INSTITUTO SUPERIOR TÉCNICO
Universidade Técnica de Lisboa

Probing the effect of ultraviolet light on biomolecules using a whey milk protein: alpha-lactalbumin

Manuel Guilherme Laranjeira Pedrosa Martins Correia

Dissertação para a obtenção do Grau de Mestre em
Engenharia Biológica

Júri

Presidente:	Prof. Luís J. P. Fonseca
Orientadores:	Prof. Duarte Miguel F. Prazeres
	Prof. Maria Teresa Neves-Petersen
	Prof. Steffen B. Petersen
Vogal:	Prof. João Pedro Conde

Dezembro 2008

ACKNOWLEDGEMENTS

First of all, I would like to thank Professor Teresa Neves-Petersen and Professor Steffen Petersen for all the support, guidance and sympathy that I felt while I was in Aalborg. I show as well my gratitude to my supervisor here in Portugal, Professor Miguel Prazeres, always available, and to Professor Helena Pinheiro for establishing the contact with the Nanobio Group.

I also thank all the help and friendship, of my coworkers, Maria Antonietta, Ane, and Gnana, always present. I convey as well my regards to Esben, who, though I did not work directly with him, was always available. I also express my gratitude to all the persons in the department, and specially Jens, who conducted the SEM-EDS experiments. Of course, I also thank my friends in Denmark which were always there for me, and evidently, the ones here in Portugal and my family.

I give my last word of appreciation to Rita, who had the patience to endure my humor in these last days.

RESUMO

A iluminação constante com luz ultravioleta de α-lactalbumina de bovino desprovida de Ca^{2+} resulta em dois efeitos progressivos na emissão dos triptófanos da proteína: aumento da intensidade e *red-shift*. As mudanças espectrais sentidas estão relacionadas com quebra paralela de pontes dissulfureto na proteína iluminada, verificada pela detecção de grupos tiol livres com o reagente de Elmann. As diferenças acima referidas são explicadas pela ausência destas pontes como agentes inibidores de fluorescência e exposição dos triptófanos ao solvente. Após iluminação prolongada observou-se que a proteína se encontrava apenas parcialmente desnaturada, numa conformação similar à nativa.

A fotólise destas pontes é atribuída ao envolvimento de espécies excitadas dos triptófanos em reacções de primeira ordem, com interconversão lenta para produtos caracterizados por *red-shift* e elevada intensidade de fluorescência. Ficou provado que um dos principais mecanismos envolve a fotoionização térmica de singletos excitados de triptófanos, com uma energia de activação de 20.5 $kJ.mol^{-1}$.

A proteína foi igualmente submetida a imobilização em nanoparticulas de ouro (AuNP) de 50.37 nm. A técnica baseia-se na afinidade de superfícies de ouro para os grupos tiol da proteína formados após irradiação com luz ultravioleta. As AuNP provenientes da reacção com proteína iluminada não mostram diferenças consideráveis em diâmetro após medição de *Dynamic Light Scattering*. Contudo, o espectro obtido por *Energy Dispersive X-ray spectroscopy* indica a presença de nitrogénio nas AuNP. Estas observações dão indícios de imobilização por formação de filme fino na superfície das AuNP. Estes complexos nanoparticula-proteína poderão ter um tremendo interesse biomédico, como transportadores moleculares ou biosensores.

Palavras-Chave: α-lactalbumina, pontes dissulfureto, inibição de fluorescência, reacção fotoquímica, imobilização assistida por luz ultravioleta, nanoparticulas de ouro.

TABLE OF CONTENTS

LIST OF ABBREVIATIONS 5
INDEX OF FIGURES 7
INDEX OF TABLES 11
1. ABSTRACT 12
2. INTRODUCTION 13
2.1. CONTEXT 13
2.2. AIM AND STRUCTURE OF THE WORK 14
3. LITERARY OVERVIEW 17
3.1. ULTRAVIOLET LIGHT 17
3.1.1. Definition, Effects of Exposure, Applications 17
3.1.2. Molecular Basis of UV light irradiation effects 18
3.2. FLUORESCENCE 20
3.2.1 Main features 20
3.2.2. Protein Fluorescence 22
3.3. ULTRAVIOLET LIGHT INDUCED REACTION MECHANISMS IN PROTEINS 27
3.3.1. Main Photochemical and Photophysical Reaction Mechanisms 27
3.3.2. Influence of external factors on the reaction mechanisms 30
3.3.3. Consequences of Protein Photo-degradation, SS Bond Breakage and Light Induced Immobilization 32
4. THE PROTEIN MODEL: α-LACTALBUMIN 35
4.1. CONTEXT AND FUNCTIONS OF THE PROTEIN 35
4.2. PRIMARY, SECONDARY & TERTIARY STRUCTURE 36
4.2.1. Main Features 36
4.2.2. Structural Elements Involved in the UV-sensitivity of LA 42
4.3. CONFORMATIONAL STABILITY OF LA 47
4.3.1. Molten Globule States 47
4.3.2. Thermal stability of LA 48
4.3.3. pH Influence in the Conformational Stability of LA 50
4.3.4. Calcium Induced Conformation Changes in LA 52
4.4 REMARKS 54
5. CHARACTERIZATION OF THE MODEL 56
5.1. PREMISSES 56
5.2. MATERIALS AND METHODS 57
5.2.1. Materials 57
5.2.2. Methods 58
5.2.2.1. Experimental Methods 58
5.2.2.2. Data Treatment and Analysis 65
5.3. RESULTS ANALYSIS AND PRESENTATION 66
5.3.1. Time-dependent Disruption of Disulphide Bridges 66
5.3.1.1. Verification and Quantification 66
5.3.1.2. Influence of external parameters 76
5.3.1.3. Effects of illumination on the secondary structure 82
5.3.2. Thermal Stability of the Protein 84
5.4. DISCUSSION 87
6. IMOBILIZATION PROCEDURE 97
6.1. PREMISSES 97
6.2. MATERIALS AND METHODS 98
6.2.1. Materials 98
6.2.2. Methods 98
6.2.2.1. Preparation of AuNP 98
6.2.2.2. Light Induced Immobilization of eLA on AuNP Surface 99
6.3. RESULTS ANALYSIS AND PRESENTATION 101
6.4. DISCUSSION 108
7. CONCLUSIONS 111
BIBLIOGRAPHY 113
APPENDIX 119
A. DENATURATION OF PROTEINS 119
B. SUPPLEMENTARY RESULTS 123
C. DEFINITIONS 137

LIST OF ABBREVIATIONS

ϕ	Quantum yield
F	Total amount of light emitted (and detected)
I_0	Incident light intensity
x	Path length in centimetres
ε	Molar extinction coefficient
c	Molar concentration of the fluorophore
3D	Three-dimensional
A	Arrhenius pre-exponentional factor for
A_{412}	Absorbance value at 412 nm
A_{ion}	Arrhenius pre-exponentional factor for Trp thermal photoionization
ASA	Accessible surface area
AuNP	Gold nanoparticles
bLA	Bovine α-lactalbumin
CD	Circular dichroism
Cys, C	Cysteine
DLS	Dynamic Light Scattering
DTNB	5,5´-dithiobis-(2-nitrobenzoic acid)
Ea	Ahrennius activation energy for the temperature dependence of exponential fluorescence increase rate *k*
Ea_{ion}	Arrhenius activation energy for Trp thermal photoionization
e_{aq}^-	Solvated aqueous electron
EDS	Energy Dispersive X-ray spectroscopy
eLA	Bovine α-lactalbumin used in the experimental procedure
EM	Electromagnetic
F/F_0	Fluorescence intensity increase

GlcNAc	N-acetylglucosamine
GT	β1,4-galactosyltransferase.
HAMLET	Human LA made lethal to tumor cells
k	Fluorescence exponential increase rate
k_{ion}	Rate constant for Trp thermal photoionization
LA	α-lactalbumin
MG	Molten-globule
MHC	Major Histocompability Complex
NMR	Nuclear magnetic resonance
Phe, F	Phenylalanine
R	Constant of perfect gases
RET	Resonance energy transfer
SDS-page	Sodium dodecyl sulfate polyacrylamide gel electrophoresis
SEM	Scanning Electron Microscopy
SEM-EDS	Scanning Electron Microscopy coupled to Energy Dispersive X-ray spectroscopy
SS	Disulphide
T	Temperature
T_d	Denaturation temperature
T_m	Temperature of mid-transition
TNB^{2-}	Nitrothiobenzoate ion
Trp, W	Tryptophan
Tyr, Y	Tyrosine
UDP-GAL	Uridine 5'-(trihydrogen diphosphate)-Galactose
UV	Ultraviolet
UVB	UV radiation in the interval 280-315 nm
λ_{max}	Emission maximum/maxima

INDEX OF FIGURES

Figure 2.1: Principle of Light Assisted Immobilization with Tryptophan (blue) close to a disulphide bridge (red) within a protein molecule (yellow). Sulphur atoms are enhanced in red. 14

Figure 3. 1: The electromagnetic spectrum. 17

Figure 3.2: The electromagnetic spectrum and molecular effects. 18

Figure 3.3: Schematic representation of the processes involved in electronic excitation. * stands for an electronic excited specie (Adapted from Prasad, 2003). 19

Figure 3.4: Typical Jablonski Diagram. The singlet ground, first, and second electronic states are depicted by S_0, S_1 and S_2 respectively. At each of these electronic energy levels the molecular or atomic species can exist in a number of vibrational levels, represented by V_1, V_2, V_3, etc. The initial absorption of light by the molecule leads into a transition to a higher energy state, S_1 or S_2 (1), from which energy can be lost in nonradiative ways, by vibrational relaxation in S_1 (2), by internal conversion (3), by external quenching (4). Molecules in the S_1 lower energetic state can undergo a downward transition by emitting fluorescence (5). Emission of fluorescence usually does not proceed until the ground state, this occurs usually by vibrational relaxation, where there is again an energy loss (6). Intersystem crossing from the singlet excited state (S_1) to the triplet state (T_1) is an alternative to fluorescence as no photon is emitted. However decay from T_1 to S_0 results in phosphorescence. The various vibrational relaxations (10^{-12}s) occur faster than the downward transitions. That is why they happen prime and after fluorescence (Adapted from Macey, 2007). 21

Figure 3.5: Absorption and emission spectra of the protein intrinsic fluorophores in pH 7 aqueous solution (Adapted from Lakowicz, 2006). 23

Figure 3.6: The two excited-state dipole moments of tryptophan (Adapted from Lakowicz, 2006) 24

Figure 3.7: Effect of tryptophan environment on the emission spectra. The higher is the exposure of the Trp in the protein structure, more will be its maxima of absorption red-shifted (1 to 4). This effect can be noticed upon the degree of unfolding of a protein. The emission spectra are those of apoazuerin Pfl, ribonuclease T_1, staphylococcal nuclease, and glugagon, for 1 to 4 respectively (Adapted from Lakowicz, 2006). 25

Figure 3.8: Channels of Trp photoionization. 30

Figure 4.1: Amino-acid composition of bLA. Data obtained using the tool ProtParam on the Expasy Server (www.espasy.org) by submitting the fasta sequence of the PDB Entry 1F6S. 37

Figure 4.2: Three-dimensional structure of LA and the functional regions of the molecule showing the location of metal ions identified in LA crystal structures. Secondary structural elements are marked (*S,* b-strand in blue; *H ,* α-helix and *h,* 3_{10} helix in red). The 8 cysteine residues are also represented, between the close pairs of cysteine are formed the 4 disulphide bridges of the protein (Adapted from Chrysina *et al.*, 2000). 39

Figure 4.3: Localization of the Aromatic Clusters I and II in the structure of bLA. apo-bLAc structure (PDB entry: 1F6R) is shown in *red*, holo-bLAc structure (PDB entry: 1F6S) is shown in *yellow,* and recombinant bLA (mLA) structure in *green*. The superposition of the structures was performed with program O (35) (Adapted from Chrysina *et al.*, 2000). 40

Figure 4.4: A – Molecular structure of lactose synthase, a complex between the catalytic domain of bovine GT (Gal-T1) and mouse LA (alpha-LA). The complex is shown with the acceptor GlcNAc. B – Stereo view of the molecular interactions between the same GT and LA. The secondary elements of LA are colored in red, while those of GT are in blue. The interactions between the proteins are principally hydrophobic. Two water molecules are trapped between the two proteins, and one of them has extensive hydrogen bonding interactions with both protein molecules. Adapted from Ramakrishnan and Qasba (2001). 41

Figure 4.5: Schematic representation of LA. Secondary structure elements and the disulfide bonds in native GLA are indicated at the top. The domain boundaries are shown as dashed lines. Each of the tryptophan residues (O) is indicated (Adapted from Vanhooren *et al.*, 2006a). 42

Figure 4.6: Crystal structure of holo-bLAc at 2.2 Á resolution (PDB entry: 1F6S) generated in *RasMol* 2.6. A- Peptide backbone is represented in grey strands. The 4 Trp and the 8 Cys residues of bLA are displayed in a stick configuration respectively in red and yellow. Dashed yellow lines represent the SS bonds of the protein highlighted by yellow arrows. Potential contact between the indole nucleus of a Trp residue and a disulphide bond is indicated mixed red-yellow dash line and the distance in Á. B- The peptide backbone is represented in grey strands and the backbone of five residues (Val27, Val92, Lys93, Lys94, and Ile95) is in blue. Val 32 is in stick configuration and in green. Contact between the indole nucleus of a Trp residue its potential quenchers is indicated in mixed red-green/blue dash line and the distance in Á. 45

Figure 4.7: Crystal structure of apo-bLAc at 2.2 Á resolution (PDB entry: 1F6S) generated in *RasMol* 2.6. A- Peptide backbone is represented in grey strands. The 4 Trp and the 8 Cys residues of apo-bLAc are displayed in a stick configuration respectively in red and yellow. Dashed yellow lines represent the SS bonds of the protein highlighted by yellow arrows. Potential contact between the indole nucleus of a Trp residue and a disulphide bond is indicated mixed red-yellow dash line and the distance in Á. B- The peptide backbone is represented in grey strands and the backbone of five residues (Val27, Val92, Lys93, Lys94, and Ile95) is in blue. Val 32 is in stick configuration and in green. Contact between the indole nucleus of a Trp residue its potential quenchers is indicated in mixed red-green/blue dash line and the distance in Á. 46

Figure 4.8: Snapshots of LA configurations in the native state (left) and molten globule state at pH 2 (right) from the molecular dynamics simulations. Helices are displayed as barrels and β-sheets as large arrows (Adapted from Tarek *et al.*, 2003)..... 51

Figure 5.1: Reaction of a thiol with Ellman's reagent, originating a mixed disulphide and one equivalent of TNB^{2-}. The extinction molar coefficients at 412 nm are displayed for the different chemical species and all refer to pH > 7.29 (Adapted from Riener *et al.*, 2002). 59

Figure 5.2: Absorbance values at 412 nm *versus* cysteine concentration in the assay. The absorbance values correspond all to a reaction time of 22minutes except for the 0µM solution. 61

Figure 5.3: Fluorescence intensity of eLA *versus* illumination time. Excitation was fixed at 295 nm and emission was monitored at 340 nm. Temperature was maintained at 25ºC using a peltier element. Measurements were performed using a RTC 2000 PTI spectrofluorimeter as described in Materials and Methods (section 5.2). 67

Figure 5.4: Effect of illumination time on the spectrum of excitation and emission. The spectra were recorded fixing the emission at 340 in the excitation spectra and the excitation at 295 in the emission one as described in Materials and Methods (Section 5.2). 68

Figure 5.5: Normalized emission spectra of illuminated samples of eLA over different time periods and non-illuminated eLA. Excitation was realized at 295nm. The spectra were first smoothed and normalized as described in Materials and Methods (section 5.2). 69

Figure 5.6: Normalized excitation spectra of illuminated samples of eLA over different time periods and non-illuminated eLA. Emission was selected at 340nm. The spectra were first smoothed and normalized as described in Materials and Methods (section 5.2). 70

Figure 5.7: Normalized excitation spectra of illuminated samples of eLA over different time periods and non-illuminated eLA. Emission was selected at 320 nm. The spectra were first smoothed and normalized as described in Materials and Methods (section 5.2). 71

Figure 5.8: Ratio between the normalized spectra with the emission fixed at 340 nm displayed in Figure 5.6. The ratio is realized between the spectra took after different periods of illumination and the spectrum of the fresh eLA. 72

Figure 5.9: Ratio between the normalized spectra with the emission fixed at 320nm displayed in Figure 5.7. The ratio is realized between the spectra took after different periods of illumination and the spectrum of the fresh eLA. 72

Figure 5.10: Values of Absorbance read at 412 nm (closed yellow circles A_{412}) *versus* illumination time. In green is displayed time-dependent fluorescence intensity increase at 340nm (F/F_0). The presence of

free thiols was evaluated after reaction with 5,5´-dithiobis-(2-nitrobenzoic acid), after 0-, 1-, 2-, 3-, 4- and 5-h of illumination with 295 nm light, considering that the free thiol concentration is proportional to the absorbance value at 412 nm, as described in Materials and Methods (Section 5.2). F/F0 values displayed consist on the ratio between the monitored values fluorescence emission at 340 nm and the initial fluorescence emission value at 340 nm obtained for the 5-h illumination session. The values were corrected for lamp intensity oscillations as described in Materials and Methods (Section 5.2). 73

Figure 5.11: Ratio of the emission values at 295 nm during the illumination sessions. The emission of 295 nm light was checked constantly during the sessions of irradiation (1h, 2h, 3h, 4h, 5h) with 295 nm light using the second channel of the spectrofluorimeter. The values are corrected for the light source oscillation and were normalized as described in Materials and Methods (Section 5.2). 75

Figure 5.12: Fluorescence intensity of Bα-L in function of the illumination time at different temperatures (9.3, 12.9, 15.6, 20.4, 24.9, 29.9 and 34.6 ºC). Excitation was realized at 295 nm and emission measured at 340 nm. Measurements were effectuated using a PTI spectrofluorimeter during 3.5 hours. The temperature of the solution was maintained constant using a Peltier element. The curves were normalized and corrected for the oscillations of lamp intensity as described in Materials and Methods (Section 5.2). 77

Figure 5.13: Linear relation between the logarithm of the rate constant ln *k* and the inverse of temperature 1/*T*. The linear regression trendline is also displayed in the plot as the equation and the root mean square error R^2. 79

Figure 5.14: Emission spectra of non-illuminated eLA at different temperatures (9.3, 12.9, 15.6, 20.4, 24.9, 29.9 and 34.6ºC). Solution temperature was previously set using the peltier element. Excitation was realized at 295nm. The spectra were first smoothed as described in Materials and Methods (section 5.2). 80

Figure 5.15: Emission spectra of eLA recorded after 3.5h of 295nm light irradiation at different temperatures (12.9, 15.6, 20.4, 24.9, 29.9 and 34.6ºC). Excitation was realized at 295nm and the temperature of the solution was still maintained after the precedent irradiation and during recording of the spectra. The spectra were first smoothed as described in Materials and Methods (section 5.2)....80

Figure 5.16: Values of absorbance at 412 nm after 20 minutes of reaction between the irradiated samples at different temperatures, and DTNB (*vide* Materials and Methods, section 5.2)....81

Figure 5.17: Fluorescence emission maximum increase at 340 nm of eLA upon prolonged 295 nm UV-light irradiation for different pH values. The points F_{max}/F_0 consist on the ratio between the maximum emission value of the time-based fluorescence emission profile (at the plateau) and the fluorescence emission at time zero. The fluorescence time-dependent curves from where these values were obtained are present in the Supplementary Results (Appendix B)....82

Figure 5.18: Fluorescence intensity of eLA *versus* illumination time. Excitation was fixed at 295 nm and emission was monitored at 340 nm. Temperature was maintained at 25ºC using a peltier element. The experiment was stopped each 2000s to remove a protein sample. The emission values are corrected for the oscillations of lamp intensity. Measurements were performed using a RTC 2000 PTI spectrometer as described in Materials and Methods (section 5.2)....83

Figure 5.19: Far-UV CD scan of 295 nm light irradiated eLA samples (0-, 2000-, 4000-, 6000-, 8000-, and 10000-s of illumination) recorded at pH 8.55 and room temperature. The measurements were realized in a JASCO J-715 spectropolarimeter. The spectra were corrected for the buffer contribution in ellipticity and smoothed as previously described in Materials and Methods (Section 5.2). Although some fluctuations are noticed, the overall trend is the partial loss of secondary structure the longer the collected sample was illuminated. 84

Figure 5.20: Normalized emission spectra of fresh eLA solutions recorded at different temperatures (10.0, 18.2, 26.0, 33.6, 41.0, 49.0, 56.5, 64.0, 71.6, and 78.7 ºC). Excitation was realized at 295nm and the temperature of the solution was set before the recording of the spectra and during the short irradiation. The spectra were smoothed and normalized as described in Materials and Methods (section 5.2)....85

Figure 5.21: Maximum of emission of eLA upon excitation at 295 nm (λ_{max}) *versus* the solution temperature. 86

Figure 5.22: Maximum of emission of eLA upon excitation at 295 nm (λ_{max}) *versus* the solution temperature. 86

Figure 6.1: Fluorescence intensity of eLA *versus* illumination time. Excitation was fixed at 295 nm and emission was monitored at 340 nm. Temperature was maintained at 25ºC using a peltier element. Measurements were performed using a RTC 2000 PTI spectrofluorimeter as described in Materials and Methods (section 6.2). 102

Figure 6.2: Absorption spectra of the supernatants of the two washes and the final resuspended AuNP solution. The box displayed within the area of the plot is a zoom of the absorption spectra of the second wash supernatant and the final resuspension of AuNP. The spectra were recorded in a UV-visible absorbance spectrophotometer as previously described in Materials and Methods (Section 6.2).....103

Figure 6.3: Absorption spectra of the final resuspension of AuNP (red), fresh AuNP (wine red) and the difference between these two (orange). Spectra were recorded using a UV-visible spectrophotometer as described in Materials and Methods (section 6.2). 104

Figure 6.4: SEM image of the final AuNP resuspension (after immobilization). Accelerating Voltage: 7.0 keV; Magnification: 18272. The squares represent the area exposed to EMS. X-ray spectra of the exposed areas are displayed in the bottom. The peaks corresponding to each atom are labeled.....106

Figure 6.5: SEM image of the final AuNP blank (fresh, non-exposed particles). Accelerating Voltage: 7.0 keV; Magnification: 29881. The squares represent the area exposed to EMS. X-ray spectra of the exposed areas are displayed in the bottom. The peaks corresponding to each atom are labeled.....107

INDEX OF TABLES

Table 4.1: Comparison of different LA structures. The values displayed are the root mean square deviations (in Å) obtained after superposition using the least square fitting function applied to C_α atoms of residues 1-120 (values in bold font) and to the core of the molecule (values in normal font). LA core comprises the residues 5-11, 23-40, 50-61, and 71-104. Apo-bLAc: Ca^{2+} depleted form of bovine LA at 2.2 Å (PDB code: 1F6R). Holo-bLAc: Ca^{2+} bound form of Bovine LA at 2.2 Å (PDB code: 1F6S). mLA: recombinant bovine LA at 2.3 Å (PDB code: 1HFZ). Baboon LA at 1.7 Å (PDB code; 1ALC). Guinea pig LA at 1.9 Å (PDB code, 1HFX). Goat LA at 2.3 Å (PDB code, 1HFY). Buffalo LA at 2.3 Å (Calderone *et al*., 1996). Human LA at 1.7 Å (Acharya *et al*., 1991). The values were calculated using the program O (Extracted from Chrysina *et al*.., 2000).....37

Table 4.2: Distances between the Trp residues of holo-bLAc and Apo-bLAc and its potential quenchers. The values were determined in *Rasmol* 2.6 using the "monitor" tool. In green are highlighted the Trp-quencher pairs for which there is direct contact (≤ 5.2 Å). 44

Table 5.1: Salts used for Buffer preparation, Molecular Formula, Purity, and Provenience. 57

Table 5.2: Composition of the solutions used for the Ellman's assays and of the two blanks. 60

Table 5.3: Conditions and settings used in the temperature-dependent illumination sessions of eLA samples. 61

Table 5.4: Buffers used for the protein solutions used in the illumination sessions and correspondent pH values. 62

Table 5.5: Selected settings in the RTC 2000 PTI spectrometer for eLA steady-state illumination.....63

Table 5.6: Experimental parameters for the standard CD spectra of a wavelength scan at 25ºC. 64

Table 5.7: Parameters values and correspondent errors, root mean square errors, and reduced chi square errors obtained after fitting of time-based fluorescence curves using equation 5.2. 78

Table 6.1: Experimental settings used in the immobilization procedures. 99

Table 6.2: Experimental atomic values obtained after EMS analysis of each exposed zone - AuNP resuspension (after immobilization). 106

Table 6.3: Experimental atomic values obtained after EMS analysis of each exposed zone - AuNP blank (fresh, non-exposed particles). 107

1. ABSTRACT

Prolonged ultraviolet illumination of Ca^{2+} depleted form of bovine α-lactalbumin (bLA) results both in progressive red-shift and increase of tryptophan fluorescence emission. Such spectral changes are related to progressive cleavage of disulphide bonds in illuminated protein molecules, verified by detection of free thiol groups with Elmann's reagent. The absence of disulphide bridges as fluorescence quenchers and dislocation of tryptophan residues to solvent accessible zones explain the emission changes. After prolonged ultraviolet-irradiation and disulphide bond cleavage, the protein is only partly denaturated, in a native-like conformation.

Photolysis of the disulphide bonds is credited to involvement of tryptophan excited species in first order reactions, slowly interconverting into high quantum yield red-shifted species. The presence of a hidden isosbestic point in successive tryptophan emission spectra suggests such equilibrium. It was proven that one of the major reaction pathways is the thermal photoionization of tryptophan excited singlet states with Arrhenius activation energy of 20.5 $kJ.mol^{-1}$.

Light induced immobilization of Ca^{2+} depleted bLA form was attempted using 50.37 nm gold nanoparticles (AuNP).The technique is based on the affinity to gold surfaces of free protein thiol groups formed upon ultraviolet-irradiation. AuNP provenient of reaction with irradiated bLA show no net difference in hydrodynamic radius compared to fresh AuNP after Dynamic Light Scattering measurements. However, Energy Dispersive X-ray spectroscopy shows unusual nitrogen contents on this reaction product. Such observations indicate that bLA might immobilize onto AuNP forming a thin film on the gold surface. The complexes nanoparticle-bLA may be of biomedical interest, as molecular carriers or biosensors.

Keywords: α-lactalbumin, disulphide bridges, fluorescence quenching, photochemical reaction, light-assisted immobilization, gold nanoparticles.

2. INTRODUCTION

2.1. CONTEXT

Nowadays, according to the physics interpretation, light encompasses the broad spectra of electromagnetic radiation from radio-waves to gamma rays. Interaction between light and matter is ubiquitous in nature and lies within numerous day-to-day commodities man uses.

Historically, light has always fascinated curious minds, since the first descriptions of light in antiquity to the proton theory of Albert Einstein. Wonder how light is constituted and how it influenced the universe around us were intriguing questions, from simple visible interactions like reflection or definition of colors to our eye-site, to others more discrete like glow in the dark mineral crystals and the photoelectric effect.

Light can indeed interplay with matter (molecules, atoms) in a several ways, that cover transfer of energy by absorption, reflection, refraction, scattering, as reversely as matter can itself emit light. Light modulates matter and *vice-versa*, and they regulate a wide number of mechanisms, equilibrium hard to follow. One of the ways of regulation consists in light-induced reactions. These are particularly fascinating since they are ultra fast, tremendously complex, and give rise to profound changes in matter.

Nature itself has particularly been mediated by light induced reactions as a principle for life across its advances. Harnessing photons to achieve photosynthesis and conversion of photons to achieve vision are two simple examples. There are also strong signs that indicate that light was essential in the genesis of life, allowing the generation of simple molecules that constituted the first living organisms.

Thus, it is not strange that crossing light and biology has raised interest for the scientific community years over years. Until recently, the task was rather difficult, due to the lack of instrumentation, which limited the survey to simple and imprecise techniques. However, in the last decades, the evolution of optical instruments, the development of laser technology, and photonic technology allowed to unravel new approaches for understanding light processes and applying light to specific needs. Biophotonics emerged as new discipline and imputed a load of knowledge into this perspective, taking advantage of new photonic tools available.

Here precisely the attention is prawn to the effects of ultraviolet (UV) light in biomolecules. Biological medium is naturally exposed to UV radiation. Ambient sunlight is constituted by photons in the visible range, but also broadens some in the UV and Infrared. Part of the UV radiation is blocked in the atmosphere, but a considerable amount of near-UV radiation still reaches earth's surface. The harmful effects of exposure to UV radiation from sunlight are widely known. In humans, prolonged direct exposure to sunlight can induce severe health

problems (*e.g.* immunosupression, skin cancer; Matsumara and Ananthaswamy, 2004). UV-irradiation can affect a wide number of organisms, such as bacteria, cyanobacteria, phytoplacton, macroalgae, plants and animals through DNA damage (Sinha and Häder, 2002). In proteins exposition to UV-light can lead to loss of structure and inactivation (Neves-Petersen *et al.*, 2002).

Uncover the molecular mechanisms and evaluate the damage that UV radiation induces in cells and biomolecules can be extremely important, not only for medical and scientifically purpose, but also for industrial applications and product quality management. For example, in the process of synthesis of antibiotics and drugs in general, which have in its constitution proteins and vitamins, there are several steps in which they are exposed to UV light, is it in analysis routines where UV spectroscopy techniques are used, or in the contact with UV radiation present in sunlight, in transfer operation or in storage procedures. There is a need of guarantying the safety of these medicaments, taking precautions, and avoid the surge of dramatic changes within biomolecules. The same is valid to similar production steps in the food industry.

On other hand, uncover the reaction mechanisms and dynamics behind these effects can also be rewarding. If one can fully acknowledge the photonic processes, maybe it will be possible to control these reactions using photons and pulses of light, mimicking nature. One could learn, for instance, how to switch on and off a particular functionality of a biocatalyst using light, thereby controlling its function in a biosensor, with a simple and practical photonic signal.

2.2. AIM AND STRUCTURE OF THE WORK

The Nanobiotechnology Group of the University of Aalborg, where this work was fulfilled, has a particular interest in the study of light induced reactions in biomolecules. The fundamental knowledge acquired over the years regarding protein structure and the effect of UV radiation allowed to develop recently a novel light assisted protein immobilization technique.

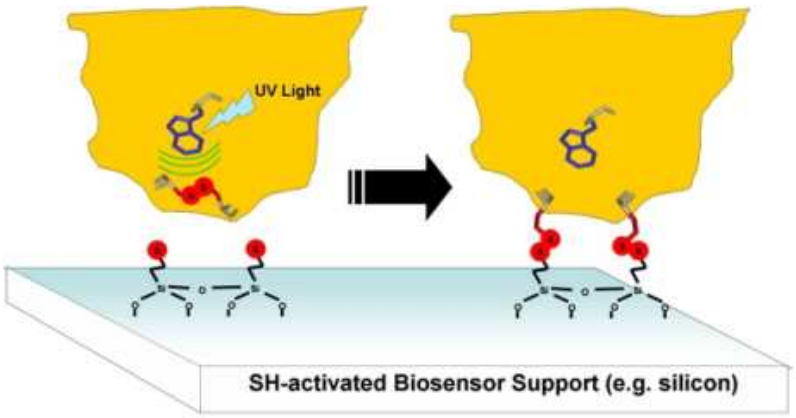

Figure 2.1: Principle of Light Assisted Immobilization with Tryptophan (blue) close to a disulphide bridge (red) within a protein molecule (yellow). Sulphur atoms are enhanced in red.

Briefly explaining, the technology behind this immobilization procedure is based on the fact that the disulphide (SS) bridges naturally present within the majority of proteins can be broken as second result of UV irradiation, in a mechanism mediated by neighbor aromatic residues. The free thiol derivated groups created upon disruption of these bonds are very reactive and can be used as linkers for covalent attachment to a surface. The surface can be for instance gold or thiol-derivatized silicon, which brings a huge span of possibilities for immobilization (*vide* Figure 2.1). With the aid of laser, the group successfully engineered specific microarrays with covalent-bounded protein. The technique allowed the immobilization of several proteins, in precise positions (directed by the laser), avoiding aggressive chemical/termochemical steps for the protein, preserving its native structural and functional properties.

However, immobilization is not an acquired fact for all proteins that contain SS bonds. The disruption of the SS bridges upon irradiation with UV light is dependent on spatial and structural properties of the protein, and external conditions, and is not always ruled by the same mechanisms. Moreover, the changes in the protein upon the disruption can be variable and of course, since proteins present different structures and a diverse number of SS bonds, and a successful immobilization is dependent on all these issues.

This project was integrated in a wider perspective that relied on developing a database of proteins that carried the necessary structural features for light induced immobilization.

The main goals of the work were therefore to evaluate a model protein on these specific characteristics, study the mechanism of the UV induced breakage of SS bridges, and eventually attempt the light assisted immobilization on a surface, engineering in that effort a potential light induced useful platform, like a set of microarrays or a biosensor.

The protein characterization relied on studying the effect of UV-light on the structural and spectroscopic features of the protein under different conditions (*e.g.* pH, temperature, concentration of the protein) using the tools available within the group. Once the ideal conditions for immobilization were established, further proceed to the immobilization procedure, and in case of success, verify the functionality of the protein via antibody or/and catalytic assay and test the sensitivity of the device.

The protein candidate studied in this work was α-lactalbumin, from bovine, used in its specific calcium depleted form. The major tool used for the characterization process was fluorescence spectroscopy. Given that some interesting results rose from the preliminary assays, regarding both the specific UV reactions triggered and structural specific features, the work proceeded further not only focused on the immobilization characteristics. The UV light induced illumination was also intended.

The organization of the work is derived from these results. On a first instance will be introduced, within a literary overview, the basic notions regarding UV light that are important for

this project. These include the characteristics of UV light irradiation effects, the basics notions of protein fluorescence (since fluorescence was used as probing tool), UV-light triggered reactions in proteins, and the specific reactions related to SS bridge disruption. It is followed by an extensive study of the model protein, α-lactalbumin, comprising the analysis of its structural and stability features. Finally, will be presented the two sets of results:

- the characterization and analysis of the protein form used;
- the immobilization procedure.

The material and methods used will evidently precede these sections, and they will be followed by the respective discussion.

Finally, the general conclusions regarding the work will be advanced.

3. LITERARY OVERVIEW

3.1. ULTRAVIOLET LIGHT

3.1.1. Definition, Effects of Exposure, Applications

UV light is considered the electromagnetic (EM) radiation (light) that present wavelengths shorter than those of the visible light, and longer than the X-rays, *i.e.* between about 400 to 10 nm, as can be observed in the electromagnetic spectrum (Figure 3.1).

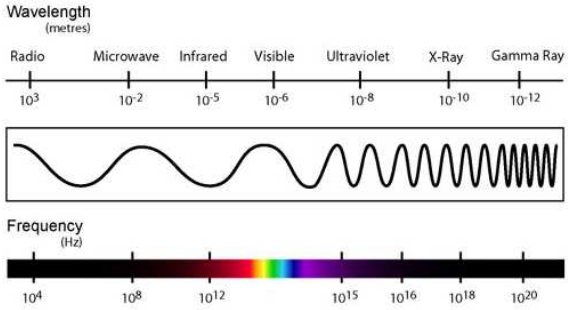

Figure 3. 1: The electromagnetic spectrum.

Since the discovery of the existence and presence of this radiation in sunlight in 1981 by the German physicist Johann Wilhelm Ritter, UV-radiation has been standing as common issue of interest for the scientific community. The effects and potential reactivity of this radiation are rather known for the last decades and in the awareness of society, mostly due to the concern regarding the harmful effects of long exposure to sunlight, which broadens part of the UV of the EM spectrum; and the destruction of the ozone layer that blocks part of the dangerous radiation.

The effects of UV irradiation surge at a molecular level but the repercussions can be verified at a larger scale. A striking example is the discoloring and degradation of surfaces exposed to sunlight, constituted by polymers, pigments or dies that suffer reactions upon the exposure.

In biological systems, which are in the line of this work, one can find a wide number of UV targets. In several organisms, exposure to diverse types of UV can lead to reduction in growth and survival, protein destruction, pigment bleaching and photoinhibition of photosynthesis (Sinha and Häder, 2002). On the human body, depending on the type of radiation and time of exposure UV light can have different effects, such as sunburn, suntan, cell-aging, and photocarcinogenesis on the skin, or welderflash and blindness (Matsumara and Ananthaswamy, 2004). The damage induced arises from molecular reactions triggered by irradiation, and the reactive species that it generates. For instance, UVB (UV radiation in the interval 280-315 nm) can induce DNA damage

by inducing the cross-linking of cytosines and thymines, provoking mutations upon repair, and further carcinogenic risks; the absorption of UV by chromophoric molecules can also lead to the formation of single oxygen or free radicals known to destroy membranes and other cellular components (Sinha and Häder, 2002).

The reactivity implicit to UV-light is also used for greater good, examples of that are its profitable use in sterilization procedures, photolithography, polymerization reactions, or laser-definition of structures.

As exposition to UV-light induces changes at the molecular level, it is widely used in as a sensor for UV sensitive species, is it in experimental analysis procedures, in spectroscopical techniques (fluorescence spectroscopy, UV-visible absorption spectroscopy, Raman spectroscopy), or microscopy (*e.g.* confocal fluorescence microscopy), or in day to day applications as UV-sensitive inks in passports or in bills to avoid forgery.

3.1.2. Molecular Basis of UV light irradiation effects

Given the broad effects noticeable on exposure to UV light it is important to first outline the molecular mechanisms that trigger such ultra-fast photophysical and photochemical reaction and give rise to detectable side-effects like fluorescence or phosphorescence.

On the verge of the molecular effects provoked by exposure of matter with UV light is the general interplay between EM radiation and matter. (Pöpp and Streller, 2006). The main interaction between light and matter consists on a process of both polarization of the molecules, bonds or atoms irradiated, and transfer of energy between the oscillating electrical field and oscillating dipoles present in molecules. The driven process has then different molecular effects on the molecular entity, depending on the wavelength of the light used. A strong interaction implies that the dipole moment in the molecule oscillates in the same frequency as the oscillation of the electrical field (Figure 3.2).

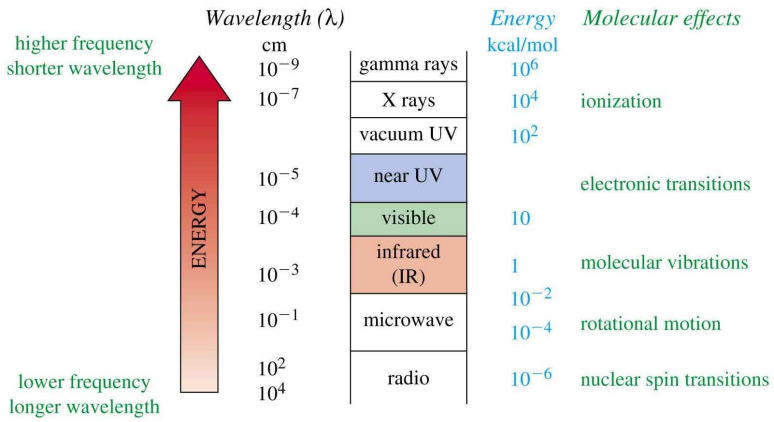

Figure 3.2: The electromagnetic spectrum and molecular effects.

For higher wavelengths and lower frequencies (like radio-waves – 100MHz) the effects can be explained with classic physics, involving for instance the alignment of polar molecules or electrons by the electrical field. For larger frequencies the interaction results in the absorption of light by the entity, as photons, resulting in the transition between energy levels, rotational, vibrational, electronic, and eventually ionization. Given that the energy of photons is dependent on frequency and wavelength, the higher the frequency, more energetic will be the transition, ultimately being the ejection of electron and ionization (Figure 3.2) (Pöpp and Streller, 2006; Macey, 2007).

The absorption of UV and visible light by an atomic or molecular specie leads particularly to the transition to higher electronic states, originating excited species with brief lifetimes (10^{-8}–10^{-9}s). Electronic transitions consist on the transfer of electrons from a lower energy orbital to a high energy orbital, such as an antibonding orbital (*e.g.* $n \rightarrow \pi^*$; $\pi \rightarrow \pi^*$). The electronic transitions only take place for a precise wavelength, since the energy gap between states is quantized. (Pöpp and Streller., 2006).

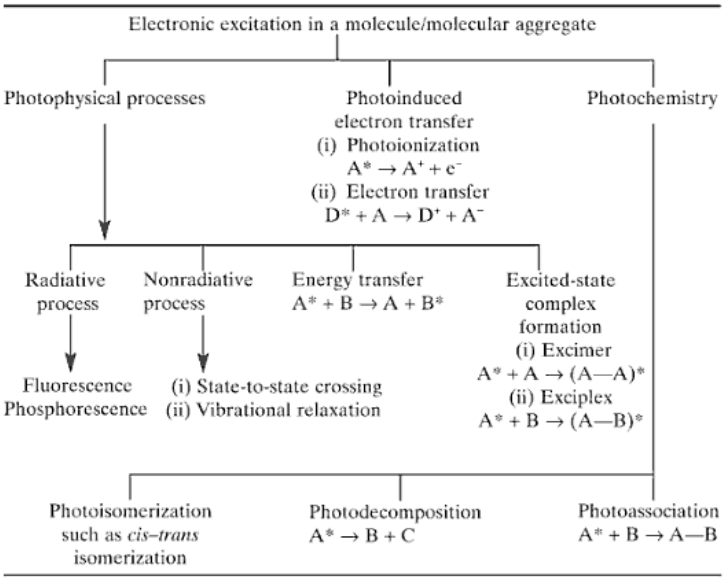

Figure 3.3: Schematic representation of the processes involved in electronic excitation. * stands for an electronic excited specie (Adapted from Prasad, 2003).

The highly energetic and unstable excited specie is then rapidly driven into a multitude of pathways as described in Figure 3.3. Its fate is uncertain, dependent on external conditions, and may even involve multiple pathways. It can involve photophysical processes, where generally the energy is dissipated or transferred, occurring the relaxation of the entity to a ground energetic state, where it is again available for further excitation. This relaxation may occur by radiative processes, such as fluorescence and phosphorescence, in case of a fluorophore; by non-radiative processes, involving heat dissipation; or by the energy transfer, is on the excitation of

other species, or formation of complexes. By other hand the molecule may not relax and enter in reactive pathways, is it by electron transfer, or chemical reactions such as photodecomposition (Prasad, 2003).

In this work not all the pathways will be in study, only those in which are driven the excited species of the model protein. Therefore, in this literature overview only these specific processes will be profoundly appreciated.

First will be addressed the phenomenon of fluorescence and the particularities of protein fluorescence. Fluorescence spectroscopy was the primary tool used both to explore the conformation of the protein and to probe the UV-reactions in the protein model.

Secondly, the pathways of excited species triggered by UV-light in proteins, and the possible resulting reactions, as possible applications for these processes, will be reviewed.

3.2. FLUORESCENCE

3.2.1 Main features

The radiative pathway mentioned before can lead to two phenomena: fluorescence and phosphorescence. They involve the emission of light from the electronically excited states and differ on the nature of the excited state. Molecules that display fluorescence (fluorophores) are typically aromatic. One example is quinine, which is present in tonic water.

Fluorescence in particular involves excited singlet states. In these, the electron on the excited orbital is paired (by opposite spin) to the second orbital in the ground-state orbital. Return to the ground-state is therefore spin-allowed and takes place quickly by emission of a photon. Fluorescence emission is a fast process: emission rates of fluorescence are usually in the scale of $10^8 s^{-1}$, resulting in a typical fluorescence lifetime around 10 ns. The fluorescence lifetime is the average time between its excitation return to the ground state.

The intensity of fluorescence light is proportional to the extinction coefficient of the fluorophore and a factor known as quantum yield (ϕ) which is the rate of photons (or quanta) emitted per photons absorbed (or quanta). The quantum yield presents values between 1 and 0 and is characteristic of each fluorophore. Fluorescence intensity measured experimentally from a fluorophore excited in solution and can be defined as:

$$F = I_0 \times \varepsilon \times c \times x \times \phi \tag{3.1}$$

where F is the total amount of light emitted (and detected), I_0 is the incident light intensity, x the path length in centimetres, ε the molar extinction coefficient, and c the molar concentration of the fluorophore.

The quantum yield is generally lower than 1 since other processes, including internal conversion, quenching of various types, and intersystem crossing compete with fluorescence to dissipate the energy gained in absorption.

There are energy losses along the invert process of emission, mainly by vibrational relaxation, or internal conversion. Thus fluorescence is not a process 100% efficient and the photons emitted are intrinsically less energetic than the photon absorbed. This is felt in spectroscopic data, as the maximum of emission spectra will always situated at longer wavelengths than the maximum of absorption spectra (Stokes Shift) (Lakowicz, 2006; Macey, 2007).

The whole process of absorption and emission can be pictured by means of a Jablonski Diagram (Figure 3.4).

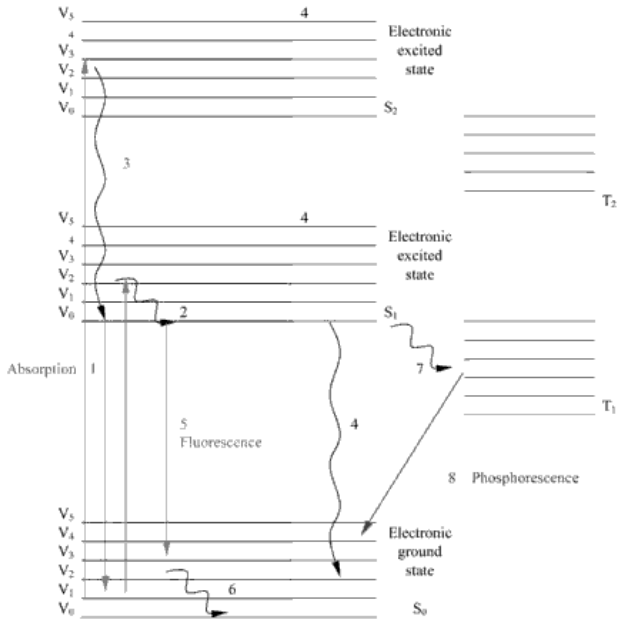

Figure 3.4: Typical Jablonski Diagram. The singlet ground, first, and second electronic states are depicted by S_0, S_1 and S_2 respectively. At each of these electronic energy levels the molecular or atomic species can exist in a number of vibrational levels, represented by V_1, V_2, V_3, etc. The initial absorption of light by the molecule leads into a transition to a higher energy state, S_1 or S_2 (1), from which energy can be lost in nonradiative ways, by vibrational relaxation in S_1 (2), by internal conversion (3), by external quenching (4). Molecules in the S_1 lower energetic state can undergo a downward transition by emitting fluorescence (5). Emission of fluorescence usually does not proceed until the ground state, this occurs usually by vibrational relaxation, where there is again an energy loss (6). Intersystem crossing from the singlet excited state (S_1) to the triplet state (T_1) is an alternative to fluorescence as no photon is emitted. However decay from T_1 to S_0 results in phosphorescence. The various vibrational relaxations (10^{-12}s) occur faster than the downward transitions. That is why they happen prime and after fluorescence (Adapted from Macey, 2007).

Before the term quenching was mentioned. In fluorescence spectroscopy quenching refers to any process that leads to the decrease in fluorescence intensity Thus, this term basically encompasses all the mechanisms involving excited electronic species that have been enumerated before, excluding fluorescence itself and the vibrational relaxations, part of the pathway of fluorescence.

It is named collisional quenching when the excited-state fluorophore is deactivated on the contact with another molecule in solution, which is named as quencher. A wide number of molecules may act as collisional quenchers, for instance oxygen, halogen, amines, and electron-deficient molecules like acrylamide, and within different mechanisms such electron transfer and intersystem crossing to the triplet state (*e.g.* quenching by halogen and heavy atoms realized by spin-orbit coupling). Another type of quenching is known as static quenching. It occurs in the ground state, and does not rely on diffusion and molecular collisions. It can for instance consist on the formation of non-fluorescent complexes between the quencher and the fluorophore. Quenching can also occur in several via several other non-molecular mechanisms, for instance attenuation of light by the fluorophore itself or other absorbing (Lakowicz, 2006).

Another important process specific to fluorescence that may occur in the excited state is resonance energy transfer (RET). It takes place whenever the emission spectrum of a fluorophore, named the donor overlaps with the absorption spectra of another molecule. The acceptor does not have to be a fluorophore. RET does not involve the emission of light by the donor, and absorption by the acceptor. The donor and acceptor are coupled by a dipole-dipole interaction. The degree of energy transfer is dependent on the spatial distance between donor and acceptor, and the extent of spatial overlap, characterized in terms of the Förster distance.
Besides these characteristic distances, the energy transfer is dependent on a broad number of parameters, as the lifetime of the donor, diffusion and if the pair is covalently bounded (Lakowicz, 2006).

3.2.2. Protein Fluorescence

Fluorescence spectroscopy is a widely used tool in protein studies, are they directed to structural features, folding, denaturation, association reactions, substrate binding, etc. It stands as a fast method of analysis, implicates low-cost operations, and provides a relatively high sensitivity.

Proteins contain three amino-acid residues that contribute to their UV fluorescence: Tyrosine (Tyr, Y), tryptophan (Trp, W), and Phenylalanine (Phe, F). These intrinsic fluorophores are particularly rare in proteins. Trp, the major contributor for protein fluorescence is usually present in 1 mole % of proteins. When proteins contain one or few fluorophores, the spectral data is easy to interpret.

For convenience of analysis the absorption and emission spectra of these amino acids in neutral solution are shown in Figure 3.5.

The emission of proteins is dominated by Trp, which absorbs at longer wavelength and presents the highest extinction coefficient. Moreover, energy absorbed by Phe and Tyr can be further transferred to Trp residues in the same protein. Phe shows the shortest absorption and

emission wavelengths, presenting a structured emission in water environment with a maximum near 282 nm. As for Tyr, the emission takes place at approximately 303 nm and is quite insensitive to solvent polarity. Oppositely, Trp emission is highly dependent on polar parameters and local environment as further can be observed. The emission of Trp in water takes place usually around 350 nm.

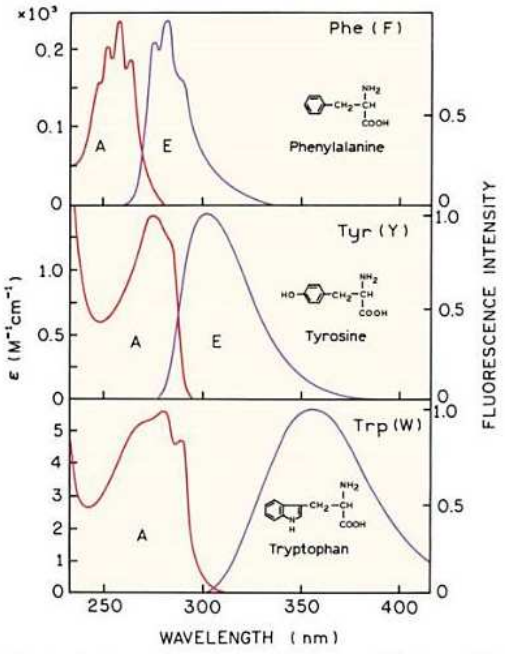

Figure 3.5: Absorption and emission spectra of the protein intrinsic fluorophores in pH 7 aqueous solution (Adapted from Lakowicz, 2006).

The excitation of protein fluorescence is generally realized at the absorption maximum 280 nm or at higher wavelengths, meaning that Phe is not excited most of times. At wavelengths longer that 295nm, as can be neatly seen in Figure 3.2, the absorption is mainly responsibility of Trp. Thus, one can excite selectively Trp fluorescence at 295-305 nm, permitting a better resolution and understanding of the spectral data (Lakowicz, 2006).

Solvent effects on Tryptophan Emission Spectra

One of the major characteristics that allow the use of protein fluorescence to extract conclusions regarding the structure features and behavior of a protein is the way Trp emission is affected by local environment.

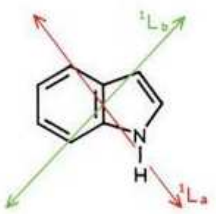

Figure 3.6: The two excited-state dipole moments of tryptophan (Adapted from Lakowicz, 2006)

Whereas the emission of Tyr is not so sensitive to local environment, Trp is highly sensitive to change in its microenvironment, especially to polar solvents. This strange duality is explained by the unique character of Trp as a fluorophore. In Tyr the emission appears two occur from only one of its two electronic states. On the contrary Trp presents two nearly isoenergetic transitions correspondent to two nearly perpendicular excited state-dipole moments, ^1L_a and ^1L_b (Figure 3.6). This electronic transitions display distinct absorption and emission, and are differently sensitive to solvent polarity. The relative population of these excited states depends first on the excitation wavelength, wavelengths higher than 290nm favor the ^1L_a transition, whereas at 270 nm is favored the other transition. By other hand the emission of ^1L_b is mostly structured, compared to the ^1L_a emission.

Depending on the solvent, emission can take place from ^1L_a or ^1L_b states, though emission from the ^1L_b is infrequent. This is due to the fact that Trp emission is highly sensitive to hydrogen bonding to the imino group. The ^1L_a transition is more sensitive to polar solvents (like ethanol), shifting to lower energy on their presence, which makes sense since this transition involves more directly the polar nitrogen atom of indole. In a complete nonpolar environment the ^1L_b state has the lower energy and may dominate the emission, whereas in the reverse situation ^1L_a dominates.

In a protein the spectral implications can be interesting for analysis. Once the ^1L_A transition shifts to lower energies with the increase of polarity and hydrogen bounding, the relative position of the Trp residues in the protein structure can be checked by the position of the emission maximum. If the Trp residue is buried inside the protein, the emission occurs at lower wavelengths. When the Trp residue is exposed in solution, typically aqueous and polar for proteins, the ^1L_a transition transits to lower energies, resulting in a red-shift[a] of fluorescence emission. This effect can be depicted in Figure 3.7, and can be used for instance to follow protein unfolding. Moreover few proteins display the characteristic structured emission of the ^1L_b transition since few Trp residues are in completely nonpolar environments. Furthermore one can specifically excite the ^1L_a at wavelengths superior to 290 nm and have a clear notion of the events (Lakowicz, 2006).

[a] A red-shift means that the maximum of emission is shifted to higher wavelengths, on opposition to a blue-shift.

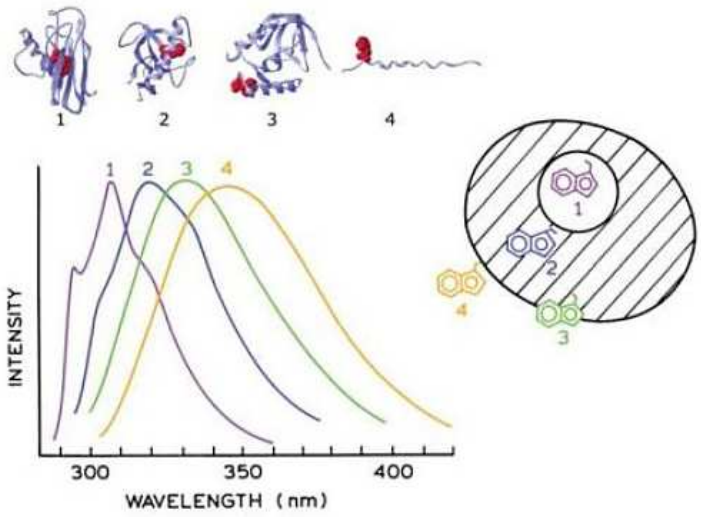

Figure 3.7: Effect of tryptophan environment on the emission spectra. The higher is the exposure of the Trp in the protein structure, more will be its maxima of absorption red-shifted (1 to 4). This effect can be noticed upon the degree of unfolding of a protein. The emission spectra are those of apoazuerin Pfl, ribonuclease T_1, staphylococcal nuclease, and glugagon, for 1 to 4 respectively (Adapted from Lakowicz, 2006).

Excited-State Ionization of Tyrosine

Tyr is regularly regarded as a simple fluorophore, and is not so sensitive to external conditions as Trp. Nonetheless Tyrosine can display complex spectral properties in certain situations. Tyr can suffer excited-state ionization, inducing the loss of the proton in the aromatic hydroxyl group. In the ground-state the pK_a of the hydroxyl group is approximately 10, while on the excited state it decreases to 4. Consequently, in neutral solution the excited state can dissociate during the lifetime of the excited state, leading to quenching of the Tyrosine fluorescence. Tyrosinate, the ionized form of Tyr, is weakly fluorescent at 350nm, an emission that can be confused with Trp fluorescence.

Nevertheless experience tells that excited state ionization is not the major decay pathway for Tyr, and for that reason it is only observed in some proteins (Lakowicz, 2006).

Resonance Energy Transfer

Due to the spectral properties of the intrinsic fluorophores, resonance energy transfer can take place between them. The spectral overlap of the absorption and emission spectra of Phe, Tyr and Trp can induce usually an energy transfer from Phe to Tyr and subsequently to Trp. This type of energy transfer has been frequently noticed in various proteins, specially the Tyr-Trp transfer, and is also accounted as a reason to the reduced contribution of Phe and Tyr in the emission of most proteins. Blue-shifted Trp residues can also transfer excitation energy to longer wavelength Trp. (Lakowicz, 2006)

Quenching of the Protein Fluorescence

Protein intrinsic chromophores are, in similarity to the other fluorophore particularly sensitive to external solvent quenching. In addition once again Trp is the most affected residue.

Besides being extremely affected with solvent polarity, Trp fluorescence is also uniquely sensitive to collisional quenching, owed seemingly to the tendency of the excited-state indole to donate electrons. Tryptophan can be quenched by externally added groups (present in the solvent) or by nearby groups in the protein. This results in highly variable quantum yields of tryptophan fluorescence. A broad number of quenching factors has been reported for Trp fluorescence:

- quenching by proton transfer to neighbor amino groups - histidine and lysine residues can be agents of such quenching;
- quenching by electron acceptors, for instance protonated carboxyl groups;
- electron transfer quenching by SSs and amides such as the ones present in the peptide backbone;
- electron transfer quenching by peptide bonds in the peptide backbone.

Similarly to RET these interactions are strongly dependent on distance, especially the rate of electron transfer, decreasing exponentially with distance. The extent of electron transfer may depend as well on the location of close charged groups, which act in stabilizing or destabilizing the charge transfer state. The quenching effect of electron transfer conjugated with RET can sometimes result that Trp residues display almost no fluorescence (Lakowicz, 2006).

Remarks

From the statements previously realized it can concluded that protein fluorescence is indeed a powerful tool, since one can extract pretty important conclusions regarding local features of the protein, where the intrinsic fluorophores are localized. For instance, while the fluorescence spectra obtained by excitation at 280 nm provide a general perspective on the protein conformation, where the generality of the residues stand, if they are quenched or not; at 295 nm we excite uniquely the Trp, and the information retrieved is far more specific of the protein areas where these are localized.

Spectral interpretation can reversely be far trickier to process. In the presence of multiple aromatic residues in the protein, particularly Trp, spectra overlap is undesirable side-effect, which occurs at most usable wavelengths. These residues are not located in the same environments in the protein, and to evaluate which residue contributes more on the fluorescence is hard to trace.

3.3. ULTRAVIOLET LIGHT INDUCED REACTION MECHANISMS IN PROTEINS

It is known that the exposure of proteins to light can induce dramatic changes in protein structure, leading eventually to its degradation, physical or chemical. Photoxidation of the protein UV sensitive species is regarded as one of the major contributors for the protein partial destruction (Kerwin and Remmele, 2006).

In proteins, the major targets of UV radiation are evidently the intrinsic fluorophores Trp, Tyr, Phe, and two important structural elements: the peptide backbone and cystines (cysteines linked by SS bridge). In aqueous solution the absorption wavelengths are 260–290 nm for Tyr, 240–270 nm for Phe, 180–230 nm for the peptide backbone, and 250–300 nm for cystines (Kerwin and Remmele, 2006). As previously described, Trp can absorb in solution through its the two dipole moments. Trp absorption maxima are centered at 220nm (ε~36000 $M^{-1}cm^{-1}$), 280nm (ε~5500 $M^{-1}cm^{-1}$) and 288nm (ε~4500 $M^{-1}cm^{-1}$) with a shoulder at 265nm (ε~4500 $M^{-1}cm^{-1}$) (Neves-Petersen *et al*., Paper Submitted).

The specific mechanisms triggered in these targets encompass the broad picture described schematically in Figure 2.2. Aside the processes in which the excited entity is relaxed to the ground state, like fluorescence, thermal relaxation or transfer of energy, the other pathways usually involve the degradation of this specie, thus termed generally photolysis or photodegradative mechanisms (Kerwin and Remmele, 2006).

In this section it is pretended to review these events in the protein intricate context, a complex net of interactions, where diverse deciding factors are in play, like the pH of the solution, temperature, polarity, nearby side-chains, etc. Since the experimental work was primarily focused in the photo-induced mechanisms in Trp, this will be the major issue in analysis. However, some notions regarding the pathways of excited states of Tyr and cystine will be introduced, pertinent to further speculations and understanding. In attention will also be the influence of the external conditions on these pathways. Evidently the particular mechanisms of SS bond disruption by UV light will be taken in strong consideration.

3.3.1. Main Photochemical and Photophysical Reaction Mechanisms

Among the natural occurring amino acids Trp displays the highest absorption in the near-UV, and is for that reason a major player in the photochemical and photophysical processes in proteins. The fate of Trp excited species (lifetime of about 3 ns) has been widely studied and reviewed in literature. Flash photolysis studies have allowed the identification of two major

pathways of non-radiative relaxation for the excited specie of tryptophan (Trp* lifetime of about 3 ns, Sherin *et al.*, 2004):

(a) ejection of an electron to the solvent, generating a solvated electron e_{aq}^- (wide absorption peak centered at ~720 nm), and a tryptophan radical cation $Trp^{\bullet+}$ (absorbs at ~560 nm) (3.2). $Trp^{\bullet+}$ rapidly deprotonates forming a indolyl neutral radical $Trp^{\bullet}$ (absorbs at ~510 nm) (3.3) (Neves-Petersen *et al.*, Paper Submitted).

$$Trp + h\nu \rightarrow Trp^{\bullet+} + e_{aq}^- \quad (3.2)$$

$$Trp^{\bullet+} \rightarrow Trp^{\bullet} + H^+ \quad (3.3)$$

The formed $Trp^{\bullet}$ can then further react with neighbor amino acids. It may, for instance, extract a hydrogen atom from a neighbor Tyr or cysteine (RSH), and self-repair, yielding reactive radical species such as cysteine neutral radical $RS^{\bullet}$ and tyrosine radical cation $Tyr^{\bullet+}$. Alternatively $Trp^{\bullet}$ might attack the peptide bond leading ultimately to its cleavage. In the presence of oxygen, it can form a peroxy radical, which can suffer further reaction producing two analogs of Trp: N-formylkyneurine and kyneurine (absorption at 300-400 nm - Snytnikova *et al.*, 2007). These two species absorb light at longer wavelengths than Trp, and upon absorption in aerobic conditions induce further damage to the protein (Kerwin and Remmele, 2006).

(b) intersystem crossing from the excited singlet state Trp to the triplet state ^3Trp (3.4 and 3.5), which absorbs at ~450 nm (lifetime of approximately 10μs). ^3Trp may afterwards transfer an electron to a nearby SS bridge yielding $Trp^{\bullet+}$ and $RSSR^{\bullet-}$ (absorbs at ~420 nm) (3.6). Under aerobic conditions the ^3Trp might also react with molecular oxygen to give once more $Trp^{\bullet+}$ and a strong reactive oxygen radical $O_2^{\bullet-}$ (3.7), which advents further damage to the protein (Neves-Petersen *et al.*, Paper Submitted; Kerwin and Remmele, 2006).

$$^1Trp + h\nu \rightarrow {}^1Trp^* \quad (3.4)$$

$$^1Trp^* \rightarrow {}^3Trp \quad (3.5)$$

$$^3Trp + RSSR \rightarrow Trp^{\bullet+} + RSSR^{\bullet-} \quad (3.6)$$

$$^3Trp + O_2 \rightarrow Trp^{\bullet+} + O_2^{\bullet-} \quad (3.7)$$

The solvated electrons e_{aq}^- yielded from the excited state ionization of Trp can latter trigger further reactive mechanisms in the protein. They may recombine with Trp, generating radical anions (3.8), or be captured by electrophylic species such as cystines (3.9), molecular oxygen (3.10), or by H_3O^+ at acidic pH (3.11).

$$e_{aq}^- + Trp \rightarrow Trp^{\bullet-} \quad (3.8)$$

$$e_{aq}^{-} + RSSR \rightarrow RSSR^{\bullet -} \quad (3.9)$$

$$e_{aq}^{-} + O_2 \rightarrow O_2^{\bullet -} \quad (3.10)$$

$$e_{aq}^{-} + H_3 0^{+} \rightarrow H^{\bullet} + H_2O \quad (3.11)$$

Cystine radicals $RSSR^{\bullet -}$ formed upon electron transfer (3.6 and 3.9) might further cleave, inducing the breakage of the SS, forming thyil radicals and thyols (3.12 and 3.13).

$$RSSR^{\bullet -} \rightarrow RS^{\bullet} + RS^{-} \quad (3.12)$$

$$RSSR^{\bullet -} + H^{+} \rightarrow RS^{\bullet} + RSH \quad (3.13)$$

The hydrogen radical resulting of electron capture at acidic pH can react with a SS bridge in the vicinity and also lead to its disruption (3.14).

$$H^{\bullet} + RSSR \rightarrow RS^{\bullet} + RSH \quad (3.14)$$

Additionally, the solvated electron e_{aq}^{-} may react with the peptide chain, to generate a hydroxide ion and a ketyl radical (3.15).

$$e_{aq}^{-} + \text{-CONH-} \rightarrow OH^{-} + \text{-}\dot{C}(OH)NH\text{-} \quad (3.15)$$

The latter can propagate along the side chain, and upon the encounter with a SS bridge react, generate once more a $RSSR^{\bullet -}$ radical, whose repercussions were already explicated, with the subsequent reductive splitting of the SS bridge (Neves-Petersen *et al*., Paper Submitted).

Evidently, cystines are also prompt to photodegradation by direct absorption of UV-light, and in the same range of wavelengths than Trp residues, primarily below 300 nm. At this event rupture can occur either in the R-S bond or in the S-S bond (3.16).

$$RSSR + h\nu \rightarrow 2RS^{\bullet} \; or \; R^{\bullet} + RSS^{\bullet} \quad (3.16)$$

The photolytical radical products $R^{\bullet}$ and $RSS^{\bullet}$ can experience further reactions with other amino acids, with molecular oxygen and possibly with water, which may respectively result in crosslinking, a variety of acids, and disproportionation to cysteine sulfonic and sulfinic acids. However, the share of this direct photodegradation is reduced, principally in proteins containing Trp and Tyr, since the molar extinction coefficient (ε) of cystine is reasonably lower than the ones of these two fluorophores (in water: ε_{280}cystine = 125 $M.cm^{-1}$; ε_{280}Trp = 5500 $M.cm^{-1}$;ε_{280}Tyr = 1490 $M.cm^{-1}$ (Walker, 2005). Moreover, the absorption wavelength is dependent on the R-S-dihedral bond angle and can red-shift to longer wavelengths that 300nm, which do were not used for excitation in this work (Kerwin and Remmele, 2006).

The photolytical yielded free thiyl radicals $RS^{\bullet}$ and thiol groups RSH can further react with other free thiol groups, is it within the protein reforming or forming a intra-disulphide bond, or externally forming SS bridges with other molecules (*e.g.* with another irradiated protein molecule resulting in aggregation). Alternatively the free thiyl radical can react with other amino acids or oxygen. Finally the thiyl radicals may even cross-link with a SS bond in a protein resulting in an unpaired electron shared between the two SS bridges followed by rupture resulting in a mixture of species: ones keeping the original bond and other with a mixed SS formed with the thiyl radical (Neves-Petersen *et al*., Paper Submitted; Kerwin and Remmele, 2006).

3.3.2. Influence of external factors on the reaction mechanisms

In the previous section were introduced a multitude of pathways that can be triggered upon UV irradiation of proteins, and the photo-induced mechanisms in Tyr and Phe were not even discussed. The succession of the mechanisms enabled by the excitation of Trp is not a determined fact. However it is strongly influenced by external conditions and by the reaction microenvironment.

First of all, external factors like pH, temperature or solvent particularities can affect the initial fate of the excited specie, is it the return to the ground state by relaxation coupled with fluorescence, ejection of an electron and ionization, or intersystem crossing.

At acidic pH values, the excited S1 state of Trp can be highly quenched due to the protonation of the NH group of the indole ring (pKa ≥ 2.2). The protonation may be followed by fast intersystem crossing into protonated triplet state $^{T}TrpH^{+}$ (pKa = 3.2, lifetime of 26 ns), suppressing significantly the return to ground state by fluorescence, and the two major non-radiative pathwaysof Trp here referred (Sherin *et al*., 2006). For pH values between 3 and 10, there is no direct influence of pH on the fate of excited Trp in solution. High pH values are generally favorable for e^{-}_{aq} formation (Kerwin and Remmele, 2006).

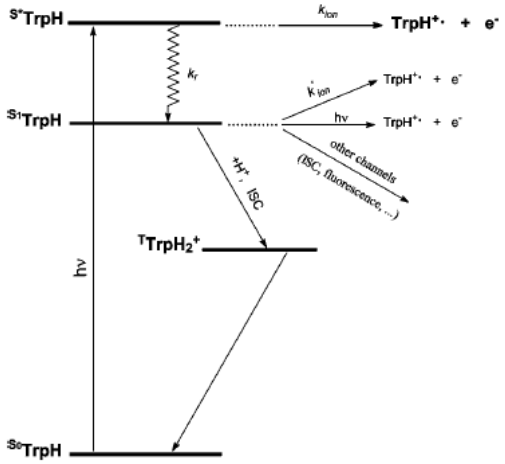

Figure 3.8: Channels of Trp photoionization.

Temperature has also a major effect on the pathway taken by the excited Trp specie. An increase of temperature from 4 to 37ºC or greater can raise e^-_{aq} formation from singlet excited Trp in solution in a fivefold fashion or more, with the parallel decrease in triplet state formation (Kerwin and Remmele, 2006).

In neutral solutions two decay pathways of Trp are dependent on temperature: the ionization of Trp excited species and intramolecular proton transfer from the protonated NH_3^+ group to the C-4 position of the indole ring, both processes being favored with the temperature increase. The second is not generally possible in proteins, since the NH_3^+ group is involved in the peptide bond and Trp residues are not generally found in N-terminals. Therefore this increase in e^-_{aq} formation with temperature can only be due from an increase in the ratio of ionized species and not the decrease in the yield of the other relaxation pathways. Fluorescence, intersystem crossing, or even internal conversions are not directly dependent on temperature (Sherin *et al.*, 2004). Photoionization of Trp can occur from diverse channels (Figure 3.8). Photoexcited Trp can absorb the second quantum of light and suffer biphotonic ionization. As already mentioned, it can undergo protonation of the indole ring, followed by intersystem crossing to the triplet state. Another precursor for the TrpH ionization is an extremely shorted-lived non-relaxed prefluorescent excited state, which apparently competes with the relaxation thermal equilibrium. Finally, singlet excited state of tryptophan may undergo thermal ionization from the S_1 relaxed state, the only process known to be temperature-dependent (Sherin et al., 2006).

The solvent used may affect also the fate of the excited specie: a raise in ionic strength or solvent polarity can stabilize the solvation of the electron, resulting in higher solution lifetimes and the probabilities of its formation (Kerwin and Remmele, 2006).

In the protein intricate environment the influence of external conditions can be felt differently since the Trp residues can be buried within the macromolecule. Thus, solvent polarity and ionic force will not affect in the same magnitude the excited state of Trp.

In a protein, another major factor that will influence the fate of the excited specie is the presence of other groups in the vicinity of the Trp residues. As previously discussed in the Protein Fluorescence section (3.2.2), Trp fluorescence is highly quenched by close groups that can accept electrons from the Trp (protonated carboxyl groups, disulphides, amides, peptide bonds) or receive protons (histidine and lysine residues). Hence, the close presence of these groups may drive the Trp excited specie in a particular pathway and favor determined mechanisms such as ionization. The mechanism of SS bond breakage can be particularly dependent on the distance between the bond and the tryptophan residue, as will be described in the next section.

On other hand external solvent conditions can also affect indirectly the photophysics and photochemistry of Trp within a protein since factors like pH, temperature, ligands or salts can

affect the conformation of the polypeptide. In experiments with the same protein, differences can be noticed from case to case if the conditions are shifted, since upon these structural changes, the relative position of the Trp residues and other groups is changed. Indeed, in tests realized in bovine serum albumin it was noticed that changes in structure induced by pH altered the final sites at which the reactive radicals resided. Analogous differences were detected between the folded and unfolded states of mellitin and beta-lactalbumin (Kerwin and Remmele, 2006).

3.3.3. Consequences of Protein Photo-degradation, SS Bond Breakage and Light Induced Immobilization

Since a wide number of mechanisms can be activated in proteins upon UV radiation, originating extremely reactive species like peroxy radicals or singlet oxygens it is natural that the structural modifications within the protein will quite serious, including the modification of amino acids, breakage of the peptide chain, and other effects reported in section 3.3.2. These modifications may lead to the structural disarrangements of binding sites and enzyme inactivation (Neves-Petersen *et al.*, 2007).

Protein photo-degradation and inactivation of enzymes or functional proteins is classically attributed to the photo-oxidation of cystines (Neves-Petersen *et al.*, 2002). SS bonds sustain the tertiary structure of the protein, and their disruption may affect terribly certain conformational features. Cystine photo-degradation is shown to be highly dependent on its microenvironment (Neves-Petersen *et al*., 2002). Additionally, in proteins cystine residues have a natural preference for aromatic residues as spatial neighbors (Petersen *et al*., 1999). The two precedent observations correlate well with the photo-induced reactions here presented. Upon excitation of Trp residues, several of the activated mechanisms may lead to breakage of intra-molecular SS bonds.

Moreover, the distance between Trp residues and the SS bonds can be an extremely important factor for the event. Studies in lysozyme and a model system allowed to verify that previously described interaction between ^{3}Trp and cystine (expression 3.5) is based on direct electron transfer between the two species. It consists on a very short range interaction that decays exponentially with the increase of distance beyond Van der Vaals overlap between the donor and acceptor (Neves-Petersen *et al.*, Paper Submitted).

Cutinase, from *Fusarium solani pisi*, has been one of the most extensive studied models since it displays only one Trp that is in direct contact with a SS bridge (closest distance ~3.8 Å). In this enzyme, the disruption of SS bond mediated by Trp excitation has been proven to be a statistical phenomenon (Neves-Petersen *et al.*, 2002). In this simple model, formation of the solvated electron from excited Trp has been noticed in the flash photolysis studies, and this yielded product follows several fates here described, including recombination with H_30^+ and SS

bonds, or with other electron scavengers. Formation of $RSSR^{\bullet -}$, which advents the splitting of SS bridge, is resultant of both solvated electron recombination and reaction with the ^{3}Trp (Neves-Petersen *et al.*, Paper Submitted). Therefore, even in this simple model, diverse pathways may be involved. For cutinase, it was also noticed that the longer the UV excitation of the aromatic residues, the larger is the proportion of broken SS bonds and free thiols, originated from splitting of $RSSR^{\bullet}$. The concentration of solvated electrons increases also over the time in the flash photolysis studies (Neves-Petersen *et al.*, 2002; Neves-Petersen *et al.*, Paper Submitted).

Though the breakage of SS bonds can induce conformational changes on the protein, the full inactivation of its properties or loss of catalytical activity in enzymes is not an acquired fact.

Besides reacting with other protein free thiols, the photo-yielded solvent accessible free thiol groups can react with gold (Au) or thiol-rich surface to form covalent bonds (Neves-Petersen *et al.*, 2006; Duroux *et al.*, 2007; Snabe *et al.*, 2006). This is the principle behind the light induced immobilization technique that was described in section 2.2. The technique makes use of the natural existence of closely spaced triads of residues aromatic/cystines that was referred previously. This constellation is ubiquitous in many protein families such as hydrolases, oxidoreductases, transferases, lyases, Major Histocompability Complex (MHC) class proteins, and membrane receptor proteins, and is present in all members of the immunoglobulin superfamily (Neves Petersen *et al.*, 2006), which make them potential and interesting targets for light-mediated immobilization.

This immobilization approach overcomes several inconvenients of classic protein immobilization techniques. The most common techniques for protein immobilization usually require one or more termochemical/chemical steps, which may have deleterious effects on the structure and function of the protein bound. The available methods rely on noncovalent adsorption or on covalent attachment to chemically modified surfaces with aldehydes, activated esters or epoxide cross-linkers. These attachment procedures lead to the random orientation of immobilized protein molecules, and poor control in the density of immobilized molecules. The methods can be also invasive, when foreign groups are introduced into the protein, which can provoke denaturation, or lower the biological activity and substrate specificity (Duroux *et al.*, 2007).

Light-induced immobilization avoids the non-specific exposure of the protein, prior or during the binding procedure, to structurally modifying chemical agents. Furthermore, the size of the area of immobilization is limited to the area of illumination. Finally, the immobilized molecules are oriented through precise and known covalent bonding onto the surface.

In the Nanobiotechnology Group of the University of Aalborg, an immobilization experimental setup is installed in a clean room for light-induced molecular immobilization (LIMI). The setup includes a laser source, whose beam can be focused onto the surface of flat quartz

slides. The slides may be thiol-derivatized, allowing the bond to the thiol groups of the protein upon illumination. The immobilization procedure implies the deposition of one microdroplet of protein solution onto the slide, and posterior exposure to the laser-beam of UV-light (Duroux *et al.*, 2007).

Using this technique several proteins belonging to the above mentioned groups were immobilized, including cutinase, lysozyme, alkaline phosphatase, immunoglobins of antigen binding, the MHC class protein I (Neves-Petersen *et al.*, 2006; Duroux *et al.*, 2007; Snabe *et al.*, 2006), bovine serum albumin and prosthetic serum albumin (Parracino, A., Personal Communication). All these proteins have a great biomedical interest since they can act as sensors for a wide number of applications. For instance, immunoglobulins have a great relevance in disease diagnostics, in microarray probing of specific diseases, or in the identification of particular biomarkers by biomolecular interaction.

With the laser setup previously, the beam can be focused to precise locations with sub-micrometer dimensions, enabling the creation of dense microarrays, immobilization of biomolecules according to specific patterns (recurring to specific masks) (Neves-Petersen *et al.*, 2006; Duroux *et al.*, 2007; Skovsen *et al*., 2008; Neves-Petersen *et al*., 2008).

An important aspect regarding the immobilization procedures that were realized is that the native and functional properties of the proteins were maintained (Duroux *et al.*, 2007; Neves-Petersen *et al.*, 2006).

The spot size of the created arrays or patterns is reduced and covers only the illuminated surface of the microdroplet, with a high density of immobilized biomolecules. Protein activity is preserved as a dense monolayer (Duroux *et al.*, 2007).

The immobilization technology is ideal to couple, proteins and peptides. It is not limited to slide immobilization. The coupling can also be realized to nanoparticles, such as gold nanospheres, that may subsequently be used as molecular carriers into cells (drug-delivering) for therapeutic applications (Parracino *et al.*, 2008).

4. THE PROTEIN MODEL: α-LACTALBUMIN

4.1. CONTEXT AND FUNCTIONS OF THE PROTEIN

Milk has been regarded for ages as an important nutritional product, derived from the experience-based acquired knowledge. However, only in the last decades has been characterized the paper of its constituents as functional foods. Whey, a by-product of cheese manufacturing, the fluid remaining after straining and curdling of milk, was once regarded as a chemical waste difficult to treat. The high costs associated to its disposal and the evolution of the analysis techniques allowed the identification of whey as a valuable co-product (Brown and Ernstrom, 1982). Indeed, whey contains a considerable fraction (20%) of the proteins from the milk; the remaining fraction, constituted mostly by caseins, is separated upon curdling. Whey proteins are globular proteins unique for its nutritional value and functional properties. Properties like emulsification or gelation raise the interest in whey proteins isolates and concentrates, making them desirable assets for a broad range of foods, (Gao *et al.*, 2008; Pedersen *et al.*, 2006).

The second major component of the whey protein agglomerate is α-lactalbumin (LA), representing about 20-25% of its composition, (Pedersen *et al*., 2006; Hong *et al*., 2002)

LA is a small (MW~14.2 kDa), acidic (isoelectric point: *IP*~4-5) calcium (Ca^{2+}) binding protein, present in the milk whey of diverse mammalians. Expressed exclusively during lactation, LA plays an important role in the biosynthesis of lactose. It resides as one of the two components of the lactose synthase complex, responsible for the catalysis of the lactose biosynthesis final step in the lactating mammary gland, as shown in expression (4.1). The other component of this enzymatic complex is β1,4-galactosyltransferase (GT), which is involved in the processing of proteins in various secretory cells by transferring galactosyl groups from Uridine 5'-(trihydrogen diphosphate)-Galactose (UDP-GAL) to glycoproteins containing N-acetylglucosamine. LA modulates the activity of GT through a reversible protein-protein interaction, increasing its affinity and specificity for glucose, and thereby changing its sugar acceptor specificity from N-acetylglucosamine (GlcNAc) to glucose, enabling the synthesis of lactose, the major carbohydrate component of the milk. The reaction occurs in the Golgi lumen of the cell, in the required presence Mn^{2+} ions. (Chysina *et al.*, 2000; Permyakov and Berliner 2000; Ramakrishnan and Qasba, 2001).

$$\text{UDP-GAL} + \text{glucose} \xrightarrow{\text{GT}/\alpha\text{-LA}} \text{lactose} + \text{UDP} \qquad (4.1)$$

Besides the natural role of LA, this protein has important characteristics that reinforce its interest as a model of study. LA contains a strong binding site for Ca^{2+} ions, which activity affects

considerably the conformation and activity in solution. Therefore, it is often chosen as a simple model for the calcium binding phenomenon in proteins, for instance in the calcium binding effects in the interaction of protein with other proteins, peptides, membranes, and low molecular weight. Moreover, this binding site responds also to other ions like Mg^{2+}, Mn^{2+} and Na^{+}, besides the existence of other Zn^{2+} binding sites, each case resulting in different conformations of the protein. The modulation of the protein structure by ions is an interesting enigma for molecular biology, particularly the functions that these conformations may have. This protein has been also studied extensively in recent years as a model for protein folding studies, particularly due to native-like conformational states that it adopts under certain conditions, called molten-globules (MGs), which are similar to protein folding intermediates.

This protein displays a close evolutionary relationship with c-type lysozyme. They share only 40% homology in amino acid sequence, but show comparable gene organization and similar three-dimensional fold (*vide supra*, section 3.2). Although structurally similar, in terms of functionality they reveal large differences. C-type lysozyme is an enzyme which binds and cleaves the glycosidic bond linkage in sugars, for instance it degrades the peptidoglycan of bacterial cell walls. Such lytic capacity is much reduced in LA, displaying in its native form only 10^{-6} of the specific activity of egg-white lysozyme. It is believed that specific amino acid substitutions in LA are responsible for the loss of the enzyme activity of lysozyme and acquisition of features required for its role in the lactose synthesis. (Chysina *et al.*, 2000; Mizuguchi *et al.*, 2000; Qasba and Kumar, 1997; Permyakov and Berliner 2000).

On other hand, some variants of LA have shown antimicrobial activity, others induction of apoptosis in tumor cells (Permyakov and Berliner 2000).

This work, aims at studying UV-light induced structural effects on LA and the temperature and pH stability of the protein. The protein used was the calcium depleted form. Hence, this chapter will focus on two major issues:

- description of the three-dimensional structure of the protein, and subsequent features important for the assessment of light-induced reactions in the protein (*e.g.* position of the fluorescent residues and the disulphide bridges);
- stability of the protein under the depletion of calcium, thermal and pH shifts.

4.2. PRIMARY, SECONDARY & TERTIARY STRUCTURE

4.2.1. Main Features

The majority of α-lactalbumins (LAs) found in mammalian's milk, including human, guinea pig, bovine, baboon, goat, and buffalo versions, are 123 amino acid residues long and share

homologous three-dimensional structures (*vide* Table 3.1). Only Rat LA distinguishes itself by containing 17 additional C-terminal residues (Permyakov and Berliner, 2000).

Table 4.1: Comparison of different LA structures. The values displayed are the root mean square deviations (in Å) obtained after superposition using the least square fitting function applied to C_α atoms of residues 1-120 (values in bold font) and to the core of the molecule (values in normal font). LA core comprises the residues 5-11, 23-40, 50-61, and 71-104. Apo-bLAc: Ca^{2+} depleted form of bovine LA at 2.2 Å (PDB code: 1F6R). Holo-bLAc: Ca^{2+} bound form of Bovine LA at 2.2 Å (PDB code: 1F6S). mLA: recombinant bovine LA at 2.3 Å (PDB code: 1HFZ). Baboon LA at 1.7 Å (PDB code; 1ALC). Guinea pig LA at 1.9 Å (PDB code, 1HFX). Goat LA at 2.3 Å (PDB code, 1HFY). Buffalo LA at 2.3 Å (Calderone *et al*., 1996). Human LA at 1.7 Å (Acharya *et al*., 1991). The values were calculated using the program O (Extracted from Chrysina *et al*.., 2000).

The deviations displayed, presenting generally values bellow 1 Å, demonstrate a high rate of structural alignment between the different versions of the protein.

	Apo-bLAc	Holo-bLAc	mLA (Bovine)	Baboon	Guinea pig	Goat	Buffalo	Human
Apo-bLAc		**0.68**	**0.8**	**0.93**	**1.01**	**0.75**	**0.8**	**0.99**
Holo-bLAc	0.39		**0.51**	**0.89**	**0.82**	**0.61**	**0.6**	**0.87**
mLA (Bovine)	0.41	0.28		**0.94**	**0.84**	**0.77**	**0.7**	**0.92**
Baboon	0.65	0.65	0.65		**1.06**	**1.06**	**1.04**	**0.41**
Guinea pig	0.57	0.44	0.44	0.66		**1.11**	**1.08**	**1.01**
Goat	0.6	0.45	0.54	0.8	0.7		**0.52**	**1.05**
Buffalo	0.53	0.95	0.48	0.76	0.63	0.27		**1.01**
Human	0.66	1	0.65	0.27	0.63	0.81	0.78	

The high homology between the first mentioned sources results in a comprehensive interchange of experimental results and subsequent interpretations realized with the different variants of the protein. For that reason, in this introductory text, when a result or interpretation will be mentioned, the specie in question will only be invocated when pertinent.

Number of amino acids: 123

Molecular weight: 14186.0

Theoretical pI: 4.80

Amino acid composition:

Ala (A)	3	2.4%
Arg (R)	1	0.8%
Asn (N)	8	6.5%
Asp (D)	13	10.6%
Cys (C)	8	6.5%
Gln (Q)	6	4.9%
Glu (E)	7	5.7%
Gly (G)	6	4.9%
His (H)	3	2.4%
Ile (I)	8	6.5%
Leu (L)	13	10.6%
Lys (K)	12	9.8%
Met (M)	1	0.8%
Phe (F)	4	3.3%
Pro (P)	2	1.6%
Ser (S)	7	5.7%
Thr (T)	7	5.7%
Trp (W)	4	3.3%
Tyr (Y)	4	3.3%
Val (V)	6	4.9%
Pyl (O)	0	0.0%
Sec (U)	0	0.0%
(B)	0	0.0%
(Z)	0	0.0%
(X)	0	0.0%

Figure 4.1: Amino-acid composition of bLA. Data obtained using the tool ProtParam on the Expasy Server (**www.espasy.org**) by submitting the fasta sequence of the PDB Entry 1F6S.

In Figure 4.1 is listed the amino-acid composition of Bovine LA (bLA), the selected model protein in this studies. The protein is rich in aromatic and cysteine (Cys, C) residues, displaying 4 tryptophans, 4 tyrosines, 4 phenylanalynes, and 8 cysteines. These residues are quite rare, existing generally in low numbers in the constitution of proteins. According to Creighton (1992), the random frequency of these residues in the amino acid composition of proteins is 1.3% for Trp, 3.2 % for Tyr, 3.9% for Phe, and 1.7% for Cys. In bLA the molar percentage of Trp and Cys is 3.3 % and 6.5%, values reasonably higher than the average, making it an unusual target of UV-triggered mechanisms.

It is important to notice that LA contains a variable number of Trp from species to species, presenting for instance 3 Trp in the human LA and 4 in the bovine and goat variant. Since the model studied is bLA, any further considerations regarding the position of Trp in LA will attend to the structure with 4 Trp at positions 26, 60, 103, and 118. Throughout this work the three-dimensional structures of bLA used for analysis correspond to the crystallized forms at 2.2Å resolution and high ionic strength by Chrysina *et al.* (2000). The two crystallized folds are: LA with Ca^{2+} bounded (holo-bLAc, PDB entry: 1F6S) and LA depleted of Ca^{2+} (apo-bLAc, PDB entry: 1F6R). The first corresponds to the native bLA, which exists in the presence of Ca^{2+} ions. The second is a Ca^{2+} depleted form, which is used for mere qualitative analysis in this section and in section 4.2.2, given that LA in the absence of Ca^{2+} displays variable configurations dependent on the solvent conditions (discussed in detail in section 4.3.4).

Tertiary Structure of Native LAs

Typically, the native tertiary structure of LAs (Ca^{2+} bound form) fold shows two sub-domains separated by a cleft: a large α-helical subdomain and a small β-sheet subdomain (further mentioned as α-subdomain and β- subdomain respectively), connected by a calcium binding loop (Figure 4.2). The α- subdomain is formed by three main α-helices (H1, H2 and H3; residues 5-11, 23-24 and 86-98 respectively) and two short 3_{10} helices[b] (h1b and h3c; residues 18-20 and 115-118 correspondingly). The β-subdomain is constituted by a serie of nonstructured loops, a small three-stranded antiparallel β-pleated sheet (S1, S2 and S3; residues 41-44, 47-50, and 55-56 respectively) and a short 3_{10} helix (h2, residues 77-80).

The high affinity Ca^{2+} binding site is located at the junction of the subdomains and is composed of a contiguous chain (residues 79-88) linking the 3_{10} helix of the β-subdomain and the helix H3 of the α-subdomain (residues 86-98). This region is considered the most rigid part of LA structure. The site includes Ca^{2+} linking highly conserved aspartates and one lysine. The ligands responsible for Ca^{2+} binding are the two carbonyl groups corresponding to Lys79 and Asp84, and three carboxyl groups corresponding to Asp82, Asp87, and Asp88. A secondary calcium binding

[b] 3_{10} helix: structure characterized by 3 residues per turn and 10-member hydrogen-bounded loops.

site was also identified 7.9 Á away from the main one (Pike *et al.*, 1996; Chrysina *et al.*, 2000; Permyakov and Berliner, 2000; Kim and Baum, 1999).

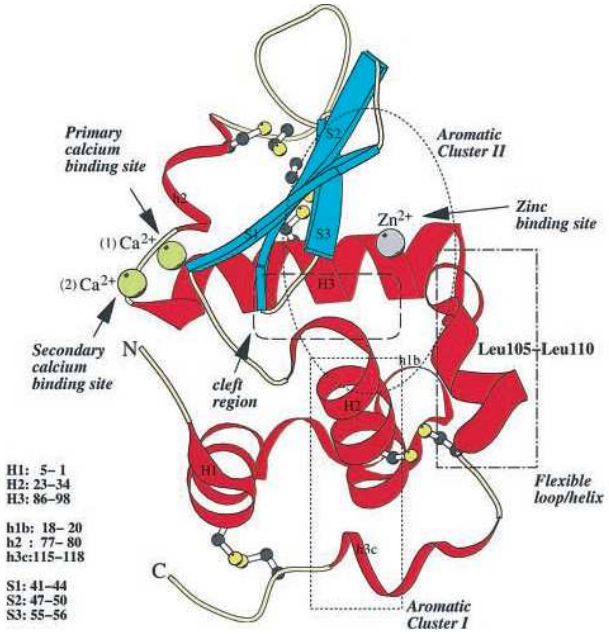

Figure 4.2: Three-dimensional structure of LA and the functional regions of the molecule showing the location of metal ions identified in LA crystal structures. Secondary structural elements are marked (*S,* b-strand in blue; *H* , α-helix and *h,* 3_{10} helix in red). The 8 cysteine residues are also represented, between the close pairs of cysteine are formed the 4 disulphide bridges of the protein (Adapted from Chrysina *et al.*, 2000).

Overall, the tertiary structure of LA is stabilized by four disulphide (SS) bridges. The SS bridge Cys73-Cys91 holds together the two subdomains, forming the Ca^{2+} binding loop. Located in the small β-sheet subdomain, another important SS bridge, Cys61-Cys77, links nonstructured loops, connecting both subdomains as well. The other two bridges, Cys6-Cys120 and Cys28-Cys111, are situated in the α-helical subdomain (Vanhooren *et al*., 2006**a**; Permyakov and Berliner, 2000), the first one being reduced with extreme rapidity (Ikegushi *et al*. 1998), and the second one plays an important stabilizing role (Wu and Kim, 1998; Horng *et al.*, 2003; Ikegushi *et al.*, 1998).

Besides the Ca^{2+} binding site, LA contains three other important structural regions: two aromatic clusters and one flexible helix/loop region.

The two aromatic clusters are integrated on two separate hydrophobic cores of the protein. They are both localized in the α-subdomain and comprise the majority of the protein fluorophores as can be observed in the structure of holo-bLAc enhanced in yellow in Figure 4.3. Together with the Ca^{2+} binding site they form the most rigid part of the structure.

.Aromatic cluster I is constituted by residues involved in interactions between one helix 3_{10} and one α helix of the α-subdomain, in a zone further from the binding site, comprising one

Phe (F31) and one Trp (W118). The aromatic cluster II, part of the second hydrophobic core (also named hydrophobic box), is formed by packed interactions between residues of the α-helices H2 and H3 and is situated in the vicinity of the cleft region located at the opposite side of the Ca^{2+} binding site (enhanced in Figure 4.2). It comprises the remaining Trp residues (W26, W60, and W104), one Tyr (Y103) and one Phe (F53) (Chrysina *et al.*, 2000; Wu *et al.*, 1998, Pike *et al*., 1996).

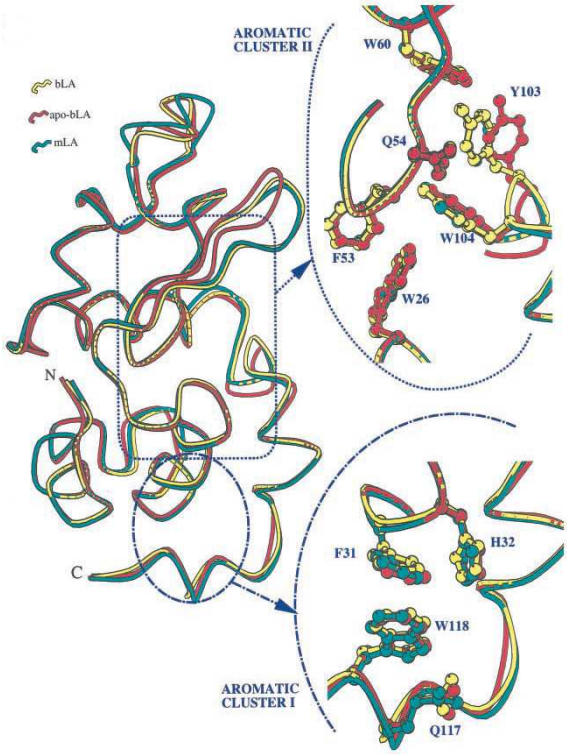

Figure 4.3: Localization of the Aromatic Clusters I and II in the structure of bLA. apo-bLAc structure (PDB entry: 1F6R) is shown in *red*, holo-bLAc structure (PDB entry: 1F6S) is shown in *yellow,* and recombinant bLA (mLA) structure in *green*. The superposition of the structures was performed with program O (35) (Adapted from Chrysina *et al.*, 2000).

The crystallized structures are very similar, only showing some small deviations. The insets show the details of packing interactions in aromatic clusters I and II (the hydrophobic box). Aromatic cluster I comprises one phenylalanine (F31) and one histidine (H32) localized in the end of helix H2, and one glutamine (Q117) and one tryptophan (W118) located in the terminal tail of LA. Aromatic cluster II contains residues from the H1, H2 and one of the 3_{10} helices, including three tryptophans (W26, W60 and W104), one tyrosine (Y103), one phenylalanine (F53), and one glutamine (Q54).

The flexible helix/loop region is constituted by the residues 105-110 (Leucine 105, Alanine 106, Histidine 107, Lysine 108, Alanine 109 and Leucine 110 - Enhanced in Figure 4.2), and is adjacent to the lower end of the cleft interacting with the C-terminal end of helix H2. It is a particularly interesting region since it flanks the aromatic cluster I and adopts different conformations, loop or distorted helix, depending of the molecular environment, particularly upon the pH of the crystallization medium. It seems that at higher pH values(6.5– 8.0) this loop adopts the helical conformation and at low pH (4.6), the “loop” conformation (Pike *et al*., 1996;

Ramakrishnan and Qasba, 2001) For both crystallized structures of bLA (apo-bLAc and holo-bLAc) this flexible region adopts a distorted helical conformation.

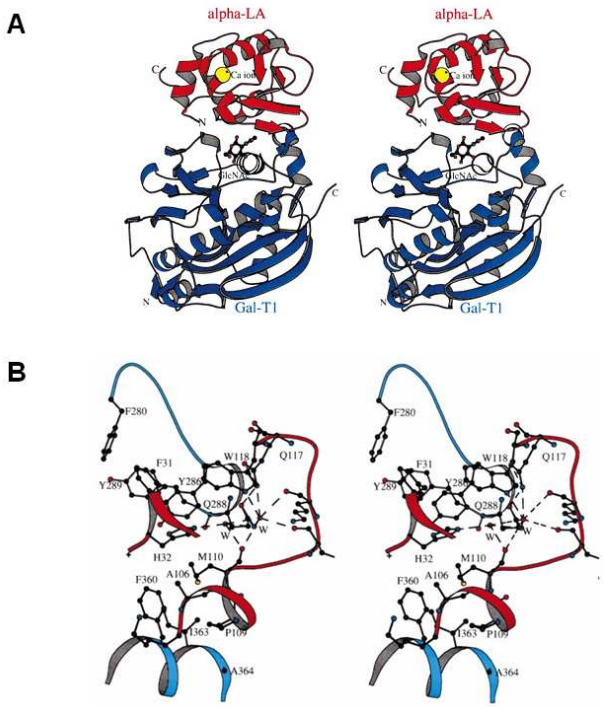

Figure 4.4: A – Molecular structure of lactose synthase, a complex between the catalytic domain of bovine GT (Gal-T1) and mouse LA (alpha-LA). The complex is shown with the acceptor GlcNAc. **B –** Stereo view of the molecular interactions between the same GT and LA. The secondary elements of LA are colored in red, while those of GT are in blue. The interactions between the proteins are principally hydrophobic. Two water molecules are trapped between the two proteins, and one of them has extensive hydrogen bonding interactions with both protein molecules. Adapted from Ramakrishnan and Qasba (2001).
.

Both aromatic cluster I and the flexible helix/loop region are particularly important for the lactose synthase regulation function, as they are the major active sites for interaction with GT. Ramakrishnan and Qasba (2001) described the structural role of both components in the catalysis reaction through a crystallographic study of the lactose synthase complex formed by recombinant mouse LA and bovine GT. The interactions between the LA and GT molecules are primarily hydrophobic and near of the acceptor site of GT (Figure 4.4 A). The aromatic cluster I of LA interacts with a corresponding hydrophobic patch in GT (Figure 4.4 B). The flexible loop/helix region of LA (in the mouse structure in a helix conformation) interacts with phenylalanine 360 and one of the α-helix of GT. Proline 109 sidechain of LA also interacts with the same α-helix of GT. Two residues of the aromatic cluster I of LA, histidine 32 and phenylanine 31 are said to be important in the binding of glucose to the complex.

In terms of structure details, it is finally important to outline the main differences between LA and c-type lysozyme. Lysozyme has the same fold organization than LA, with the two distinct

subdomains. The main differences reside on the non-existence of a Ca^{2+} binding site in lysozyme and in the cleft region, in which is located the binding site for monosaccharides in lysozyme. In LA the cleft region is blocked by Tyr 103. The truncations of the site, along with amino acid substitutions in the lower reaches of the cleft perturb the capability of LA to bind monosaccharides (Pike *et al.*, 1996).

4.2.2. Structural Elements Involved in the UV-sensitivity of LA

The location of the major part of the protein fluorophores in bLA has already been mentioned as they integrate primarily the two aromatic clusters of the protein. In this project, the most important positions are those of the Trp residues, since the intrinsic Trp fluorescence was used to probe their position within the protein (and the local structure), and the Trp residues were selectively excited to study the UV-induced reactions.

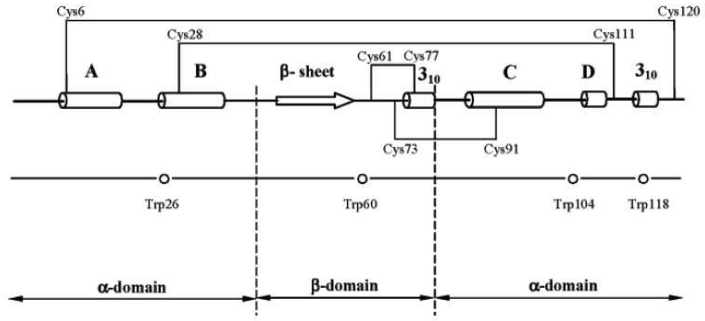

Figure 4.5: Schematic representation of LA. Secondary structure elements and the disulfide bonds in native GLA are indicated at the top. The domain boundaries are shown as dashed lines. Each of the tryptophan residues (O) is indicated (Adapted from Vanhooren *et al.*, 2006**a**).

The four Trp, major contributors for the protein fluorescence, are all located in the two clusters of bLA. Trp 26, Trp 60 and Trp 104, constituents of the aromatic cluster II are buried within the protein, displaying low values of accessible surface area[c] (ASA) in holo-bLAc: 0, 2.06, and 5.86 $Å^2$ respectively. Trp 118, present in the aromatic cluster I, is more exposed to the solvent with a calculated ASA of 30.3 $Å^2$. In apo-bLAc, the Ca^{2+} depleted form at high ionic strength, the tendency is the same, though Trp 60 is quite more exposed and Trp 104 the inverse. The ASA determined values for apo-bLAc are respectively 0, 0.12, 9.45, and 26.73 $Å^2$ for Trp 26, Trp 60, Trp 104 and Trp 118.

Trp 60, the only one of these residues that belongs to the β-subdomain (Figure 4.5), is located near two disulphide bonds (Cys61-Cys77 and Cys73-Cys91) in native bLA as can be depicted in the three-dimensional representation of holo-bLAc (Figure 4.6 A).

[c] The ASA values were calculated using the program *Surface Racer*© 5.4, upon submission of the PDB files for holo-bLA (1F6S) and apo-bLA (1F6R), considering a probe radius of 1.4 Å that approximates the radius of a water molecule, and the Van der Vaals radii sets of Richards – 1977 (Tsodikov *et al.*, 2000).

Considering a 5.2 Á cut-off distance for Van der Vaals contact between two atoms in proteins (as defined in Li and Nussinov, 1998), Trp60 is in direct contact with Cys73-Cys91 (calculated value of 4.67 Á) and very close to Cys 61-Cys77 (6.43 Á), which make them potential targets of UV-induced reduction, and consequently probable quenchers of Trp60 fluorescence. Trp 118, located in the opposite end of bLA, in direct contact with Cys28-Cys-118 (5.15 Á), is another likely trigger of UV induced SS bond disruption.

As observed by Vanhooren *et al*.(2006**b**) for goat LA, the indole side-chains of Trp60 and Trp118 in bLA are located on opposite sides of those of Trp26 and Trp104, that form a couple. The indoles side-chains of these two coupled Trp residues are in direct contact with each-other (calculated distance of 3.78 Á in *RasMol* – data not displayed in Figure 4.6), adequate situation for exchange and resonance of their excitation energy. Trp26 and Trp104 are not in direct contact with any SS bond. However, the indole ring of Trp104 and a potential quenching group, the peptide bond of Val92-Lys93, are within the delimited contact (calculated distance of 5.06 Á) as can be pictured in Figure 4.6 A.

In the same zone of the peptide backbone, the peptide bond Lys94-Ile95 is in direct contact with Trp 60 (3.76 Á) and may act also as quencher for this fluorophore. Similarly, Trp118 is also in presence of other quenching groups, other than the SS bond Cys28-Cys111. Its indole ring is in direct contact with the imizidole ring of one histidine (His32, 3.86 Á) and close to the peptide bond between Val27 and Cys26 (6.62 Á).

The characteristics of the Trp residues in the structure of apo-bLAc are similar to those of the correspondent residues in holo-bLAc described, which is natural given high homology degree of the two folds (see deviation values in Table 4.1, superposed structures in Figure 4.3 and section 4.3.5). In fields A and B of Figure 4.7 is represented the three-dimensional structure of apo-bLAc with the relative positions of Trp regarding correspondingly the SS bonds and the other potential quenchers. It can be noticed in both fields that the direct contacts mentioned for holo-bLAc are maintained, meaning that for this form of the Ca2+ depleted LA, the same UV-reactions noticed in native bLA may also occur.

The relative distances calculated for both structures are summarized in Table 4.2, where are also present other proximity distance values between SS bonds and Trp residues.

Experimental observations sustain partly the observations here realized. Through fluorescence studies using mutants of human LA containing only one Trp residue, Chakraborty *et al.* (2001) proved that the fluorescence signal of Trp 60 and Trp 118 is significantly quenched by disulphide bonds in their vicinity. Native human LA contains only three Trp residues, lacking Trp 26. However the structures of bLA and human LA are very similar, so the same quenching should occur in bLA, as suggest the distances here determined.

Table 4.2: Distances between the Trp residues of holo-bLAc and Apo-bLAc and its potential quenchers. The values were determined in *Rasmol* 2.6 using the "monitor" tool. In green are highlighted the Trp-quencher pairs for which there is direct contact (≤ 5.2 Å).

Pair		Distance (Å)	
Tryptophan	**Potential Quencher**	**Holo-bLAc**	**Apo-bLAc**
Trp26	Trp104	3.78	3.61
Trp26	Cys28-Cys111	8.37	8.38
Trp26	Cys6-Cys120	14.81	13.36
Trp60	Cys61-Cys77	6.43	6.24
Trp60	Cys73-Cys91	4.67	4.20
Trp60	Lys94-Ile95	3.76	4.09
Trp104	Val92-Lys93	5.06	5.08
Trp104	Cys28-Cys111	9.06	8.95
Trp104	Cys73-Cys91	7.80	7.93
Trp118	Cys6-Cys120	9.60	8.07
Trp118	Cys28-Cys111	5.15	4.74
Trp118	His32	3.86	4.12
Trp118	Val27-Cys28	6.62	5.70

More recently, Vanhooren et al. (2006**b**) studied the fluorescence of four mutants of goat LA, each one lacking one of the Trp residues. Compared to the wild-type the fluorescence of mutants lacking Trp60, Trp104 and Trp118 was higher, while for the mutant lacking Trp 26 it was lower. First of all, these results indicate that Trp26 dominates fluorescence, which can be explained by the lack of quenching groups around it (which is also verified in bLA). The increase in Trp fluorescence of the other mutants is explained differently. Trp60 and Trp118 are highly quenched by vicinal groups, including the disulphide bonds (observed as well in bLA). There are strong evidences that in LA these groups indirectly quench the group Trp26-Trp104, by transfer of energy to Trp60 and Trp118 (Sommers and Kronman, 1980; Vanhooren *et al.*, 2005). Despite the exchange of excitation between Trp 26 and Trp 104, there is an increase of fluorescence intensity in the mutant lacking Trp 104. This could be again due to the presence of quenchers of Trp 104 (again here verified for bLA), and indirect quenching of Trp26 by transfer of energy from Trp26 to Trp104. Resuming, in the mutants lacking Trp60, Trp104 and Trp118, the indirect quenching of Trp26 by the quenchers and the transfer of energy from Trp26 to each of these residues would not occur, resulting in the increase of fluorescence yield.

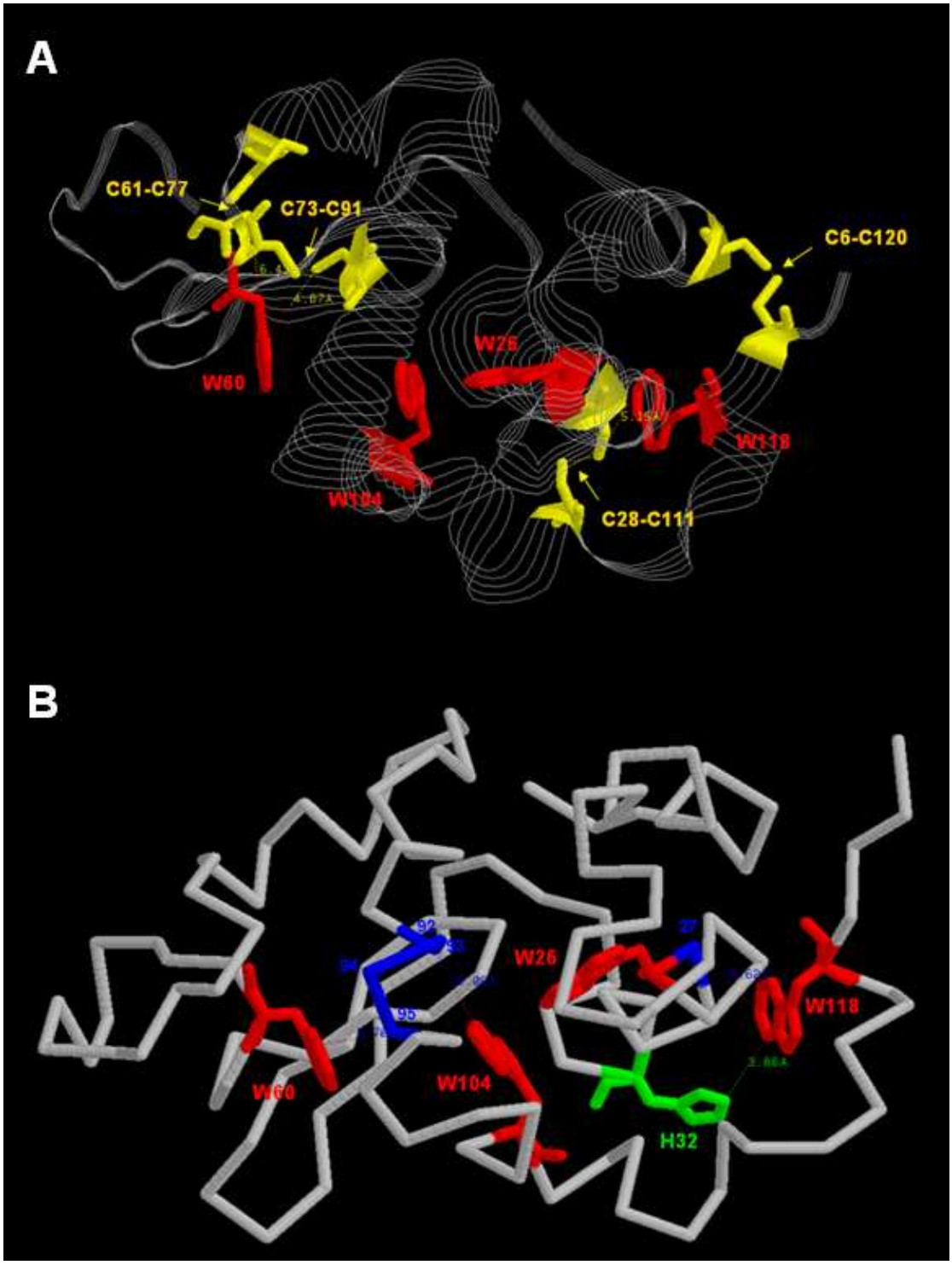

Figure 4.6: Crystal structure of holo-bLAc at 2.2 Å resolution (PDB entry: 1F6S) generated in *RasMol* 2.6. **A-** Peptide backbone is represented in grey strands. The 4 Trp and the 8 Cys residues of bLA are displayed in a stick configuration respectively in red and yellow. Dashed yellow lines represent the SS bonds of the protein highlighted by yellow arrows. Potential contact between the indole nucleus of a Trp residue and a disulphide bond is indicated mixed red-yellow dash line and the distance in Å. **B-** The peptide backbone is represented in grey strands and the backbone of five residues (Val27, Val92, Lys93, Lys94, and Ile95) is in blue. Val 32 is in stick configuration and in green. Contact between the indole nucleus of a Trp residue its potential quenchers is indicated in mixed red-green/blue dash line and the distance in Å.

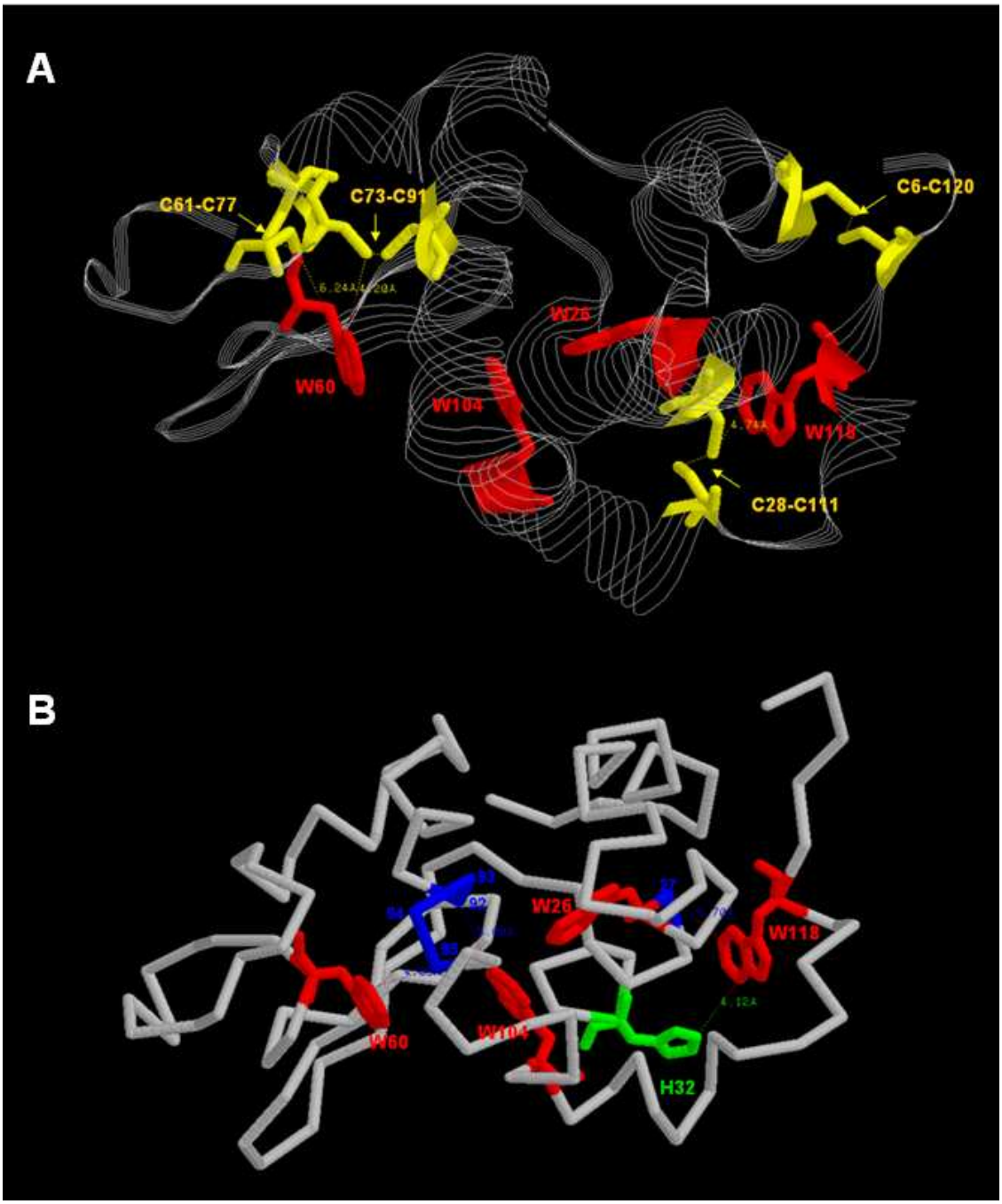

Figure 4.7: Crystal structure of apo-bLAc at 2.2 Å resolution (PDB entry: 1F6S) generated in *RasMol* 2.6. A- Peptide backbone is represented in grey strands. The 4 Trp and the 8 Cys residues of apo-bLAc are displayed in a stick configuration respectively in red and yellow. Dashed yellow lines represent the SS bonds of the protein highlighted by yellow arrows. Potential contact between the indole nucleus of a Trp residue and a disulphide bond is indicated mixed red-yellow dash line and the distance in Å. B- The peptide backbone is represented in grey strands and the backbone of five residues (Val27, Val92, Lys93, Lys94, and Ile95) is in blue. Val 32 is in stick configuration and in green. Contact between the indole nucleus of a Trp residue its potential quenchers is indicated in mixed red-green/blue dash line and the distance in Å.

4.3. CONFORMATIONAL STABILITY OF LA

The denaturation of proteins is evidently closely related to the stability of their structures. For LA a great deal of studies has been carried out using denaturation and unfolding procedures, is it in the ambit of protein folding studies, or in the context of aggregation studies of the protein for food engineering. For insight into protein stability and denaturation phenomena please see Appendix A (Denaturation of Proteins). It was not integrated in this part to avoid the natural succession in the text.

In the next section the denaturation of LA (the molten globule states) will be discussed, followed by a literature overview on the conformational stability under the conditions stated previously (temperature, pH, absence of calcium).

4.3.1. Molten Globule States

Globular proteins, and specially LA, have been extensively studied protein models for the understanding of protein stability, folding, and unfolding. Proteins can exist in particular low-entropy but energically equivalent states, “quasi-native” states, usually called molten-globules (MGs), that do not involve major changes in protein structure (Damodaran and Paraf, 1997; Chang *et al.*, 2001). These states are created under a wide variety of conditions, generated at equilibrium after unfolding upon the exposition to acid solutions, mild denaturants, by remotion of protein-bound prosthetic groups or metal ions, as well as protein chain truncation (Laureto *et al.*, 2002).

A molten globule (MG) state has been classically described as a relatively compact folding state of the protein, a collapsed state of the whole polypeptide chain, that retains some native-like secondary structure and overall backbone-folding topology, but lacks some of the specific side-chain interactions of the native structure that permit the existence of a clear tertiary arrangement. “Globule” refers to the structure compactness and “molten” to the increased enthalpy and entropy on the transition from the native to the new state. The MG state may therefore be interpreted as a stable partially folded conformation that can be distinguished from either the native or the fully denaturated form. (Laureto *et al.*, 2002; Van Dael *et al.*, 2005; Tarek *et al.*, 2003; Damodaran and Paraf, 1997).

MG-like states are particularly attractive since they have been shown to resemble kinetic intermediates in the folding process of the proteins, LA being one of these cases (Wijesinha-Bettoni *et al.*, 2007; Tarek *et al.*, 2003). The full understanding of the mechanism of protein folding, an active quest in molecular biology and biophysics nowadays, requires the knowledge of the structure, relative energetics and dynamics of the species populating the folding pathways of the protein. The acquired knowledge could help to understand the nature and role of these

diverse kinetic intermediates, intriguing for itself along the folding pathway. In some cases they display progressive structural shifts along the folding process, while in other situations one can find intermediates that display large structural deviations in comparison with the precedents, yielding conformers that even delay the process. (Van Dael *et al.*, 2005). MG-like states can be used as a model to fulfill these needs of analysis, besides presenting the advantage fact of being formed at equilibrium, permitting an easier identification and characterization with the help of spectroscopy techniques, on opposition to the case of regular protein folding intermediates, seemingly intricate due to their transient nature (Laureto *et al*., 2002).

Although the MG is currently accepted as a concept, there have been raised several polemics around its meaning, particularly if it should be considered as thermodynamically distinct state in comparison to the unfolded one (Laureto *et al.*, 2002; Pfeil *et al.*, 1998). The structure of the MG is highly heterogeneous and disordered and, like the large majority of denaturated or partial denaturated state of proteins, it comprises also a large number of conformational isomers (Chang *et al.*, 2001), complicating the achievement of a structural picture of this its conformational states.

In the specific case of LA, unfolding of the protein to MG-like states has been reported upon exposition of the protein to acid solutions (acid denaturation), to mild denaturants (*e.g.* with guanidine hydrochloride at neutral pH LA suffers a three-state denaturation from the native state N, with an intermediate MG-like state and the further fully denaturated form), thermal variations, in cases of calcium depletion at low ionic strength, among others (Kuwajima *et al.*, 1996; Laureto *et al.*, 2002). In this thesis, relevant notions about the thermal stability of the protein, its conformational state at different pHs, and structural changes induced by calcium depletion will be mentioned. The focus will not be the MG and the study of folding intermediates. Nevertheless, discussing the MG state is inevitable, given that the thematic in issue and the MG are intrinsically related, and along the chapter some questions will be raised

4.3.2. Thermal stability of LA

The thermal stability of a protein is an intricate and complex issue: Thermal induced changes involve primarily the destabilization of major non-covalent interactions. Hydrogen bonds, electrostatic, and Van der Vaals interactions, which stabilize the native structure mainly at the different secondary level of its structure, are exothermic (enthalpy driven) in nature. Hence, they are destabilized at high temperatures and stabilized at low temperatures. However, the peptide hydrogen bonds are mainly buried in the interior of the protein, so they remain stable at a wide range of temperatures. In contrast, hydrophobic interactions are endothermic (entropy driven), and favored with the temperature increase, and the hydrophobic residues are more susceptible of interacting with water at lower temperatures. Another important factor is the conformational

entropy of the polypeptide chain: with a temperature increase, the thermal kinetic energy of the polypeptide chain increases, which greatly facilitates the unfolding of the polypeptide chain (Fennema, 1996).

The thermal stability of proteins is consequently strongly dependent on the amino-acid content and on the network of bonds in the protein structure. In fact, the first observed change in a protein's structure upon temperature increase will be the unfolding on its tertiary structure, due to the weakening and breakage of long-range interactions. The progressive flexibility obtained by the protein chain leads to solvent exposure of groups once buried. Cooperative hydrogen bonds will now maintain the secondary structure of the protein. Then the disruption of non-covalent interactions leads the unfolding, and the hydrophobic groups, on the unfolding and hydration of the structure, take a role in the rearrangement of the structure, since they interact less with water. On the other hand, the stability of the proteins can also be compromised by lowering of temperature, such as myoglobin that displays maximum stability around 30ºC, and that upon storage below 0ºC suffers cold-induced denaturation. Protein stability depends on the relative magnitude of contributions from polar and non-polar interactions. When polar interactions are favored in a protein, it will be more stable at low temperatures than at higher temperatures, while when non-polar interactions are favored, the protein will be more stable at ambient temperature than at low temperatures (Fennema, 1996).

LA has a high content in hydrophobic amino-acids (like Leu, Cys, Ile ; *vide* Figure 3.1), factor that can contribute positively for its thermal stability (Fennema, 1996). This is reinforced by the compact tertiary structure of globular proteins and the absence of free thiols groups (Wang *et al.*, 2006). Indeed, in its native conformation, at physiologic conditions (whey milk), neutral pH and calcium-rich environment, LA shows a high thermal stability. In these conditions, the T_d (denaturation temperature) (~62%) is the lowest among the whey proteins but this process is 90% reversible, as measured by calorimetry (Chaplin and Lyster, 1986; Wit and Klarenbeek, 1984). Irreversible changes happen in the native protein only at 70-80ºC, which results in minimum protein aggregation. At a temperature superior to 90ºC aggregation is fully noticed (McGuffey *et al*., 2007). The thermal unfolding is also appointed to form partly denaturated species with characteristics similar to MG-like conformations, these species being noticed at temperatures superior to 60 ºC. These partially unfolded state exhibit an increased linear dimension and hydrophobicity as well as better accessibility of the disulfide bonds to a thiol exchange reaction (Wijesinha-Bettoni *et al.*, 2007; Vanderheeren and Hanssens, 1994; Wang *et al.*, 2006).

Though native LA can be classified as thermal resistant protein (maintaining its structure intact at high temperatures), it is not always the case since its conformation is largely affected by external solvent conditions, thus so is its stability. Indeed, any denaturation transition in LA is highly dependent on metal ion concentration and pH values (Permyakov and Berliner, 2000).

Thermal stability data is very useful in terms of providing clues on the structural effects induced to the protein by different external parameters, like pH or other solvent specificities (Pedersen *et al.*, 2006). Structural changes are detectable since the protein will have a different susceptibility to thermal unfolding upon changes in physic chemical parameters of the solution. For that reason it is a tool frequently used on studies with LA, involving pH or calcium concentration changes.

4.3.3. pH Influence in the Conformational Stability of LA

At neutral pH LA and at temperature way below its T_d is in its native state in the milk whey (Gao *et al.* 2008). From preliminary studies it was concluded that LA undergoes intermolecular interactions leading to varying degrees of polymerization depending on the pH. At acidic pH values, the protein is characterized a rapid reversible association and slow aggregation. Between pH 6 and 8.5 there is very little association, being the protein in a native-like structure and above pH 9.5 there is expansion without aggregation (Boye *et al.*, 1997). It is interesting in the ambit of this study to look at the molecular changes that occur at these different pH values.

As mentioned before, the isoelectric point of native LA is determined by previous analysis to be around 4-5 (acidic protein).

Therefore, upon pH shifts towards acidic values, LA turns progressively more positively charged. The titrable groups of the protein (with different pK_as) will be gradually protonated at low pH values, leading ultimately to the denaturation of the protein due to electrostatic repulsion forces. The transition to a denaturated state happens progressively, as a cooperative event, triggered by the protonation of residues in the calcium binding pocket, rich in Glu and Asp (model pK_as around 4-5, Creighton, 1992), leading to Ca^{2+} release from the protein (Pedersen *et al.*, 2006; Kim and Baum, 1998). This event takes place in the vicinity of the isoelectric point, as described by nuclear magnetic resonance (NMR) and near-UV (250-400 nm) CD spectroscopy (Kim and Baum, 1998), in agreement with previous studies (Griko et al., 1994). Above pH 5.0 the protonation of residues does not contribute to the formation of a compact denaturated state. The transition is noticed below 4.2, where larger population of denaturated states is detected, displaying a reduced signal at 280 nm (in the near-UV) in the CD spectrum (Kim and Baum, 1998). Probably, the structure is destabilized for two reasons: the release of calcium and the possible to breakage of salt bridges mediated by the protonation of Asp and Glu. The result is a structure with fewer constraints, and risking concomitant rupture of H-bonds.

The acidic pH-induced unfolding results in a calcium depleted acid denaturated form (A-state), a MG-like conformal state, which is analogous to an early protein folding intermediate, and frequently regarded as the MG *prototype*, usually defined at pH 2 (De Laureto et al. Kim and Baum, 1998). In this form, the thermal stability of the protein is largely affected, the T_d lowers from 62ºC at pH 8 to 32ºC at pH 2.5 (Pedersen *et al.* 2006).

This partly folded state retains some of its tertiary features, in a bipartite structure conformation. When pH drops, the helical content of the native structure, constituted by the α-subdomain plus helix 3_{10} h2 (residues 1-37 and 85-123) is preserved, albeit dynamical, with the typical helical secondary structure retained by helices H2 and H3, formed by loose hydrophobic interactions. On the other hand, the majority of the β-subdomain, encompassing the three β-strands of the protein (residues 38-84) is disordered and unstructured (Laureto *et al.*, 2002, Kuwajima *et al.*, 1996).

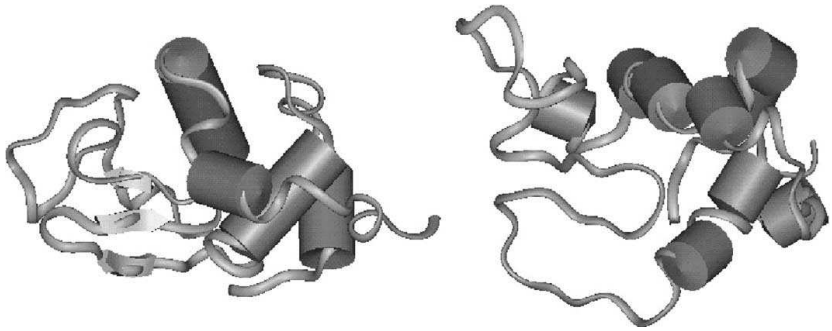

Figure 4.8: Snapshots of LA configurations in the native state (left) and molten globule state at pH 2 (right) from the molecular dynamics simulations. Helices are displayed as barrels and β-sheets as large arrows (Adapted from Tarek *et al.*, 2003).

This bipartite picture of LA can be confirmed by snapshots of LA generated from molecular dynamics simulations displayed in Figure 4.8 (Tarek *et al.*, 2003). Two snapshots are represented: to the left is displayed protein in its native conformation (pH 8) and to the right in its A-state (pH 2). It can be clearly noticed the loss of the structure in the β-subdomain (triple-stranded antiparallel β-sheet) when pH is lowered to pH 2, while most of the α-subdomain (helices) is conserved.

The reduced signal obtained with near-UV CD spectroscopy (De Laureto *et al.*, 2002; Kim and Baum, 1999), in consonance with quenching experiments with acrylamide (Pedersen *et al.*, 2006), indicate that, at low pH, some specific and rigid side-chain packing of aromatic chromophores of the protein is possibly lost, and that an opening of the hydrophobic part of the protein may occur.

Although at low pH Trp 26 and Trp 104 (part of the aromatic cluster II) remain buried in the acid state and the hydrophobic cluster that they integrate is maintained, there is a clear possibility of structural re-arrangement in this area, as documented by nuclear magnetic resonance (NMR) and hydrogen exchange of tryptophan indole ions (Kuwajima et al., 1996). The observed conformational change is likely to be in this area since the main stabilizing hydrophobic core is considered to be oppositely the aromatic box I. An analysis of a set of point mutations in the α-subdomain of the protein led to consider this subset of hydrophobic residues (aromatic box I) most important for the formation of the native-like topology (Wu and Kim, 1998; Permyakov and Berlinder, 2001), as it could be for the maintenance of the α-subdomain structure.

This expected opening of the structure and the exposure of certain hydrophobic parts of the protein are confirmed by the following observations.

- the radius of gyration of native calcium-loaded LA is 15.7 Á in contrast with the value of 17.2 Á for the acid molten globule Permyakov and Berliner, 2000);
- it is a highly hydrated conformation comprising 270 bound water molecules (Permyakov and Berliner, 2000);
- the mass density of the interior of the protein is 5% less and the intrinsic compressibility coefficient two times higher than in the native protein (Permyakov and Berliner, 2000);
- a 15-fold increase in hydrophobicity is noticed when it converts to the acid state (Gao *et al.*, 2008).

LA retains therefore a globular shape in acidic conditions however swollen when compared to the native state. At very low pH values the opening of the structure leads eventually to protein aggregation (Pedersen *et al.*, 2006).

The effect of alkaline pHs in the structure of the protein is less described in literature. Upon shift to basic pH values, the protein will become negatively charged. At pH 9 the protein is probably quite stable, since no aggregation is still observed and no thermal transition is noticed in differential scanning calorimetry experiments (Boye *et al.*, 1997). At higher pH values, the destabilized negative charged protein may loose a large part of its favorable electrostatic interactions leading to its partial denaturation, mentioned to have a MG-like conformation (Harata and Muraki, 1992).

4.3.4. Calcium Induced Conformation Changes in LA

Chelating agents, metal cations, and buffer components are known to induce dramatical structural changes in the LA molecule and thereby alter its binding properties in solution (Griko *et al.*, 1999). In particular, the influence of the Ca^{2+} ion will be discussed.

The native form of the LA is the calcium-bound, which is the major form under physiological conditions (milk whey) (Hong *et al.*, 2002). However, during the refolding process LA is mainly in its calcium depleted form (named apo-LA on opposition of holo-LA, which is the metal-ion bounded form), and the role of binding of Ca^{2+} in lactose synthesis is still unclear (Permyakov and Berliner, 2000). LA assumes probably other forms than the calcium-bound *in vivo* in the variable environments where it intervenes, and the apo-form is probably one of them.

The binding of Ca^{2+} to LA induces prominent changes in its 3D structure and function but not the secondary structure (Permyakov and Berliner, 2000). The calcium ion in LA has a structural role, being required for folding and native SS bond formation in the reduced denaturated protein (Chrysina *et al.*, 2000). In the denatured form, with the disulphide bridges

intact, LA refolds slowly to its native structure, a process at least 2 orders faster upon Ca^{2+} binding by folding intermediates (Kuwajima *et al*., 1989)

Though several reports exist on the role of calcium in the stabilization of LA structure, there is no agreement about the conformation of the calcium depleted form of LA, probably due to its structural instability. Divergent opinions are reported, shifting from a classical MG devoid of the cooperative thermal transition, to a partly native folded state with some maintained native proprieties and oppositely showing cooperativity (Laureto *et al.*, 2001).

The apo-LA thermal stability has been probed by differential calorimetry, fluorescence emission, Raman spectroscopy, and near UV-CD at different solvent conditions (pH, ionic strength). All observed T_m (temperature of mid-transition) values were lower than the T_m of the native Ca^{2+} bound state (Hendrix *et al.*, 1996; Wilson *et al.*, 1995; Laureto *et al.*, 2001; Veprintsev *et al*., 1997; Pfeil, 1998; Wijesinha-Bettoni *et al*., 2001). T_m is reported to be highly dependent of the physic chemical parameters of the solution.

One important solvent parameter that can affect the results and the conformation of apo-LA is ionic strength. NaCl and KCl were both shown to stabilize substantially the folded state: in the presence of 0.5 M NaCl the thermal stability is reported to increase by 30ºC (Wijesinha-Bettoni *et al.*, 2001). The stability of calcium-bound LA is not influenced by variations in ionic strength at neutral pH indicating that no charged groups affect protein stability in this pH range. However removal of calcium ion exposes negatively charged residues originally coordinated to Ca^{2+} in the holo-LA, destabilizing the conformation of the protein (Griko *et al*., 1999). The salt stabilizing effect is probably due to ionic interactions and not a specific binding effect of the cations like Ca^{2+} replacement, achieved by partial neutralization of the unfavorable charge. This is supported by previously referred X-ray crystallography studies (Chrysina *et al.*, 2000) and NMR studies (Wijesinha-Bettoni *et al.*, 2001) carried on apo-LA in the presence of high contents of salts. In both studies only subtle changes are observed between the apo and the calcium loaded form, at the calcium binding sites. Parallel to the minor instability in the structure, no ion was found in binding site in the crystallized apo-LA and no chemical shifts were observed in the aspartates of the calcium binding site, excluding this way any Ca^{2+} substitution.

Without the stabilizing presence of calcium in the binding site, LA is also more vulnerable to pH shifts. Between pH 5.5 and 8.5, apo-LA is stable, in similarity to the native form. However, its stability decreases remarkably below pH 5 (Griko *et al.*, 1999)

Crystallographic studies show the presence of a more open cleft structure in the Ca depleted form, induced by a perturbation of interactions between the α and β-subdomain of LA at an inter-subdomain region located it at the edge of the hydrophobic box. The authors argue that this perturbation propagated from the main calcium binding pocket, where a small expansion is observed (at high ionic strength), causing a slight tilt of the helix 3_{10} h2 relatively to the H3-helix, leading to the disruption of some of the native interactions in the Aromatic Cluster II. The NMR

studies concurs partially with the crystallization study showing that the major shifts occur in the residues on the main Ca^{2+} binding loop and on the nearby α-helix(H3-helix). Nonetheless, the NMR chemical shifts in the Aromatic Cluster II are not so elevated (mostly for the Tyr103, which is the residue that shows a wider change in the crystallographic study). These small divergences in both studies may be attributed to differences between the crystallized form and the solution (NMR) form of apo-LA, or simply by differences in the experimental conditions used in both studies.

The areas with changed structure in the calcium depleted form are the same areas where the MG of the A-state (LA at pH 2) is apparently altered, which could signify that this form at high ionic strength is representative of an initial step for the transition to a MG-form. The MG-conformation could be favored at low ionic strength, with a further dispersion of these zones.

Studies using limited proteolysis on apo LA (Laureto *et al.*, 2002), where the conformation was well characterized as native-like by means of near-UV CD show that the destabilization of apo LA under different denaturating conditions (moderate heating, presence of Trifluoroethanol and Oleic acid), occurs only in residues 34-57, giving origin to a MG like conformation. These residues are part of the β-subdomain, the major zone disordered in the A-form. One can imagine therefore apo-LA in terms of a compact protein with a short disordered segment, easily destabilized by ionic strength, temperature, among others, that in under strong destabilization resembles the A-state pictured in Figure 4.8.

4.4 REMARKS

From this literary overview of the protein, some broad notions can be traced about its reaction to destabilizing conditions. The unfolding of LA comes generally in a bipartite fashion, with the β-lobe more disorganized and the α-lobe retaining some compactness, which makes sense since the two sub-domains are well separated as can be depicted from the three-dimensional structure of the native protein (Figure 4.2). The apo-form is less stable and reacts in an amazing diversity upon diverse solvent conditions, implying that, for each experimental approach, a judicious characterization of the specific effects of different solvent factors on protein structure must precede premature speculation and discussion of controversial results.

However, it is interesting to observe that the molecular flexibility of LA is probably influenced and controlled by solvent conditions and modulated by binding ions, which might serve as a regulatory mechanism for this protein.

Indeed, in the several biochemical roles advanced for the protein other than the intervention in the lactose biosynthesis, LA is not in its native conformation. Calcium-depleted forms, as the one analyzed in this study, are known to interact with lipid membranes and oleic acid. The association of LA with the latter is known to generate a multimeric MG variant, HAMLET

(human LA made lethal to tumor cells) that induces apoptosis specifically in tumor cells. (Permyakov and Berliner, 2000; Laureto *et al.*, 2002; Fisher *et al.*, 2004). Furthermore, a MG state of the human protein has been shown to have antimicrobial activity (Wijesinha-Bettoni *et al.*, 2007).

It makes sense also, that in the different environments of the human and mammals' body, LA assumes different conformations. The reactivity to different metal ions is a possible regulating mechanism.

For the reasons presented above the apo-forms of LA are by itself clearly attractive models of study, though care must be taken on analysis.

On the other hand it is important to analyze the protein and the apo-form as models for the study of UV reactions. As a model, LA is not a simple case of study like *Fusarium solani pisi* cutinase that displays only one Trp and one SS bond, which allows the link between the excitation of Trp and disruption of SS-bridge to be easily made. Moreover, the four Trp residues of LA are located in different environments of the protein, exposed to different quenchers and may be enrolled in a wide number of interactions. Such variety makes not only the process of fluorescence data analysis quite harder, since it is not easy to understand how the Trp residues contribute for the protein intrinsic fluorescence, as it opens doors for a wide number of possible UV triggered mechanisms. However, the richness of SS bonds and Trp residues in this small protein suggests that the SS induced breakage in study is probable in several ways.

In fact, the disruption of SS bonds in LA upon Trp excitation has been verified for Ca^{2+} loaded and apo-versions of bovine, human (Permyakov *et al*., 2003), and goat (Vanhooren et al., 2002; Vanhooren *et al.*, 2006**a**) LA. In these studies was proven the light-induced breakage of two SS bonds in human and goat LA: Cys61-Cys77 and Cys 73-91. Additionally, in the studies regarding the goat version (for apo and Ca^{2+} loaded LA) was proven the disruption of Cys6-Cys120. Strangely, no breakage of the bond Cys28-Cys111 was found in either study. This bridge is in close Van der Vaals contact with Trp 118, and its photo-reduction would be more expected than the others SS bonds. This SS bond is located in a zone with very high preference for native-like topology. Thus, this activated SS bond may not be susceptible to cleaving, or even upon cleaving, the resulting thiyl radicals may not tend to migrate away for each-other, and the SS bond may reform before any other reaction (Vanhooren *et al.*, 2006**a**).

Studying an apo-form is presumably more difficult since the structure is more instable and unpredictable. Nevertheless, the SS bridges in this state are probably still intact and the aromatic residues compact even in a MG-like state. It is appealing to probe the effects of UV light on apo-bLAs since they are not so well characterized in this particularity. The characteristics of apo-forms may be also favorable for an immobilization procedure since the disulphide bonds of LA are in principle less stable, and possibly it will adhere easily onto surfaces due to the stronger inherent hydrophobic character of these forms (compared to the native LA).

5. CHARACTERIZATION OF THE MODEL

5.1. PREMISSES

The main goals of the characterization procedure were, as previously stated, to evaluate the protein model as a candidate for light induced immobilization and check the ideal conditions to proceed with this technique with the model. Taking in consideration the main features of the model chosen, a calcium depleted form of LA, the characterization procedure regarded two distinct issues, reflected in the organization of the results here presented.

First it was needed to verify the SS bond light induced disruption for the apo-form of LA obtained in solution. As stated before, from literature it is known that this mechanism can occur in calcium depleted forms of the protein but it was desirable to verify it, and confirm its specific features for the apo-form and the conditions used. Moreover, it was important to check the impact of distinct factors such as temperature or pH in the UV-sensitivity of the protein in order to plan a desired immobilization.

On a second hand, it was required to qualify and define the specific apo-form obtained in the experimental conditions used above. Calcium depleted forms LA are particularly unstable, and for that reason it was important to figure out the conformation that it adopts initially in solution, and assure if the model is stable during the experiments, focusing already in the immobilization procedure. Furthermore, for comparisons with other works, this step is clearly essential.

The primary tool used for both sets of analyses was fluorescence spectroscopy. The basic principles and concepts behind the analysis procedure will be described throughout the results presentation.

To avoid confusions with either the native form or other apo-forms of the protein, the protein form used in the experiments and described in the Materials and Methods (section 5.2.1) will be further named as eLA, standing for “bovine α-lactalbumin used in the experimental procedure”.

5.2. MATERIALS AND METHODS

5.2.1. Materials

Protein Solutions

Bovine α-Lactalbumin from bovine milk type III was purchased from Sigma-Aldricht (product labeled as L6010a) as lyophilized powder and the same was used without any further preparation in all the experiments here mentioned. The product in question had been previously prepared directly from raw, unpasteurized milk, purified by ion-exchange chromatography using DEAE-agarose, and depleted of calcium via remotion by precipitation with sodium sulphate. The degree of purity is ≥85% (Sigma Product Information, www.sigmaaldrich.com).

eLA concentrations in solution were determined by absorbance at 280nm using an extinction molar coefficient of 28500 $M^{-1}.cm^{-1}$ (Masaki *et al.*, 2000; Permyakov *et al.*, 2003)

Buffer Preparation

In all spectroscopy studies protein and other solutions were dissolved in buffers prepared with Milli-Q water (conductivity below 0.2 µS.cm-1). The salts used for buffer preparation, as the respective purity and their provenience are displayed in Table 5.1.

Table 5.1: Salts used for Buffer preparation, Molecular Formula, Purity, and Provenience.

Buffer	Salt	Formula	Purity	Provenience
Tris HCl	TRIZMA® BASE	$NH_2C(CH_2OH)_3$	≥99.9%	Sigma
Phosphate Buffer	Potassium Phosphate Monobasic	KH_2PO_4	≥99.0%	Sigma
	Potassium Phosphate Dibasic ACS Reagent	K_2HPO_4	≥98.0%	Sigma-Aldricht
Sodium Citrate	Sodium Citrate Tribasic Dihydrate	HOC(COONa)(CH2COONa)2 · 2H2O	≥99.0%	Sigma-Aldricht
Sodium Carbonate	Sodium Carbonate Anydrous	Na_2CO_3	≥98.0%	Fluka

pH of the prepared buffer stock solutions was adjusted by addition of hydrochloric acid 2.5 M and sodium hydroxide 2 M and pH values were checked using a standard pHmeter (PHM 210).

Ellman's reagent

DTNB (5,5´-dithiobis-(2-nitrobenzoic acid)) or Ellman's reagent was purchased from Molecular Probes (Invitrogen) as a powder. 1 mM of this powder was dissolved in TRIS HCl 100 mM. The pH was adjusted to 6.56 in order to favor the dissolution. 0.7 mM DTNB stock used in the experiments consisted on the supernatant extracted. The stock concentration was determined by absorbance at 324nm using an extinction molar coefficient for DTNB in TRIS HCl of 16600 $M^{-1}.cm^{-1}$ (Riddles *et al.*, 1983). The stock solution was stored in the fridge at 4 ºC.

Cysteine solutions

L-Cysteine was obtained from Fluka as a lyophilized powder (degree of purity ≥ 98.5%). A 200 mM stock solution was prepared in Tris HCl 10 mM pH 7.56 after weighting in an analytical balance. All solutions used experimentally were diluted from this stock.

5.2.2. Methods

5.2.2.1. Experimental Methods

Time-dependent Fluorescence Emission of eLA

UV-light triggered reaction mechanisms in eLA were probed by monitoring the time-dependent fluorescence intensity of eLA upon constant irradiation with UV-light. A 1.86 µM eLA solution was prepared after dilution in TRIS HCl 25 mM pH 8.55 from a stock solution of the protein. Three milliliters of the prepared solution was illuminated in a quartz macro cuvette (1 cm pathlenght) in diverse irradiation sessions each of them corresponding to different illumination duration (1h, 2h, 3h, 4h, 5h), this way characterizing the extent of the reaction. Continuous illumination at 295 nm was realized using a 75-W Xenon arc lamp coupled to a monochromator from a RTC 2000 PTI spectrometer. Temperature was maintained constant at 25 ºC in the thermostated cuvette by means of a peltier element installed in the spectrofluorimeter, and controlled externally by a thermometer plunged in the solution. The sample was continuously magnetically stirred at 900 rpm to preserve the homogeneity of the solution. The fluorescence intensity of eLA at 340 nm was monitored during the plenitude of the sessions through the detector 1 of the equipment, and the emission at 295 nm, the scattering of the light, was scanned synchronously in the detector 2, turning on the time-based mode of the equipment. Emission was detected through two photomultiplier tubes each coupled to a monochromator. Excitation and emission slits were set at 5 nm.

In the PTI software used to control the experiment, real-time correction was enabled, set at 1.8 V for excitation at 295 nm, in order to correct the oscillations of the lamp in excitation. Two

data sets of emission *versus* time are obtained in this procedure for both channels (detectors), one with the detected values and one with the correction applied. In the results analysis and presentation the corrected values are only used when mentioned.

After each illumination emission and excitation spectra were recorded. The slits were all maintained at 5nm. Excitation in the emission spectra was realized first at 295 nm and secondly at 280 nm. Emission was fixed at 340 nm in the channel 1 and 320 nm in the channel 2 for the excitation spectra.

The same emission and excitation spectra were realized for in the same conditions with the fresh solution (non-illuminated), and with just the buffer (TRIS HCl 25 mM pH 8.55), in order to correct for *Raman Contribution* (see definition in Appendix C).

Detection of free Thiol Groups with DTNB on UV illumination of eLA

Detection and quantification of the free protein thiol groups was carried on with the spectrophotometric assay based on the reaction of thiol groups with DTNB As can be observed in Figure 5.1, when the thiolate ion ($R\text{-}S^-$) or a thiol (R-SH) reacts with the Ellman's reagent ($DTNB^{2-}$ in solution), a mixed disulphide and one equivalent of nitrothiobenzoate ion (TNB^{2-}) are formed. The latter absorbs intensively at 412 nm (ε_{412} = 14150 $M^{-1}.cm^{-1}$), while the mixed disulphide and $DTNB^{2-}$ show the same weak absorption signal at this wavelength. Hence, the net change in molar absorptivity at 412nm felt upon the reaction is equal to the molar absorptivity of the intensely colored by-product TNB^{2-}, which is by its turn proportional to the concentration of the $R\text{-}S^-$ or/and R-SH that reacted (Riener *et al.*, 2002, Neves-Petersen *et al.*, 2002).

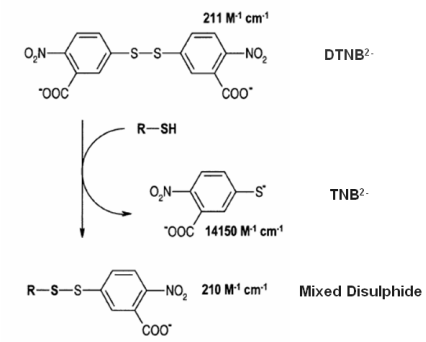

Figure 5.1: Reaction of a thiol with Ellman's reagent, originating a mixed disulphide and one equivalent of TNB^{2-}. The extinction molar coefficients at 412 nm are displayed for the different chemical species and all refer to pH > 7.29 (Adapted from Riener *et al.*, 2002).

In order to realize the quantification procedure on α-LA, after each of the illumination sessions described in the previous section, the irradiated solutions present in the cuvette were extracted. An excess of DTNB (100 µL of a 0.7 mM stock solution of DTNB in Tris HCl) was added to 900 µL of each of the illuminated solutions (immediately after the extraction) and to 900 µL of a non-illuminated eLA. The absorbance at 412 nm was measured with a UV/visible

spectrophotometer (UV1 VWR International – Thermo Electron Corporation), and using always 1 –cm path quartz cuvettes. The absorbance of the solution was checked immediately after mixing of the two components, and on several turns in the following minutes. The sample was kept in the dark between measurements, and agitated manually before each reading. The absorbance value at 412 nm stabilized after approximately 20 minutes of reaction. For quantification was considered the absorbance value read at 22 minutes of reaction. Furthermore, absorbance at 412 nm was checked immediately after manual agitation for two blanks, a protein blank and a reagent blank, in order to correct the assay determined absorbances. The compositions of the assay solution and of the two blanks are described in table 5.2:

Table 5.2: Composition of the solutions used for the Ellman's assays and of the two blanks.

	Absorbance Value	**Volume (µL)**	**Components and Concentration**	**pH**
DETECTION ASSAY:	$A_{412S\ 22min}$	900	eLA 1.86 µM Illuminated and non-illuminated	8.55
		100	DTNB 0.7 mM	6.75
REAGENT BLANK:	A_{412r}	900	Tris HCl 25 mM	8.55
		100	DTNB 0.7mM	6.75
PROTEIN BLANK:	A_{412p}	900	eLA 1.86 µM non-illuminated	8.55
		100	Tris HCl 100 mM	6.75

Since the detection assay on the non-illuminated protein was not realized in the same time scale than the illumination of the eLA 1.86 µM samples, the blanks were repeated for this one. The final values of absorbance (A_{412}) are proportional to the number of free thiol groups present in the protein that react with DTNB and were determined using the following expression:

$$A_{412} = A_{412S\ 22\,min} - A_{412R} - A_{412S} \quad (5.1)$$

To evaluate the sensibility of the assay, the same procedure was realized for diluted L-cysteine solutions of known concentration. L-Cysteine presents a single thiol group that reacts easily with the Ellman's reagent and for that reason is often used as a thiol standard (Riener *et al.*, 2002). 900 µL of each solution and of buffer used for dilution (Tris HCl 10 mM pH 7.56) were mixed each turn with 100 mM. Once more the absorbance at 412nm was checked immediately after mixing. For the cysteine solutions the protocol was the same than before, with the stabilized value after 22 minutes of reaction registered. The absorbance values obtained in this fashion are plotted in function of cysteine concentration in the calibration curve obtained (Figure 5.2) A reasonable linear correlation is noticed between the two variables, which reinforces the reliability of the assay used.

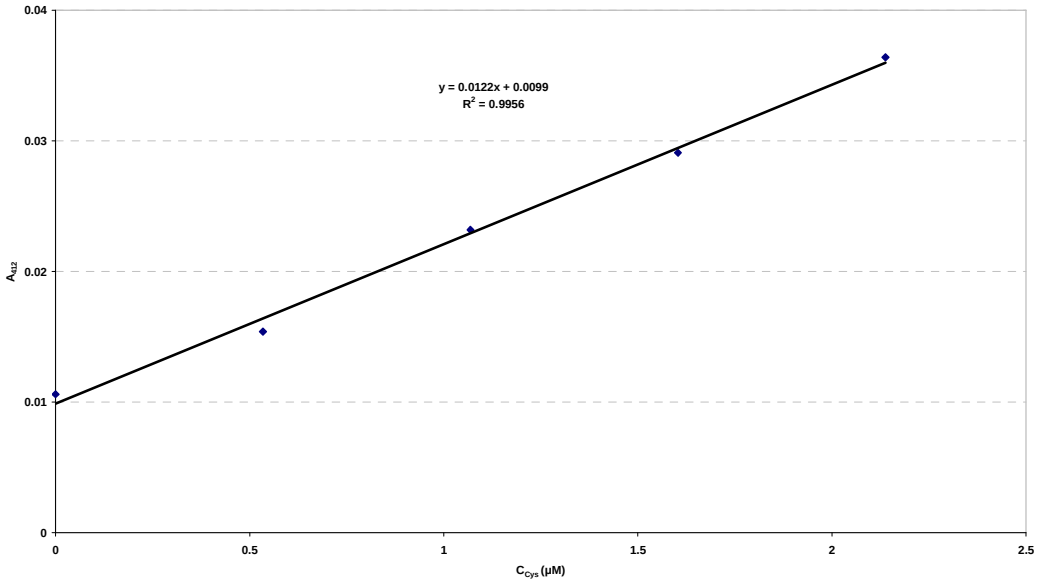

Figure 5.2: Absorbance values at 412 nm *versus* cysteine concentration in the assay. The absorbance values correspond all to a reaction time of 22minutes except for the 0µM solution.

Time-dependent Fluorescence Emission of eLA at different temperatures

The effect of temperature in eLA UV-sensitivity was investigated using the same approach as the previously described study of extent of reaction mechanisms over the irradiation time. The time-dependent fluorescence intensity of eLA was once more monitored using the same steady-state setup in the RTC 2000 PTI spectrometer with constant irradiation with UV-light. However, in this case the solution in the cuvette was maintained at different temperatures in the diverse sessions, and illumination was always carried out over the same duration. The experimental set-up used for the constant UV-light irradiation was identical and the procedures realized prior and after the sessions were exactly the same. Thus, here will only be described the conditions used on all illumination sessions, summarized in Table 5.3.

Table 5.3: Conditions and settings used in the temperature-dependent illumination sessions of eLA samples.

Protein sample	eLA 1.85µM in Tris HCl 25mM pH 8.55
Volume (mL)	3
Stirring (rpm)	900
Irradiation duration (h)	3.5
Excitation wavelength (nm)	295
Wavelength set in Detector 1 (nm)	340
Wavelength set in Detector 2 (nm)	295
Real-time Correction - Excitation at 295 nm	1V

Temperature was maintained constant throughout the each session at the value of interest, and the sessions were realized respectively at 9.3, 12.9, 15.6, 20.4, 24.9, 29.9 and 34.6ºC. Emission spectra were also recorded in the end of each session, upon excitation at 295 nm and 280 nm, as well as excitation spectra fixing the emission in detector 1 at 340 nm and in detector 2 at 320 nm. Temperature was still maintained constant in these recordings. Moreover, these measurements were performed in fresh samples of the protein, at each of the temperatures above mentioned, considering the same delay time to reach each temperature, and with just the buffer (TRIS HCl 25 mM pH 8.55), in order to correct for *Raman Contribution*.

In all experiments and procedures excitation and emission slits were set at 5 nm.

The detection of free thiol groups was also realized in the end of each irradiation session, except for the irradiation session realized at 9.3 ºC. The protocol used was exactly the same than for quantification procedure of different irradiation times, with the Ellman's assay. The difference here resided on the samples used for detection, all collected from the irradiation procedures of 3.5 h described in this session. The absorbance value considered was the one at 20 minutes of reaction, since the value at 412 nm stabilized earlier. Protein and Reagent blanks were also realized for each trial.

Time-dependent Fluorescence Emission of eLA at different pH values

The study of pH influence in the UV-sensitivity of eLA was in all similar to the one realized in the previous section. All conditions and experimental set-ups of illumination were equal except the temperature, which was maintained constant at 25 ºC in all sessions, the illuminated sample, which presented different pH values from session to session, and the voltage selected for Real-time correction, which was 1.81 V for the selected excitation at 295 nm.

Table 5.4: Buffers used for the protein solutions used in the illumination sessions and correspondent pH values.

pH	Buffer
4.56	Sodium Citrate 0.01 M
5.7	Phosphate Buffer 0.1 M
6.48	Phosphate Buffer 0.1 M
7.56	Tris HCl 10 mM
8.55	Tris HCl 25 mM
9.48	Sodium Carbonate 0.05 M
10.49	Sodium Carbonate 0.05 M

eLA concentration in the cuvette was always 1.85 μM, but the buffer used for the previous dilution was different, each of them specific for the pH value pretended (Table 5.4).

eLA UV-light irradiation coupled to CD measurements

The far UV-region of a circular dichroism (CD) spectrum assures a qualitative evaluation on the average secondary structure content of proteins (Neves-Petersen *et al.*, 2002). In particular, proteins containing a high content in α-helix, such as LAs, present a strong double minimum in far-UV CD spectra, at 222 nm and 210-208 nm. The intensity of these peaks reflects the amount of helicity in these proteins (Fasman *et al.*, 1996). Hence, CD spectroscopy was used to scan the relative changes induced by UV illumination in the conformation of eLA.

Table 5.5: Selected settings in the RTC 2000 PTI spectrometer for eLA steady-state illumination.

Temperature (ºC)	25.2
Stirring (rpm)	900
Excitation wavelength (nm)	295
Wavelength set in Detector 1 (nm)	340
Wavelength set in Detector 2 (nm)	295
Excitation slit (nm)	5
Emission slits (nm)	3
Real-time Correction - Excitation at 295nm	1 V

For that purpose a eLA sample was irradiated with 295 nm light using the same spectrofluorimeter and a similar experimental set-up than the referred in the previous sections. In order to obtain a clear far-UV CD spectra, a higher concentration of eLA was illuminated, 11.5 μM, and a 10 mM concentration was selected for the buffer (Tris HCl pH 8.55). The settings used for the illumination procedure are resumed in Table 5.5.

Before illumination, 3.5 mL of the eLA sample were introduced in the cuvette. The sample was illuminated during 10000 s but each 2000 s the experiment was stopped to remove a 300 μL sample for the further analysis. The stability of each removed sample (2000 s, 4000 s, 6000 s, 8000 s, and 10000 s) was immediately evaluated after extraction by far-UV CD spectroscopy. Non-illuminated eLA and the buffer were also probed by far-UV CD with the respective purposes of comparison and correction of the spectra.

The experimental parameters selected for acquiring the standard CD spectra are listed in Table 5.6. The 300 μL samples were placed in a quartz macrocuvette, with a pathlenght of 0.1 cm to check the amount of secondary structural feature of eLA in function of the illumination time. The CD wavelength scans were realized at room temperature in a JASCO J-715 spectropolarimeter and the measurements were controlled by the JASCO hardware manager.

Table 5.6: Experimental parameters for the standard CD spectra of a wavelength scan at 25ºC.

Parameters	
Mode	CD/HT
Range	240-200 nm
Band width (nm)	0.5
Resolution	1.0
Accumulation	3
Speed (nm/min)	5
Sensitivity (mdeg)	100
Response (s)	1
Buffer	10mM Tris HCl (pH 8.55)
Sample	eLA 11.5 µM
Test	0-, 2000-, 4000-, 6000-, 8000-, 10000-s illumination

Experimental set-up used for acquiring the fluorescence emission spectra at different temperatures

For obtaining a thermal unfolding profile of the protein form used approach consisted on recording the intrinsic fluorescence emission of the protein in a wide range of temperatures. For that aim, emission spectra of fresh samples of protein at different temperatures were recorded using the previously described RTC 2000 PTI spectrometer.

Two sets of spectra were measured, in one the excitation was fixed at 280 nm and in the other at 295nm. In the first set of experiments eLA concentration in the samples was 16.63 µM, while in the second 17.54 µM. In both protein in the samples was solubilized in 25 mM Tris HCl at pH 8.55.

The sample volume in the 1-cm path cuvette was 3mL and the stirring was maintained in the scans constantly at 650 nm. The excitation slits were selected at 5 nm, while the emission slits at 1 nm. Spectra were recorded with an integration time of 0.1 seconds. The pretended solution temperature was reached through the peltier element and the same hold time (at the temperature pretended) was selected in the PTI software. Since the scans were realized progressively (from the lowest to the highest temperature), after the introduction of a new fresh sample, the temperature pretended was reached rapidly and in a similar time gap in all cases. Temperature was maintained during the scans. Spectra with excitation fixed at 280 nm were recorded at 10.2, 18.2, 26.1, 33.6, 40.9, 49.4, 56.3, 63.9, 71.1, and 77.4 ºC. Spectra with excitation fixed at 295 nm were measured at 10.0, 18.2, 26.0, 33.6, 41.0, 49.0, 56.5, 64.0, 71.6, and 78.7 ºC.

The spectra with the excitation fixed at 295 nm were also realized with the buffer, in order to correct for *Raman Contribution*. No temperature effect was noticed in the *Raman Contribution* and for that reason only the spectra registered at 26.0 ºC was used for correction. The equivalent spectra were not recorded for the excitation fixed at 280 nm since the Raman signal does not affect in this case the maximum of emission.

5.2.2.2. Data Treatment and Analysis

Raman Correction

In certain emission and excitation spectra it was necessary to correct the values for *Raman Contribution* (*vide* Definition in Appendix C). The corrected emission values consisted simply on the subtraction between the original ones and the values obtained for the buffer, which at the wavelengths in play only absorbed and emitted light derived from the vibration of water molecules.

Smoothing Procedures

Some spectra obtained throughout the results displayed a considerable noise that was not convenient for visualization and for calculation procedures. Thus, in certain cases, which are outlined along the results presentation, a smoothing treatment of the data points was required. All smoothing procedures were performed by adjacent averaging in the program *Origin 7.5*. The emission and the far-UV CD spectra were smoothed using a 5 points average, while for the excitation spectra a 2 points average was chosen. Smoothing operations were realized prior to normalization procedures, if both were carried out.

Data Normalization

The normalized emission values of emission spectra, excitation spectra, and time-based fluorescence measurements consisted on the ratio between each data point (emission value) and the maximum value of emission registered in the whole spectra or over the entire illumination session.

Fittings and Plots

Non-linear fitting operations were realized using the program *Origin 7.5*. Linear fittings and plotting of the data were performed in *Excel*.

5.3. RESULTS ANALYSIS AND PRESENTATION

5.3.1. Time-dependent Disruption of Disulphide Bridges

5.3.1.1. Verification and Quantification

The first step of the characterization procedure consisted on verifying and quantifying the disruption of SS bonds upon UV irradiation on eLA. The stability issues of the protein will not be presented in this section; they will be addressed later on. It is just important to state that the experiments were realized at 25 ºC, and in 25mM of Tris HCl at pH 8.55, conditions for which eLA should be still stable. To probe the breakage of disulphide bonds over time, the intrinsic Trp fluorescence was scanned in solution, under constant illumination of UV light. Changes in the fluorescence intensity can provide clues regarding the UV induced mechanisms, since upon irradiation, the excited Trp species can be driven in a multitude of pathways, and consequently the fluorescence emission is indirectly affected. Particularly, it is known that in LA SS bonds quench substantially the excited state of Trp residues in LA. Upon breakage, the resultant thiols no longer act as quenching agents. Therefore, an increase in Trp fluorescence intensity may occur, if the broken SS bond was previously quenching a Trp residue.

Time-dependent fluorescence profile upon UV light exposure

The time-dependent fluorescence intensity of eLA at 340 nm upon illumination using 295 nm light is presented in Figure 5.3. During the first 6000 seconds (~1.7 hours) an accentuated increase in fluorescence (~17%) is observed, followed by stabilization in a short plateau region (from 2h to 3h of illumination) where the fluorescence intensity remains stable, and a posterior decrease in the counts.

This increase in fluorescence intensity is in agreement with a light-induced transformation of eLA. It could be due do light-induced separation between quenching groups and Trp residues or photoinduced chemical changes in the same groups (*e.g.* cleavage of SS bonds). The Trp residues, selectively excited, would no longer be as initially quenched, and could fluoresce more. As the sample is irradiated, the larger would be the number of protein molecules photo-transformed (with the quenching groups damaged), since they are spread in the agitated medium. At a certain point few would be the non-transformed protein molecules in solution, as the fluorescence intensity remains constant in the plateau, until other mechanisms overrule, which lead probably to the photobleaching (photodegradation) of Trp residues and decay in Trp fluorescence.

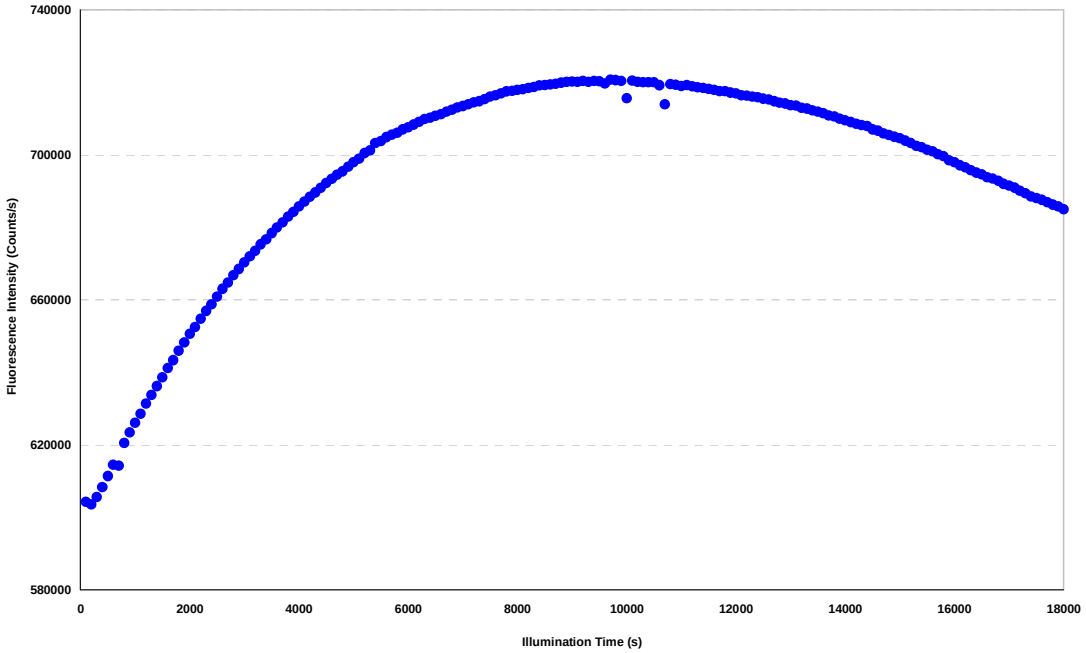

Figure 5.3: Fluorescence intensity of eLA *versus* illumination time. Excitation was fixed at 295 nm and emission was monitored at 340 nm. Temperature was maintained at 25ºC using a peltier element. Measurements were performed using a RTC 2000 PTI spectrofluorimeter as described in Materials and Methods (section 5.2).

The fluorescence profile displayed in Figure 5.3 corresponds to an illumination session of 5 h. In order to characterize the fluorescence behavior of the protein intrinsic fluorophores (Trp, Tyr and Phe) along the illumination procedure, the same experiment was also performed during other illumination periods (1h, 2h, 3h, 4h) (*vide* Materials and Methods, section 5.2). The fluorescence emission profiles obtained at 340nm were very similar to the one shown on Figure 5.3 (*vide* Figure B1, Supplementary Results in Appendix B), confirming the reproducibility of the 5h results.

Excitation (emission set at 340 and 320 nm) and emission spectra (excitation at 295 and 280 nm) were recorded at the end of each illumination session and for a fresh sample of eLA. The spectra were corrected for *Raman contribution* (description in Materials and Methods, section 5.4).

An assembly of the results respecting the first three hours of illumination (where the increase in fluorescence intensity is still observed), is displayed in Figure 5.4, including the emission spectra read after excitation at 295 and the excitation spectra taken with emission fixed at 340 nm. The increase in intensity is confirmed in the in the excitation spectra over the first 2 h of illumination and is correlated with the increase in the fluorescence readings in the emission spectra. In fact, in Figure 5.4, the emission is only probed at 340 nm and it is important to assure that the fluorescence increase is not just dependent on a possible wavelength shift of Trp

emission. Indeed, as can be noticed in Figure 5.4 the emission spectrum becomes strongly red-shifted with the illumination of the protein, presenting a maximum around 322 nm at the start of illumination and migrating until approximately 338 nm in the plateau region (~3h). Oppositely the excitation spectrum turns slightly blue shifted with the illumination of the protein.

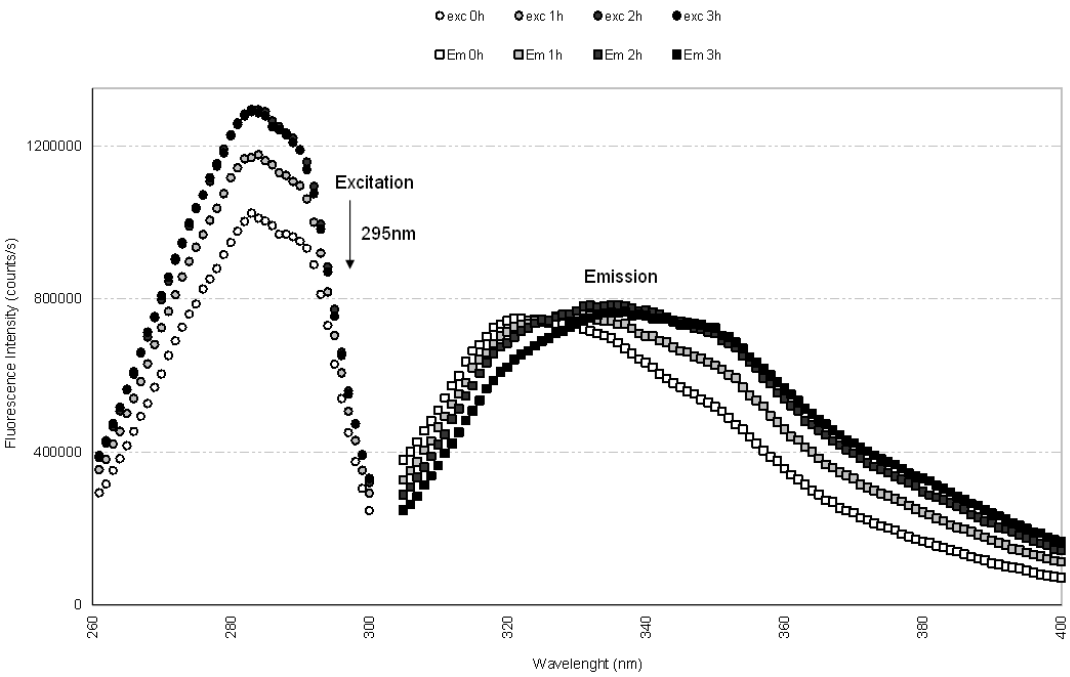

Figure 5.4: Effect of illumination time on the spectrum of excitation and emission. The spectra were recorded fixing the emission at 340 in the excitation spectra and the excitation at 295 in the emission one as described in Materials and Methods (Section 5.2).

The gradual red-shift of Trp fluorescence is clearly observed in Figure 5.5, where are gathered the normalized emission spectra recorded upon 295 nm light excitation for all irradiation sessions broadening the different time periods of illumination. It continues besides the plateau region (irradiation time > 2h), though the wavelength distance between emission maxima of two consecutive spectra turns lower with the extent of illumination. Ultimately the maximum of emission is swept to 340 nm at 5h of illumination. The first important detail that should be outlined is the existence of a red shoulder between 345 nm and 355 nm in the spectrum taken for the fresh sample. The emission of the four eLA Trp residues is overlapped in the emission spectra. This zone may be resultant of the fluorescence contribute of a Trp residue which sensitive to polarity due to solvent exposure, and thus emitting at higher wavelengths. From the structural analysis performed previously the most likely candidate would be Trp 118, which presents the higher ASA values for the crystallized proteins (*vide* section 4.2.2), and is located in a separate zone of the protein (aromatic cluster I). The remaining Trp residues dominate the emission, and should be more buried in the non-illuminated eLA, since the emission maximum of the spectrum

is located around 322 nm. Indeed, the other Trp residues of bLA (Trp 26, Trp 108 and Trp 60) are quite shielded from solvent and integrate aromatic cluster II, comprised within the main hydrophobic core of the protein.

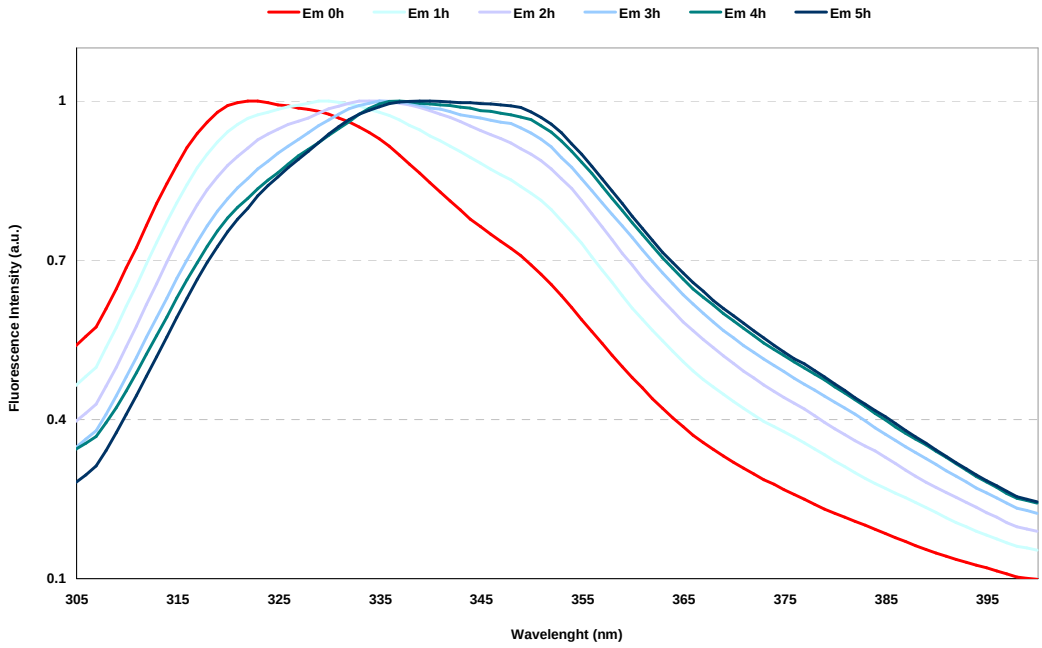

Figure 5.5: Normalized emission spectra of illuminated samples of eLA over different time periods and non-illuminated eLA. Excitation was realized at 295nm. The spectra were first smoothed and normalized as described in Materials and Methods (section 5.2).

The constant irradiation results in an increase of the fluorescence contribution in the shoulder region, while at lower wavelengths a blue shoulder is gradually formed (~315-325 nm). The shifts here described can be derived from the migration of one or more specific Trp residue(s) to more solvent accessible zones of the protein. It could be due to opening of the SS bonds e reconfiguration of the aromatic clusters of the protein, which results at least in the local unfolding of eLA in these zones.

Upon normalization, another interesting feature is also unveiled: the emission spectra took after 2, 3, 4 and 5h of illumination apparently cross each-other at approximately 337 nm. This crosspoint can be eventually an *isosbestic point* (see definition - Appendix C). Though different interpretations can be provided for the existence of *isosbestic points* in sets of electronic spectra, the situation in this case is probably simpler to read. Only one chemical specie should be involved, since the Trp residues are selectively excited. Thus, the *isosbestic* point could indicate the presence of an equilibrium in a photo induced reaction. On the reagent side would be present the Trp species which are characterized by an emission at lower wavelengths, which are slowly inter-converting into red-shifted products species, object of the illumination and possibly SS-bond breakage.

For the correspondent normalized spectra read after excitation at 280 nm (*vide* Figure B2, Supplementary Results – Appendix B), the red-shift is also visible, and takes place over the same distances. Such results indicate that Trp dominates fluorescence emission in the protein. This is expected since near 280 nm the Tyr groups are responsible for only one-fifth of goat LA absorption (Vanhooren *et al.*, 2002), which is similar to bLA in structure. The red shoulder is still visible for the non-illuminated sample, while the *isosbestic* point is not clear anymore.

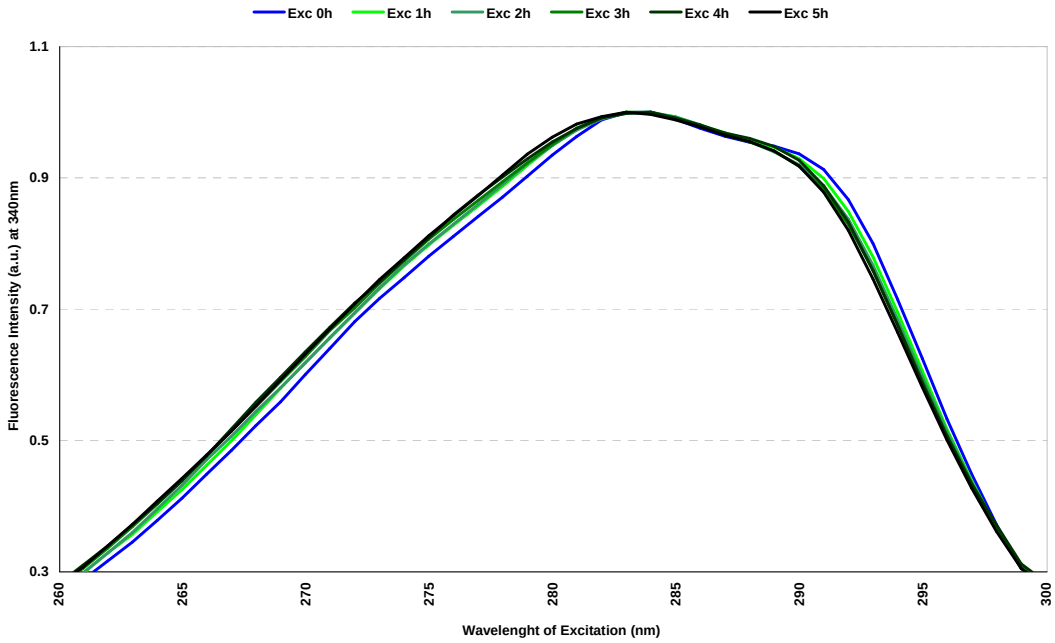

Figure 5.6: Normalized excitation spectra of illuminated samples of eLA over different time periods and non-illuminated eLA. Emission was selected at 340nm. The spectra were first smoothed and normalized as described in Materials and Methods (section 5.2).

The normalization of the excitation spectra provides further insight into the events in play. Both the spectra recorded with emission fixed at 340 nm and 320 nm (Figure 5.6 and Figure 5.7 respectively) show, in similarity to the observed for the emission spectra, that the fluorescence behavior of the intrinsic fluorophores is affected all along the illumination, even in the decay region. This shift signifies that with the illumination of the protein occurs an increase of the proportion of species that are excited at lower wavelengths in detriment of species excited at higher wavelengths.

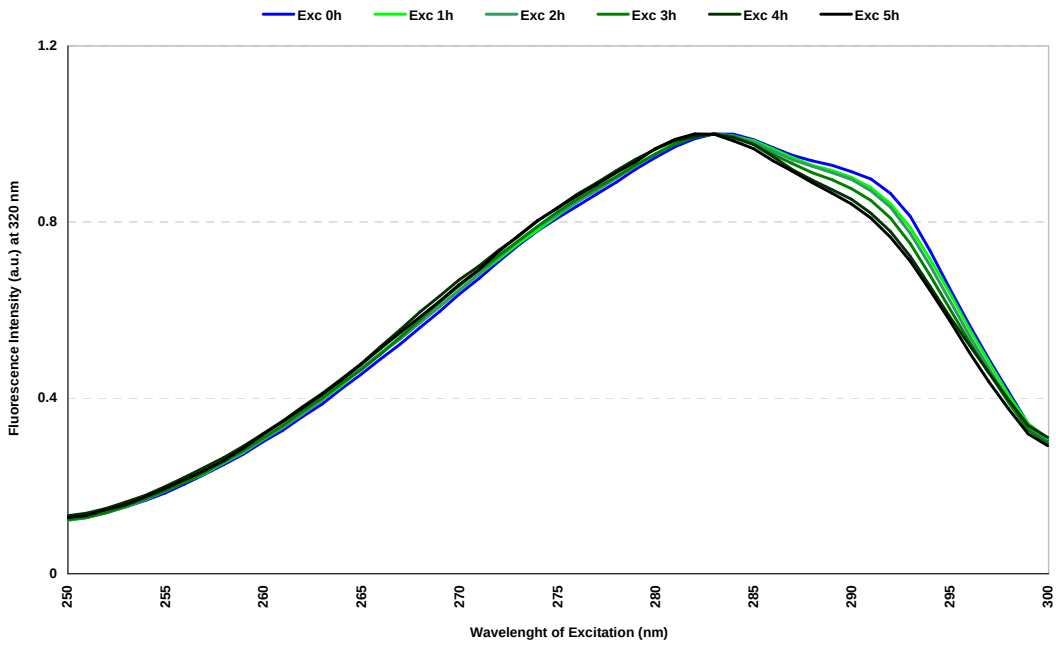

Figure 5.7: Normalized excitation spectra of illuminated samples of eLA over different time periods and non-illuminated eLA. Emission was selected at 320 nm. The spectra were first smoothed and normalized as described in Materials and Methods (section 5.2).

For an emission around 320 nm, this result is expected, since Trp species, as observed previously, tend to emit at higher wavelengths with the long-term irradiation, resulting in a reduced number of Trp emitting in that area and in an increase in proportion of the other protein fluorophores (Phe and Tyr) that are excited at lower wavelengths. This predictable shift is most likely reflected in the normalized excitation spectra on a large shoulder-decrease clearly visible in Figure 5.5 (285-296 nm interval).

The ratios between the normalized excitation spectra of the illuminated samples and the spectrum of the fresh sample provide an enhanced resolution on the spectral changes (Figures 5.8 and 5.9). In both plots (with emission fixed at 340 nm and 320 nm) can be observed a gradual ratio decrease in the zone where Trp selectively absorbs (290-306 nm), coupled to an increase in ratio below 283 nm that turns more intense at lower wavelengths. In the plot correspondent to the excitation spectra with emission fixed at 320 nm, there is a larger decrease of the ratio in magnitude and the specific spectral change spreads in a wider area (282-300 nm). This is mainly due to the overlapping effect of the shoulder-decrease before mentioned.

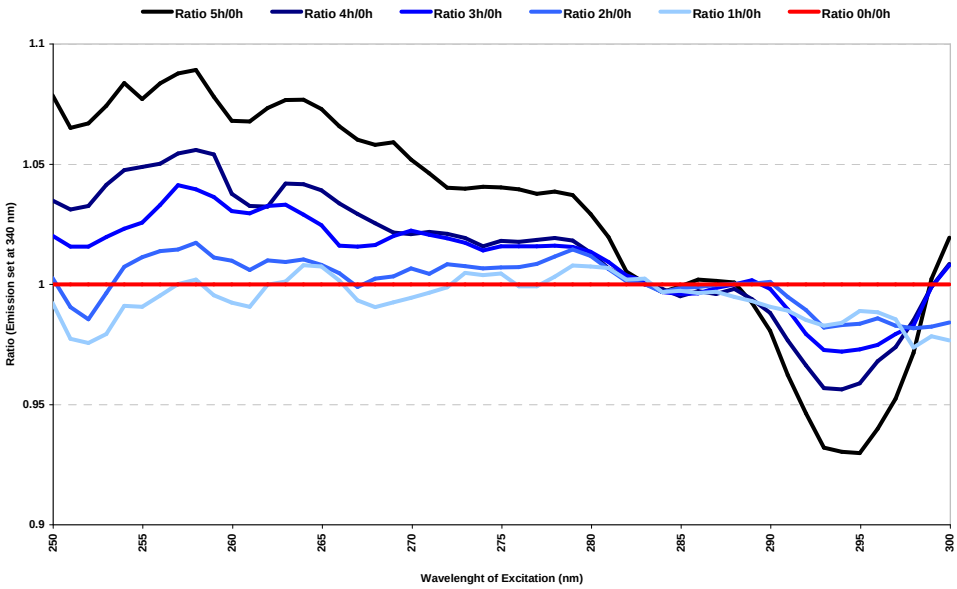

Figure 5.8: Ratio between the normalized spectra with the emission fixed at 340 nm displayed in Figure 5.6. The ratio is realized between the spectra took after different periods of illumination and the spectrum of the fresh eLA.

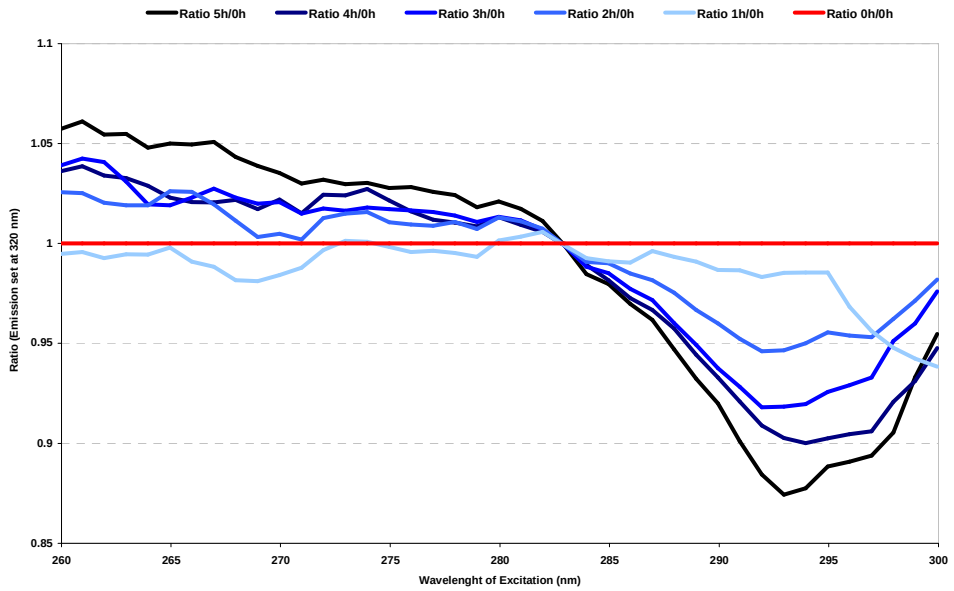

Figure 5.9: Ratio between the normalized spectra with the emission fixed at 320nm displayed in Figure 5.7. The ratio is realized between the spectra took after different periods of illumination and the spectrum of the fresh eLA.

This effect, whose causes were already advanced, may not be the only influence felt when fixing the emission 320 nm. The same event that affects the other excitation spectra

(emission fixed at 340 nm) could also be influencing the ratios at this wavelength. This general event that is characterized by a gradual decrease of ratio at 283-305 nm and increase at 290-305 nm could be due to the photobleaching of Trp residues. Upon illumination the proportion of Trp in the excited population would diminish, provoking the increase in proportion of other protein fluorophores (Tyr, Phe) in the population.

Quantification of the SS bond light-induced breakage with DTNB

In order to verify and quantify the possible disruption of the disulfide bridges under the UV illumination, a reaction assay was performed with DTNB after each illumination session previously mentioned (1h, 2h, 3h, 4h and 5h) and for a sample of non-illuminated eLA (*vide* Materials and Methods, section 5.2). In Figure 5.10 are displayed the absorbance values at 412 nm (A_{412}) obtained for each irradiation time and the time-dependent fluorescence emission increase at 340 nm obtained for the session of 5-h illumination.

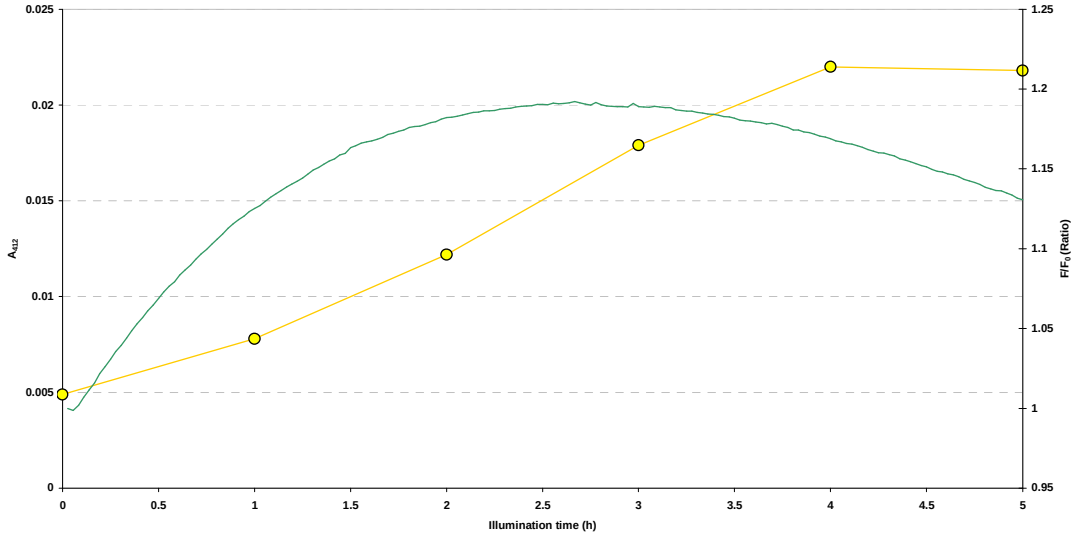

Figure 5.10: Values of Absorbance read at 412 nm (closed yellow circles A_{412}) *versus* illumination time. In green is displayed time-dependent fluorescence intensity increase at 340nm (F/F_0). The presence of free thiols was evaluated after reaction with 5,5´-dithiobis-(2-nitrobenzoic acid), after 0-, 1-, 2-, 3-, 4- and 5-h of illumination with 295 nm light, considering that the free thiol concentration is proportional to the absorbance value at 412 nm, as described in Materials and Methods (Section 5.2). F/F0 values displayed consist on the ratio between the monitored values fluorescence emission at 340 nm and the initial fluorescence emission value at 340 nm obtained for the 5-h illumination session. The values were corrected for lamp intensity oscillations as described in Materials and Methods (Section 5.2).

It can be noticed that A_{412} increases rapidly with Trp excitation in the first three hours of illumination, corresponding to the same zone where is noticed an exponential increase in fluorescence intensity. In the decay zone a raise of A_{412} is still noticed (between the assays realized for 3 and 4h of illumination) culminating in a lower value obtained at 5 h of illumination. Since the free thiol concentration is proportional to the value read at 412 nm (*vide* Materials and

Methods section 5.4), these results indicate that the continuous illumination with 295 nm induces an increase in thiol concentration. Therefore, it is confirmed in eLA the excitation of Trp residues provokes the cleavage of SS bonds. However, from these results no direct correlation can be realized between the increase of fluorescence intensity and breakage of SS bonds. Probably the absence of the SS bonds and other sterical configurations provoked by the breakage provoke a direct of indirect increase in fluorescence.

One of the absorbance values obtained was not expected. The value for 0 h of illumination presented a residual value, even after deduction of the blanks (*vide* Materials and Methods section 5.2). This result is doubtful since the protein even in the apo-form should not display any free thiol groups, since the four SS bridges should not easily be broken or reduced without the presence of an external agent. One plausible reason resides on the fact that the experiments with illuminated samples and the non-illuminated one were not realized in the same time frame. The blank assays were realized separately also, which could raise differences in the detection capacity of the instrument, and in the solution of DTNB stored in the cold. Indeed when compared the corrected spectra (reagent blank subtracted) of the irradiated samples and the fresh one (*vide* Figure B3 Supplementary Results – Appendix B), the characteristic peak of the absorbing 412 nm TNB^{2-} is only noticeable for the first ones. Nonetheless, ideally, the whole experiment should be repeated, which at the time was not possible.

Static light scattering

Since the irradiation of eLA leads to the presence of free thiol groups it was important to verify during the illumination procedure that there was no association or aggregation of protein molecules by means of inter SS bond formation. This was realized by simple measurement of the intensity of the light scattered in the illuminated samples. Upon illumination with light the dipoles set in oscillation emit also a secondary radiation with the same wavelength of incoming radiation, called Rayleigh scattering, or elastic scattering. For particles much smaller that the wavelength of light (radius $R < \lambda / 20$), which is the case of small globular proteins such as eLA , the intensity of the scattered light is only dependent on the size of the particles and not on the structure or their concentration. Therefore, if protein monomers associate, there should be a large increase in the emission signal at the wavelength of excitation.

In this line of thought the 295 nm emission of the samples irradiated with 295 nm light was constantly monitored in each of the previously mentioned illumination sessions (1h, 2h, 3h, 4h and 5h). The time-course of the normalized scattered light during each illumination is displayed in Figure 5.11. In the illumination sessions of 2h, 3h, 4h and 5h a decrease in intensity is noticed in the majority of the illumination session, despite that in the profiles of the 3h and 4h session there is a small initial increase in fluorescence. In the session of 1h illumination there is an increase in emission, though the slope turns less steep in the last minutes. Curiously, these

sessions in which an increase in 295 nm emission is found, present all a small initial decrease in the 340 nm fluorescence, for unknown reasons. Possibly, if the session of 1h illumination was proceeded, the decrease in light scattering intensity would be verified further in time. Despite these small incongruences, these results indicate that, in principle, very little or even no association takes place between proteins upon illumination with 295 nm UV light and for the concentration value here used.

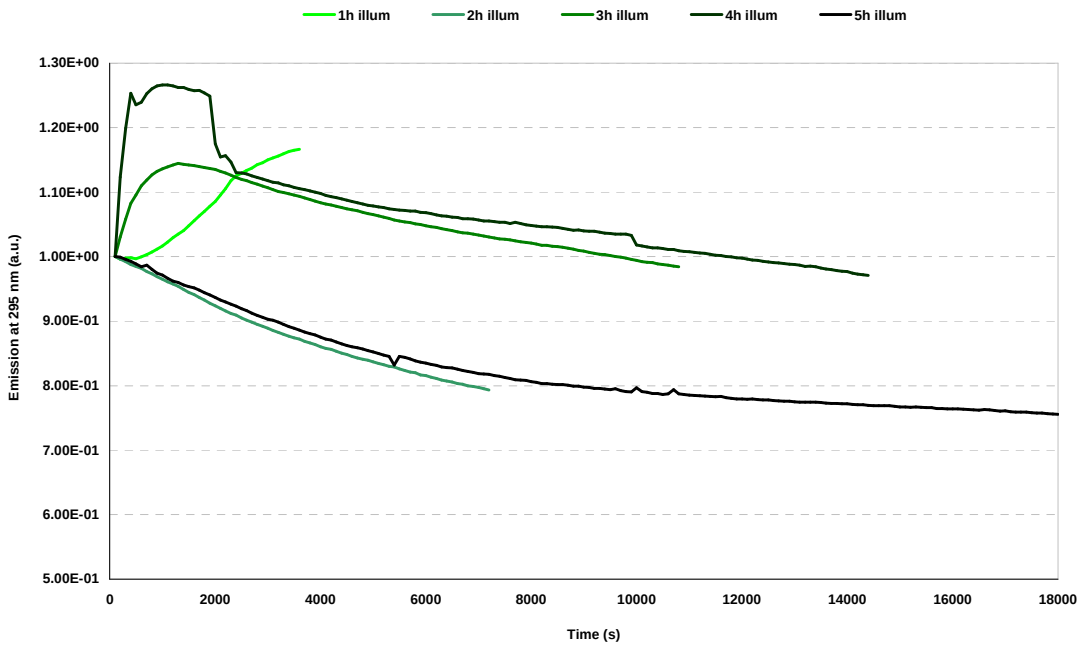

Figure 5.11: Ratio of the emission values at 295 nm during the illumination sessions. The emission of 295 nm light was checked constantly during the sessions of irradiation (1h, 2h, 3h, 4h, 5h) with 295 nm light using the second channel of the spectrofluorimeter. The values are corrected for the light source oscillation and were normalized as described in Materials and Methods (Section 5.2).

Choice of the Concentration

The majority of the illumination sessions realized in the characterization procedure were run using protein solutions with concentrations of about 2 μM. This reference value was chosen in virtue of earlier experiments with the protein. From these trials it was deduced that higher concentrations could imply longer illumination sessions for obtaining the whole fluorescence emission profile (zone of fluorescence increase, plateau, decay) (Data not shown). Since the all the profile is needed for analysis, this time gap could complicate the scaling and planning of the experimental procedures and even jeopardize the integrity of the protein. Using high concentrations of protein can also have natural implications in a good fluorescence reading of the sample, *e.g.* inner filter effect. Higher concentrations could also drive to a closer proximity

between protein molecules. Upon disruption of the SS bonds this proximity can favor the possibility of cross-linking.

5.3.1.2. Influence of external parameters

In sequence to the verification of SS bond disruption upon UV illumination it was interesting to check the effect of external parameters like temperature or pH in the mechanisms involved. Such evaluation could, for instance, help to understand the conditions in which the immobilization process would be more favored.

Temperature Dependence

To study the effect of temperature on the photo-triggered mechanisms in eLA a similar approach than the one realized for the verification procedure was realized. In this case, instead of illumination time, the changed variable from session to session was temperature.

The normalized time-based fluorescence measurements realized with emission fixed at 340 nm upon constant irradiation with 295 nm light are displayed in Figure 5.12. The fluorescence time-dependent profile recorded for the majority of the temperatures follows the same tendency than the presented in Figure 5.3, *i.e.* a strong initial increase in fluorescence intensity, followed by stabilization in a plateau region, and eventually a decay phase (only visible for some temperatures in the 3.5 hours of illumination). The exception to this common fluorescence behavior is the experiment at the most elevated temperature, 34.6 ºC, for which can be noticed a constant decay in fluorescence emission all along the illumination session.

As can be observed in Figure 5.12, in the trial realized at 9.3 ºC data points are lacking in the last 2000 seconds of illumination, resulting in an incomplete profile. This was due to experimental problems. Unfortunately, it revealed difficult to maintain the solution temperature at such low values with the peltier element used, during the whole period of illumination. The profile here displayed corresponds to the experiment for which the peltier element remained longer efficient. Thus, the data points in display correspond to the phase where the temperature was still maintained at 9.3 ºC.

The effect of temperature is at first sight evident. The lower the temperature is, the steeper the slope of initial fluorescence increase, originating fluorescence increases superior to 25 % for the three lowest temperatures. Coupled to this, is the fact that for lower temperatures, the plateau is only reached further in time. Only for the illumination procedures realized at 12.9 and 15.9 ºC, it is hard to trace this general pattern, since they present very similar profiles, which is natural since the temperature margin between these two experiments is the lowest among all.

Assuming that the increase in fluorescence is originated from SS bond breakage as described in the previous section, this influence of temperature in the fluorescence increase

indicates that at least one of the processes or reactions that originate this rupture in this protein is temperature dependent.

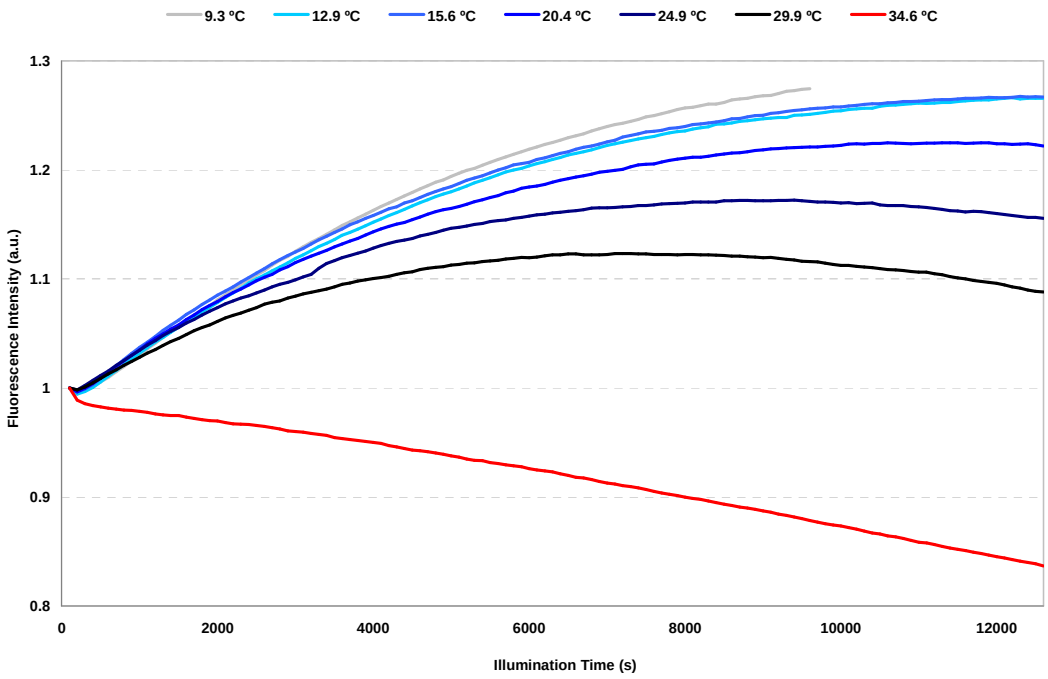

Figure 5.12: Fluorescence intensity of Bα-L in function of the illumination time at different temperatures (9.3, 12.9, 15.6, 20.4, 24.9, 29.9 and 34.6 ºC). Excitation was realized at 295 nm and emission measured at 340 nm. Measurements were effectuated using a PTI spectrofluorimeter during 3.5 hours. The temperature of the solution was maintained constant using a Peltier element. The curves were normalized and corrected for the oscillations of lamp intensity as described in Materials and Methods (Section 5.2).

In order to understand the effect of temperature in the kinetics of a possible reaction, the fluorescence emission time-based curves obtained for the different temperatures (Figure 5.12) were fitted using an exponential function. Since for the curve obtained at 24.9 ºC within this experimental set-up presented a deviation around 3000s, for the fitting was used a different run realized also at 24.9 ºC within the same time period, with a very similar profile.

$$F(t) = C_1 + C_2 e^{-kt} \tag{5.2}$$

The curves were fitted according to Equation 5.2, where $F(t)$ is the fluorescence intensity measured at time t, C_1 and C_2 are constants, and k the rate constant of exponential fluorescence increase. The physical interpretation of this equation is that the irradiation of Trp species (one or more Trp of the protein) induces a first order reaction involving only one protein molecule.

A fitting criterion was adopted, to overcome the divergence in the temperature profiles, and to exclude the initial small decrease in fluorescence (first minutes). The fitting was realized in all assays for the data sets between the first point in time which that majored 80% of the

maximum fluorescence emission and the first that overcome 95% of the maximum fluorescence emission, so only in the emission increase zone. This way the fittings are comparable since they were realized considering data points located in same zone of the profiles for all temperatures. The fittings were also realized for the normalized data points. The fitted parameters, as the correspondent errors, mean square errors (R^2), and reduced Chi square errors, for each of the fitted temperature curves, are displayed in Table 5.8.

Table 5.7: Parameters values and correspondent errors, root mean square errors, and reduced chi square errors obtained after fitting of time-based fluorescence curves using equation 5.2.

T (ºC)	C_1	C_2	k (s^{-1})	R^2	Red. Chi^2
9.3	1.37 ± 0.004	-0.402 ± 0.003	1.64E-04 ± 2.73E-06	0.99986	4.90E-07
12.9	1.33 ± 0.002	-0.356 ± 0.001	1.71E-04 ± 1.44E-06	0.99995	1.41E-07
15.6	1.32 ± 0.002	-0.340 ± 0.001	1.87E-04 ± 1.67E-06	0.99994	1.60E-07
20.4	1.25 ± 0.002	-0.274 ± 0.001	2.26E-04 ± 2.57E-06	0.99992	1.42E-07
24.9	1.20 ± 0.003	-0.221 ± 0.002	2.49E-04 ± 5.64E-06	0.99989	9.28E-08
29.9	1.16 ± 0.008	-0.174 ± 0.007	2.88E-04 ± 2.07E-05	0.99977	6.39E-08

The fitting curves, and the correspondent residual plots, are present in the supplementary results (Appendix B) for further insight.

The fitted values obtained for the constants show that temperature affects the time-dependent fluorescence intensity of the sample in a bivalent fashion. Both constants C_1 and C_2 decrease (in module) with rise of temperature, whereas the rate constant k increases. The values of C_1 and C_2 cannot be used to quantify any phenomenon, since the values used for fitting were normalized, to overcome possible divergences between the diverse experiments. Despite this fact, the important notion that should be extracted is that these two constants counteract the effect of the rate constant upon temperature change, and dominate the shape of the curve. This explains why in the curves of Figure 5.12 the slope of fluorescence intensity is steeper with the decrease of temperature, while the rate constant of exponential increase k decreases.

On the contrary to the other constants, k has a physical meaning, characterizing the one-step reaction. The constant should thus be dependent on temperature in accordance to the Arrhenius law:

$$k = Ae^{-Ea/RT} \tag{5.3}$$

where Ea is the energy of activation ($J.mol^{-1}$), R the universal gas constant for perfect gases (8.135 $J.K^{-1}.mol^{-1}$), and T the temperature in Kelvin. The linear relationship between the logarithm

of the rate constant values displayed in Table 5.8 and the inverse of temperature is confirmed in Figure 5.13, with the correspondent linear fitting and mean square error (R^2).

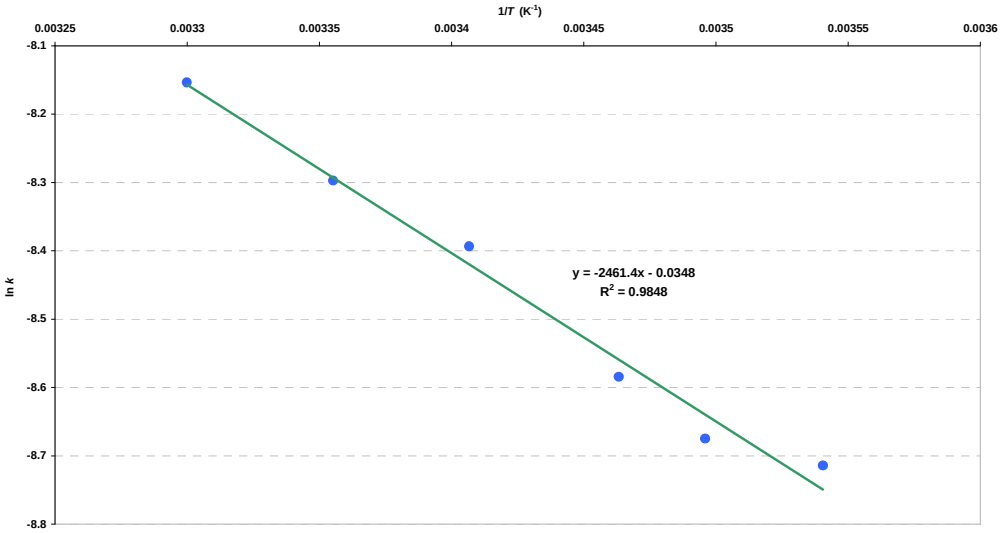

Figure 5.13: Linear relation between the logarithm of the rate constant ln *k* and the inverse of temperature 1/*T*. The linear regression trendline is also displayed in the plot as the equation and the root mean square error R^2.

The energy of activation can be then calculated from the slope of the linear regression (-*Ea*/*R*). The energy of activation obtained characterizes the process affected by temperature, presenting a value of about 20.5 kJ.mol^{-1}.

Following the same approach than the used in the study of illumination time influence, excitation (emission set at 340 and 320nm for each channel) and emission spectrum (excitation at 295 and 280nm) were also recorded after each fluorescence illumination session (run at different temperatures) and for fresh samples of α-L (with the temperature set previously in the spectrofluorimeter). To be noticed that the spectra were corrected for *Raman contribution*. The emission spectra recorded upon excitation at 295nm before and after illumination (3.5 h) are displayed respectively in Figures 5.14 and 5.15.

When comparing both figures it is possible to confirm the raise of Trp emission noticed in fluorescence time-based profiles (Figure 5.12) for the temperatures concerned (15.6 to 29.9 ºC), coupled here again to a red-shift, presenting the same transition spectral traces (upon illumination) than the ones focused at 25 ºC in section 5.2.1.1. For evident reasons it was not possible to record the emission spectrum after illumination at 9.3 ºC. The fluorescence increase screened in emission is again coupled to the increase in the excitation of the protein fluorophores as depicted in the excitation spectra taken (Data not shown).

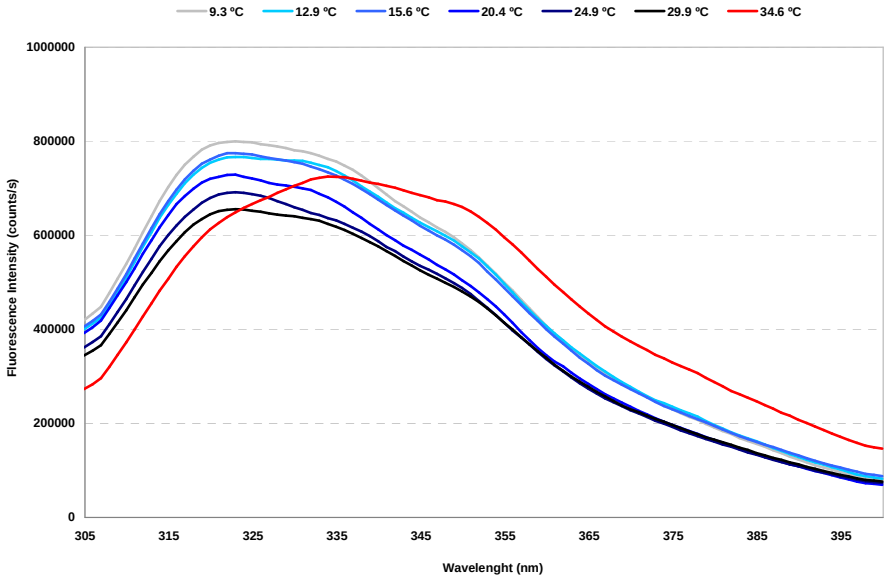

Figure 5.14: Emission spectra of non-illuminated eLA at different temperatures (9.3, 12.9, 15.6, 20.4, 24.9, 29.9 and 34.6ºC). Solution temperature was previously set using the peltier element. Excitation was realized at 295nm. The spectra were first smoothed as described in Materials and Methods (section 5.2).

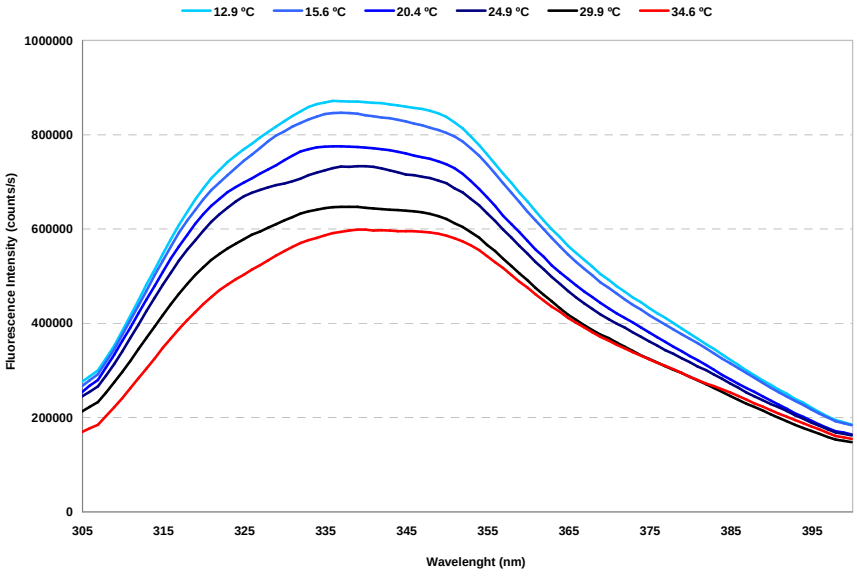

Figure 5.15: Emission spectra of eLA recorded after 3.5h of 295nm light irradiation at different temperatures (12.9, 15.6, 20.4, 24.9, 29.9 and 34.6ºC). Excitation was realized at 295nm and the temperature of the solution was still maintained after the precedent irradiation and during recording of the spectra. The spectra were first smoothed as described in Materials and Methods (section 5.2).

In the fresh solutions, at 34.6 ºC Trp fluorescence is already red-shifted to 334 nm when compared to the lower temperatures, which present all the same emission maximum at approximately 323 nm. This could explain the absence of a fluorescence increase profile, in virtue

of a structural modification of the protein. Nonetheless, illumination at this temperature provokes a red-shift of 4nm in the emission maximum coupled to the decrease in the counts.

The emission spectra recorded at 280 nm (*vide* Figures B16 and B17 Supplementary Results – Appendix B) display the same pattern, indicating roughly that between 29.9 ºC and 34.6 ºC there should be a thermal transition in this form of eLA.

This matter will be further discussed when addressed the thermal stability of the protein.

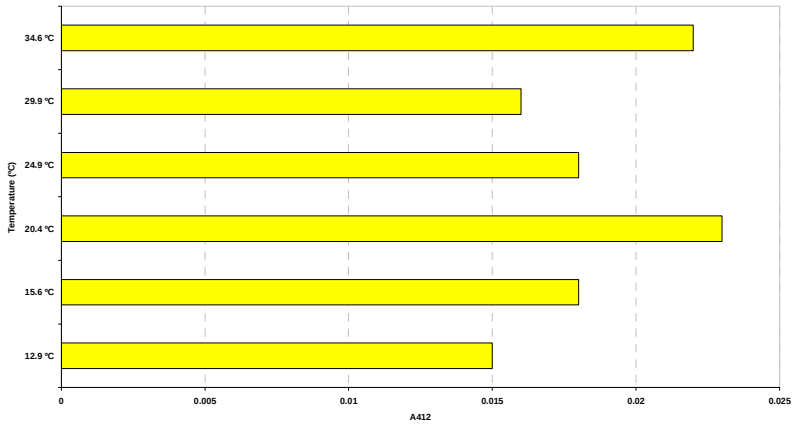

Figure 5.16: Values of absorbance at 412 nm after 20 minutes of reaction between the irradiated samples at different temperatures, and DTNB (*vide* Materials and Methods, section 5.2).

The Ellman's assay with DTNB was also performed immediately after each illumination session to verify the presence of free thiols and the breakage of the SS bonds, in the irradiated solutions. As can be noticed in Figure 5.16 there a relatively strong absorbance signal was noticed after mixing with DTNB for all the samples, with the same magnitude as the values for the plateau region in the verification procedure presented before (section 5.2.1.1), attesting the presence of free thiols, even after irradiation at 34.6 ºC. No explicit correlation with temperature can be outlined, just in the three lowest temperatures there seems to exist an increase in thiol concentration with the temperature increase.

pH Dependence

The influence of pH on UV light-triggered reaction mechanisms was studied considering the same approach than the used in the case of temperature. The time-dependent fluorescence intensity at 340nm upon irradiation with 295 nm UV-light was checked for diverse solutions of eLA, which were prepared from different buffers and presenting different pH values (4.56, 5.7, 6.48, 7.56, 8.55, 9.48, and 10.49). The corresponding time-based fluorescence profiles are displayed in Figure B18 in the Supplementary Results section (*vide* Appendix B).

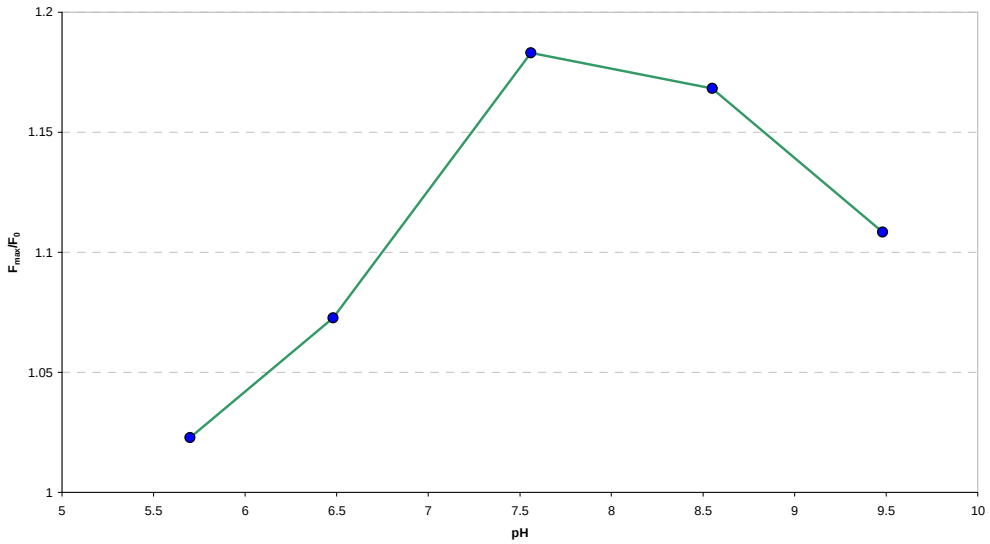

Figure 5.17: Fluorescence emission maximum increase at 340 nm of eLA upon prolonged 295 nm UV-light irradiation for different pH values. The points F_{max}/F_0 consist on the ratio between the maximum emission value of the time-based fluorescence emission profile (at the plateau) and the fluorescence emission at time zero. The fluorescence time-dependent curves from where these values were obtained are present in the Supplementary Results (Appendix B).

No increase in fluorescence emission was noticed for the solutions characterized by extreme pH values (4.56 and 10.49), just a constant decay. For the intermediate pH values, an increase in fluorescence was noticed with the same time-dependent profile than the presented in Figure 5.3. The maximum fluorescence emission increase (emission at the plateau) obtained for each of these pH values at 340 nm is displayed in Figure 5.17. The higher values of increase are noticed for pH values near neutrality: 7.56 and 8.55. This probably indicates that at neutral pH values the quenching of the Trp residues is less prominent. However, it is not possible to affirm, based only on these results, that the photo-degrading mechanism of quenchers or cleavage or SS bonds is favored at these pH values. Since the protein is in the apo-form the conformational structure is strongly affected by the pH of the solution. Moreover the buffers used presented diverse ionic strengths and the implications to protein conformation could be variant and unpredictable from experiment to experiment. Thus, one cannot predict if the relative positions of the quenchers relative to the Trp are affected.

5.3.1.3. Effects of illumination on the secondary structure

Acknowledged that irradiation of eLA with 295 nm UV light induced specific structural changes in this form of eLA, including the breakage of SS bonds, and exposure of Trp residues, it was important to evaluate the implications of such modifications in the general conformation of the protein. For that aim, far-UV circular dichroism (CD) spectroscopy was used to check possible conformational changes in the secondary structure of the protein over different periods of UV-light illumination, complementing the fluorescence studies presented in 5.2.1.1.

As previously described in Materials and Methods, a 11.5 µM eLA sample was irradiated with 295 nm, and the fluorescence intensity was monitored at 340 nm. The experiment was stopped each 2000s to remove a sample for further analysis. The stability of each removed sample (2000s, 4000s, 6000s, 8000s, and 10000s) and of a non-illuminated one was evaluated by far-UV CD spectroscopy. The steady-state fluorescence profile of the entire illumination session is displayed in Figure 5.18.

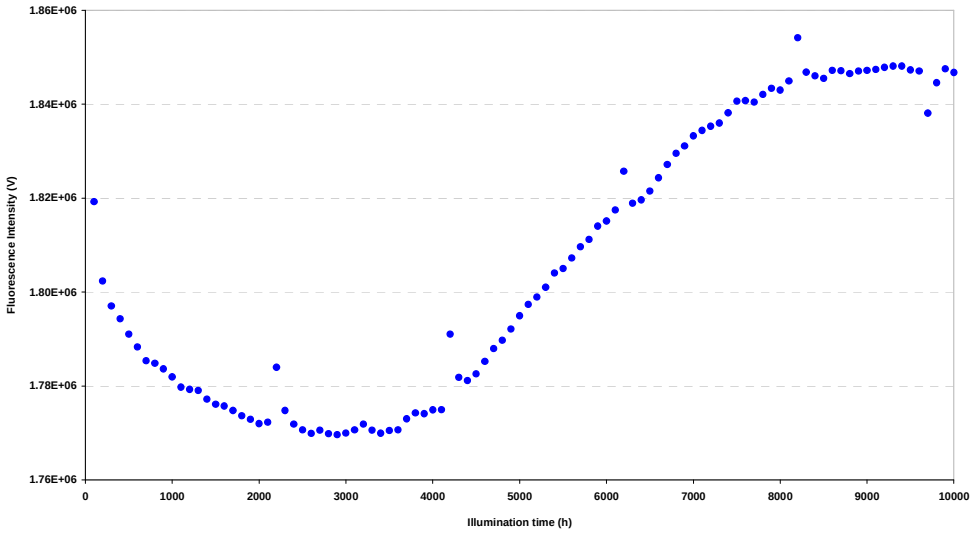

Figure 5.18: Fluorescence intensity of eLA *versus* illumination time. Excitation was fixed at 295 nm and emission was monitored at 340 nm. Temperature was maintained at 25ºC using a peltier element. The experiment was stopped each 2000s to remove a protein sample. The emission values are corrected for the oscillations of lamp intensity. Measurements were performed using a RTC 2000 PTI spectrometer as described in Materials and Methods (section 5.2).

The time-dependent fluorescence emission upon irradiation with 295 nm of the 11.5 µM protein sample is similar to the previously observed in the verification procedure (Figure 5.3) and in the temperature experiments (Figure 5.12), just with the difference in a small decrease in intensity in the early phase of the experiment.

The effects of illumination on the secondary structure can be observed in Figure 5.19, where is displayed an overlay of the recorded far-UV CD spectra. Although some fluctuations are noticed, the overall trend is the partial loss of the secondary structure the longer the sample was illuminated, with progressive slight loss of ellipticity. Although these changes are noticed, irradiated eLA should still present a considerable amount of secondary features, since the spectra of the irradiated spectra still present the minimum at ~210-208 nm.

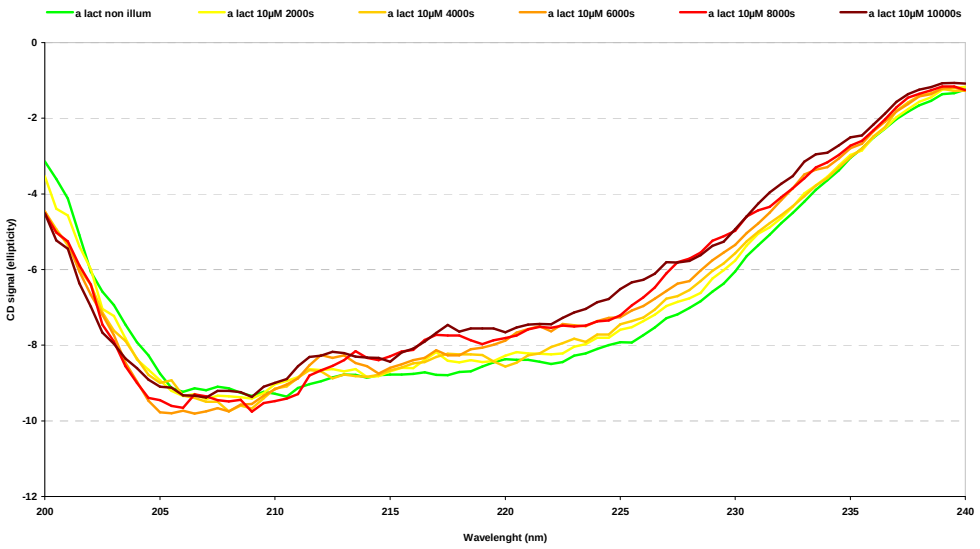

Figure 5.19: Far-UV CD scan of 295 nm light irradiated eLA samples (0-, 2000-, 4000-, 6000-, 8000-, and 10000-s of illumination) recorded at pH 8.55 and room temperature. The measurements were realized in a JASCO J-715 spectropolarimeter. The spectra were corrected for the buffer contribution in ellipticity and smoothed as previously described in Materials and Methods (Section 5.2). Although some fluctuations are noticed, the overall trend is the partial loss of secondary structure the longer the collected sample was illuminated.

It is not possible to correlate the increase of fluorescence with the changes in the secondary structure. The experimental set-up should affect the fluorescence emission, since the volume removed at each stop (clearly visible in the time profile by a raise in fluorescence emission) is considerable (8% of the initial volume), resulting in a final volume of 2 mL compared to an initial of 3.5 mL. The usage of this setup was forced by the experimental conditions needed in a clear far-UV CD scan. Protein concentration of approximately 10 µM is needed for a clear spectra in far-UV CD, along with a buffer concentration of 10 mM (*vide* Material and Methods). In the required conditions the fluorescence profiles were extremely different at each illumination session, probably due to the joint effect of using higher concentrations and lower ionic strength. This last variable specially is probably the destabilizing factor, rendering the protein more sensitive to external changes.

Nonetheless, with the approach used, the effect on the secondary structure is clear, even if the effect over illumination time could not be reasonably quantified.

5.3.2. Thermal Stability of the Protein

As was advanced in the literary review realized over α-LA (Chapter 4), this protein, especially in its apo-form, is very sensitive to external factors, like ionic strength or temperature. Thus, it is required to evaluate the conformation adopted by the protein in the experimental conditions used for characterization. Once again, fluorescence spectroscopy was used to the

thermal stability of the protein form, since temperature was the main destabilizing agent in the experiments, and to explore the conformational features of the protein, in the apo-form obtained.

The thermal stability of the protein was checked by probing the intrinsic fluorescence of fresh solutions of protein stabilized at a wide range of temperatures (10-80ºC). The emission of the protein at a certain temperature was checked by excitation of fresh 17.54 µM eLA solutions at 295 nm and at 280 nm.

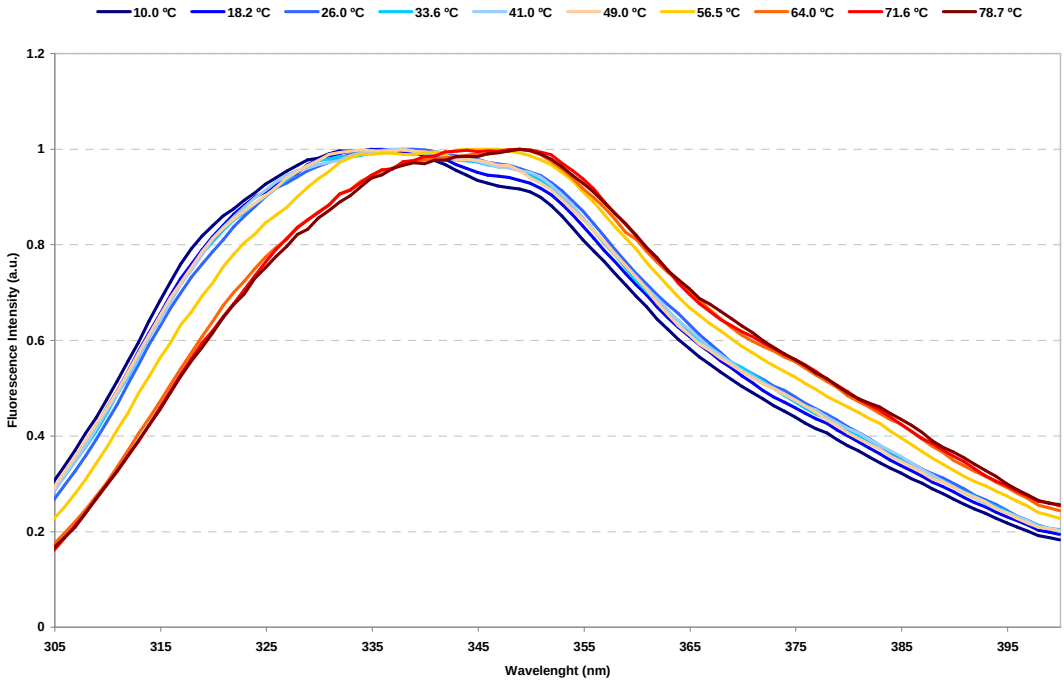

Figure 5.20: Normalized emission spectra of fresh eLA solutions recorded at different temperatures (10.0, 18.2, 26.0, 33.6, 41.0, 49.0, 56.5, 64.0, 71.6, and 78.7 ºC). Excitation was realized at 295nm and the temperature of the solution was set before the recording of the spectra and during the short irradiation. The spectra were smoothed and normalized as described in Materials and Methods (section 5.2).

The solution temperature was set previously, considering the same hold stabilization time for each temperature, and the resulting emission spectra after excitation at 295nm were corrected for *Raman contribution* as described in Materials and Methods (Section 5.2). In Figure 5.20 are displayed the normalized emission spectra correspondent to excitation with 295 nm light for the different temperatures tested. A red-shift is noticeable in Trp fluorescence when the spectrum is taken at higher temperatures. This red-shift is quite similar to the observed when the protein is irradiated with UV-light (section 5.2.1.1), with an increase in the population of exposed Trp in the red-shoulder area, which is severed at temperatures higher than 48.0 ºC. Besides the red-shift is there is a decrease in fluorescence emission with the temperature increase, which can be noticed in the original spectra (non-normalized – *vide* supplementary results, Appendix B). This was already verified in the temperature characterization (section 5.3.1.2). In the spectra recorded

upon excitation at 280 nm, the same red-shift is noticed, as also the increase in fluorescence counts (*vide* supplementary results, Appendix B).

In order to clearly visualize the occurring red-shift, the wavelengths values of emission maxima (λ_{max}) after excitation at 295 and 280 nm are plotted in function of temperature in Figures 5.21 and 5.22.

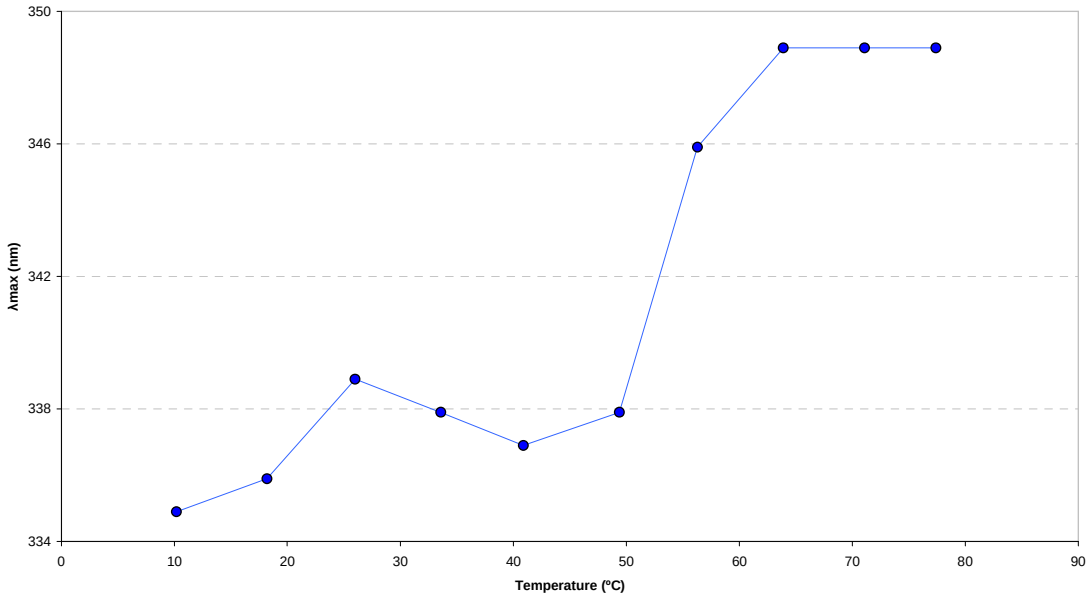

Figure 5.21: Maximum of emission of eLA upon excitation at 295 nm (λ_{max}) *versus* the solution temperature.

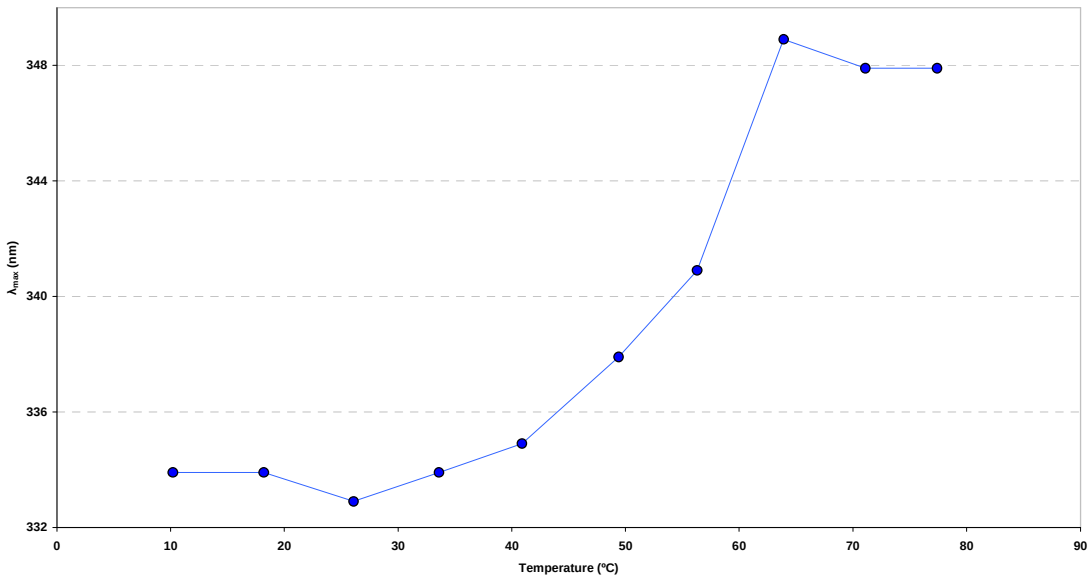

Figure 5.22: Maximum of emission of eLA upon excitation at 295 nm (λ_{max}) *versus* the solution temperature.

The first important fact that should be retained from both figures is that the λ_{max} noticed in these results for low temperatures (<25ºC) are quite higher than the observed in the temperature characterization procedure (Figures 5.14 and B.16 in Appendix - λ_{max} ~322-324 nm for excitation at 295 nm and 280 nm). The main experimental difference between the two sets of experiments is eLA concentration, which here is ten times higher. The Trp residues, sensitive to solvent polarity, are here more exposed, for higher concentrations of eLA.

Both the figures describe in a general form the thermal unfolding of the protein. Upon excitation at 295 nm there are two experimental points that could be outliers and erroneous, the ones corresponding to temperatures of 28.0 and 33.6 ºC. The unfolding at 295 nm (Figure 5.22) characterizes only the Trp residues, and probably only part of them, given the already debated increase of fluorescence intensity in the red shoulder area of the spectrum for high temperatures. If the two experimental points before mentioned are not considered, the profile of the unfolding denotes a transition characterized with by T_m between 50 and 70 ºC. The thermal unfolding is more patent in the points obtained from the excitation procedures realized at 280 nm (Figure 5.21), characterizing the exposure of part of both Trp and Tyr residues of the protein, and shows more clearly the existence of a cooperative thermal transition of the apo-form in these conditions, with a T_m between 40 and 70 ºC.

In the temperature characterization procedure, a strong wavelength red-shift was felt between spectra of lower temperatures, 29.9 and 34.6 ºC, from ~323 nm of λ_{max} to 334 nm (Figures 5.14 and B16) . The strong shift in that case probably induces a conformational transition in eLA since after 3.5 h of illumination, only at 34.6 ºC is not noticed an increase in fluorescence intensity.

This particular thermal transition is not noticeable in these results. The aromatic clusters should be already partly destabilized at this range of temperatures as described before. Since the concentration is higher in these experiments, it could be that the impact of ionic strength in eLA (the concentration of the buffer is the same in both experimental procedures) is more felt in the experiments realized for the temperature characterization procedure. Thus, these eLA samples, which are more concentrated, could be more instable.

5.4. DISCUSSION

Before analyzing specifically the UV sensitivity of the protein model it is important to clarify the conformational features of the apo-forms of LA obtained here in solution. In most part of the characterization procedure eLA concentration was ~2 µM in 25 mM Tris HCl pH 8.55. In non-irradiated samples corresponding to these conditions and at low temperatures Trp emission is typically centered at ~322 nm (*vide* Figures 5.5 and 5.14). In solution and at neutral pH Ca^{2+} loaded bLA shows a fluorescence emission maximum of 325 nm (Engel *et al.*, 2002). The

proximity of both values indicates that most of the Trp residues in the eLA apo-form are buried as in native bLA. Moreover in diverse procedures the behavior of this eLA apo-form upon exposure to UV-light is similar, showing similar spectral traces, and reproducible results.

To study the stability of the eLA in solution, its thermal unfolding was probed by fluorescence spectroscopy (section 5.3.2). However, these experiments were conducted using higher concentrations of eLA (17.44 μM) and spectral changes in Trp emission were noticed for low temperatures (<30ºC). Probably the ionic strength is not high enough to stabilize completely eLA in the absence of calcium for these concentrations. Nonetheless, eLa at 17.54 μM (and in 25mM Tris HCl pH 8.55) presents apparently a cooperative thermal unfolding in the regions where Trp is located. MG forms of eLA, which are typical products of LA unfolding under denaturating conditions, do not present usually a cooperative unfolding (Pfeil *et al.*, 1998), and generally are an equilibrium mixture of substates (Chang *et al.*, 2001), so probably this form of eLA in solution presents still a native-like structure, as the model described for apo-LA in Chapter 4. In the temperature characterization realized for the form of eLA at 2 μM, the Trp emission spectra of non-irradiated samples show a possible conformational transition between 29.9 and 34.6 ºC (Figure 5.14), which was not observed in this thermal denaturation. The fluorescence behavior at 34.6 ºC upon continuous UV-irradiation is markedly different than at lower temperatures, not presenting an increase in fluorescence intensity at 340 nm. It is possible that this transition, not observed in the thermal unfolding, is a first step of eLA unfolding, in which the aromatic clusters are disarranged, particularly relatively to quenching groups, not yielding the same fluorescence spectral changes than at low temperatures.

At low temperatures (<29.9 ºC) for the samples of ~2μM, eLA should be stable in solution, presenting a native-like conformation, and retain the majority of the packing interactions in the aromatic clusters, as it is indicated by he degree of Trp burial. The Trp emission spectra of all non-irradiated of eLA shows an interesting red-shoulder, which is not noticed in previous fluorescence experiments is it with bLA (Engel *et al.*, 2002), or apo and native goat LA (Vanhooren et al., 2002). This shoulder could derived from the fluorescence contribute of the more exposed Trp118, attending that this Trp may be less quenched in this form of LA displaying an increased fluorescence than usual, and that the aromatic cluster I may be more disarranged. Trp118 could be extremely more exposed than expected.

It is patent, though, that the concentration of eLA and buffer influenced tremendously the experiments, which is natural considering the analysis of the protein model realized before (Chapter 4). For instance in CD experiments, which were conducted at the lowest ionic strength (10 mM Tris HCl pH 8.55), no reproducible results for the time-dependence of the fluorescence emission of eLA were obtained. eLA in solution adopts probably in these conditions a more unstable conformation.

Prolonged excitation of Trp residues in eLA induces an increase in fluorescence yield coupled with a red-shift in Trp emission. This fluorescence behavior of this apo-version of bLA (2 µM sample) was observed for temperatures below 29.9 ºC. It correlates well with previous observations realized in Ca^{2+} loaded and depleted human, bovine (Permyakov *et al*., 2003) and goat (Vanhooren et al., 2002; Vanhooren *et al.*, 2006**a**) forms of LA, for which light induced SS bond breakage was noticed.

The increase in fluorescence yield with the illumination time is presumably related to the progressive cleavage of SS bonds mediated by Trp excitation, and with the absence of these groups as potential quenchers. In eLA the time-dependent profile of fluorescence emission at 340 nm shows a relatively strong increase in intensity in the first hours of illumination of (Figure 5.3 and 5.12). The rate at the fluorescence intensity increases seems to diminish in an exponential way. This was confirmed by the fitting procedures realized in the temperature characterization (Section 5.3.2 – Table 5.7). Fluorescence quantum yields stabilize latter in a plateau region, with a final decrease in last minutes of irradiation. Such time-dependent emission profile has been observed previously in other UV sensitive proteins like cutinase (Neves-Petersen et al., 2002) and horseradish peroxidase H2 (Neves-Petersen *et al.*, 2007). In both cases the increase in fluorescence yield was attributed to putative light-induced dissociation and/or photoinduced damage of strong fluorescence quenchers proximal to aromatic residues of the proteins. While in horseradish peroxidase H2, this increase was attributed to damage of the close prosthetic group, in cutinase was proven the direct relationship with disulphide bond cleavage. Cutinase displays only one Trp residue in direct contact with a disulphide bond and for that reason it is easy to relate the two events (*vide* Sections 3.3.3 and 4.4). The increase in thiol groups was found to be correlated to the time-dependency of fluorescence increase. In bLA, the richness in SS bonds, Trp residues and other quenchers requires a more extensive analysis to prove that cleaving of SS bonds is really the cause of this phenomenon, and determine the Trp residue(s) involved. To be noticed that the fluorescence increase noticed on eLA is quite reduced when compared to the observed in cutinase (*vide* Figure 5.3 - a maximum of 19% increase is registered in the plateau *vs* an increase superior to 8 fold in cutinase), and the plateau phase is only reached way further in illumination time.

For eLA, disruption of SS bonds was observed upon prolonged excitation of Trp residues recurring to the Elmann's assay (Figure 5.10), but the experimental data is insufficient to relate directly the cleavage and fluorescence increase. For an apo-form of goat LA (which presents the same four Trp residues and a similar structure to native bLA – *vide* Table 4.1), Vanhooren et al. (2003) noticed that upon constant UV light irradiation the rate at which the free thiol groups were formed apparently decreased in an exponential way. Such rate dependence, noticed at different temperatures and also for Ca^{2+} loaded forms of goat LA, is concordant with the remarks above. This correlation indicates that the relation exist probably, and could be verified upon repetition

and optimization of the Elmann's assays here executed. A larger number of samples irradiated during different periods of 295 nm-light should be tested.

The fluorescence increase felt at 340 nm is also partly provoked by the pronounced red-shift in eLA Trp fluorescence. After 5 h of constant irradiation Trp emission maximum is swept from 322 nm to 340 nm (Figure 5.5), which indicates a progressive local unfolding of eLA under irradiation, as Trp residues are dislocated to solvent accessible areas of eLA. Trp in water has an emission maximum of 348 nm, and the fully denaturated form of native goat LA on 6 M guanidinium hydrochloride has a maximum of emission of 345 nm (Vanhooren et al., 2006**a**). Thus, the hydrophobic clusters of eLA should not be completely unfolded upon irradiation. Curiously, emission around 340 nm is a typical property of molten globule forms of LA, particularly the acidic form at pH 2 (Vanhooren et al., 2002).

It is hard to predict the global conformational changes that the tertiary structure of eLA suffers upon irradiation. As stated previously, breakage of Cys61-Cys77 and Cys73-91 was found in goat and human LA upon Trp prolonged excitation (Vanhooren *et al.*, 2006**a**; Permyakov *et al.*, 2000). As mentioned before Cys73-91 holds together the two subdomains of LA and Cys61-Cys77 is located within the β-subdomain. Upon their breakage the α-subdomain remains structured while the β-subdomain is disarranged, as shows a construct of LA where the cysteines that form this SS bonds are substituted by alanines (Wu *et al.* 1995). In goat LA is also found the light-induced cleavage of Cys6-Cys120 (Vanhooren *et al.*, 2006**a**). The three-disulphide form of LA with a reduced Cys6-Cys120 is similar to intact native LA in secondary and tertiary structure (Moriarty *et al.*, 2000). The far-UV CD spectra of eLA irradiated samples here recorded (Figure 5.19) show a progressive but low loss of secondary features on irradiation with 295 nm light. The helical structures of eLA should be retained even after illumination. Vanhooren *et al.* (2003) noticed similar changes far-UV CD spectra for an apo-version of goat LA. Reversely the far UV spectrum recorded by the same authors revealed profound losses of ellipticity. These remarks indicate that the UV-triggered cleavage of disulphide bridges in LA induces the loosening of the tertiary structure of the protein, mostly in the aromatic clusters (where are located the intrinsic fluorophores), but not in the secondary features, maintaining most of the α-helical content.

Upon continuous Trp excitation in human α-LA, Permyakov *et al.*(2003), found three types of protein components after gel chromatography of the irradiated sample. One was representative of the native protein (emission upon excitation centered at ~328-329 nm), the other with a red-shifted Trp fluorescence (emission maxima at ~339-340 nm), and the last with non-tryptophan fluorescence. In the eLA Trp emission spectra recorded here after distinct durations of irradiation at 25ºC (Figure 5.5), the formation of such red-shifted species is also noticed. Upon illumination, there is a progressive increase of intensity in the red-shoulder region

of the spectrum, dislocating the emission maximum to 340 nm. The blue-shoulder formed gradually with irradiation could advent of the overlapped emission of the remaining native protein portion that did not suffer any conformational changes (*e.g.* splitting of SS bonds). The presence of an *isosbestic point* indicates that a reaction may occur yielding these red-shifted Trp species from lower wavelength emitting Trp species. The red-shifted species display also higher fluorescence quantum yields, this indicating that they should be related to the SS-bond breakage. The validity of this *isosbestic point* could be discussible, since it is originated from the normalization of spectra. However, in several other procedures was proven that hidden *isosbestic points* such as this one may appear after normalization of electronic spectra and have a significative meaning (Panda and Datta, 2008; Pouet *et al.*, 2004). Here, since the two species present divergences in fluorescence quantum yield, it is not possible to notice the *isosbestic point* without normalizing.

The last component described by Permyakov et al. (2000) displaying nontryptophan fluorescence corresponds evidently to the protein fraction that has its Trp residues photochemically degraded by exposure to UV-light. The photochemical destruction of Trp residues is probably the main responsible for the decay of fluorescence intensity felt after 2.5 h of illumination (Figure 5.3). It also explains the increasing the blue shift displayed in the excitation spectra with the extent of illumination (Figures 5.6 and 5.7). The ratio of Trp available to be excited is diminished, which results in a raise in ratio of Tyr and Phe excited, which absorb at lower wavelengths (Figures 5.8 and 5.9). Upon excitation at 313 nm this component in human LA emits with a maximum centered at ~417 nm, resembling the emission of N-formylkynurenine. The absorption spectra of irradiated goat LA present a shoulder at 310-325 nm, which increases with time of irradiation. Oppositely to the observations in human LA, the irradiated protein does not fluoresce upon excitation at these wavelengths. Therefore, it is possible that several fates for Trp photochemical destruction exist, depending on the specie and conditions. It is important to empathize that human LA possesses only three Trp residues, lacking the most fluorescent Trp 26, which could greatly influence these reaction pathways.

It is interesting to look more profoundly into the equilibrium translated by the presence of an *isosbestic point*. For the light-induced cleavage of the SS bond in cutinase, Neves-Petersen et al. (2002), proposed a theoretical model which assumed a chemical exchange between two species that slowly interconvert. The original species are the protein molecules with their SS bonds intact, yielding the photo-cleaved species that are characterized by a higher quantum fluorescence yield. Due to internal processes after Trp excitation the excited low quantum yield species would convert to high the high quantum yield species. The conversion is regarded in the model as a probabilistic event, and the time-dependent fraction of low quantum yield species depends on factors such as power of the irradiation or the absorption (volume, concentration).

The model successfully described the time-dependency of the fluorescence intensity in cutinase (increase).

The presence of an *isosbestic point* in the eLA successive spectra suggests that a similar event occurs in this protein, with the UV triggered conversion between the original low quantum yield species to transformed species characterized by a red-shifted emission and higher quantum yields. The presence of these two elements in the separated products of human LA irradiation supports such reaction mechanism.

It was not possible to fit the time-dependent fluorescence curves of eLA with the expressions resultant of the model proposed by Neves-Petersen et al. (2002), since the application of model can not be applied satisfactorily in the experimental conditions used the irradiation procedure of eLA. Certain criteria are not fulfilled, such as the full illumination of sample volume.

Alternatively, the temperature time-dependent fluorescence eLA curves (Figure 5.13) were fitted with an exponential function. It is assumed that excited Trp are involved in a first order reaction, and that the extent of the reaction (rate constant) is proportional to the rate constant of fluorescence exponential increase (*k*). The products of the reaction would be the 340 nm fluorescent Trp species. In this model possible reactions that lead to fluorescence intensity decrease are despised, such as the reverse reaction or photo-destruction of Trp residues. In that case a bi or tri-exponential function should be used for fitting, and the decay phase of the profile should be included. Irradiation was realized always for 3.5 h and the decay phase was not present in most of the profiles. With the determination of *k* for different temperatures it was expected to learn more about the possible reaction kinetics.

The errors obtained for the fittings (Table 5.8) and the fitting curves and residues (Supplementary Results in Appendix B), indicated that the model above can successfully be applied to describe the time-dependent fluorescence of eLA.

The values of the fitted parameters show, as evidenced in the presentation of the results, two distinct tendencies. *k* increases with the temperature raise, while C_1 and C_2 diminish. The increase of *k* with temperature signifies that the reaction mechanism in which the Trp excited species of eLA are driven is favored by temperature increase. On the other hand, the Trp excited species, upon involvement in reaction pathways do not radiate emitting fluorescence, which explains the diminishment of fluorescence for higher temperatures, mathematically translated in the values of C_1 and C_2.

As advanced before, for Trp alone in solution an increase of temperature from 4 to 37 ºC can raise aqueous electron formation (e_{aq}^-) from excited singlet Trp states in a fivefold way or more (*vide* section 3.3.2). The increase of *k* with temperature quite considerable, the fitted value at 29.9 ºC is almost the double of the one at 9.3 ºC. The only decay pathway of Trp excited

species that is known to be temperature dependent is the thermal ionization from the S_1 relaxed state (5.4) (*vide* section 3.3.2).

$$^1\mathrm{Trp} \xrightarrow{k_{ion}} \mathrm{Trp}^{\bullet+} + e_{aq}^{-} \quad (5.4)$$

Sherin *et al.* (2003) studied the temperature dependence of Trp excited states ionization. This group determined that the rate constant of Trp thermal ionization (k_{ion}) at pH 7.1 varied with temperature according to the Arrhenius Law yielding pre-exponential factor $A_{ion} = 2.3\times10^{15}$ s and energy of activation Ea_{ion} = 50 kJ/mol. As described in the Analysis of the results *k* shows similar temperature dependence with an Ahrrenius activation energy Ea = 20.5 kJ/mol. The values of the activation energies are quite proximal indicating the thermal photoionization is one of the major mechanisms activated upon excitation of the Trp species, and precedes the increase in fluorescence intensity. The energy of activation required for photoionization in eLA is smaller than for Trp in solution. In eLA the presence of other groups in the vicinity of Trp residues could both favor the ionization of the excited Trp, diminishing the energy barrier required for this mechanism. For instance, it is known that lysine and histidine may quench the Trp excited species by proton transfer to neighbor amino groups. The proximity of electron acceptor groups such as protonated carboxyl groups, SS bonds, amides, and the peptide bond could be another factor (section 3.2.2). Indeed, while studying the 3D structures of the two bLAs (Figures 4.6 and 4.7), the close proximity of lysine residues, SS bonds and peptide chain was referred.

This mechanism yields the formation of a solvated e_{aq}^-, which as described previously (*vide* section 3.3.1). The e_{aq}^- may trigger a wide number of photoinduced mechanisms in proteins, including the breakage of SS bonds. The latter probably occurs in eLA, if the correlation between SS bond breakage and exponential fluorescence increase is considered. In that case it would be probably the sole pathway described by exponential fluorescence increase upon e_{aq}^- electron release. Temperature dependence is observed for all the temperature curves, so this mechanism is expected to occur in the range of temperatures 9.3 – 29.9 ºC. For higher temperatures it is not excludable that the same mechanism occurs. In fact cleavage of SS bond is noticed at 34.6 ºC. eLA is probably folded differently at this temperature, implying changes in the positions of the Trp residues and probably the quenching groups, which modify its fluorescence behavior.

The cleavage of SS bonds upon e_{aq}^- release can occur by several mechanisms (*vide* section 3.3.1), is it by direct capture of the e_{aq}^- by the cystine residues (5.5), or indirectly implying the reaction with the peptide chain (5.6), yielding of ketyl radical $-\dot{C}(OH)NH-$ that can propagate along the chain and react with the SS bond.

$$e_{aq}^{-} + RSSR \rightarrow RSSR^{\bullet -} \quad (5.5)$$

$$e_{aq}^{-} + \text{-CONH-} \rightarrow OH^{-} + \text{-}\dot{C}(OH)NH\text{-} \quad (5.6)$$

The second mechanism does not depend on the distance between the excited Trp residues and SS bond, as the first one or as the electron transfer from the triplet state ^{3}Trp (*vide* sections 3.3.1 and 3.3.3)., Vanhooren *et al.* (2006**a**) observed that the light-cleavage SS bonds in goat LA is associated with the cross-linking of cysteine with lysine residues. Such event is noticed for breakage of Cys6-Cys120 and Cys73-Cys91 with formation of Cys6-Lys122 and Cys91-Lys79 or Cys73-Cys93 (only one free thiol radical is formed in each case). Through the construction of four goat LA mutants, each one with a Trp residue substituted by a Phe, this group discovered also that the breakage of Cys6-Cys120 is exclusively mediated by Trp26. The two entities are too distant for a direct contact (in goat LA the distance is 14.5 Á), so a plausible mechanism would be a propagation reaction like the described here (5.6). The formation of Cys6-Lys122 sustains such possibility. Moreover, lysine radicals are known to form intramolecular –S–NH– with cysteine residues when radicals (Fu et al., 2002). The similarity between bLA and goat LA, and the observed distance between the two referred entities in holo-bLAc and apo-bLAc (14.81 and 13.36 Á respectively) indicate that the cross-linking could also occur in eLA.

By the same approach Vanhooren *et al.* (2006**a**) determined the mutual presence of Trp26 and Trp104 may be essential for the photo-cleavage of Cys73-Cys91 in goat-LA. Again the distances between these Trp residues and this bonds are far elevated (10.9 and 7.7 Á), and the lysine cross-linking is found, indicating a possible important contribute of e_{aq}^{-} in the cleavage.

Evidently, it is not excluded that other mechanisms are involved in the fluorescence increase and SS bond breakage, such as the electron transfer from the triplet state to neighbor SS bonds. Indeed for goat LA, Trp60 is the major contributor for SS bond cleavage and is in proximity of the broken Cys 61-77 and Cys73-Cys91. Furthermore, for the first of the bonds no cross-linking with lysine was observed.

Observation of the successive Trp emission spectra of eLA (Figure 5.5), for which the *isosbestic point* is visualized, can help to trace some conclusions regarding the Trp species involved in the reaction mechanisms. If the red-shoulder present in the emission spectrum at 0h irradiation represents truly the fluorescence contribute of Trp118, this residue should not be involved in reaction equilibrium translated by the *isosbestic point* and possibly in the fluorescence increase. In fact for goat LA Trp 118 is considered the Trp residue that contributes the less to the thiol formation. This is likely due to the fact that Cys28-Cys111 is not found broken after illumination (Vanhooren *et al.*, 2006**a**).

One of the other Trp residues should be involved in this equilibrium upon excitation, the most likely being Trp26, that dominates emission in LA (*vide* section 4.2.2).

As mentioned before the contribute constants C_1 and C_2 counteract the increase of fluorescence dictated for higher values of *k* with temperature raise. The increase of temperature favors the yielding of e_{aq}^-. This should result in an increase of SS bond formation and consequently of fluorescence quantum yield. However e_{aq}^- can be driven to other reaction pathways (*e.g.* reaction with molecular oxygen or H_30^+ ion from the buffer – section 3.3.2) and induce further damage to the Trp residues or to the protein itself. Therefore, at higher temperature these mechanisms are also favored, which would explain also the decrease in fluorescence yield for higher temperatures.

Finally it is important to discuss other important experimental indications regarding eLA as a candidate for eLA immobilization. Assuming that the increase in fluorescence is correlated to the cleavage of SS bonds the pH characterization procedure indicates that neutral pH values favor the breakage mechanisms (Figure 5.17). At alkaline pH values the production of e_{aq}^- should be favored, but eLA is also more unstable, which could invalidate the increase in fluorescence, and does not interest for immobilization since the molecule is not kept intact.

Static light scattering measurements in eLA (Figure 5.11) indicate that little or almost no association takes place between eLA molecules with broken SS bonds. In the studies realized by Permyakov *et al.* (2003), the SDS-page electrophoresis data of the illuminated human LA showed no oligomeric forms. Oppositely, SDS-page and gel filtration results of Vanhooren *et al.* (2003), demonstrate that after 6 h UV-irradiation of an apo-form of goat LA monomers, dimmers, trimers and polymers are formed. However the fraction of intact monomers (0.66) is still considerably high. Therefore it should be expected that the indications of the static light measurements are accurate and polymerization by intra-SS bounding is not a problem for the proposed light-induced immobilization. However, it is hard to predict which thiol reactive group would be immobilized.

The implications of SS bond breakage in the structure of the protein are difficult to predict, as advanced *supra*. UV-modified human LA shows no cooperative thermal spectral changes, showing that the protein should be mostly in a denaturated form (Permyakov *et al.*, 2002). The implications to the protein functionality are not well defined. The UV-changed component of human LA above mentioned still shows Ca2+ binding capability, though with lower affinity than the native-like human LA (Permyakov *et al.*, 2002). Since several conformational changes are expected near or in the active site (aromatic cluster I, and hydrophobic cores)for lactose synthase regulation, it is expected that eLA looses most of this functionality in the products of irradiation (340 nm Trp emitting proteins – with SS bonds broken). In native-like goat LA ~35 % of the original lactose synthase regulatory activity is conserved after 3 h irradiation (Vanhooren et al., 2006**a**). However it is not known if this activity is originated from the still intact

goat LA or photo-transformed protein. This test should be realized in eLA in the photo-transformed protein after separation of the irradiation products.

Since the cleavage of three disulphide bonds can be expected in LAs (Cys61-Cys77, Cys73-91 and Cys6-Cys120), a potential immobilization of eLA onto a surface could occur by all these three possibilities, which would have different impacts on the protein structure. Of the three disulphide bonds, Cys6-Cys120 should be the most accessible for surface binding upon cleavage, since it is locate in exposed areas of both holo-bLAc and apobLAc. On the other hand, Cys61-Cys77 and Cys73-Cys91 are almost completely shielded from the solvent, which would difficult an immobilization. Additionally, only for Cys6-Cys120 is not noticed cross-linking with lysine residues in goat LA, so two thyil radicals could be available for reaction, and the radicals should be free of sterical interference in the bounding. Nonetheless, the effects of illumination on the position of these Cys radicals are not known.

Resuming, characterizing eLA as a potential candidate light-induced immobilization candidate is a delicate issue. Light-immobilization onto thiol derivatized surface or gold surfaces should be expected since the formation of thiol groups is confirmed and is favored by prolonged illumination with UV-light. However, the reaction mechanisms in which are driven the excited species of Trp are extremely complex and no strong conclusions can be taken for the best conditions for immobilization. Neutral pH and low temperatures should be preferable since the protein should be relatively stable and the cleavage of SS bonds still takes place. Moreover the calcium depleted forms of eLA revealed in solution a high instability upon slight changes in solvent conditions.

6. IMOBILIZATION PROCEDURE

6.1. PREMISSES

During the extent of the project, considering the progressive uptake of information resultant of eLA characterization, several light immobilization procedures were tried. The disruption of SS bonds in the protein upon Trp excitation was early confirmed using the Elmann's reaction, as displayed in the characterization results. Therefore it was assumed that free thiol groups should be present to react with thiol derivatized surfaces or gold upon prolonged UV-illumination, at least in the experimental conditions used in that assay.

Before and during this project, immobilization of eLA in quartz derivatized slides was tried using the LIMI technology developed by the group, and previously described. For a wide number of solvent conditions and eLA concentrations, (covering the used in the characterization procedure), and output power, the immobilization was not successful (Parracino, A., Kold, A., Personal Communication).

As an alternative, light induced immobilization was attempted in solution, using gold nanoparticles (AuNP). Bain *et al.* (1989) demonstrated that molecules carrying thiol groups can absorb with extreme efficiency onto gold surfaces, upon the covalent binding of the thiol moiety to the gold atoms in the surface. As previously reviewed (section 3.3), the thiol groups provenient from photo-reduction in proteins are very reactive, which should facilitate the covalent bonding,

In solution eLA is perfectly hydrated and the molecules can be homogeneously illuminated upon stirring. Furthermore, with the agitation of the medium, the reaction between the free solvent thiol groups of the protein and the gold atoms of the nanoparticles surface is promoted. Moreover, if well dispersed in solution, AuNP provide a high surface area for immobilization.

The light-immobilization into AuNP was realized with a similar experimental set-up than the used in characterization for probing the fluorescence time-based emission of eLA. An eLA sample is constantly illuminated with UV-light in the spectrofluorimeter, in order to break the disulphide bonds. The kinetics of cleavage are already known, since similar experiments were realized during the characterization procedure of eLA, and the fluorescence emission of the protein can be probed during the experiment. At the desired moment, AuNP can be introduced in the cuvette to react the produced thiol groups of the protein in solution. This can be either during the process, by pausing the illumination session, or in the beginning, before this procedure. Replacement of one molecule with another is favored by using an excess of a new molecule while providing enough heat and/or sonication (Templeton *et al.*, 1999). Consequently, the concentration of eLA used in solution was always approximately 2.5 times higher than the

concentration of AuNP after addition. Heat and/or sonication were not possible to use in risk of damaging the protein, so during reaction, magnetic agitation was always promoted. After reaction the particles (with or without eLA immobilized) and eLA were separated by centrifugation, due to the difference in molecular weight.

The size estimation of separated, fresh particles and eLA was carried out using Dynamic Light Scattering (DLS). The purification technique (removal of excess protein) and characterization of immobilization procedure (verification of protein immobilization into AuNp were studied using UV-visible spectroscopy. Additional characterization was realized by probing the fluorescence of the nanoparticles, and by further measurements using Scanning Electron Microscopy coupled to Energy Dispersive X-ray spectroscopy (SEM-EDS).

6.2. MATERIALS AND METHODS

6.2.1. Materials

Preparation of AuNP

Sodium Citrate ($C_6H_5Na_3O_7.2H_2O$), Gold (III) chloride tryhydrate ($HAuCl_4,3H_2O$) were procured from E-Merck. 0.01 M Au^{3+} and 0.1 M sodium citrate mother solutions were used for synthesis.

Protein and Buffer Solutions

Protein and buffer solutions were prepared using the same sources and procedures than the presented in the Materials section of the eLA characterization procedure (Section 5.2.1).

6.2.2. Methods

6.2.2.1. Preparation of AuNP

Gold cation in the form of $AuCl_4^-$ can be reduced by using biocompatible weaker reducing agents (Cushing *et al.*, 2004). Moreover, the reducing agent can also serve as an organic capping agent that is normally used to prevent agglomeration of nucleated particles. Turkevich process is the well-known example for the same, where the synthesis of citrate capped AuNP was carried out by boiling a mixture of dilute $HAuCl_4$ and sodium citrate (Enüstun *et al.*, 1963).

2 ml of the 0.01 M gold salt solution transferred into 48 ml of de-ionized water. The solution was heated to boil on constant stirring. On boiling, 0.4 ml of 0.1 M sodium citrate solution was added rapidly and left at the same temperature and stirring for 30 min. The solution turned to deep red color of characteristic gold colloids indicating the reduction of Au^{3+} to metallic gold (Au^0).

The suspension was cooled to room temperature and washed twice with water using the centrifugation technique. The suspension was centrifuged at 10000 RPM for 10 min. and supernatant liquid that contains very small particles, excess surfactant and reaction byproduct salts was decanted. Bottom agglomerated particles were re-dispersed in water and the same process was repeated for another time. After second wash, bottom settled citrate coated gold particles re-dispersed in buffer solution. The suspension was used for characterization and further immobilization experiments. From the molarities of the above reaction, the concentration of gold nanoparticles (AuNP) and citrate surfactant is determined. Respective concentrations of 0.4 mM and 0.8 mM were obtained.

6.2.2.2. Light Induced Immobilization of eLA on AuNP Surface

Two immobilization procedures of eLA were realized. The experimental set-up for immobilization was the same than the used for probing the time-dependent fluorescence emission of eLA (described in Section 5.2.2.1). In both procedures two milliliters of eLA solution was illuminated in a quartz macro cuvette (1 cm pathlenght). Illumination was stopped at a certain point to introduce AuNP solution, and continued afterwards with AuNP in solution. Continuous illumination at 295 nm was once more realized in the previously described RTC 2000 PTI spectrometer. Emission was monitored using the two detection channels of the spectrometer. Real-time correction was not enabled. Magnetic stirring of the illuminated sample was kept during the extent of both procedures. Temperature inside the cuvette was maintained constant using a peltier element.

The experimental settings used in both immobilization procedures (A and B) are described in Table 6.1.

Table 6.1: Experimental settings used in the immobilization procedures.

Immobilization Procedure	**A**	**B**
Protein sample	eLA 10 μM in Tris HCl 10 mM pH 8.55	
Volume (mL)	2	
AuNP sample	AuNP 400 μM in Tris HCl 10 mM pH 8.55	
Volume of AuNP solution introduced (μL)	20	15
NP concentration in the cuvette (μM)	3.96	3
Time of introduction of AuNP (h)	1	1.7
Total time of illumination (h)	2.3	4
Temperature (ºC)	25.2	25
Stirring (rpm)	900	
Excitation wavelength (nm)	295	295
Wavelength set in Detector 1 (nm)	340	330
Wavelength set in Detector 2 (nm)	295	330
Excitation slits (nm)	5	
Emission slits (nm)	3	5

In the case of the immobilization procedure B the illuminated sample was removed and stored at 4 ºC and under constant agitation overnight to promote reaction b between the thiol groups and the gold surface.

After illumination in procedure A, and reaction in procedure B, the samples were washed twice to remove the excess of protein which did not bind to the AuNP. Each time (wash), the samples were centrifuged at 13400 rpm in a Minispin® (Eppendorf) during 10-15 minutes. After centrifugation the AuNP were clearly visible in the bottom of the liquid as a black color agglomerate. The supernatant was removed and AuNP were resuspended in 10 mM Tris HCl pH 8.55. AuNP dispersed immediately in solution, showing that they were still stable. After the two washes the final resuspension should contain almost no free eLA in solution.

6.2.2.2. Characterization Procedure

UV-visible Absorption Spectroscopy

Thermo scientific UV-Visible spectrophotometer (model: VWK International UV1 v4.60) was used to characterize the diverse washing steps of the separation procedure after immobilization procedure A (the two supernatants), the final resuspension of AuNP resulting of immobilization procedure A, and a AuNP blank (fresh sample of 3.96 µM concentration in 10 mM Tris HCl pH 8.55). The absorption spectra were recorded between 200 and 600 nm. The measurements were performed in black 1 cm path length cuvettes.

Fluorescence Spectroscopy

Measurements were once more carried out in RTC 2000 PTI spectrometer in a black 1 cm path length cuvette. The analyzed samples were the diverse washing steps of the separation procedure after immobilization procedure A (the two supernatants), the final resuspension of AuNP resulting of immobilization procedure A, and a AuNP blank (fresh sample of 3.96 µM concentration in 10 mM Tris HCl pH 8.55). Emission Spectra were recorded upon excitation at 280 nm. Emission and excitation slits were fixed at 5 nm. The final spectra are resultant of average of 3 spectra. The same measurements were realized with 10 mM Tris HCl pH 8.55 in order to correct for *Raman Contribution*. All the precedent spectra were corrected by subtraction of the emission spectrum of this buffer.

Dynamic Light Scattering (DLS)

DLS experiments were performed in a NanoZS, a zeta sizer from Malvern. The instrument automatically fits the autocorrelation function with various fitting algorithms to extract

the diffusion coefficient and Stokes-Einstein equation uses to convert the diffusion coefficient to the hydrodynamic radius. The average size and size distribution of fresh AuNP, eLA and AuNP after immobilization were estimated. For that purpose were used respectively a freshly prepared solution of 10 μM AuNP (in 10 mM Tris HCl pH 8.55), the supernatant of the first wash from immobilization procedure A, and the final resuspension of AuNP from immobilization procedure A. The measurements were realized in 1 cm path length disposable polystyrene cuvettes.

Scanning Electron Microscopy – Energy Dispersive X-ray spectroscopy (SEM-EDS)

Carl Zeiss 1540XB SEM-EDS was used for estimation of AuNP composition. Scanning electron microscopy (SEM) images were collected optimizing the voltage between 5 - 12 kV on silicon substrate where the dried AuNP particles are placed. X-rays, which are also produced by the interaction of electrons with the sample was detected by Energy Dispersive X-ray Spectroscopy (EDS). In order to improve the EDS analysis in SEM, the sample was excited with X-rays. During the X-ray acquisition for particle's composition analysis, the electron beam focused over the particle projection area. The X-ray spectrum was acquired for 60s, at an acceleration voltage of 12 kV. NORAN system six version 2.0 software from Thermo Fischer scientific was used to analyze the EDS data.

Two samples were analyzed using SEM-EDS:

- final resuspension provenient from immobilization procedure B;
- AuNP blank - diluted fresh sample prepared from the mother solution containing 3μM of AuNP in 10 mM Tris HCl pH 8.55.

6.3. RESULTS ANALYSIS AND PRESENTATION

In the first immobilization procedure (Immobilization A) a sample of eLA was illuminated with 295 nm light in the spectrofluorimeter as described in Materials and Methods (Section 6.2). The time-profile of fluorescence emission at 340 nm is displayed in Figure 6.1.

An increase in fluorescence is observed during the first hour of illumination. The experiment was stopped after approximately 1 hour of illumination to introduce the AuNP, which can be noticed in the profile by a temporary intensity decrease. Considering the previous trials with the Elmann's reagent, it was assumed that the increase fluorescence intensity is proportional to the number of free thiol groups formed. By introducing the AuNP in an advanced part of the illumination session it was pretended that free thiol groups were already formed upon mixing with the protein solution. After one hour of illumination there should be already a considerable number of broken SS, translated by an 13% increase in fluorescence intensity. Furthermore, in the

characterization procedure of eLA it was noticed that for breakage of a considerable amount of SS bridges, was required a considerable exposition time to UV. The late introduction of AuNP permits to avoid that they interfere with the process of illumination (e.g. scattering of the light). After the introduction of the AuNP, an increase in fluorescence intensity is still noticed, though the slope is less steep. After ~1.8 h of illumination a plateau is reached, followed by a decay phase until the end of the session (~2.3 h).

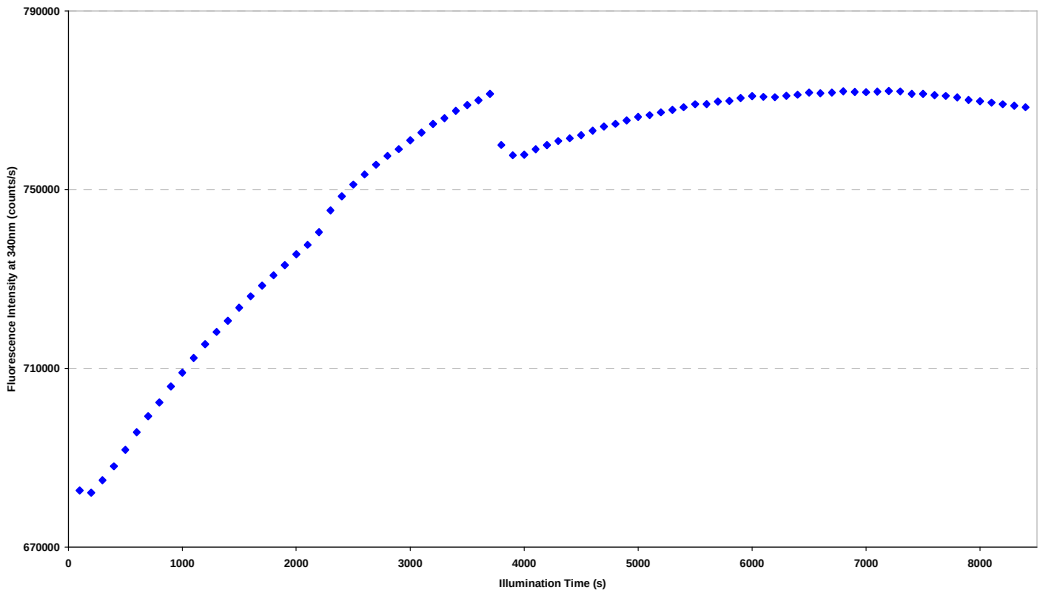

Figure 6.1: Fluorescence intensity of eLA *versus* illumination time. Excitation was fixed at 295 nm and emission was monitored at 340 nm. Temperature was maintained at 25ºC using a peltier element. Measurements were performed using a RTC 2000 PTI spectrofluorimeter as described in Materials and Methods (section 6.2).

The elastic scattering of the light was monitored during the whole extent of the session, by probing the emission at 295 nm in the second channel of the spectrofluorimeter. The emission did not increase, just decayed, even after the introduction of AuNP (Data not Shown), suggesting that no aggregation took place through inter-disulphide bonding between protein molecules.

Subsequently, the irradiated solution (containing the AuNP) was centrifuged and washed twice, as described in Materials and Methods, in order to remove the excess of protein. Three solutions were stored, one correspondent to supernatant of the first wash, the equivalent of the second wash, and the resuspended AuNP (with eLA immobilized or not). These samples were characterized through UV-absorption, Fluorescence Spectroscopy and DLS as described previously in Materials and Methods (Section 6.2).

In Figure 6.2 are displayed the absorption spectra of the liquid supernatants obtained after each wash procedure. In the spectrum recorded with the supernatant extracted from the first wash (in green), two typical protein peaks are clearly observed, at 220 nm and 280 nm, wavelengths for which the peptide bonds and aromatic residues respectively absorb. After the

first wash the majority of the protein in excess is removed, since in the spectra corresponding to the supernatant resultant of the second wash and resuspended AuNP (blue and red respectively, visible in the zoomed area), these two peaks are not sharp anymore. The peak corresponding to gold (~520 nm) is only visible for the spectrum of resuspended AuNP which confirms that the separation was successful.

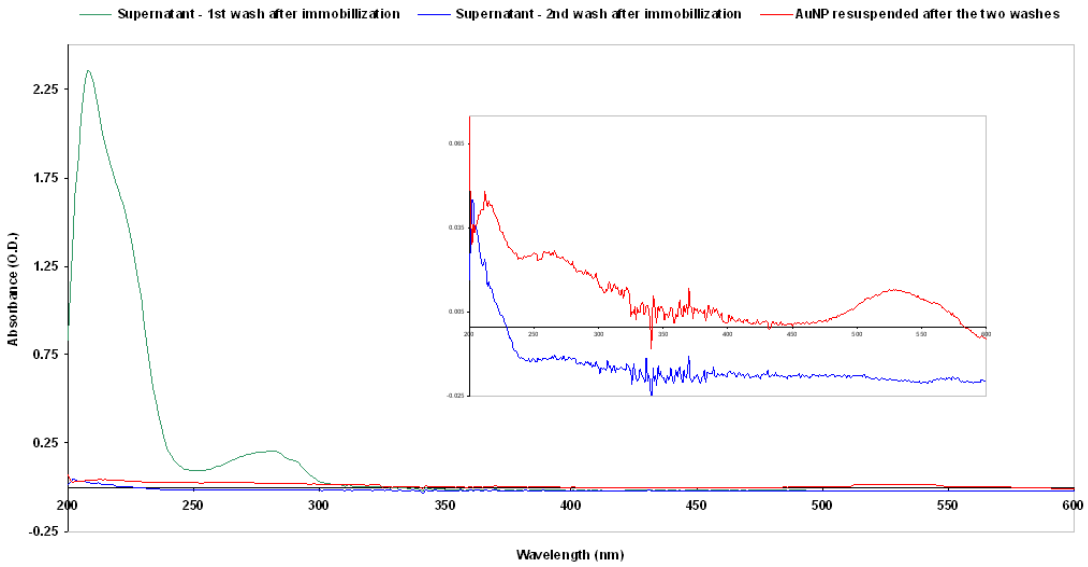

Figure 6.2: Absorption spectra of the supernatants of the two washes and the final resuspended AuNP solution. The box displayed within the area of the plot is a zoom of the absorption spectra of the second wash supernatant and the final resuspension of AuNP. The spectra were recorded in a UV-visible absorbance spectrophotometer as previously described in Materials and Methods (Section 6.2)

In Figure 6.3 are displayed the absorption spectra of the resuspended AuNP (red), and a fresh solution of AuNP prepared with the same concentration (wine red). The gold peak is present in either one of the spectra. The difference between these two spectra (orange), shows a peak at 220 nm, which could represent the absorption of peptide bonds of immobilized eLA. The absorption peak of the aromatic residues is not so clear. There could be a peak indeed, but centered at ~260 nm.

The fluorescence characterization data reflects similar results. The fluorescence emission spectrum of the supernatant resultant of the first wash (upon excitation with 280 nm light) presents a broad peak centered at ~335 nm (*vide* Figure B22 – Supplementary Results, Appendix B). The supernatant resultant of the first wash still displays some protein intrinsic fluorescence, but with far lower emission counts. Compared to the latter, the resuspended AuNP seemingly display no emission peak upon excitation with 280 nm (*vide* Figure B23 – Supplementary Results, Appendix B). The emission spectra difference between the resuspended AuNP and the fresh AuNP displays however a peak at ~335 nm (*vide* Figure B24 –

Supplementary Results, Appendix B), though at these low fluorescence counts the accuracy of the results is not to be trusted.

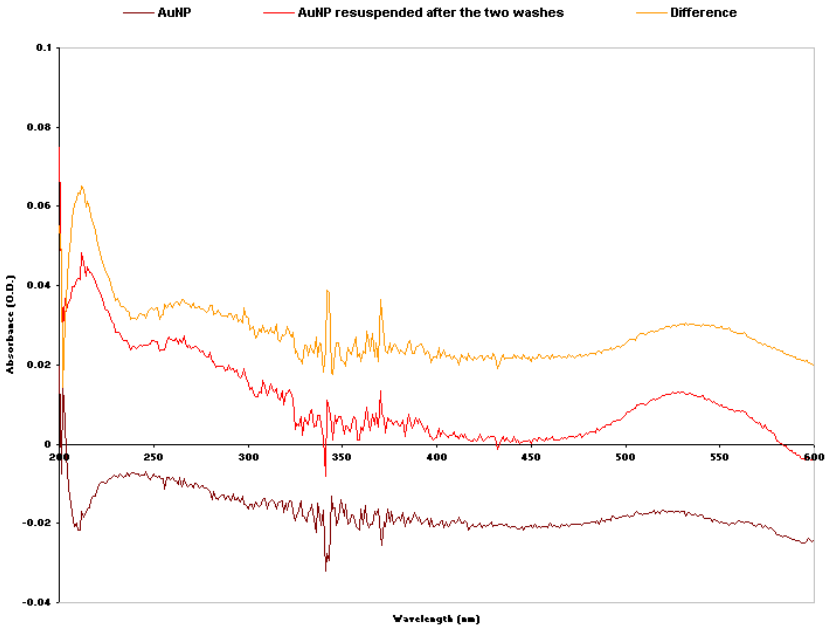

Figure 6.3: Absorption spectra of the final resuspension of AuNP (red), fresh AuNP (wine red) and the difference between these two (orange). Spectra were recorded using a UV-visible spectrophotometer as described in Materials and Methods (section 6.2).

To confirm if eLA was successfully immobilized onto the AuNP, the size of eLA, fresh AuNP, and the final resuspended AuNP was estimated using DLS. For a solution of 10 μM of fresh AuNP the measurements show an intense peak at 50.37 nm (*vide* Figure B25 – Supplementary Results, Appendix B). The measurement realized for the final resuspension of AuNP shows a modest difference in AuNP size after the immobilization procedure, presenting an intense peak at 50.81 nm (*vide* Figure B26 – Supplementary Results, Appendix B). eLA size was estimated by DLS measurement of the second wash supernatant. The peak which probably corresponds to the protein, at ~5.5 nm (*vide* Figure B27 – Supplementary Results, Appendix B), is not the most intense (15% intensity), showing that the sample may have been contaminated with some larger impurity. Nonetheless, given the probable hydrodynamic diameter (5.5 nm) of eLA, these results do not support a scenario of a successful immobilization, since no significative difference is noticed between the diameter values of the two tested particles.

In order to check the previous results the immobilization procedure was repeated (Immobilization B). This rehearsal presented some differences. After the illumination procedure the removed irradiated mixture of protein and AuNPs was left overnight at 4ºC under constant

agitation. This way it was expected to promote the binding reaction, and allow all the free thiol groups of the protein to react with the AuNP. The AuNP were also introduced latter in the illumination process, after about 1.7h of illumination, which proceeded until a final time of 4h.

Fluorescence emission was probed at 330 nm upon excitation with 295 nm light and no increase in fluorescence was noticed (Data not shown).

After overnight reaction the sample was submitted to the same washing protocol. The characterization procedure was this turn realized using SEM-EDS. The images obtained for the final resuspension of AuNP (after immobilization) and for the AuNP blank (fresh sample) are displayed in the Figures 6.4 and 6.5 respectively. In both images are visible the groups of AuNP. The enhanced areas in the images (1 and 2), corresponding to two distinct zones where AuNP were or not present, were analyzed though EDS.

The X-ray spectra of the two exposed areas (Figures 6.4 and 6.5) can provide quantitative information of the particles constitution. However this information may not correlate exactly the particles content due to the presence of the buffer salts and surfactant. Moreover, the sample placed on the sample holder may not be homogeneous and the amount of sample may be variable between detections. Furthermore, individual AuNP are in nanometer size, and the area exposed (> 2.5 μm in length and height) comprise a large portion of area non-occupied by AuNP, in which other molecules could be present.

However, this experimental analysis qualitatively confirms the presence of the elements C, O, N, Si, Au and Cl (Fig. 5). C and O peaks can be expected from sodium citrate surfactant and the buffer salts; the N peak can also be expected from the buffer salts and Au from AuNP. Proteins display also high contents in N, C and O, so these peaks could also be representative of eLA attached to AuNP.

In Figure 6.4, exposed area 2 does not contain any AuNP, since no Au peak is noticed in the X-ray spectrum, and presents all the atomic entities of the buffer salts (Tris HCl). Therefore this area should be representative of atomic composition of the buffer salts and surfactant. In the spectrum corresponding to exposed area 1, the presence of AuNP is confirmed by a gold peak at ~2.1 kV. A peak of smaller intensity is also noticed for nitrogen. In Figure 6.5, the X-ray spectrum, corresponding to the zone where fresh AuNP lay (exposed area 1) shows again the Au peak and quite reduced N peak this time.

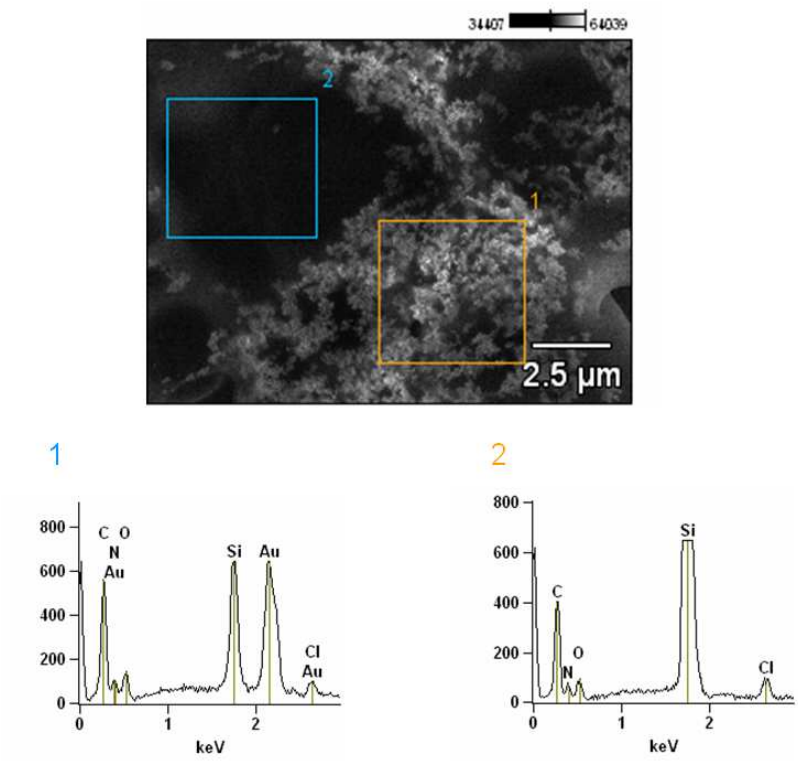

Figure 6.4: SEM image of the final AuNP resuspension (after immobilization). Accelerating Voltage: 7.0 keV; Magnification: 18272. The squares represent the area exposed to EMS. X-ray spectra of the exposed areas are displayed in the bottom. The peaks corresponding to each atom are labeled.

Table 6.2: Experimental atomic values obtained after EMS analysis of each exposed zone - AuNP resuspension (after immobilization).

Parameter	ZAF Value		Weight %		Atomic %	
Atom/Exposed area	**1**	**2**	**1**	**2**	**1**	**2**
C	1.84	3.95	16.41	24.84	46.34	41.78
N	2.06	3.01	6.63	4.5	16.07	6.49
O	1.7	1.96	4.77	2.99	10.1	3.77
Si	0.88	1.06	12.09	62.87	14.6	45.22
Cl	0.97	1.21	3.23	4.79	3.09	2.73
Au	1.34		56.87		9.79	

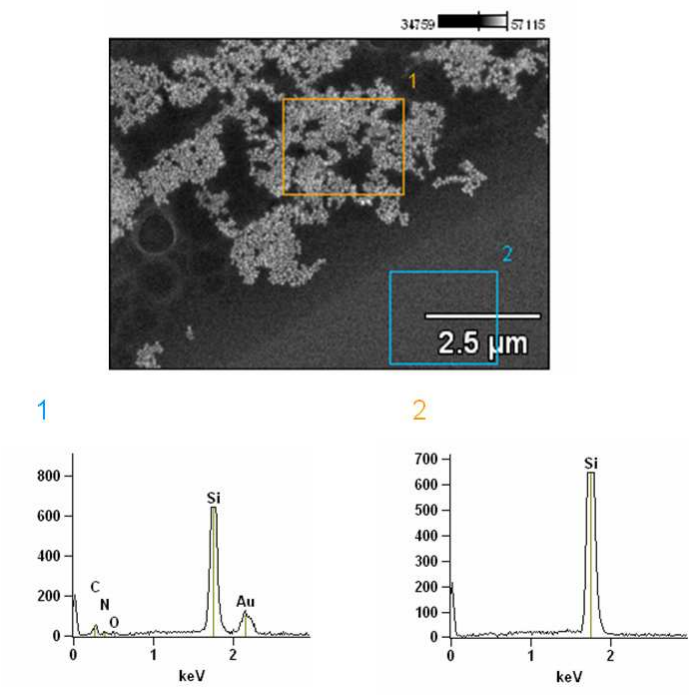

Figure 6.5: SEM image of the final AuNP blank (fresh, non-exposed particles). Accelerating Voltage: 7.0 keV; Magnification: 29881. The squares represent the area exposed to EMS. X-ray spectra of the exposed areas are displayed in the bottom. The peaks corresponding to each atom are labeled.

Table 6.3: Experimental atomic values obtained after EMS analysis of each exposed zone - AuNP blank (fresh, non-exposed particles).

Parameter	ZAF Value		Weight %		Atomic %	
Atom/Exposed area	**1**	**2**	**1**	**2**	**1**	**2**
C	3.07		6.14		17.77	
N	2.18		2.32		5.76	
O	1.63		1.22		2.65	
Si	0.91	1	54.59	100	67.52	100
Au	1.53		35.73		6.3	

The experimental EMS values (Tables 6.2 and 6.3), provide further insight into the possible AuNP composition. In the zone where resuspended AuNP lay (exposed area 1 – Figure 6.4) the atomic content in N (16.07 %) is considerably higher compared to the zone characterizing the exposed buffer and the surfactant (6.49 %) (exposed area 2 – Table 6.2). As said before, the homogeneity of the sample can not be assured and the quantity of sample tested

may not be the same in both areas. However, such a difference of values could indicate that eLA is in fact immobilized on the surface of AuNP, though in low quantities. The ratio between N and atomic content of gold could be a reasonable indicative of the presence of eLA in the AuNP. The values of these ratios for the zone where resuspended (exposed area 1 – Figure 6.4) and fresh (exposed area 1 – Figure 6.5) are present are respectively 0.117 and 0.065. Though the particles can behave differently in solution and the two analyses can present divergences, the value for the resuspended AuNP is almost the double, providing another indication of successful immobilization.

6.4. DISCUSSION

The results obtained from the two immobilization procedures of eLA onto AuNP are contradictory. The DLS analysis of immobilization A shows no apparent difference in hydrodynamic diameter between the product of immobilization (final resuspended AuNP) and the fresh AuNP. Though the surfactant surrounds AuNP in the fresh sample, the width of the surface film it may form should not be even detectable, while with eLA immobilized, a macromolecule, a difference in hydrodynamic diameter should be noticed. The UV-absorption characterization procedure shows on the other hand some indications of possible immobilization. In the difference spectra between final resuspended and fresh AuNP a peak is observed at 220 nm, where peptide bond absorbs, and a residual peak is found at ~260 nm, where aromatic residues absorb. Furthermore, these peaks are not found or very reduced in supernatant of the second wash, excluding the possibility of being representative of free eLA in solution. However the fluorescence spectroscopy characterization shows once more negative results, with no emission upon 280 nm excitation in the resuspended AuNP.

Oppositely, immobilization procedure B provides a scenario of successful immobilization, since the resuspended AuNP provenient from this procedure present, seemingly present nitrogen contents, after characterization analysis with SEM-EDS.

The two immobilization procedures present differences, not only in protocol (diverse times of introduction of AuNP, longer time of irradiation reaction in immobilization B) but also in the fluorescence behavior of eLA upon irradiation. The increase in fluorescence intensity was not noticed in immobilization B, while for immobilization A the typical increase described in eLA characterization procedure is noticed. These divergences in fluorescence behavior spell once more the instability noticed eLA once the low ionic strength is too low. The immobilizations were realized with eLA concentration of 10 μM in 10 mM TrisHCl. It corresponds to the lowest case in ionic strength. At the time of the experiments the knowledge regarding apo-forms of bLA was limited. In future immobilizations this effect should be considered. Nonetheless the breakage of

SS bonds could be expected, even in these destabilized forms. The denaturated forms of LA are generally folded in MG-like conformations, and part of the native interactions should be kept.

Light-induced immobilization of other proteins onto nanoparticles was already attempted in the Nanobiotechnology group of the University of Aalborg. Bovine Serum Albumin and Prosthetic Serum Albumin were already successfully immobilized onto gold coated magnetite nanoparticles and AuNP respectively (Personal Communication, Parracino A.). After immobilization it was found not that not also Bovine Serum Albumin molecules are covalently bounded on the surface of the nanoparticles, but also that they form aggregates around the immobilized protein, increasing the measured hydrodynamic diameter in DLS from 27.4 to 200 nm (Parracino *et al.*, 2008). Another protein, esterase, an enzyme that does not present SS bonds, but contains four free cysteines, was immobilized through affinity reaction with gold coated magnetite nanoparticles, without the use of light. The average hydrodynamic diameter of the particles (DLS), protein and complex of protein and nanoparticles was respectively 37 nm, 49.4 nm and 74.6 nm, signifying that the enzyme forms a single layer on the gold surface.

Evidently, each protein can display a particular mechanism of immobilization and attachment to the gold derivatized nanoparticles, depending on its structural and chemical features. Though LA immobilization to metallic surfaces is not well described in literature, there are several reports concerning the adsorption properties of LA. Upon interaction with colloidal polystyrene nanospheres native bLA the protein adsorbs particularly well on the polystyrene surface through stable hydrophobic interactions (neutral pH - both LA and polystyrene are negatively charged) and hardily desorbs. Upon adsorption bLA suffers denaturation to a partly folded state and remains in a MG-like conformation (Engel *et al.*, 2002). LA also adsorbs particularly well onto negatively charged planar poly(acrylic) acid brushes (Holmann *et al.*, 2007). Neutron Reflectometry data showed that despite its net negative charge (neutral pH), LA was penetrating deeply into the polymeric brush. Moreover, no protein accumulation was found at the inner poly(styrene) or the outer solution interface of the polymeric brush. Total Internal Reflection Fluorescence data indicated also a high degree of reorientational mobility of LA within polymeric brush. It was concluded that this high mobility of LA within the polymeric brush could partially be understood by the presence of repulsive electrostatic interactions.

Upon thiol immobilization to the gold surface, eLA might also rearrange in a partly denaturated form as the described above. Since eLA is negatively charged and upon adsorption does not tend to accumulate, aggregation of the protein is not expected, due to electronic repulsion. Hence, the eLA molecules may occupy completely the surface of the AuNP, forming a thin film, not allowing other molecules to adsorb.

Given that eLA is a particularly small protein (average hydrodynamic radius obtained from DLS is 5.5 nm), the difference in hydrodynamic radius of the complex AuNP-eLA may not be distinguishable within the resolution of the DLS measurements, unlike esterase. Moreover the

hydrodynamic radius of the AuNP may not be constant, which could yield some divergences between samples.

Nevertheless, such event does not overrule the unsatisfactory results obtained on the Fluorescence Spectroscopy characterization, where no fluorescence emission is found for the resuspended AuNP.

Gold is known for having a polemic and discussible paper in fluorescence emission. Classically, gold is known to be a stronger fluorescence quencher. However it has been advanced recently that gold may also have a reverse role, enhancing the fluorescence of fluorophores. Fluorophores on the excited may undergo near-field interactions with metal particles to create plasmons, a phenomenon called Metal-Enhanced Fluorescence (MEF). MEF by was already verified for AlexaFluor derivatized Rat Immunoglobin G immobilized in gold films (Zhang and Lakowicz, 2006). According to radiating plasmons model for MEF the absorption component of metal particle extinction contributes to quenching, while the scattering component contributes to MEF. Therefore the size of gold particles may have a particular influence on the paper of gold in fluorescence.

Here, the estimated hydrodynamic radius of AuNP is 50.37 nm, which could signify a high light scattering yield from the particles. However if total adsorption of eLA on the surface is considered, this implies that the aromatic residues are in direct or almost in direct contact with the gold molecules, which could favor the quenching of their fluorescence by the gold (Zhang and Lakowicz, 2006), explaining the emission spectrum obtained. Furthermore, quenching of fluorescence was observed recently by Delphino and Cannistaro (2009) for the well described hybrid complex of Azurin-AuNP. In this case azurin molecules form a monolayer in the surface of the 20 nm AuNP. Binding of azurin molecules to the AuNP surface results in the red shift of the nanoparticle resonance plasmon band and in the quenching of the azurin single tryptophan fluorescence signal.

Even if the model advanced (thin film of eLA around the AuNP) explains partly the results obtained for both immobilizations, and the SEM-EMS results point out the binding of eLA to AuNP, the data presented here is not sufficient to prove a successful light-induced immobilization of eLA.

7. CONCLUSIONS

The first step of this experimental work consisted on evaluating bLA as a potential candidate for light-assisted immobilization. Calcium depleted form of bLA was chosen as model for this characterization procedure. This choice reflected both the biomedical interest of apo-LA forms (regarding its potential functionality), and the need of further investigating the light induced cleavage of SS bonds in these LA forms, which was not so well characterized.

The characterization procedure of apo-bLA forms brought evidence of some interesting results. Prolonged irradiation of a native-like apo-bLA resulted in an increase in fluorescence yield, coupled to a pronounced red-shift in Trp fluorescence. These spectral changes are probably caused by involvement of Trp excited species into first order reactions that will yield conformational changes on the protein, as indicate the hidden *isosbestic* point and the exponential fluorescence increase at 340 nm. The original Trp excited species are converted upon reaction to high fluorescence quantum yield and red-shifted products. Breakage of SS bonds is probably another product of this reaction. Upon cleavage of these bridges in eLA, the quenching of the Trp residues is considerably reduced, explaining the raise in Trp emission. This cut-back is probably due to the absence of these bonds as strong fluorescence quenchers, but can also advent of photodegradation and displacement of other quenching groups upon cleavage. For instance it is known that the SS bonds breakage in goat-LA can be resultant of crosslinking of a cysteine to a lysine. The latter can be a strong fluorescence quencher, as integrated in the peptide bond. Furthermore, the red-shifted emission of the product Trp species indicates a displacement of these residues to solvent accessible areas upon cleavage. It could also alter the appetence of the red-shifted Trp species for quenching.

One of mechanisms activated upon Trp irradiation and responsible of SS bond cleavage is the thermal photoionization of excited singlet Trp species and production of e_{aq}^-, as pointed out by the temperature dependency of the exponential rate of fluorescence increase.

Acquirement of fluorescence lifetime components and use of flash photolysis studies in bLA is a next step for understanding deeply the mechanisms and Trp residues involved in the UV-triggered reactions here described.

Though these observations provide supplemental knowledge on the UV-triggered mechanisms in apo-forms of bLA, and LA in general, the informations regarding apo-bLA as candidate for light-assisted immobilization are scarce.

The verified presence of free thiol groups is evidently a fulfilled criterion for the technique. Nevertheless it is not known which thiol groups will be available to react with a derivatized surface upon immobilization. They are detected by the Elmann's reagent and Cys6-Cys120, that suffers photlysis in goat LA, is in an accessible region, so they should be solvent accessible, but it is not

excludable that sterical interferences exist. SS bond breakage seemingly is favored at low temperatures and neutral pH, another indication that should be considered for immobilization.

The integrity of the protein and its functionality is not guaranteed upon UV-light irradiation. The polypeptide probably reorganizes as a MG-form maintaining most of its native-like structural features (mostly secondary content), but drastical changes are expected in the aromatic clusters, which could jeopardize the active site for lactase synthase activity and other potential functionalities.

The instability and unpredictability of bLa in an apo-form is an additional problem for using this model. Slight modifications in the experimental conditions, typically required for using diverse analytical techniques, resulted in large discrepancies in results obtained. In the future, it would be preferable to use the most stable Ca^{2+} loaded form, in order to have reproducible results. The UV-sensitivity of both forms could also be compared this way.

The final evaluation of apo-bLA as candidate was performed by executing the light-immobilization procedure on gold nanoparticles. The results suggest the possibility of thin-film formation on the AuNP surface. Even so, these experiments consisted only on a test phase, since at the time the knowledge of the apo-form of bLA was reduced, as also the UV-sensitivity of the candidate. The conditions used in both immobilizations destabilized particularly apo-bLA. In the future higher ionic strengths should be used.

The model for thin-film formation in apo-bLA should be confirmed by rehearsal of the immobilization and all the characterization procedures. Labeling of the protein with a powerful fluorophore may also help in characterization procedure. Moreover it would allow the use of other identification techniques (for the tagging of eLA onto the fold surface), such as fluorescence and confocal microscopy.

Light-induced immobilization of LA onto gold AuNP has a considerable biomedical interest. Given the broad range of LA functional properties, upon binding to AuNP, this complex could be used futurelly as biosensor for a wide number of metal ions, or as molecular carrier. The latter application is particularly appealing given two possible distinct LA functions: lactose synthase regulation and anti-tumorogenic agent. Moreover, the protein can be successfully delivered in the interior of cells. This is due to the nature of covalent bond that links the thiol to the gold surface, resulting in the detachment of the protein when the carrier (AuNP) enters the reducing cell environment. The specific delivery of the protein to certain cells can also be controlled by magnetic field, if the AuNP are substituted by gold coated magnetite nanoparticles, which above certain dimensions, display paramagnetic properties.

Concluding, this work brought further insight into UV-light activated mechanisms in Ca^{2+} depleted forms of LA, especially in what respects the breakage of SS bonds. In this form LA is not the best candidate for light-induced immobilization, since it is very unstable and susceptible to conformational changes.

BIBLIOGRAPHY

Acharya KR, Ren JS, Stuart DI, Phillips DC, Fenna RE. (1991) *Crystal structure of human alpha-lactalbumin at 1.7 A resolution*. J Mol Biol., **221**(2), 571-81.

Bain C.D., Troughton E.B., Tao Y.T., Evall J., Whitesides G.M. and Nuzzo R.G. (1989), *Formation of Monolayer Films by the Spontaneous Assembly of Organic Thiols from Solution onto Gold*. J. Am. Chem. Soc*.,* **111**, 321-335.

Boye J. I., I. Alli and A. A. Ismail. (1997). *Use of Differential Scanning Calorimetry and Infrared Spectroscopy in the Study of Thermal and Structural Stability of α-Lactalbumin*. J. Agric. Food Chem., **45**, 1116-1125

Brown R. J. and Ernstron C. A. (1982). *Incorporation of Ultrafiltration Concentrated Whey Solids into Cheddar Cheese for Increased Yield*. J. Dairy Sci., **65**, 2391-2395

Calderone V., M. G. Giuffrida, D. Viterbo, L. Napolitano, D. Fortunato, A. Conti, K. R. Acharya. (1996). *Amino acid sequence and crystal structure of buffalo α-lactalbumin.* FEBS Letters, **394**, 91-95

Canet D, K. Doering, C. M. Dobson, and Y. Dupont. (2001). *High-Sensitivity Fluorescence Anisotropy Detection of Protein-Folding Events: Application to α-Lactalbumin.* Biophysical Journal, **80**, 1996–2003

Chakraborty S., Ittah V., Bai P., Luo L., Haas E., Peng Z.Y. (2001) *Structure and dynamics of the alpha lactalbumin molten globule: fluorescence studies using proteins containing a single tryptophan residue*. Biochemistry, **40**, 7228–7238

Chang J-Y and Li L. (2001). *The Structure of Denatured a-Lactalbumin Elucidated by the Technique of Disulfide Scrambling.* The Journal of Biological Chemistry, **276**, 13, Issue of March 30, pp. 9705–9712

Chaplin L. C. and Lyster, R. L. J. (1986). *Irreversible heat denaturation of bovine α-lactalbumin*. Journal of Dairy Research, **53**, 249–258.

Chrysina E.D., K. Brew and K. R. Acharya. (2000). *Crystal structures of apo- and holo-bovine alpha-lactalbumin at 2.2-Å resolution reveal an effect of calcium on inter-lobe interactions.* J Biol Chem, **275**, 37021– 37029.

Creighton T. E. (1992) *Proteins: Structures and Molecular Properties*. W. H. Freeman; Second Edition

Cushing B. L., Kolesnichenko V. L., O'Connor C. J. (2004) *Recent advances in the liquid-phase syntheses of inorganic nanoparticles.* Chem. Rev., **104**, 3893-3946

Damodaran and Paraf (1997) *Food proteins and their applications*. Marcel Dekker Inc, New York

Delfino I., Cannistraro S. (2009) *Optical investigation of the electron transfer protein azurin–gold nanoparticle system*. Biophysical Chemistry, **139**, 1–7

Duroux M, E. Skovsen, M. T. Neves-Petersen, L. Duroux, L. Gurevich and S. B. Petersen. (2007). *Light-induced immobilisation of biomolecules as an attractive alternative to microdroplet dispensing-based arraying Technologies*. Proteomics, **7**, 3491–3499

Engel M. F. M., C. P. M. van Mierlo and A. J. W. G. Visser. (2002). *Kinetic and Structural Characterization of Adsorption-induced Unfolding of Bovine α-Lactalbumin.* The Journal of Biological Chemistry, **277**, 3, Issue of March 29, 10922–10930

Enüstün B. V., Turkevich J. (1963) *Coagulation of Colloidal Gold.* J. Am. Chem. Soc., **85** (21), 3317–3328

Fasman G. D. (1996) *Circular Dichroism and the Conformational Analysis of Biomolecules*. Springer

Fenemma O. (1996) *Food Chemistry.* Marcel Dekker Inc, New York

Fischer W., L. Gustafsson, A-K Mossberg, J. Gronli, S. Mork, R. Bjerkvig and C. Svanborg. (2004). *Human α-Lactalbumin Made Lethal to Tumor Cells (HAMLET) Kills Human Glioblastoma Cells in Brain Xenografts by an Apoptosis-Like Mechanism and Prolongs Survival*. Cancer Research, **64**, 2105–2112

Fu X. Y., Mueller D. M., and Heinecke J. W. (2002) *Generation of intramolecular and intermolecular sulfenamides, sulfinamides, and sulfonamides by hypochlorous acid: A potential pathway for oxidative cross-linking of low-density lipoprotein by myeloperoxidase*. Biochemistry, **41**, 1293-1301.

Gao C., R. Wijesinha-Bettoni, P. J. Wilde, E. N. C. Mills, L. J. Smith and A. R. Mackie. (2008). *Surface Properties Are Highly Sensitive to Small pH Induced Changes in the 3-D Structure of α-Lactalbumin.* Biochemistry, **47**, 1659-1666

Griko Y. V. and Remeta D. P. (1999). *Energetics of solvent and ligand-induced conformational changes in α-lactalbumin.* Prot Sci, **8**, 554–561.

Griko YV, Freire E, Privalov PL. (1994) *Energetics of the α-lactalbumin states: A calorimetric and statistical thermodynamic study*. Biochemistry, **33**, 1889-1899.

Harata K. and Muraki S. M. (1992). *X-ray Structural Evidence for a Local Helix-Loop Transition in α-Lactalbumin.* The Journal of Biological Chemistry, **267**, 3, 1419-1421

Hendrix T. M., Y. V. Griko and P.L. Privalov. (1996). *Energetics of structural domains in α-lactalbumin*. Prot Sci, **5**, 923–931.

Hollmann O., Steitz R., Czeslik C. (2008) *Structure and dynamics of α-lactalbumin adsorbed at a charged brush interface*. Phys. Chem. Chem. Phys.,**10**, 1448–1456

Hong Y-H and Creamer L. K. (2002). *Changed protein structures of bovine β-lactoglobulin B and α-lactalbumin as a consequence of heat treatment*. International Dairy Journal, **12** (2002) 345–359

Horng C-H, S. J. Demarest, and D. P. Raleigh. (2003) *pH-Dependent Stability of the Human α-Lactalbumin Molten Globule State: Contrasting Roles of the 6-120 Disulfide and the β-Subdomain at Low and Neutral pH.* PROTEINS: Structure, Function, and Genetics, **52**,193–202

Ikeguhi M., M. Fujino, M. Kato, K. Kuwajima and S. Sugai. (1998). *Transition state in the folding of α-lactalbumin probed by the 6-120 disulfide bond.* Protein Science, **7**, 1564-1574.

Kerwin B. A, and Remmele R. L. Jr. (2006). *Protect from Light: Photodegradation and Protein Biologics*. Journal of Pharmaceutical Sciences, **96**, 6, 1468-1479

Kim S. and Baum J. (1998). *Electrostatic interactions in the acid denaturation of α-lactalbumin determined by NMR.* Protein Science, **7**, 1930-1938.

Kuwajima K. (1996). *The molten globule state of α-lactalbumin*. FASEB J,**10**,102–109

Kuwajima K., Y. Ogawa, and S. Sugai. (1979). *Application of the pH-Jump Method to the Titration of Tyrosine Residues in Bovine α-Lactalbumin.* Biochemistry, 878

Kuwajima, K., Mitani M., Sugai, S. (1989) *Characterization of the critical state in protein folding. Effects of guanidine hydrochloride and specific Ca_2^+ binding on the folding kinetics of alpha-lactalbumin*. J Mol Biol., **206**(3), 547–561.

Lakowicz J. R. (2006). *Principles of Fluorescence Spectroscopy*. Springer, 3rd edition

Laureto P. P., E. Frare, R. Gottardo and A. Fontana. (2002). *Molten Globule of Bovine α-Lactalbumin at Neutral pH Induced by Heat, Trifluoroethanol, and Oleic Acid: A Comparative Analysis by Circular Dichroism Spectroscopy and Limited Proteolysis*. PROTEINS: Structure, Function, and Genetics, **49**, 385–397

Li A-J and Nussinov R. (1998). *A Set of van der Waals and Coulombic Radii of Protein Atoms for Molecular and Solvent-Accessible Surface Calculation, Packing Evaluation, and Docking.* PROTEINS: Structure, Function, and Genetics, **32**, 111–127

Macey M. (2007) *Flow Cytometry: Principles and Applications*. Humana Press; 1st edition

Masaki K., Masuda R., Takase K., Kawano K. and Nitta K. (2000) *Stability of the molten globule state of a domain-exchanged chimeric protein between human and bovine α-lactalbumins*. Protein Engineering, **1**, 1-4

Matsumura Y and Ananthaswamy H. N. (2004). *Toxic effects of ultraviolet radiation on the skin.* Toxicology and Applied Pharmacology, **195**, 298–308

McGuffey M. K., D. E. Otter, J. H. van Zanten and E. A. Foegeding. (2007) *Solubility and aggregation of commercial α-lactalbumin at neutral pH.* International Dairy Journal, **17**, 1168–1178

Mizuguchi M., D. Hashimoto, M. Sakurai and K. Nitta. (2000). *Cold Denaturation of α-Lactalbumin*. PROTEINS: Structure, Function, and Genetics, **38**, 407–413

Moriarty D.F., Demarest S.J., Robblee J., Fairman R., Raleigh D.P. (2000) *Local interactions and the role of the 6–120 disulfide bond in_α-lactalbumin: implications for formation of the molten globule state*. Biochim Biophys Acta,**1476**, 9–19.

Neves-Petersen M. T., M. Duroux, E. Skovsen, L. Duroux and S. B. Petersen. (2008) Journal of Nanoscience and Nanotechnology, in print.

Neves-Petersen M. T., S. Klitgaard, A. S. L. Carvalho, S. B. Petersen, M. R. A. de Barros and E. Pinho e Melo. (2007) *Photophysics and Photochemistry of Horseradish Peroxidase A2 upon Ultraviolet Illumination.* Biophysical Journal, **92**, 2016–2027

Neves-Petersen M. T., S. Klitgaard, E. Skovsen, T. Pascher, T. Polivka, A. Yartsev, V. Sundström and S. B. Petersen. (Paper submitted). *Flash photolysis of cutinase: identification and decay kinetics of transient intermediates formed upon UV excitation of aromatic residues*.

Neves-Petersen M. T., Z. Gryczynski, J. Lakowicz, P. Fojan, S. Pedersen, E. Petersen and S. B. Petersen. (2002). *High probability of disrupting a disulphide bridge mediated by an endogenous excited tryptophan residue.* Protein Sci., **11**, 588-600

Neves-Petersen M.T., Snabe T., Klitgaard S., Duroux M., Petersen S.B. (2006) *Photonic activation of disulfide bridges achieves oriented protein immobilization on biosensor surfaces.* Protein Sci., **15**, 343-51

Panda D. and Datta A. (2008) *Implications of Area Normalization of Multi-Component Spectra*. Appl. Spectrosc., **62**, 341-344

Parracino A., Prakash G., Kold A., Correia M., Neves-Petersen M.T., and Petersen S. B. (2008) *Novel photonic immobilisation technique provides a new approach to couple biomolecules onto superparamagnetic nanoparticles for nano-medical applications*.

Conference Talk, **NanoSMat 2008** - 3rd International Conference on Surfaces, Coatings and Nanostructured Materials

Pedersen J. B., P. Fojan, J. Sorensen and S. B. Petersen. (2006) *Towards Control of Aggregational Behaviour of α-Lactalbumin at Acidic pH.* J. Fluoresc., **16**, 611–621

Permyakov E. A. and Berliner L. J. (2000). *α-Lactalbumin: Structure and function*. FEBS Lett, **473**, 269–274.

Permyakov E. A., S. E. Permyakov, G. Y. Deikus, L. A. Morozova-Roche, V. M. Grishchenko, L. P. Kalinichenko and V. N. Uversky. (2003). *Ultraviolet Illumination-induced Reduction of α-Lactalbumin Disulfide Bridges.* PROTEINS: Structure, Function, and Genetics, **51**, 498–503

Petersen, M.T.N., Jonson, P.H., and Petersen, S.B. (1999) *Amino acid neighbours and detailed conformational analysis of cysteines in proteins.* Protein Eng. **12**, 535–548.

Pfeil W. (1998). *Is the molten globule a third thermodynamic state of proteins? The example of alpha-lactalbumin*. Prot Struct Funct Genet, **30**, 43–48

Pike A. C. W., K. Brew and K. R. Acharya1. (1996). *Crystal structures of guinea-pig, goat and bovine α-lactalbumin highlight the enhanced conformational flexibility of regions that are significant for its action in lactose synthase.* Structure, **4**, 691–703

Pöpp J. and Strelle M. (2008) *Biophotonics - Visions for Better Health Care*. Wiley-VCH, 1st edition

Pouët M., Baures E., Vaillant S., and Thomas O. (2004) *Hidden Isosbestic Point(s) in Ultraviolet Spectra*. Appl. Spectrosc., **58**, 486-490

Prasad N. (2003) Introduction to biophotonics. Wiley

Qasba P. K. and Kumar S. (1997). *Molecular Divergence of Lysozymes and α-Lactalbumin*. Critical Reviews in Biochemistry and Molecular Biology, **32**, 4, 255-306

Ramakrishnan B. and Qasba P. K. (2001). *Crystal Structure of Lactose Synthase Reveals a Large Conformational Change in its Catalytic Component, the b1,4-Galactosyltransferase-I.* J. Mol. Biol., **310**, 205-218

Riddles P. W., Blakeley R. L., Zerner B. (1983). *Reassessment of Ellman's reagent*. Meth. Enzymol., **91**: 49–60

Riener C. K., Kada G., Gruber H. J. (2002) *Quick measurement of protein sulfhydryls with Ellman's reagent and with 4,4'-dithiodipyridine*. Anal. Bioanal. Chem., **373**, 266–276

Sherin P. S., O. A. Snytnikova and Y. P. Tsentalovich. (2004). *Tryptophan photoionization from prefluorescent and fluorescent states*. Chemical Physics Letters, **391**, 44–49

Sherin P. S., Snytnikova O. A., Tsentalovich Y. P. (2006) *Competition between ultrafast relaxation and photoionization in excited prefluorescent states of tryptophan and indole*. The Journal OF Chemical Physics, **125**, 144511

Sinha R. P. and Häder D. P. (2002). *UV-induced DNA damage and repair: a review*. Photochem. Photobiol. Sci., **1**, 225–236

Skovsen E., M. T., Neves-Petersen, A. Kold, L. Duroux and S. B. Petersen. (2008) Journal of Nanoscience and Nanotechnology, in print.

Snabe T., Røder G. A., Neves-Petersen M. T., Buus S., Petersen S. B., (2006) *Oriented coupling of major histocompatibility complex (MHC) to sensor surfaces using light*

assisted immobilisation technology. Biosens. Bioelectron. 2006, **21**, 1553–1559

Snytnikova O. A., P. S. Sherin, L. V. Kopylova, and Y. P. Tsentalovich. (2007). *Kinetics and mechanism of reactions of photoexcited kynurenine with molecules of some natural compounds*. Russian Chemical Bulletin, International Edition, **56**, 4, 732—738

Sommers, P. B., and Kronman, M. J. (1980) *Comparative fluorescence properties of bovine, goat, human and guinea pig α-lactalbumin. Characterization of the environments of individual tryptophan residues in partial folding conformers*. Biophys. Chem.,**11**, 217-232.

Tarek M., D. A. Neumannb and D. J. Tobias. (2003) *Characterization of sub-nanosecond dynamics of the molten globule state of α-lactalbumin using quasielastic neutron scattering and molecular dynamics simulations.* Chemical Physics, **292**, 435–443

Templeton A.C., Cliffel D.E., and Murray R.W. (1999) *Redox and Fluorophore Functionalization of Water-Soluble, Tiopronin-Protected Gold Clusters.* J. Am. Chem. Soc., **121**, 7081-7089

Tsodikov O. V., M. T. Jr. Record, and Y. V. Sergeev. (2002*). A novel computer program for fast exact calculation of accessible and molecular surface areas and average surface curvature.* J. Comput. Chem., **23**, 600-609.

Van Dael H., A. Chedad, A. Vanhooren and I. Hanssens (2005). *Influence of experimental conditions and Trp mutations on the stability and the folding characteristics of goat α-lactalbumin.* Journal of Molecular Structure, **744–747**,155–160

Vanderheeren G. and Hanssens I. (1994) *Thermal Unfolding of Bovine α-Lactalbumin. Comparison of circular dichroism with hydropphobicity measurements*. The journal of Biological Chemistry, **269**, 10, 7090-7094

Vanhooren A., B. Devreese, K. Vanhee, J. Van Beeumen and I. Hanssens. (2002). *Photoexcitation of Tryptophan Groups Induces Reduction of Two Disulfide Bonds in Goat α-Lactalbumin*. Biochemistry, ***41,*** 11035-11043

Vanhooren A., Chedad A., Farkas V., Majer Z., Van Dael H., Joniau M., Hanssens I., (2005) *Tryptophan to phenylalanine substitution allows to differentiate between short and long range conformational changes during denaturation of goat α-lactalbumin*. Proteins, **60**, 118–130

Vanhooren A., E. Illyes, Z. Majer and I. Hanssens. (2006**b**). *Fluorescence contributions of the individual Trp residues in goat α-lactalbumin*. Biochimica et Biophysica Acta, **1764**, 1586–1591

Vanhooren A., K. De Vriendt, B. Devreese, A. Chedad, A. Sterling, H. Van Dael, J. Van Beeumen and I. Hanssens. (2006**a**). *Selectivity of Tryptophan Residues in Mediating Photolysis of Disulfide Bridges in Goat α-Lactalbumin*. Biochemistry, **45**, 2085-2093

Veprintsev D.B., S. E. Permyakov, E. A. Permyakov, V. V. Rogov, K. M. Cawtherm and L. J. Berliner. (1997). *Cooperative thermal transitions of bovine and human apo-lactalbumins: evidence for a new intermediate state*. FEBS Lett, **412**, 625–628.

Walker J. M. (2005) *The Proteomics Protocols Handbook*, Humana Press, 571-607

Wang Q., A. Tolkach and U. Kulozik. (2006). *Quantitative Assessment of Thermal Denaturation of Bovine α-Lactalbumin via Low-Intensity Ultrasound, HPLC, and DSC.* J. Agric. Food Chem., **54**, 6501-6506

Wijesinha-Bettoni R, C. M. Dobson and C. Redfield. (2001). *Comparison of the structural and dynamical properties of holo and apo bovine alpha-lactalbumin by NMR spectroscopy.*

JMol Biol, **307**, 885–898.

Wijesinha-Bettoni R., C. Gao, J. A. Jenkins, A. R. Mackie, P. J. Wilde, E. N. C. Mills and L. J. Smith. (2007). *Heat Treatment of Bovine α-Lactalbumin Results in Partially Folded, Disulfide Bond Shuffled States with Enhanced Surface Activity*. Biochemistry, **46**, 9774-9784

Wilson G., S. J. Ford, A. Cooper, L. Hecht, Z. Q. Wen and L. D. Barron. (1995). *Vibrational Raman Optical Activity of a-Lactalbumin: Comparison with Lysozyme, and Evidence for Native Tertiary Folds in Molten Globule States*. J. Mol. Biol., **254**, 747–760

Wit J. N. and Klarenbeek, G. (1984). *Effects of various heat treatments on structure and solubility of whey proteins*. Journal of Dairy Science, **67**, 2701–2710.

Wu L. C. and Kim P.S. (1998). *A Specific Hydrophobic Core in the α-Lactalbumin Molten Globule*. J. Mol. Biol., **280**, 175-182

Wu, L. C., Peng, Z., and Kim, P. S. (1995) *Bipartite structure of the α-lactalbumin molten globule*. *Nature Struct. Biol.* 2, 28 1-286

Zhang J. and Lakowicz J. R. (2007) *Metal-enhanced fluorescence of an organic fluorophore using gold particles*. Opt. Express, **15**, 2598-2606

APPENDIX

A. DENATURATION OF PROTEINS

The denaturation processes of proteins are frequently used as simplified situations for the analysis of phenomena such as protein stability, folding, and unfolding. Indeed, denaturation appears like an unfolding process, reversal occurring when refolding takes place, and can be use to mimic such mechanisms.

The denaturation generally is considered like a two-state sharp transition from native (N) to denaturated (D) protein, where the structure of the protein is disordered under a certain stress (*e.g.* heat, mild denaturant like urea), and its functionality can be remarkably lost.

This is simplistic description of the process that does not consider the eventual intermediate transitions occurring during protein denaturation. At any instant of time a protein molecule in population of an unfolding protein has a unique conformation which is not static, but constantly being altered by rotation around single bounds. The kinetic pathways of unfolding and refolding process in denaturation phenomenon can be determined by which intermediate conformational state (I_i) the molecule passes through, where the reaction can be described as a succession of transitions, as it can be depicted in Figure A1.

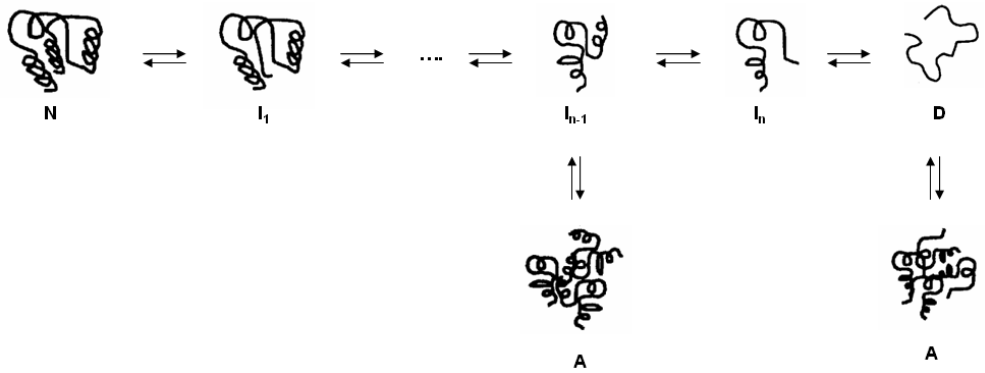

Figure A1: Schematic representation of the kinetic pathways of unfolding and folding in a denaturation process. The states are pictured as a hypothetic protein during its unfolding. Letters: N – native protein; I_i – intermediate species; D – denaturated form; A – state of aggregation.

The general picture given by Figure A1 can be further explored, and simplified for specific cases. Along the process, denaturation can be reversible or irreversible, depending on the transient state where the defolding is, *i.e.* if the reverse path is still energetically viable. Some of intermediates are also stable enough and can exist in equilibrium states. The extent of denaturation can be also variable, affecting largely or not the structure of the protein (on the

quaternary, tertiary, secondary structure), is it confined to a region specific region and resulting only on the partial unfolding of the protein, or involving the complete molecule.

The denaturation can also consist in a “all-or-none” reaction that shows cooperativity nature, or in a more confusing process where the transition is not defined from molecule to molecule in the pool of denaturating species generating even diverse intermediate forms. In a cooperative unfolding there will be no partially unfolded molecules in the set, since structures that exist partly intact or partly are not thermodynamically stable and only exist transiently. In this case the denaturation process can be really approximated to a two-state unfolding (taking place from the native or a transient thermodynamically stable specie to the denatured final form or stable denaturated specie).

Though each protein possesses a unique native three-dimensional structure, the same protein can also adopt several different structures according to the type and extent of denaturating treatment.

Aggregated species (A) may also be formed at different steps of the process, either in the case stable intermediate (due mainly to hydrophobic interactions between exposed hydrophobic groups during denaturation), or in the advent of the denaturated form (disulphide and hydrogen bonding, as ionic forces are responsible for bonding (Damodaran and Paraf, 1997).

Thus, each case must be separately considered, and specific models of defolding must be for the protein in study.

The analysis of denaturation processes is clearly an important issue. Usually, a physical or chemical property of the protein that is related with its structure is measured along an increase in the denaturating conditions (for instance a denaturant concentration or temperature). The property can indicate the local unfolding of a protein, like the fluorescence emission of the protein chromophores (using fluorescence spectroscopy), or the global unfolding of the protein, accessed for instance with the ellipticity measured at far-UV (using circular dichroism spectroscopy), helpful in characterizing of the peptide bond in proteins. In that way a profile can be obtained that describes the denaturating process, and the eventual changes in protein structure, along the diverse intermediates formed. The typical profiles for a two-state denaturation showing cooperativity are illustrated in Figure A2. They show the shift in signal (y) when one pass from a native specie (y'_N and y_N) to a denaturated form (y'_D and y_D), signal this that characterizes a part of the structure and its shift in position.

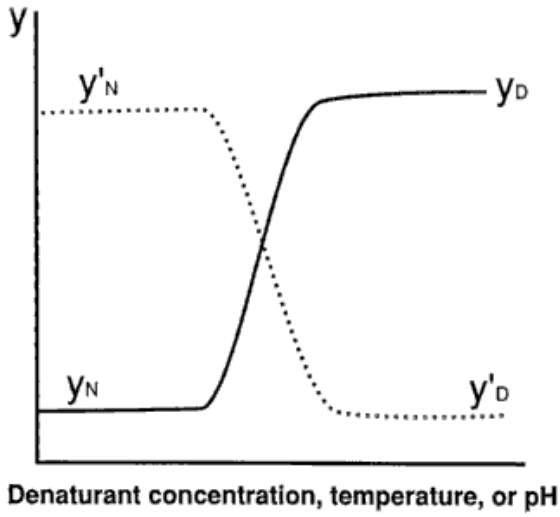

Figure A2: Typical protein denaturation curves; *y* represents any measurable physical or chemical property of the protein that varies with protein conformation; y_N and y_D are the values for the native and denaturated state respectively (Adapted from Fenemma, 1996).

It is also important to notice that monomeric proteins that contain two or more domains with different properties may exhibit multiple transition steps in a unfolding profile.

The denaturation curves further allow the quantification of the denaturation process. When cooperativity is present in a transition between two species, the "two-state transition" model can be applied. For this model the equilibrium between the native and the denaturated state in the cooperative transition region can be expressed as:

$$N \underset{}{\overset{K_D}{\rightleftharpoons}} D \qquad \text{(A.1)}$$

$$K_D = [D]/[N] \qquad \text{(A.2)}$$

where K_D is the equilibrium constant. Since the concentration of denaturated protein molecules in the absence of a denaturant is extremely low, estimation of this constant is not possible. However, in the transition region, where the concentration of denaturant is sufficiently high, an increase in the population of denaturated protein specie allows the determination of the apparent equilibrium constant, K_{app}. In the transition region, where both native and denaturated protein species are present, the value of *y* is given by:

$$y = f_N y_N + f_D y_D \qquad \text{(A.3)}$$

where *fn* and *fd* are the fractions of the protein in the native and denaturated state, and y_N and y_D are y values for the native and denaturated states respectively. From Figure A2 one can deduce the values of each fraction (here is considered that the denaturated specie has a higher signal, the inverse would imply the correspondent calculations):

$$f_N = (y_D - y)/(y_D - y_N) \quad \text{(A.4)}$$

$$f_D = (y - y_N)/(y_D - y_N) \quad \text{(A.5)}$$

Since the fractions of denaturant and native protein are correspondent to their concentrations, the apparent equilibrium constant is then obtained by:

$$K_{app} = f_D / f_N = (y - y_N)/(y - y_D) \quad \text{(A.6)}$$

The free energy of denaturation is finally given by:

$$\Delta G_{app} = -RT \ln K_D \quad \text{(A.7)}$$

R is the perfect gas constant in J.mol^{-1}.K^{-1}, T temperature in K. A plot of $-RT \ln K_D$ versus denaturant signal (concentration, temperature, pH) results in a straight line. The value of mid-transition is the value for which the free energy of denaturation ΔG_{app} is zero, *i.e.* at equilibrium.

In the case of chemical denaturants, the enthalpy of change ΔH_D can be obtained from the variation of the free energy change with temperature using the Van't Hoff equation.

$$\Delta H_D = -R \frac{d \ln K_D}{d(1/T)} \quad \text{(A.7)}$$

One can compare the process under different conditions (which would rely on a variable distinct from the responsible for denaturation) by means of the value at mid-transition, is it the temperature of mid-transition (T_m), concentration of denaturant at mid-transition (C_m), or pH of mid-transition (pH_m). The value of mid-transition will then one for which in the set of proteins in analysis, half of them are still in the original state and half of them in the denaturated one. One classical example is the melting temperature, or denaturation temperature (T_d), which is simply the T_m for proteins and other biomolecules that present a two-state sharp thermal transition (from the N-state to the D-state). It is often used characterize the thermal denaturation of several enzymes and proteins, and other biomolecules, like for instance the DNA on its denaturation from double to single chain (Damodaran and Paraf, 1997; Fenemma, 1996).

B. SUPPLEMENTARY RESULTS

Time-dependent Disruption of Disulphide Bridges

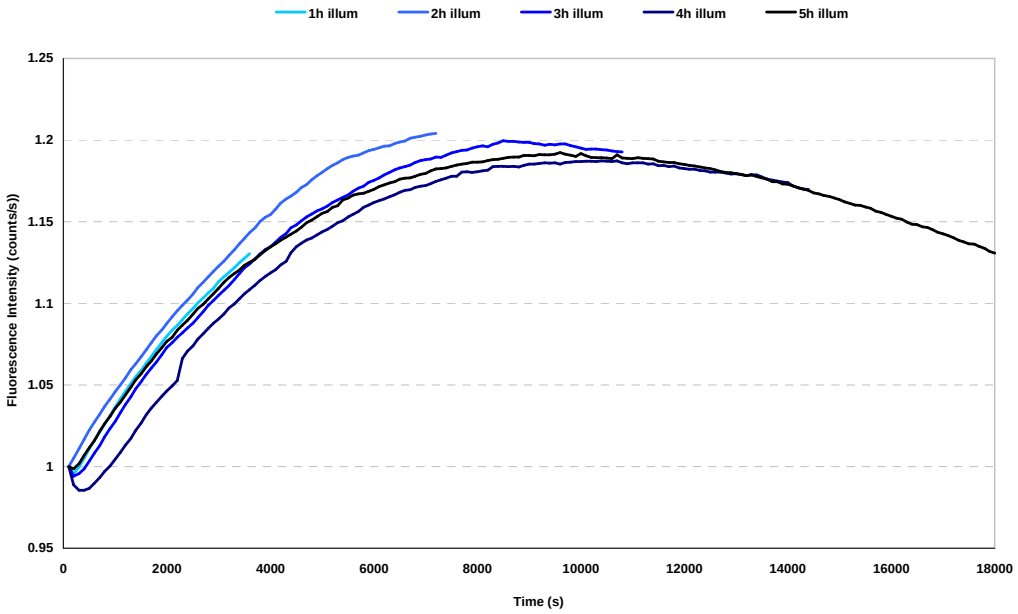

Figure B.1: Fluorescence intensity of eLA *versus* illumination time in the diverse irradiation sessions (1-, 2-, 3-, 4-, and 5-h). Excitation was fixed at 295 nm and emission was monitored at 340 nm. Temperature was maintained at 25ºC using a peltier element. Measurements were performed using a RTC 2000 PTI spectrofluorimeter. The curves were normalized and corrected for the oscillations of lamp intensity as described in Materials and Methods (Section 5.2).

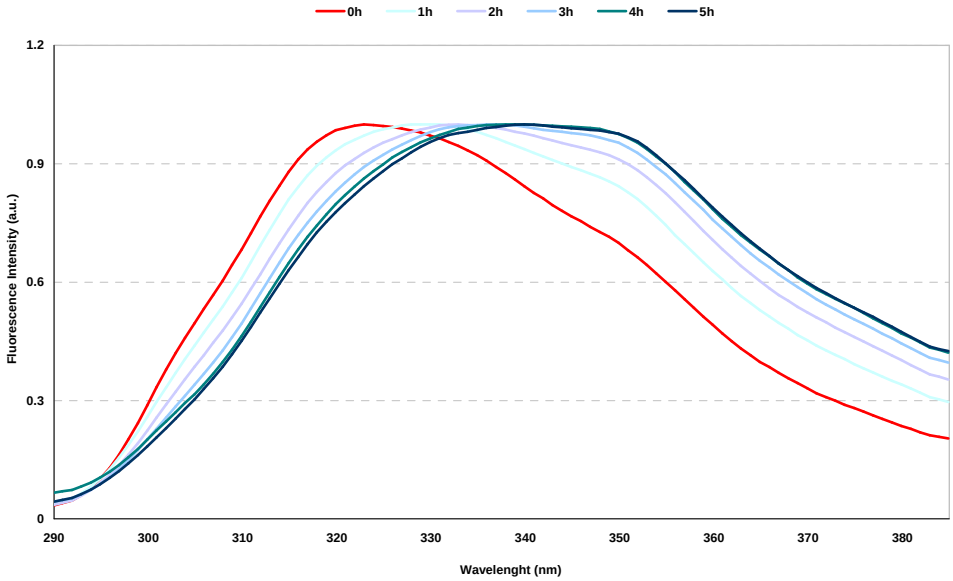

Figure B.2: Normalized emission spectra of illuminated samples of eLA over different time periods and non-illuminated eLA. Excitation was realized at 280 nm. The spectra were first smoothed and normalized as described in Materials and Methods (section 5.2).

Figure B.3: Corrected absorbance spectra recorded after 22 minutes of reaction between irradiated (1-, 2-, 3-, 4-, and 5-h) and non-irradiated (0h) eLA and DTNB. The correction was realized by subtracting the experimentally obtained spectra and the spectra for the reagent blanks, enlighten by colored dashes in the Plot. The characteristic peak at 412 nm can be noticed for the irradiated samples, while for the non-irradiated sample, no peak is visible, the value at 412 nm being merely residual.

Influence of temperature in the time-dependent fluorescence emission of eLA - Fitting Results

9.3 ºC

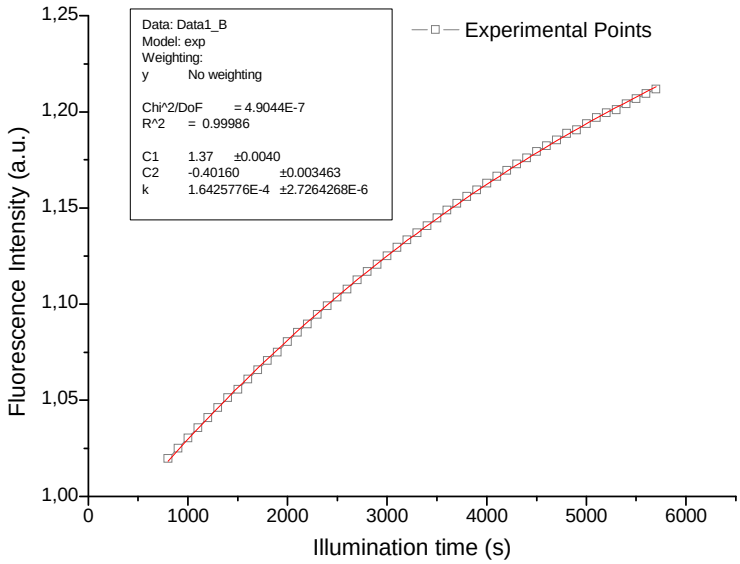

Figure B.4: Fitting curve obtained for fluorescence time-dependent intensity at 340 nm upon irradiation with 295 nm UV-light for 9.3 ºC (red). The experimental points are also displayed (squares). In the box are presented the fitting parameters, correspondent errors, mean square error, and chi square error.

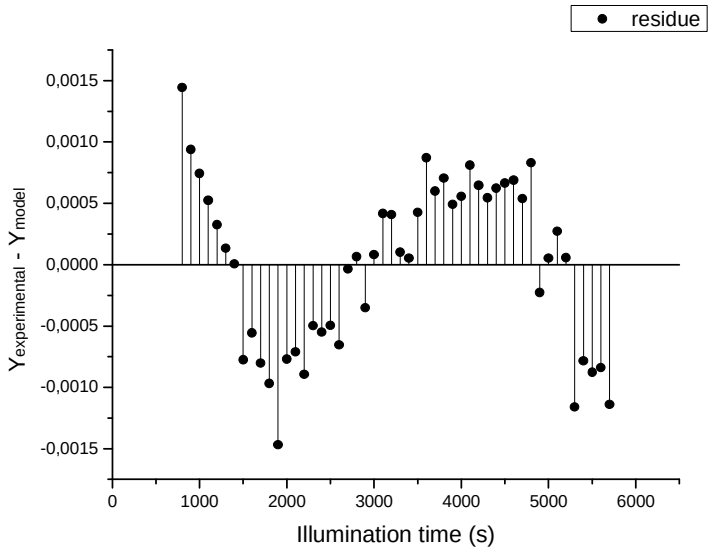

Figure B.5: Residual Plot obtained for the fitting of the fluorescence time-dependent intensity curve obtained at 9.3 ºC. Each residue corresponds on the difference between the experimental point and the value predicted by the model.

12.9 ºC

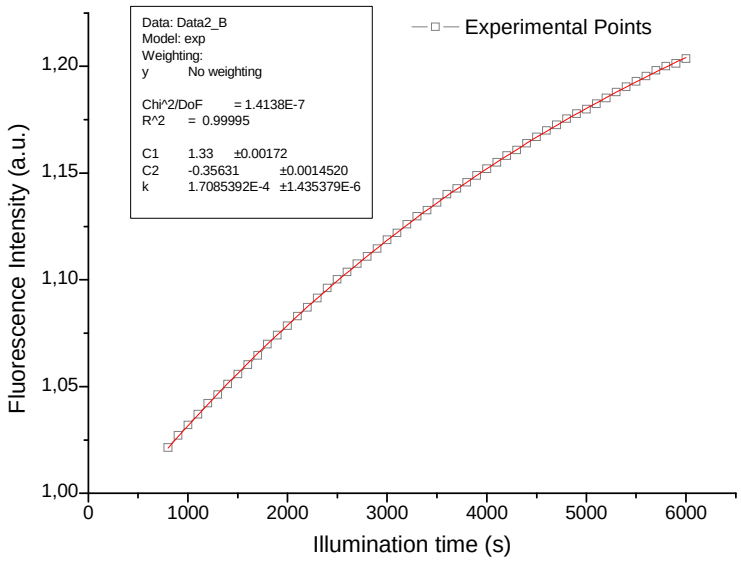

Figure B.6: Fitting curve obtained for fluorescence time-dependent intensity at 340 nm upon irradiation with 295 nm UV-light for 12.9 ºC (red). The experimental points are also displayed (squares). In the box are presented the fitting parameters, correspondent errors, mean square error, and chi square error.

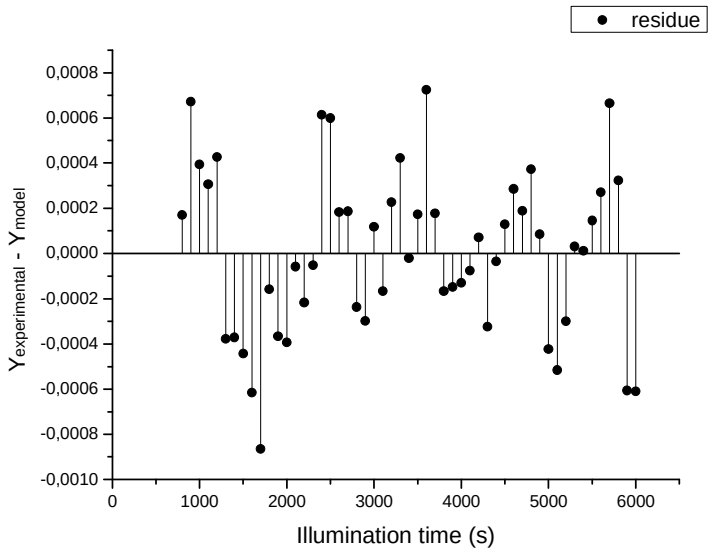

Figure B.7: Residual Plot obtained for the fitting of the fluorescence time-dependent intensity curve obtained at 12.9 ºC. Each residue corresponds on the difference between the experimental point and the value predicted by the model.

15.6 ºC

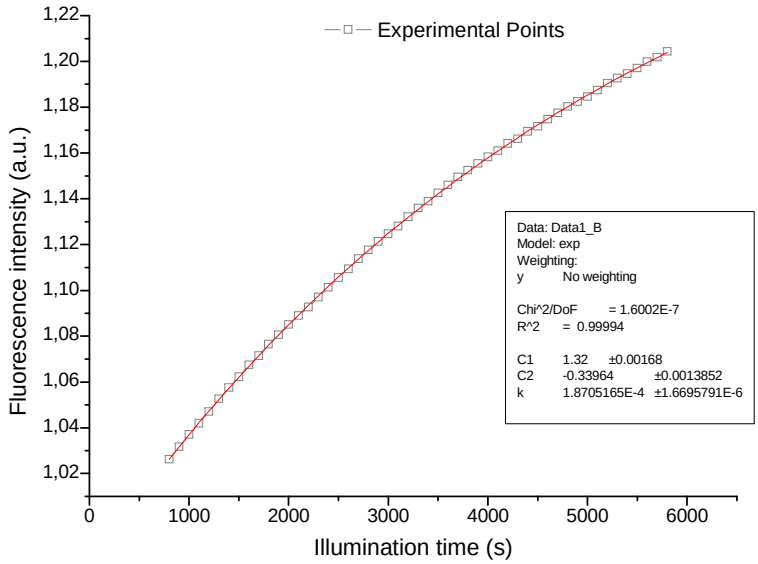

Figure B.8: Fitting curve obtained for fluorescence time-dependent intensity at 340 nm upon irradiation with 295 nm UV-light for 15.6 ºC (red). The experimental points are also displayed (squares). In the box are presented the fitting parameters, correspondent errors, mean square error, and chi square error.

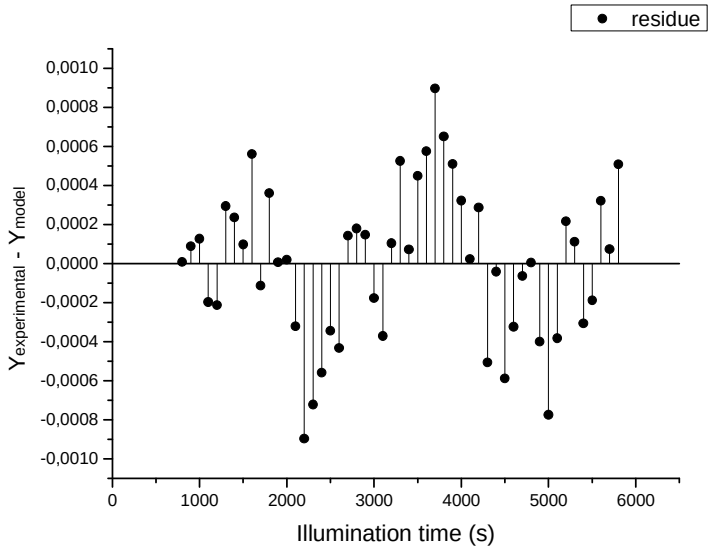

Figure B.9: Residual Plot obtained for the fitting of the fluorescence time-dependent intensity curve obtained at 15.6 ºC. Each residue corresponds on the difference between the experimental point and the value predicted by the model.

20.4 ºC

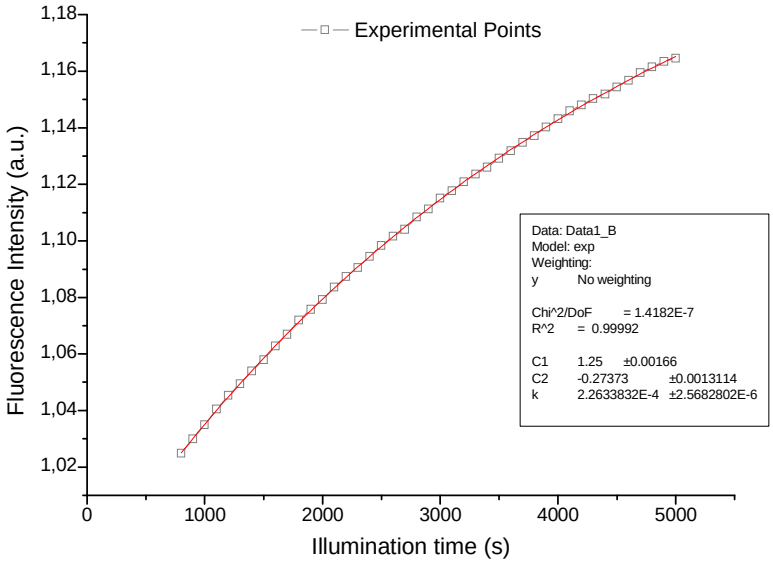

Figure B.10: Fitting curve obtained for fluorescence time-dependent intensity at 340 nm upon irradiation with 295 nm UV-light for 20.4 ºC (red). The experimental points are also displayed (squares). In the box are presented the fitting parameters, correspondent errors, mean square error, and chi square error.

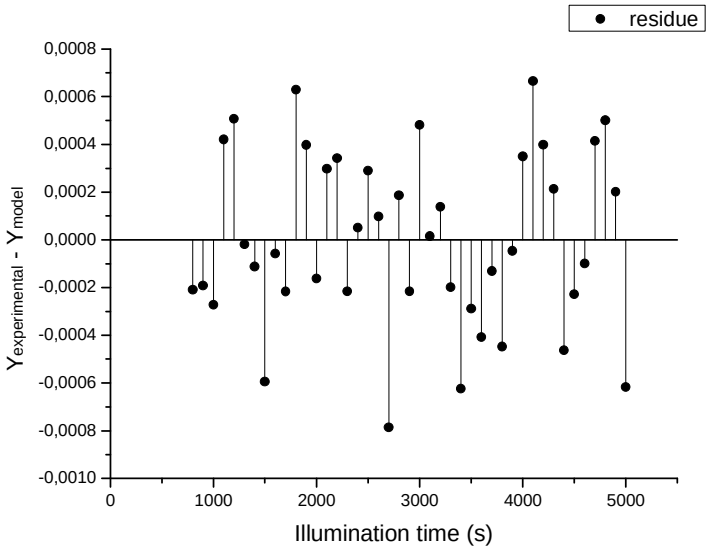

Figure B.11: Residual Plot obtained for the fitting of the fluorescence time-dependent intensity curve obtained at 20.4 ºC. Each residue corresponds on the difference between the experimental point and the value predicted by the model.

24.9 ºC

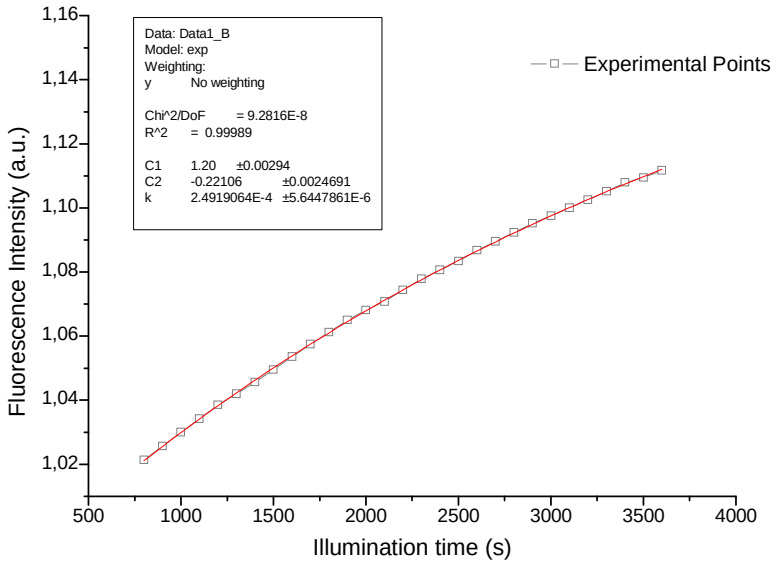

Figure B.12: Fitting curve obtained for fluorescence time-dependent intensity at 340 nm upon irradiation with 295 nm UV-light for 24.9 ºC (red). The experimental points are also displayed (squares). In the box are presented the fitting parameters, correspondent errors, mean square error, and chi square error.

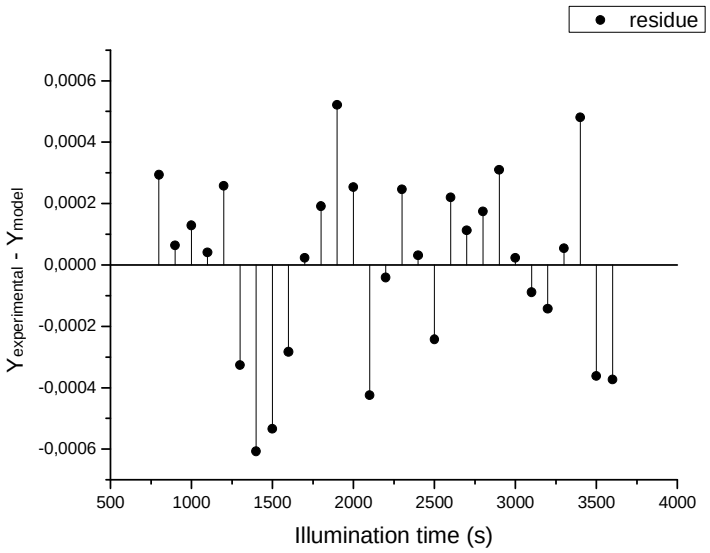

Figure B.13: Residual Plot obtained for the fitting of the fluorescence time-dependent intensity curve obtained at 24.9 ºC. Each residue corresponds on the difference between the experimental point and the value predicted by the model.

29.9 ºC

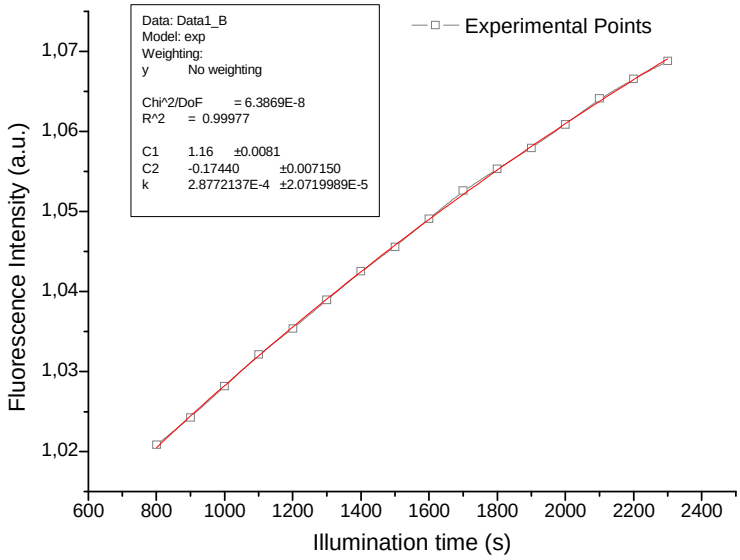

Figure B.14: Fitting curve obtained for fluorescence time-dependent intensity at 340 nm upon irradiation with 295 nm UV-light for 29.9 ºC (red). The experimental points are also displayed (squares). In the box are presented the fitting parameters, correspondent errors, mean square error, and chi square error.

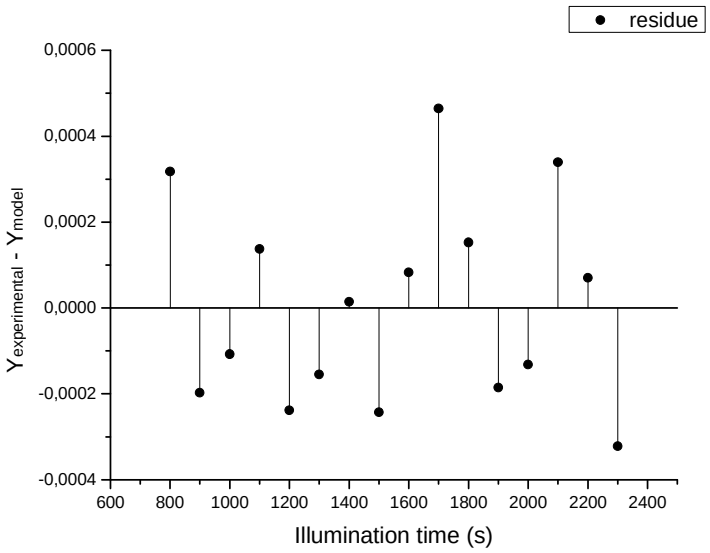

Figure B.15: Residual Plot obtained for the fitting of the fluorescence time-dependent intensity curve obtained at 29.9 ºC. Each residue corresponds on the difference between the experimental point and the value predicted by the model.

Influence of temperature in the time-dependent fluorescence emission of eLA – Emission Spectra

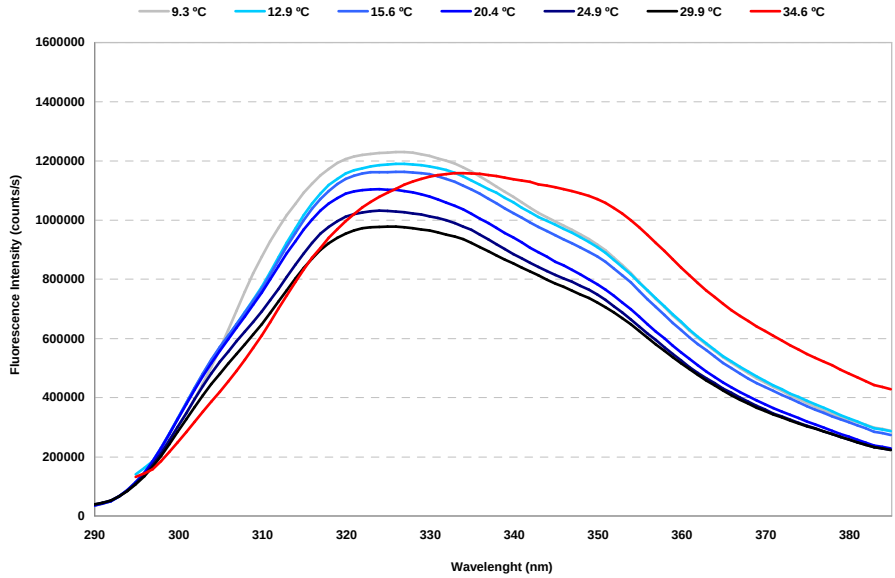

Figure B.16: Emission spectra of non-illuminated eLA at different temperatures (9.3, 12.9, 15.6, 20.4, 24.9, 29.9 and 34.6ºC). Solution temperature was previously set using the peltier element. Excitation was realized at 280 nm. The spectra were first smoothed as described in Materials and Methods (section 5.2).

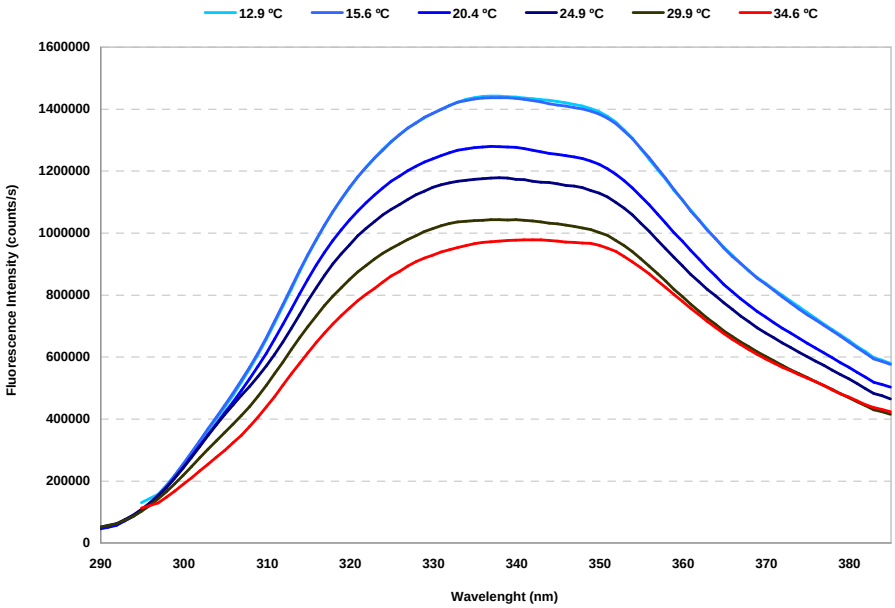

Figure B.17: Emission spectra of eLA recorded after 3.5h of 295 nm light irradiation at different temperatures (12.9, 15.6, 20.4, 24.9, 29.9 and 34.6ºC). Excitation was realized at 280 nm and the temperature of the solution was still maintained after the precedent irradiation and during recording of the spectra. The spectra were first smoothed as described in Materials and Methods (section 5.2).

Influence of pH in the time-dependent fluorescence emission of eLA

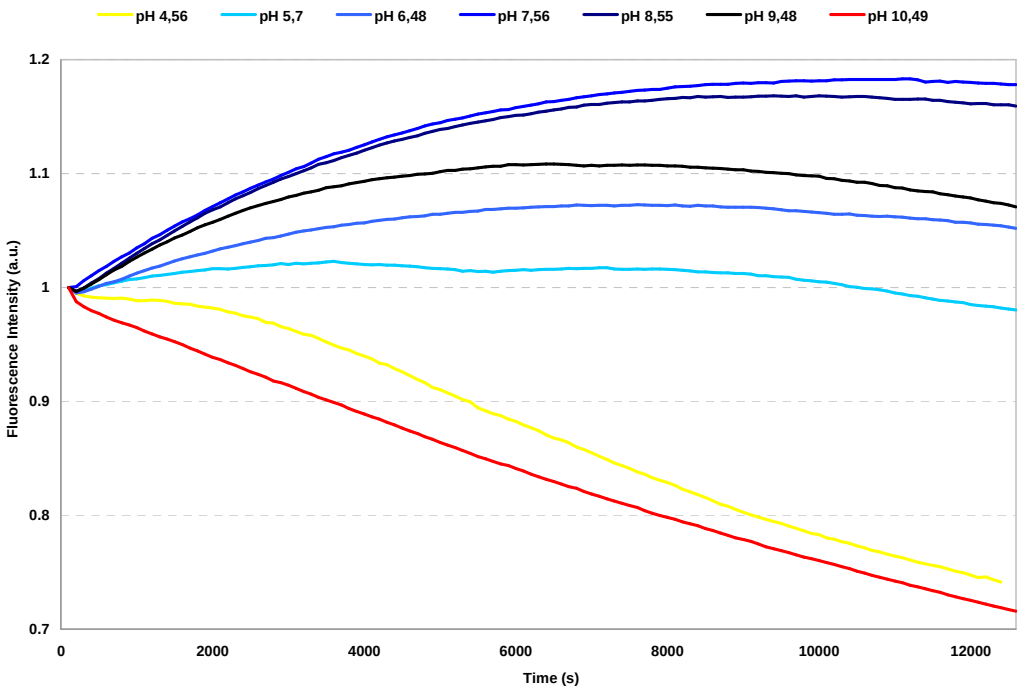

Figure B.18: Fluorescence intensity of Bα-L in function of the illumination time at pH values (4.56, 5.7, 6.48, 7.56, 8.55, 9.48, and 10.49). Excitation was realized at 295 nm and emission measured at 340 nm. Measurements were effectuated using a PTI spectrofluorimeter during 3.5 hours. The temperature of the solution was maintained constant using a Peltier element. The curves were normalized and corrected for the oscillations of lamp intensity as described in Materials and Methods (Section 5.2).

Temperature Influence on Fluorescence Emission

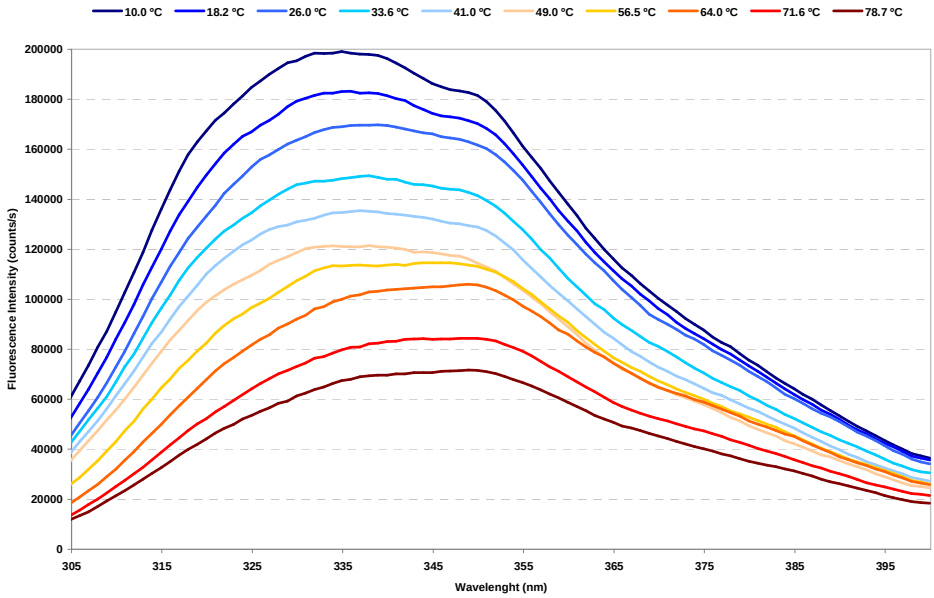

Figure B.19: Emission spectra of fresh eLA solutions recorded at different temperatures (10.0, 18.2, 26.0, 33.6, 41.0, 49.0, 56.5, 64.0, 71.6, and 78.7 ºC). Excitation was realized at 295 nm and the temperature of the solution was set before the recording of the spectra and during the short irradiation. The spectra were smoothed as described in Materials and Methods (section 5.2).

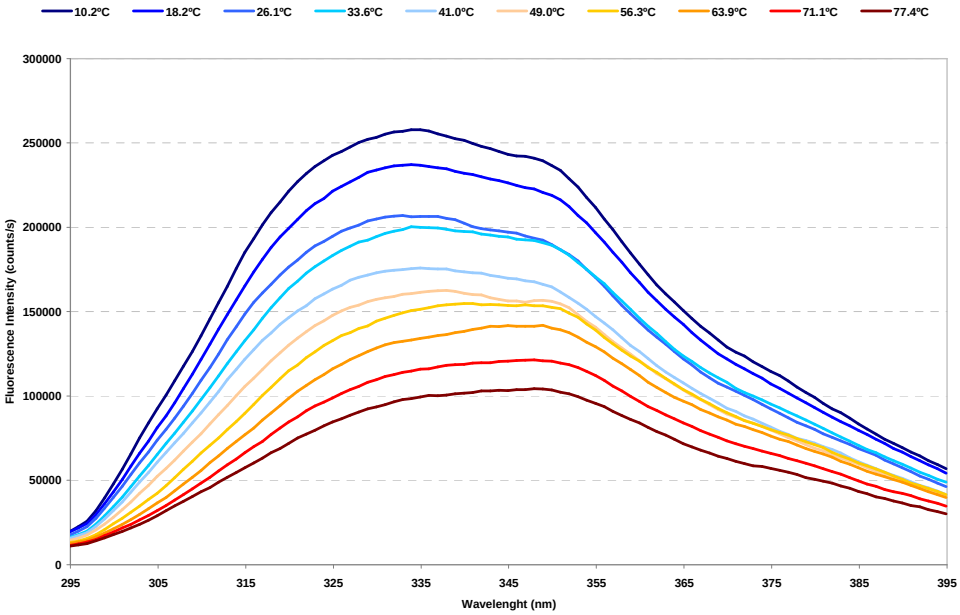

Figure B.20: Emission spectra of fresh eLA solutions recorded at different temperatures (10.2, 18.2, 26.1, 33.6, 40.9, 49.4, 56.3, 63.9, 71.1, and 77.4 ºC). Excitation was realized at 280 nm and the temperature of the solution was set before the recording of the spectra and during the short irradiation. The spectra were smoothed as described in Materials and Methods (section 5.2).

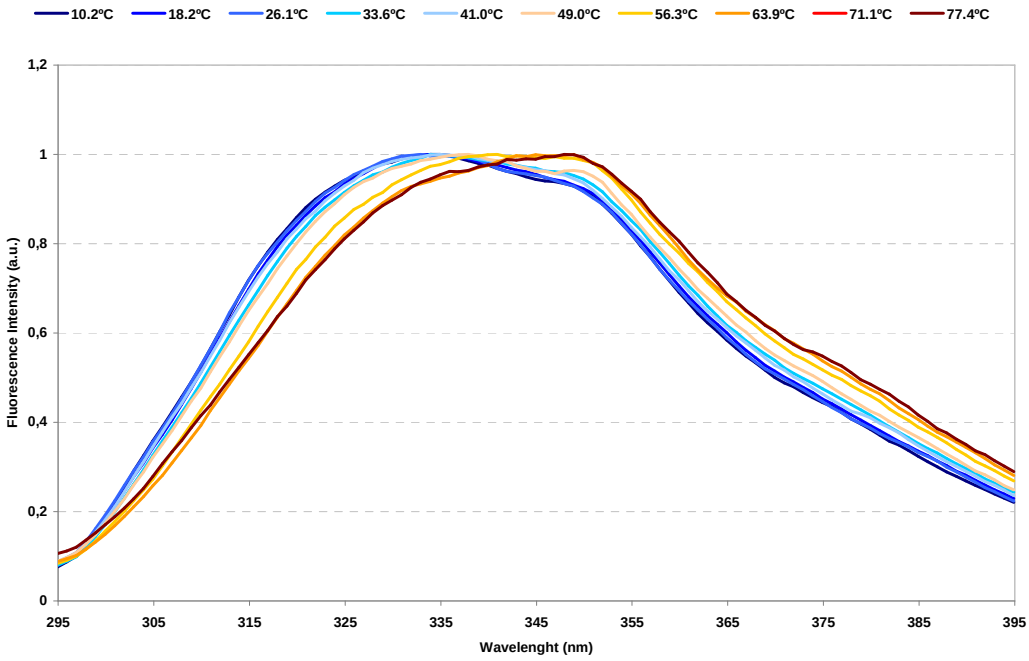

Figure B.21: Normalized emission spectra of fresh eLA solutions recorded at different temperatures (10.2, 18.2, 26.1, 33.6, 40.9, 49.4, 56.3, 63.9, 71.1, and 77.4 ºC). Excitation was realized at 280 nm and the temperature of the solution was set before the recording of the spectra and during the short irradiation. The spectra were smoothed and normalized as described in Materials and Methods (section 5.2).

Immobilization Procedure

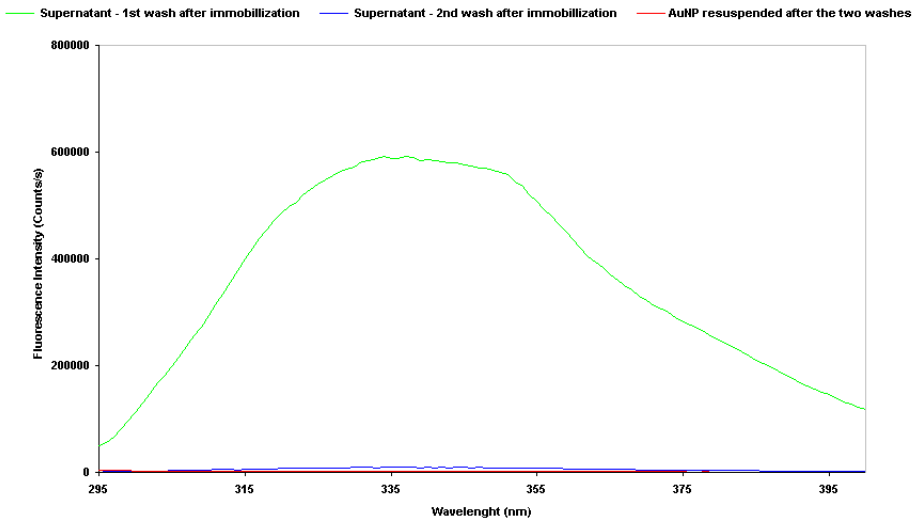

Figure B.22: Emission spectra of the supernatants of the two washes and the final resuspended AuNP solution. The spectra are corrected for *Raman contribution*. The spectra were recorded in a PTI spectrofluorimeter as previously described in Materials and Methods (Section 6.2)

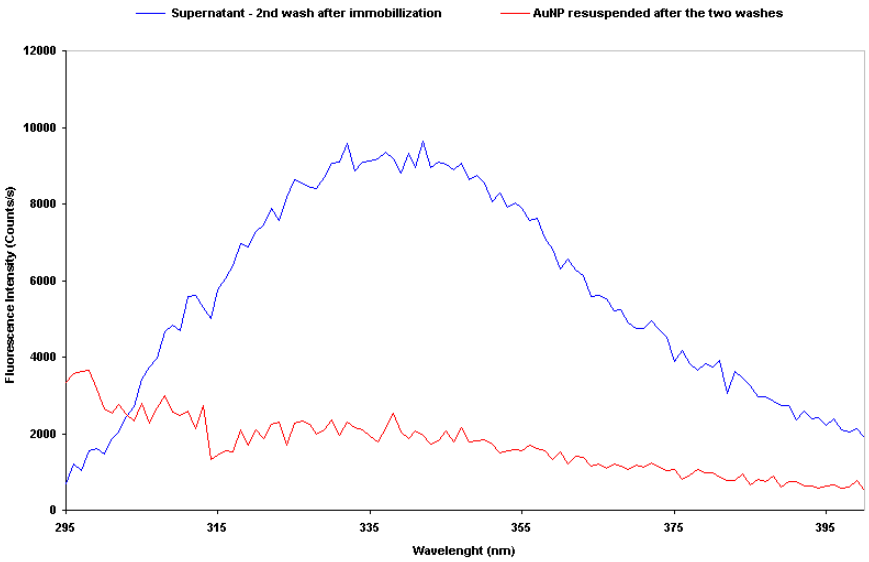

Figure B.23: Emission spectra of the supernatants of the second wash and the final resuspended AuNP solution. The spectra are corrected for *Raman contribution*. The spectra were recorded in a PTI spectrofluorimeter as previously described in Materials and Methods (Section 6.2)

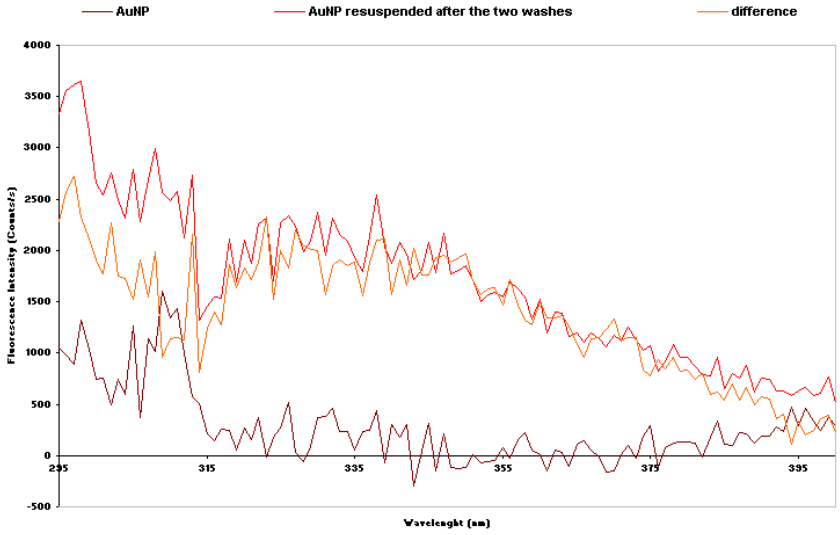

Figure B.24: Emission spectra of the final resuspended AuNP solution, a fresh solution of AuNP and the difference between them. The spectra are corrected for *Raman contribution*. The spectra were recorded in a PTI spectrofluorimeter as previously described in Materials and Methods (Section 6.2)

		Diam. (nm)	% Intensity	Width (nm)
Z-Average (d.nm): 22,86	Peak 1:	50,37	82,4	19,64
PdI: 0,596	Peak 2:	3,398	17,6	1,059
Intercept: 0,820	Peak 3:	0,000	0,0	0,000

Result quality : Refer to quality report

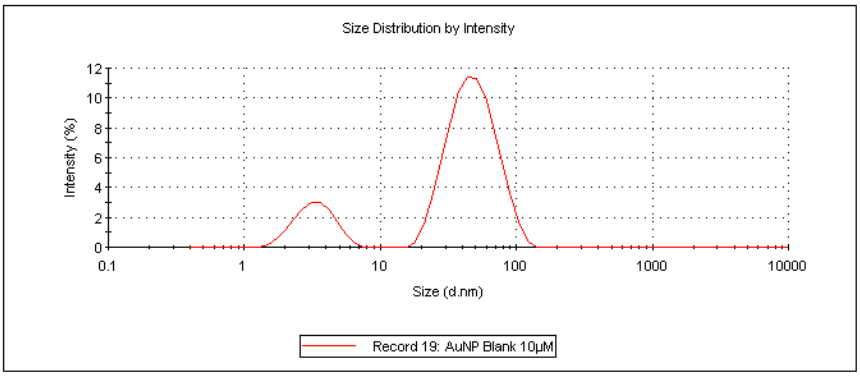

Figure B.25: Size distribution by Intensity. The intensity is related to the number of measurements that originated a peak with for a certain particle size. A strong intensity means that in solution is present a considerable amount of molecules with the particular size where the peak is centered. Results obtained for a AuNP fresh solution of 10 µM. The dynamic light scattering measurements were realized in a Zeta Sizer NANO ZS as described in Materials and Methods (section 6.2).

		Diam. (nm)	% Intensity	Width (nm)
Z-Average (d.nm): 34,01	Peak 1:	72,10	85,0	29,98
PdI: 0,622	Peak 2:	5,477	15,0	1,976
Intercept: 0,667	Peak 3:	0,000	0,0	0,000

Result quality : Refer to quality report

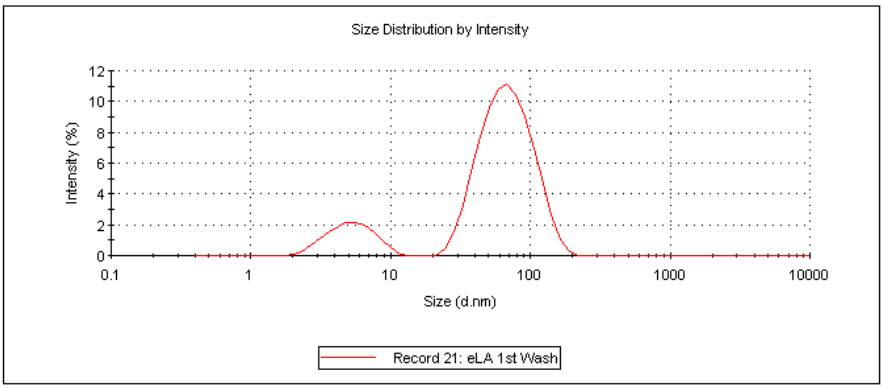

Figure B.26: Size distribution by Intensity. The intensity is related to the number of measurements that originated a peak with for a certain particle size. A strong intensity means that in solution is present a considerable amount of molecules with the particular size where the peak is centered. Results obtained for the supernatant of the first wash. The dynamic light scattering measurements were realized in a Zeta Sizer NANO ZS as described in Materials and Methods (section 6.2).

			Diam. (nm)	% Intensity	Width (nm)
Z-Average (d.nm):	25,90	Peak 1:	50,81	86,3	20,84
PdI:	0,579	Peak 2:	3,767	13,7	1,170
Intercept:	0,829	Peak 3:	0,000	0,0	0,000
Result quality :	Refer to quality report				

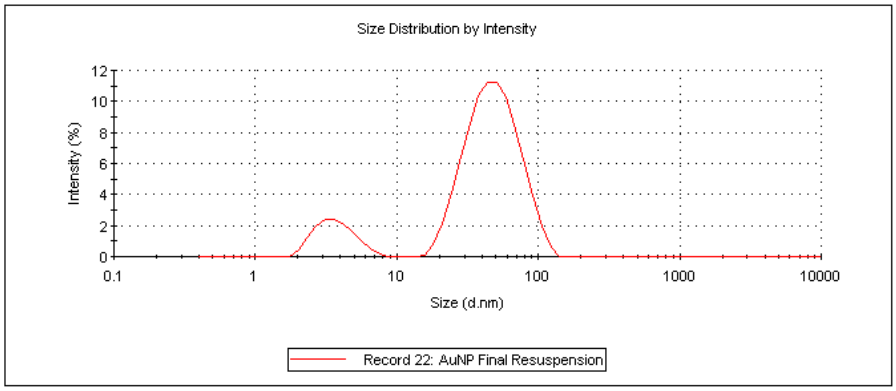

Figure B. 27: Size distribution by Intensity. The intensity is related to the number of measurements that originated a peak with for a certain particle size. A strong intensity means that in solution is present a considerable amount of molecules with the particular size where the peak is centered. Results obtained for the final resuspension of AuNP. The dynamic light scattering measurements were realized in a Zeta Sizer NANO ZS as described in Materials and Methods (section 6.2).

C. DEFINITIONS

Raman Contribution

Spectral data obtained experimentally upon excitation of a certain fluorophore in solution do not translate explicitly the real emission of this molecule. A wide number of factors can affect the signal and distort the observation. Raman scattering can be one of these artifacts, and it will occur from all solvents. For water the Raman peak appears at a wavenumber 3600 cm^{-1} lower than the wavenumber of the incident EM radiation. For excitation at 280 nm the Raman peak from water surges at ~311 nm, which can interfere with protein intrinsic fluorophores emission. Highly fluorescence samples generally dominate the emission and overwhelm the Raman peak. However, if the gain of the instrument is increased to compensate a diluted solution or a low fluorescing sample, the Raman peak may become significant and distort the emission spectrum (Lakowicz et al., 2006).

Isosbestic Point

Isosbestic points are commonly found when spectra plotted on the same chart are taken for a set of solutions where two or more absorbing components are present varying their proportions from solution to solution, provided that their total concentration is constant. The

meaning of isosbestic points is though polemic, and the knowledge about them is still scarce. An isosbestic point can arise in diverse situations, for instance:

- when the electronic spectra are taken on a solution where a chemical reaction is taking place, in which case the two absorbing components are a reactant and a product A and B;
- a solution where the two absorbing species A and B are in equilibrium and their relative proportions are controlled by the concentration of some other component (*e.g.* the protonated and deprotonated forms of a acid-base indicator; in this case the other component would be hydrogen ions);
- in the spectra of two unrelated components non-interacting components that present the same total concentration.

In all these examples, A (and/or B) may be either a single *chemical species* or a mixture of chemical species present in invariant proportion. If A and B are single chemical species, isosbestic points will appear at all wavelengths at which their molar absorption coefficients (formerly called extinction coefficients) are the same. (A more involved identity applies when A and B are mixtures of constant proportion.) (IUPAC, Pouet *et al.*, 2004)

INSTITUTO SUPERIOR TÉCNICO
Universidade Técnica de Lisboa

Probing the effect of ultraviolet light on biomolecules using a whey milk protein: alpha-lactalbumin

Manuel Guilherme Laranjeira Pedrosa Martins Correia

Dissertação para a obtenção do Grau de Mestre em
Engenharia Biológica

Júri

Presidente:	Prof. Luís J. P. Fonseca
Orientadores:	Prof. Duarte Miguel F. Prazeres
	Prof. Maria Teresa Neves-Petersen
	Prof. Steffen B. Petersen
Vogal:	Prof. João Pedro Conde

Dezembro 2008

ACKNOWLEDGEMENTS

First of all, I would like to thank Professor Teresa Neves-Petersen and Professor Steffen Petersen for all the support, guidance and sympathy that I felt while I was in Aalborg. I show as well my gratitude to my supervisor here in Portugal, Professor Miguel Prazeres, always available, and to Professor Helena Pinheiro for establishing the contact with the Nanobio Group.

I also thank all the help and friendship, of my coworkers, Maria Antonietta, Ane, and Gnana, always present. I convey as well my regards to Esben, who, though I did not work directly with him, was always available. I also express my gratitude to all the persons in the department, and specially Jens, who conducted the SEM-EDS experiments. Of course, I also thank my friends in Denmark which were always there for me, and evidently, the ones here in Portugal and my family.

I give my last word of appreciation to Rita, who had the patience to endure my humor in these last days.

RESUMO

A iluminação constante com luz ultravioleta de α-lactalbumina de bovino desprovida de Ca^{2+} resulta em dois efeitos progressivos na emissão dos triptófanos da proteína: aumento da intensidade e *red-shift*. As mudanças espectrais sentidas estão relacionadas com quebra paralela de pontes dissulfureto na proteína iluminada, verificada pela detecção de grupos tiol livres com o reagente de Elmann. As diferenças acima referidas são explicadas pela ausência destas pontes como agentes inibidores de fluorescência e exposição dos triptófanos ao solvente. Após iluminação prolongada observou-se que a proteína se encontrava apenas parcialmente desnaturada, numa conformação similar à nativa.

A fotólise destas pontes é atribuída ao envolvimento de espécies excitadas dos triptófanos em reacções de primeira ordem, com interconversão lenta para produtos caracterizados por *red-shift* e elevada intensidade de fluorescência. Ficou provado que um dos principais mecanismos envolve a fotoionização térmica de singletos excitados de triptófanos, com uma energia de activação de 20.5 $kJ.mol^{-1}$.

A proteína foi igualmente submetida a imobilização em nanoparticulas de ouro (AuNP) de 50.37 nm. A técnica baseia-se na afinidade de superfícies de ouro para os grupos tiol da proteína formados após irradiação com luz ultravioleta. As AuNP provenientes da reacção com proteína iluminada não mostram diferenças consideráveis em diâmetro após medição de *Dynamic Light Scattering*. Contudo, o espectro obtido por *Energy Dispersive X-ray spectroscopy* indica a presença de nitrogénio nas AuNP. Estas observações dão indícios de imobilização por formação de filme fino na superfície das AuNP. Estes complexos nanoparticula-proteína poderão ter um tremendo interesse biomédico, como transportadores moleculares ou biosensores.

Palavras-Chave: α-lactalbumina, pontes dissulfureto, inibição de fluorescência, reacção fotoquímica, imobilização assistida por luz ultravioleta, nanoparticulas de ouro.

TABLE OF CONTENTS

LIST OF ABBREVIATIONS 5
INDEX OF FIGURES 7
INDEX OF TABLES 11
1. ABSTRACT 12
2. INTRODUCTION 13
2.1. CONTEXT 13
2.2. AIM AND STRUCTURE OF THE WORK 14
3. LITERARY OVERVIEW 17
3.1. ULTRAVIOLET LIGHT 17
3.1.1. Definition, Effects of Exposure, Applications 17
3.1.2. Molecular Basis of UV light irradiation effects 18
3.2. FLUORESCENCE 20
3.2.1 Main features 20
3.2.2. Protein Fluorescence 22
3.3. ULTRAVIOLET LIGHT INDUCED REACTION MECHANISMS IN PROTEINS 27
3.3.1. Main Photochemical and Photophysical Reaction Mechanisms 27
3.3.2. Influence of external factors on the reaction mechanisms 30
3.3.3. Consequences of Protein Photo-degradation, SS Bond Breakage and Light Induced Immobilization 32
4. THE PROTEIN MODEL: α-LACTALBUMIN 35
4.1. CONTEXT AND FUNCTIONS OF THE PROTEIN 35
4.2. PRIMARY, SECONDARY & TERTIARY STRUCTURE 36
4.2.1. Main Features 36
4.2.2. Structural Elements Involved in the UV-sensitivity of LA 42
4.3. CONFORMATIONAL STABILITY OF LA 47
4.3.1. Molten Globule States 47
4.3.2. Thermal stability of LA 48
4.3.3. pH Influence in the Conformational Stability of LA 50
4.3.4. Calcium Induced Conformation Changes in LA 52
4.4 REMARKS 54
5. CHARACTERIZATION OF THE MODEL 56
5.1. PREMISSES 56
5.2. MATERIALS AND METHODS 57
5.2.1. Materials 57
5.2.2. Methods 58
5.2.2.1. Experimental Methods 58
5.2.2.2. Data Treatment and Analysis 65
5.3. RESULTS ANALYSIS AND PRESENTATION 66
5.3.1. Time-dependent Disruption of Disulphide Bridges 66
5.3.1.1. Verification and Quantification 66
5.3.1.2. Influence of external parameters 76
5.3.1.3. Effects of illumination on the secondary structure 82
5.3.2. Thermal Stability of the Protein 84
5.4. DISCUSSION 87
6. IMOBILIZATION PROCEDURE 97
6.1. PREMISSES 97
6.2. MATERIALS AND METHODS 98
6.2.1. Materials 98
6.2.2. Methods 98
6.2.2.1. Preparation of AuNP 98
6.2.2.2. Light Induced Immobilization of eLA on AuNP Surface 99
6.3. RESULTS ANALYSIS AND PRESENTATION 101
6.4. DISCUSSION 108
7. CONCLUSIONS 111
BIBLIOGRAPHY 113
APPENDIX 119
A. DENATURATION OF PROTEINS 119
B. SUPPLEMENTARY RESULTS 123
C. DEFINITIONS 137

LIST OF ABBREVIATIONS

ϕ	Quantum yield
F	Total amount of light emitted (and detected)
I_0	Incident light intensity
x	Path length in centimetres
ε	Molar extinction coefficient
c	Molar concentration of the fluorophore
3D	Three-dimensional
A	Arrhenius pre-exponentional factor for
A_{412}	Absorbance value at 412 nm
A_{ion}	Arrhenius pre-exponentional factor for Trp thermal photoionization
ASA	Accessible surface area
AuNP	Gold nanoparticles
bLA	Bovine α-lactalbumin
CD	Circular dichroism
Cys, C	Cysteine
DLS	Dynamic Light Scattering
DTNB	5,5´-dithiobis-(2-nitrobenzoic acid)
Ea	Ahrennius activation energy for the temperature dependence of exponential fluorescence increase rate *k*
Ea_{ion}	Arrhenius activation energy for Trp thermal photoionization
e_{aq}^-	Solvated aqueous electron
EDS	Energy Dispersive X-ray spectroscopy
eLA	Bovine α-lactalbumin used in the experimental procedure
EM	Electromagnetic
F/F_0	Fluorescence intensity increase

GlcNAc	N-acetylglucosamine
GT	β1,4-galactosyltransferase.
HAMLET	Human LA made lethal to tumor cells
k	Fluorescence exponential increase rate
k_{ion}	Rate constant for Trp thermal photoionization
LA	α-lactalbumin
MG	Molten-globule
MHC	Major Histocompability Complex
NMR	Nuclear magnetic resonance
Phe, F	Phenylalanine
R	Constant of perfect gases
RET	Resonance energy transfer
SDS-page	Sodium dodecyl sulfate polyacrylamide gel electrophoresis
SEM	Scanning Electron Microscopy
SEM-EDS	Scanning Electron Microscopy coupled to Energy Dispersive X-ray spectroscopy
SS	Disulphide
T	Temperature
T_d	Denaturation temperature
T_m	Temperature of mid-transition
TNB^{2-}	Nitrothiobenzoate ion
Trp, W	Tryptophan
Tyr, Y	Tyrosine
UDP-GAL	Uridine 5'-(trihydrogen diphosphate)-Galactose
UV	Ultraviolet
UVB	UV radiation in the interval 280-315 nm
λ_{max}	Emission maximum/maxima

INDEX OF FIGURES

Figure 2.1: Principle of Light Assisted Immobilization with Tryptophan (blue) close to a disulphide bridge (red) within a protein molecule (yellow). Sulphur atoms are enhanced in red. 14

Figure 3. 1: The electromagnetic spectrum. 17

Figure 3.2: The electromagnetic spectrum and molecular effects. 18

Figure 3.3: Schematic representation of the processes involved in electronic excitation. * stands for an electronic excited specie (Adapted from Prasad, 2003). 19

Figure 3.4: Typical Jablonski Diagram. The singlet ground, first, and second electronic states are depicted by S_0, S_1 and S_2 respectively. At each of these electronic energy levels the molecular or atomic species can exist in a number of vibrational levels, represented by V_1, V_2, V_3, etc. The initial absorption of light by the molecule leads into a transition to a higher energy state, S_1 or S_2 (1), from which energy can be lost in nonradiative ways, by vibrational relaxation in S_1 (2), by internal conversion (3), by external quenching (4). Molecules in the S_1 lower energetic state can undergo a downward transition by emitting fluorescence (5). Emission of fluorescence usually does not proceed until the ground state, this occurs usually by vibrational relaxation, where there is again an energy loss (6). Intersystem crossing from the singlet excited state (S_1) to the triplet state (T_1) is an alternative to fluorescence as no photon is emitted. However decay from T_1 to S_0 results in phosphorescence. The various vibrational relaxations (10^{-12}s) occur faster than the downward transitions. That is why they happen prime and after fluorescence (Adapted from Macey, 2007). 21

Figure 3.5: Absorption and emission spectra of the protein intrinsic fluorophores in pH 7 aqueous solution (Adapted from Lakowicz, 2006). 23

Figure 3.6: The two excited-state dipole moments of tryptophan (Adapted from Lakowicz, 2006) 24

Figure 3.7: Effect of tryptophan environment on the emission spectra. The higher is the exposure of the Trp in the protein structure, more will be its maxima of absorption red-shifted (1 to 4). This effect can be noticed upon the degree of unfolding of a protein. The emission spectra are those of apoazuerin Pfl, ribonuclease T_1, staphylococcal nuclease, and glugagon, for 1 to 4 respectively (Adapted from Lakowicz, 2006). 25

Figure 3.8: Channels of Trp photoionization. 30

Figure 4.1: Amino-acid composition of bLA. Data obtained using the tool ProtParam on the Expasy Server (www.espasy.org) by submitting the fasta sequence of the PDB Entry 1F6S. 37

Figure 4.2: Three-dimensional structure of LA and the functional regions of the molecule showing the location of metal ions identified in LA crystal structures. Secondary structural elements are marked (*S,* b-strand in blue; *H ,* α-helix and *h,* 3_{10} helix in red). The 8 cysteine residues are also represented, between the close pairs of cysteine are formed the 4 disulphide bridges of the protein (Adapted from Chrysina *et al.*, 2000). 39

Figure 4.3: Localization of the Aromatic Clusters I and II in the structure of bLA. apo-bLAc structure (PDB entry: 1F6R) is shown in *red*, holo-bLAc structure (PDB entry: 1F6S) is shown in *yellow,* and recombinant bLA (mLA) structure in *green*. The superposition of the structures was performed with program O (35) (Adapted from Chrysina *et al.*, 2000). 40

Figure 4.4: A – Molecular structure of lactose synthase, a complex between the catalytic domain of bovine GT (Gal-T1) and mouse LA (alpha-LA). The complex is shown with the acceptor GlcNAc. B – Stereo view of the molecular interactions between the same GT and LA. The secondary elements of LA are colored in red, while those of GT are in blue. The interactions between the proteins are principally hydrophobic. Two water molecules are trapped between the two proteins, and one of them has extensive hydrogen bonding interactions with both protein molecules. Adapted from Ramakrishnan and Qasba (2001). 41

Figure 4.5: Schematic representation of LA. Secondary structure elements and the disulfide bonds in native GLA are indicated at the top. The domain boundaries are shown as dashed lines. Each of the tryptophan residues (O) is indicated (Adapted from Vanhooren *et al.*, 2006a). 42

Figure 4.6: Crystal structure of holo-bLAc at 2.2 Á resolution (PDB entry: 1F6S) generated in *RasMol* 2.6. A- Peptide backbone is represented in grey strands. The 4 Trp and the 8 Cys residues of bLA are displayed in a stick configuration respectively in red and yellow. Dashed yellow lines represent the SS bonds of the protein highlighted by yellow arrows. Potential contact between the indole nucleus of a Trp residue and a disulphide bond is indicated mixed red-yellow dash line and the distance in Á. B- The peptide backbone is represented in grey strands and the backbone of five residues (Val27, Val92, Lys93, Lys94, and Ile95) is in blue. Val 32 is in stick configuration and in green. Contact between the indole nucleus of a Trp residue its potential quenchers is indicated in mixed red-green/blue dash line and the distance in Á. 45

Figure 4.7: Crystal structure of apo-bLAc at 2.2 Á resolution (PDB entry: 1F6S) generated in *RasMol* 2.6. A- Peptide backbone is represented in grey strands. The 4 Trp and the 8 Cys residues of apo-bLAc are displayed in a stick configuration respectively in red and yellow. Dashed yellow lines represent the SS bonds of the protein highlighted by yellow arrows. Potential contact between the indole nucleus of a Trp residue and a disulphide bond is indicated mixed red-yellow dash line and the distance in Á. B- The peptide backbone is represented in grey strands and the backbone of five residues (Val27, Val92, Lys93, Lys94, and Ile95) is in blue. Val 32 is in stick configuration and in green. Contact between the indole nucleus of a Trp residue its potential quenchers is indicated in mixed red-green/blue dash line and the distance in Á. 46

Figure 4.8: Snapshots of LA configurations in the native state (left) and molten globule state at pH 2 (right) from the molecular dynamics simulations. Helices are displayed as barrels and β-sheets as large arrows (Adapted from Tarek *et al.*, 2003)..... 51

Figure 5.1: Reaction of a thiol with Ellman's reagent, originating a mixed disulphide and one equivalent of TNB^{2-}. The extinction molar coefficients at 412 nm are displayed for the different chemical species and all refer to pH > 7.29 (Adapted from Riener *et al.*, 2002). 59

Figure 5.2: Absorbance values at 412 nm *versus* cysteine concentration in the assay. The absorbance values correspond all to a reaction time of 22minutes except for the 0µM solution. 61

Figure 5.3: Fluorescence intensity of eLA *versus* illumination time. Excitation was fixed at 295 nm and emission was monitored at 340 nm. Temperature was maintained at 25ºC using a peltier element. Measurements were performed using a RTC 2000 PTI spectrofluorimeter as described in Materials and Methods (section 5.2). 67

Figure 5.4: Effect of illumination time on the spectrum of excitation and emission. The spectra were recorded fixing the emission at 340 in the excitation spectra and the excitation at 295 in the emission one as described in Materials and Methods (Section 5.2). 68

Figure 5.5: Normalized emission spectra of illuminated samples of eLA over different time periods and non-illuminated eLA. Excitation was realized at 295nm. The spectra were first smoothed and normalized as described in Materials and Methods (section 5.2). 69

Figure 5.6: Normalized excitation spectra of illuminated samples of eLA over different time periods and non-illuminated eLA. Emission was selected at 340nm. The spectra were first smoothed and normalized as described in Materials and Methods (section 5.2). 70

Figure 5.7: Normalized excitation spectra of illuminated samples of eLA over different time periods and non-illuminated eLA. Emission was selected at 320 nm. The spectra were first smoothed and normalized as described in Materials and Methods (section 5.2). 71

Figure 5.8: Ratio between the normalized spectra with the emission fixed at 340 nm displayed in Figure 5.6. The ratio is realized between the spectra took after different periods of illumination and the spectrum of the fresh eLA. 72

Figure 5.9: Ratio between the normalized spectra with the emission fixed at 320nm displayed in Figure 5.7. The ratio is realized between the spectra took after different periods of illumination and the spectrum of the fresh eLA. 72

Figure 5.10: Values of Absorbance read at 412 nm (closed yellow circles A_{412}) *versus* illumination time. In green is displayed time-dependent fluorescence intensity increase at 340nm (F/F_0). The presence of

free thiols was evaluated after reaction with 5,5´-dithiobis-(2-nitrobenzoic acid), after 0-, 1-, 2-, 3-, 4- and 5-h of illumination with 295 nm light, considering that the free thiol concentration is proportional to the absorbance value at 412 nm, as described in Materials and Methods (Section 5.2). F/F0 values displayed consist on the ratio between the monitored values fluorescence emission at 340 nm and the initial fluorescence emission value at 340 nm obtained for the 5-h illumination session. The values were corrected for lamp intensity oscillations as described in Materials and Methods (Section 5.2). 73

Figure 5.11: Ratio of the emission values at 295 nm during the illumination sessions. The emission of 295 nm light was checked constantly during the sessions of irradiation (1h, 2h, 3h, 4h, 5h) with 295 nm light using the second channel of the spectrofluorimeter. The values are corrected for the light source oscillation and were normalized as described in Materials and Methods (Section 5.2). 75

Figure 5.12: Fluorescence intensity of Bα-L in function of the illumination time at different temperatures (9.3, 12.9, 15.6, 20.4, 24.9, 29.9 and 34.6 ºC). Excitation was realized at 295 nm and emission measured at 340 nm. Measurements were effectuated using a PTI spectrofluorimeter during 3.5 hours. The temperature of the solution was maintained constant using a Peltier element. The curves were normalized and corrected for the oscillations of lamp intensity as described in Materials and Methods (Section 5.2). 77

Figure 5.13: Linear relation between the logarithm of the rate constant ln *k* and the inverse of temperature 1/*T*. The linear regression trendline is also displayed in the plot as the equation and the root mean square error R^2. 79

Figure 5.14: Emission spectra of non-illuminated eLA at different temperatures (9.3, 12.9, 15.6, 20.4, 24.9, 29.9 and 34.6ºC). Solution temperature was previously set using the peltier element. Excitation was realized at 295nm. The spectra were first smoothed as described in Materials and Methods (section 5.2). 80

Figure 5.15: Emission spectra of eLA recorded after 3.5h of 295nm light irradiation at different temperatures (12.9, 15.6, 20.4, 24.9, 29.9 and 34.6ºC). Excitation was realized at 295nm and the temperature of the solution was still maintained after the precedent irradiation and during recording of the spectra. The spectra were first smoothed as described in Materials and Methods (section 5.2)....80

Figure 5.16: Values of absorbance at 412 nm after 20 minutes of reaction between the irradiated samples at different temperatures, and DTNB (*vide* Materials and Methods, section 5.2)....81

Figure 5.17: Fluorescence emission maximum increase at 340 nm of eLA upon prolonged 295 nm UV-light irradiation for different pH values. The points F_{max}/F_0 consist on the ratio between the maximum emission value of the time-based fluorescence emission profile (at the plateau) and the fluorescence emission at time zero. The fluorescence time-dependent curves from where these values were obtained are present in the Supplementary Results (Appendix B)....82

Figure 5.18: Fluorescence intensity of eLA *versus* illumination time. Excitation was fixed at 295 nm and emission was monitored at 340 nm. Temperature was maintained at 25ºC using a peltier element. The experiment was stopped each 2000s to remove a protein sample. The emission values are corrected for the oscillations of lamp intensity. Measurements were performed using a RTC 2000 PTI spectrometer as described in Materials and Methods (section 5.2)....83

Figure 5.19: Far-UV CD scan of 295 nm light irradiated eLA samples (0-, 2000-, 4000-, 6000-, 8000-, and 10000-s of illumination) recorded at pH 8.55 and room temperature. The measurements were realized in a JASCO J-715 spectropolarimeter. The spectra were corrected for the buffer contribution in ellipticity and smoothed as previously described in Materials and Methods (Section 5.2). Although some fluctuations are noticed, the overall trend is the partial loss of secondary structure the longer the collected sample was illuminated. 84

Figure 5.20: Normalized emission spectra of fresh eLA solutions recorded at different temperatures (10.0, 18.2, 26.0, 33.6, 41.0, 49.0, 56.5, 64.0, 71.6, and 78.7 ºC). Excitation was realized at 295nm and the temperature of the solution was set before the recording of the spectra and during the short irradiation. The spectra were smoothed and normalized as described in Materials and Methods (section 5.2)....85

Figure 5.21: Maximum of emission of eLA upon excitation at 295 nm (λ_{max}) *versus* the solution temperature. 86

Figure 5.22: Maximum of emission of eLA upon excitation at 295 nm (λ_{max}) *versus* the solution temperature. 86

Figure 6.1: Fluorescence intensity of eLA *versus* illumination time. Excitation was fixed at 295 nm and emission was monitored at 340 nm. Temperature was maintained at 25ºC using a peltier element. Measurements were performed using a RTC 2000 PTI spectrofluorimeter as described in Materials and Methods (section 6.2). 102

Figure 6.2: Absorption spectra of the supernatants of the two washes and the final resuspended AuNP solution. The box displayed within the area of the plot is a zoom of the absorption spectra of the second wash supernatant and the final resuspension of AuNP. The spectra were recorded in a UV-visible absorbance spectrophotometer as previously described in Materials and Methods (Section 6.2).....103

Figure 6.3: Absorption spectra of the final resuspension of AuNP (red), fresh AuNP (wine red) and the difference between these two (orange). Spectra were recorded using a UV-visible spectrophotometer as described in Materials and Methods (section 6.2). 104

Figure 6.4: SEM image of the final AuNP resuspension (after immobilization). Accelerating Voltage: 7.0 keV; Magnification: 18272. The squares represent the area exposed to EMS. X-ray spectra of the exposed areas are displayed in the bottom. The peaks corresponding to each atom are labeled.....106

Figure 6.5: SEM image of the final AuNP blank (fresh, non-exposed particles). Accelerating Voltage: 7.0 keV; Magnification: 29881. The squares represent the area exposed to EMS. X-ray spectra of the exposed areas are displayed in the bottom. The peaks corresponding to each atom are labeled.....107

INDEX OF TABLES

Table 4.1: Comparison of different LA structures. The values displayed are the root mean square deviations (in Å) obtained after superposition using the least square fitting function applied to C_α atoms of residues 1-120 (values in bold font) and to the core of the molecule (values in normal font). LA core comprises the residues 5-11, 23-40, 50-61, and 71-104. Apo-bLAc: Ca^{2+} depleted form of bovine LA at 2.2 Å (PDB code: 1F6R). Holo-bLAc: Ca^{2+} bound form of Bovine LA at 2.2 Å (PDB code: 1F6S). mLA: recombinant bovine LA at 2.3 Å (PDB code: 1HFZ). Baboon LA at 1.7 Å (PDB code; 1ALC). Guinea pig LA at 1.9 Å (PDB code, 1HFX). Goat LA at 2.3 Å (PDB code, 1HFY). Buffalo LA at 2.3 Å (Calderone *et al*., 1996). Human LA at 1.7 Å (Acharya *et al*., 1991). The values were calculated using the program O (Extracted from Chrysina *et al*.., 2000).....37

Table 4.2: Distances between the Trp residues of holo-bLAc and Apo-bLAc and its potential quenchers. The values were determined in *Rasmol* 2.6 using the "monitor" tool. In green are highlighted the Trp-quencher pairs for which there is direct contact (≤ 5.2 Å). 44

Table 5.1: Salts used for Buffer preparation, Molecular Formula, Purity, and Provenience. 57

Table 5.2: Composition of the solutions used for the Ellman's assays and of the two blanks. 60

Table 5.3: Conditions and settings used in the temperature-dependent illumination sessions of eLA samples. 61

Table 5.4: Buffers used for the protein solutions used in the illumination sessions and correspondent pH values. 62

Table 5.5: Selected settings in the RTC 2000 PTI spectrometer for eLA steady-state illumination.....63

Table 5.6: Experimental parameters for the standard CD spectra of a wavelength scan at 25ºC. 64

Table 5.7: Parameters values and correspondent errors, root mean square errors, and reduced chi square errors obtained after fitting of time-based fluorescence curves using equation 5.2. 78

Table 6.1: Experimental settings used in the immobilization procedures. 99

Table 6.2: Experimental atomic values obtained after EMS analysis of each exposed zone - AuNP resuspension (after immobilization). 106

Table 6.3: Experimental atomic values obtained after EMS analysis of each exposed zone - AuNP blank (fresh, non-exposed particles). 107

1. ABSTRACT

Prolonged ultraviolet illumination of Ca^{2+} depleted form of bovine α-lactalbumin (bLA) results both in progressive red-shift and increase of tryptophan fluorescence emission. Such spectral changes are related to progressive cleavage of disulphide bonds in illuminated protein molecules, verified by detection of free thiol groups with Elmann's reagent. The absence of disulphide bridges as fluorescence quenchers and dislocation of tryptophan residues to solvent accessible zones explain the emission changes. After prolonged ultraviolet-irradiation and disulphide bond cleavage, the protein is only partly denaturated, in a native-like conformation.

Photolysis of the disulphide bonds is credited to involvement of tryptophan excited species in first order reactions, slowly interconverting into high quantum yield red-shifted species. The presence of a hidden isosbestic point in successive tryptophan emission spectra suggests such equilibrium. It was proven that one of the major reaction pathways is the thermal photoionization of tryptophan excited singlet states with Arrhenius activation energy of 20.5 $kJ.mol^{-1}$.

Light induced immobilization of Ca^{2+} depleted bLA form was attempted using 50.37 nm gold nanoparticles (AuNP).The technique is based on the affinity to gold surfaces of free protein thiol groups formed upon ultraviolet-irradiation. AuNP provenient of reaction with irradiated bLA show no net difference in hydrodynamic radius compared to fresh AuNP after Dynamic Light Scattering measurements. However, Energy Dispersive X-ray spectroscopy shows unusual nitrogen contents on this reaction product. Such observations indicate that bLA might immobilize onto AuNP forming a thin film on the gold surface. The complexes nanoparticle-bLA may be of biomedical interest, as molecular carriers or biosensors.

Keywords: α-lactalbumin, disulphide bridges, fluorescence quenching, photochemical reaction, light-assisted immobilization, gold nanoparticles.

2. INTRODUCTION

2.1. CONTEXT

Nowadays, according to the physics interpretation, light encompasses the broad spectra of electromagnetic radiation from radio-waves to gamma rays. Interaction between light and matter is ubiquitous in nature and lies within numerous day-to-day commodities man uses.

Historically, light has always fascinated curious minds, since the first descriptions of light in antiquity to the proton theory of Albert Einstein. Wonder how light is constituted and how it influenced the universe around us were intriguing questions, from simple visible interactions like reflection or definition of colors to our eye-site, to others more discrete like glow in the dark mineral crystals and the photoelectric effect.

Light can indeed interplay with matter (molecules, atoms) in a several ways, that cover transfer of energy by absorption, reflection, refraction, scattering, as reversely as matter can itself emit light. Light modulates matter and *vice-versa*, and they regulate a wide number of mechanisms, equilibrium hard to follow. One of the ways of regulation consists in light-induced reactions. These are particularly fascinating since they are ultra fast, tremendously complex, and give rise to profound changes in matter.

Nature itself has particularly been mediated by light induced reactions as a principle for life across its advances. Harnessing photons to achieve photosynthesis and conversion of photons to achieve vision are two simple examples. There are also strong signs that indicate that light was essential in the genesis of life, allowing the generation of simple molecules that constituted the first living organisms.

Thus, it is not strange that crossing light and biology has raised interest for the scientific community years over years. Until recently, the task was rather difficult, due to the lack of instrumentation, which limited the survey to simple and imprecise techniques. However, in the last decades, the evolution of optical instruments, the development of laser technology, and photonic technology allowed to unravel new approaches for understanding light processes and applying light to specific needs. Biophotonics emerged as new discipline and imputed a load of knowledge into this perspective, taking advantage of new photonic tools available.

Here precisely the attention is prawn to the effects of ultraviolet (UV) light in biomolecules. Biological medium is naturally exposed to UV radiation. Ambient sunlight is constituted by photons in the visible range, but also broadens some in the UV and Infrared. Part of the UV radiation is blocked in the atmosphere, but a considerable amount of near-UV radiation still reaches earth's surface. The harmful effects of exposure to UV radiation from sunlight are widely known. In humans, prolonged direct exposure to sunlight can induce severe health

problems (*e.g.* immunosupression, skin cancer; Matsumara and Ananthaswamy, 2004). UV-irradiation can affect a wide number of organisms, such as bacteria, cyanobacteria, phytoplacton, macroalgae, plants and animals through DNA damage (Sinha and Häder, 2002). In proteins exposition to UV-light can lead to loss of structure and inactivation (Neves-Petersen *et al.*, 2002).

Uncover the molecular mechanisms and evaluate the damage that UV radiation induces in cells and biomolecules can be extremely important, not only for medical and scientifically purpose, but also for industrial applications and product quality management. For example, in the process of synthesis of antibiotics and drugs in general, which have in its constitution proteins and vitamins, there are several steps in which they are exposed to UV light, is it in analysis routines where UV spectroscopy techniques are used, or in the contact with UV radiation present in sunlight, in transfer operation or in storage procedures. There is a need of guarantying the safety of these medicaments, taking precautions, and avoid the surge of dramatic changes within biomolecules. The same is valid to similar production steps in the food industry.

On other hand, uncover the reaction mechanisms and dynamics behind these effects can also be rewarding. If one can fully acknowledge the photonic processes, maybe it will be possible to control these reactions using photons and pulses of light, mimicking nature. One could learn, for instance, how to switch on and off a particular functionality of a biocatalyst using light, thereby controlling its function in a biosensor, with a simple and practical photonic signal.

2.2. AIM AND STRUCTURE OF THE WORK

The Nanobiotechnology Group of the University of Aalborg, where this work was fulfilled, has a particular interest in the study of light induced reactions in biomolecules. The fundamental knowledge acquired over the years regarding protein structure and the effect of UV radiation allowed to develop recently a novel light assisted protein immobilization technique.

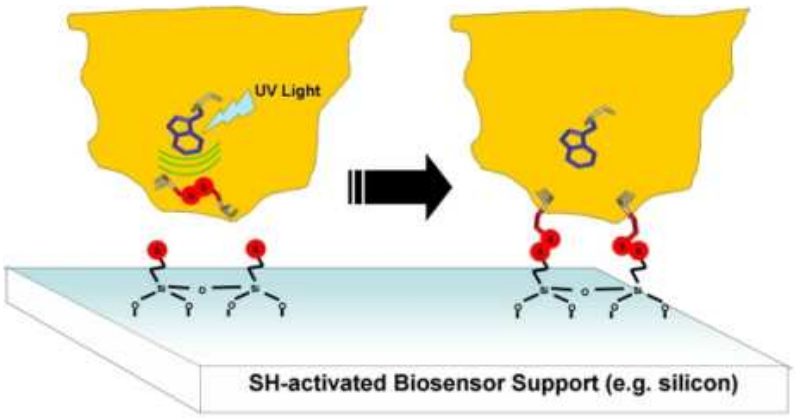

Figure 2.1: Principle of Light Assisted Immobilization with Tryptophan (blue) close to a disulphide bridge (red) within a protein molecule (yellow). Sulphur atoms are enhanced in red.

Briefly explaining, the technology behind this immobilization procedure is based on the fact that the disulphide (SS) bridges naturally present within the majority of proteins can be broken as second result of UV irradiation, in a mechanism mediated by neighbor aromatic residues. The free thiol derivated groups created upon disruption of these bonds are very reactive and can be used as linkers for covalent attachment to a surface. The surface can be for instance gold or thiol-derivatized silicon, which brings a huge span of possibilities for immobilization (*vide* Figure 2.1). With the aid of laser, the group successfully engineered specific microarrays with covalent-bounded protein. The technique allowed the immobilization of several proteins, in precise positions (directed by the laser), avoiding aggressive chemical/termochemical steps for the protein, preserving its native structural and functional properties.

However, immobilization is not an acquired fact for all proteins that contain SS bonds. The disruption of the SS bridges upon irradiation with UV light is dependent on spatial and structural properties of the protein, and external conditions, and is not always ruled by the same mechanisms. Moreover, the changes in the protein upon the disruption can be variable and of course, since proteins present different structures and a diverse number of SS bonds, and a successful immobilization is dependent on all these issues.

This project was integrated in a wider perspective that relied on developing a database of proteins that carried the necessary structural features for light induced immobilization.

The main goals of the work were therefore to evaluate a model protein on these specific characteristics, study the mechanism of the UV induced breakage of SS bridges, and eventually attempt the light assisted immobilization on a surface, engineering in that effort a potential light induced useful platform, like a set of microarrays or a biosensor.

The protein characterization relied on studying the effect of UV-light on the structural and spectroscopic features of the protein under different conditions (*e.g.* pH, temperature, concentration of the protein) using the tools available within the group. Once the ideal conditions for immobilization were established, further proceed to the immobilization procedure, and in case of success, verify the functionality of the protein via antibody or/and catalytic assay and test the sensitivity of the device.

The protein candidate studied in this work was α-lactalbumin, from bovine, used in its specific calcium depleted form. The major tool used for the characterization process was fluorescence spectroscopy. Given that some interesting results rose from the preliminary assays, regarding both the specific UV reactions triggered and structural specific features, the work proceeded further not only focused on the immobilization characteristics. The UV light induced illumination was also intended.

The organization of the work is derived from these results. On a first instance will be introduced, within a literary overview, the basic notions regarding UV light that are important for

this project. These include the characteristics of UV light irradiation effects, the basics notions of protein fluorescence (since fluorescence was used as probing tool), UV-light triggered reactions in proteins, and the specific reactions related to SS bridge disruption. It is followed by an extensive study of the model protein, α-lactalbumin, comprising the analysis of its structural and stability features. Finally, will be presented the two sets of results:

- the characterization and analysis of the protein form used;
- the immobilization procedure.

The material and methods used will evidently precede these sections, and they will be followed by the respective discussion.

Finally, the general conclusions regarding the work will be advanced.

3. LITERARY OVERVIEW

3.1. ULTRAVIOLET LIGHT

3.1.1. Definition, Effects of Exposure, Applications

UV light is considered the electromagnetic (EM) radiation (light) that present wavelengths shorter than those of the visible light, and longer than the X-rays, *i.e.* between about 400 to 10 nm, as can be observed in the electromagnetic spectrum (Figure 3.1).

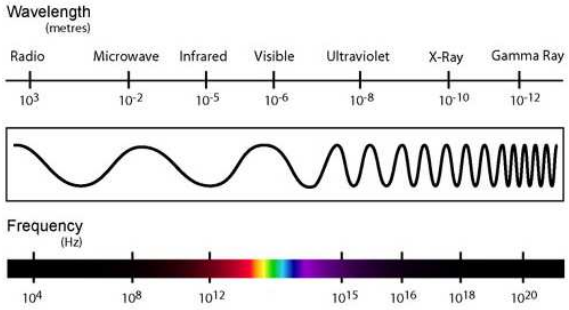

Figure 3. 1: The electromagnetic spectrum.

Since the discovery of the existence and presence of this radiation in sunlight in 1981 by the German physicist Johann Wilhelm Ritter, UV-radiation has been standing as common issue of interest for the scientific community. The effects and potential reactivity of this radiation are rather known for the last decades and in the awareness of society, mostly due to the concern regarding the harmful effects of long exposure to sunlight, which broadens part of the UV of the EM spectrum; and the destruction of the ozone layer that blocks part of the dangerous radiation.

The effects of UV irradiation surge at a molecular level but the repercussions can be verified at a larger scale. A striking example is the discoloring and degradation of surfaces exposed to sunlight, constituted by polymers, pigments or dies that suffer reactions upon the exposure.

In biological systems, which are in the line of this work, one can find a wide number of UV targets. In several organisms, exposure to diverse types of UV can lead to reduction in growth and survival, protein destruction, pigment bleaching and photoinhibition of photosynthesis (Sinha and Häder, 2002). On the human body, depending on the type of radiation and time of exposure UV light can have different effects, such as sunburn, suntan, cell-aging, and photocarcinogenesis on the skin, or welderflash and blindness (Matsumara and Ananthaswamy, 2004). The damage induced arises from molecular reactions triggered by irradiation, and the reactive species that it generates. For instance, UVB (UV radiation in the interval 280-315 nm) can induce DNA damage

by inducing the cross-linking of cytosines and thymines, provoking mutations upon repair, and further carcinogenic risks; the absorption of UV by chromophoric molecules can also lead to the formation of single oxygen or free radicals known to destroy membranes and other cellular components (Sinha and Häder, 2002).

The reactivity implicit to UV-light is also used for greater good, examples of that are its profitable use in sterilization procedures, photolithography, polymerization reactions, or laser-definition of structures.

As exposition to UV-light induces changes at the molecular level, it is widely used in as a sensor for UV sensitive species, is it in experimental analysis procedures, in spectroscopical techniques (fluorescence spectroscopy, UV-visible absorption spectroscopy, Raman spectroscopy), or microscopy (*e.g.* confocal fluorescence microscopy), or in day to day applications as UV-sensitive inks in passports or in bills to avoid forgery.

3.1.2. Molecular Basis of UV light irradiation effects

Given the broad effects noticeable on exposure to UV light it is important to first outline the molecular mechanisms that trigger such ultra-fast photophysical and photochemical reaction and give rise to detectable side-effects like fluorescence or phosphorescence.

On the verge of the molecular effects provoked by exposure of matter with UV light is the general interplay between EM radiation and matter. (Pöpp and Streller, 2006). The main interaction between light and matter consists on a process of both polarization of the molecules, bonds or atoms irradiated, and transfer of energy between the oscillating electrical field and oscillating dipoles present in molecules. The driven process has then different molecular effects on the molecular entity, depending on the wavelength of the light used. A strong interaction implies that the dipole moment in the molecule oscillates in the same frequency as the oscillation of the electrical field (Figure 3.2).

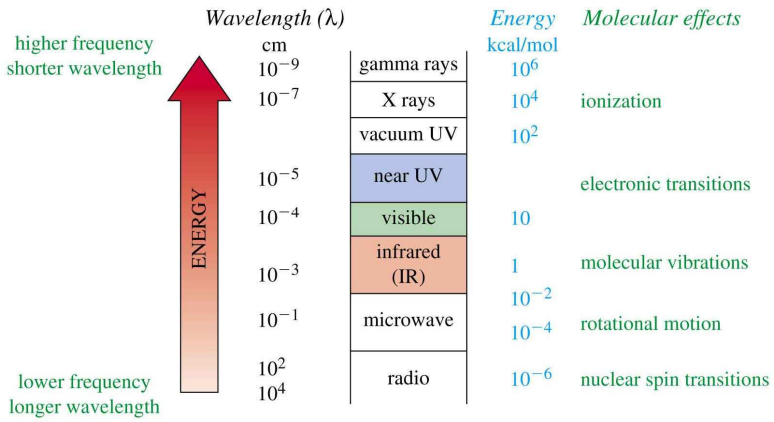

Figure 3.2: The electromagnetic spectrum and molecular effects.

For higher wavelengths and lower frequencies (like radio-waves – 100MHz) the effects can be explained with classic physics, involving for instance the alignment of polar molecules or electrons by the electrical field. For larger frequencies the interaction results in the absorption of light by the entity, as photons, resulting in the transition between energy levels, rotational, vibrational, electronic, and eventually ionization. Given that the energy of photons is dependent on frequency and wavelength, the higher the frequency, more energetic will be the transition, ultimately being the ejection of electron and ionization (Figure 3.2) (Pöpp and Streller, 2006; Macey, 2007).

The absorption of UV and visible light by an atomic or molecular specie leads particularly to the transition to higher electronic states, originating excited species with brief lifetimes (10^{-8}–10^{-9}s). Electronic transitions consist on the transfer of electrons from a lower energy orbital to a high energy orbital, such as an antibonding orbital (*e.g.* $n \rightarrow \pi^*$; $\pi \rightarrow \pi^*$). The electronic transitions only take place for a precise wavelength, since the energy gap between states is quantized. (Pöpp and Streller., 2006).

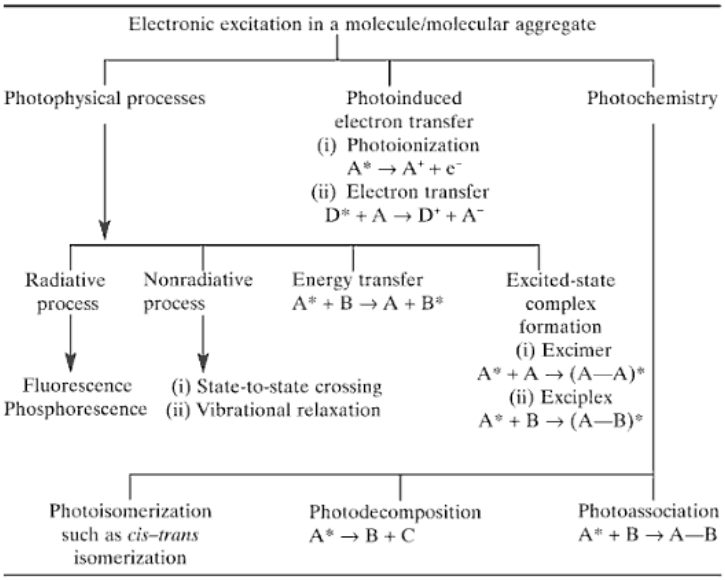

Figure 3.3: Schematic representation of the processes involved in electronic excitation. * stands for an electronic excited specie (Adapted from Prasad, 2003).

The highly energetic and unstable excited specie is then rapidly driven into a multitude of pathways as described in Figure 3.3. Its fate is uncertain, dependent on external conditions, and may even involve multiple pathways. It can involve photophysical processes, where generally the energy is dissipated or transferred, occurring the relaxation of the entity to a ground energetic state, where it is again available for further excitation. This relaxation may occur by radiative processes, such as fluorescence and phosphorescence, in case of a fluorophore; by non-radiative processes, involving heat dissipation; or by the energy transfer, is on the excitation of

other species, or formation of complexes. By other hand the molecule may not relax and enter in reactive pathways, is it by electron transfer, or chemical reactions such as photodecomposition (Prasad, 2003).

In this work not all the pathways will be in study, only those in which are driven the excited species of the model protein. Therefore, in this literature overview only these specific processes will be profoundly appreciated.

First will be addressed the phenomenon of fluorescence and the particularities of protein fluorescence. Fluorescence spectroscopy was the primary tool used both to explore the conformation of the protein and to probe the UV-reactions in the protein model.

Secondly, the pathways of excited species triggered by UV-light in proteins, and the possible resulting reactions, as possible applications for these processes, will be reviewed.

3.2. FLUORESCENCE

3.2.1 Main features

The radiative pathway mentioned before can lead to two phenomena: fluorescence and phosphorescence. They involve the emission of light from the electronically excited states and differ on the nature of the excited state. Molecules that display fluorescence (fluorophores) are typically aromatic. One example is quinine, which is present in tonic water.

Fluorescence in particular involves excited singlet states. In these, the electron on the excited orbital is paired (by opposite spin) to the second orbital in the ground-state orbital. Return to the ground-state is therefore spin-allowed and takes place quickly by emission of a photon. Fluorescence emission is a fast process: emission rates of fluorescence are usually in the scale of $10^8 s^{-1}$, resulting in a typical fluorescence lifetime around 10 ns. The fluorescence lifetime is the average time between its excitation return to the ground state.

The intensity of fluorescence light is proportional to the extinction coefficient of the fluorophore and a factor known as quantum yield (ϕ) which is the rate of photons (or quanta) emitted per photons absorbed (or quanta). The quantum yield presents values between 1 and 0 and is characteristic of each fluorophore. Fluorescence intensity measured experimentally from a fluorophore excited in solution and can be defined as:

$$F = I_0 \times \varepsilon \times c \times x \times \phi \tag{3.1}$$

where F is the total amount of light emitted (and detected), I_0 is the incident light intensity, x the path length in centimetres, ε the molar extinction coefficient, and c the molar concentration of the fluorophore.

The quantum yield is generally lower than 1 since other processes, including internal conversion, quenching of various types, and intersystem crossing compete with fluorescence to dissipate the energy gained in absorption.

There are energy losses along the invert process of emission, mainly by vibrational relaxation, or internal conversion. Thus fluorescence is not a process 100% efficient and the photons emitted are intrinsically less energetic than the photon absorbed. This is felt in spectroscopic data, as the maximum of emission spectra will always situated at longer wavelengths than the maximum of absorption spectra (Stokes Shift) (Lakowicz, 2006; Macey, 2007).

The whole process of absorption and emission can be pictured by means of a Jablonski Diagram (Figure 3.4).

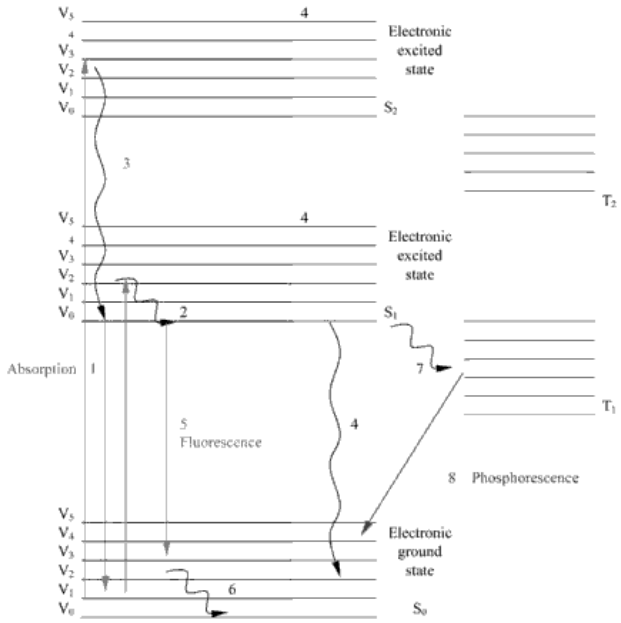

Figure 3.4: Typical Jablonski Diagram. The singlet ground, first, and second electronic states are depicted by S_0, S_1 and S_2 respectively. At each of these electronic energy levels the molecular or atomic species can exist in a number of vibrational levels, represented by V_1, V_2, V_3, etc. The initial absorption of light by the molecule leads into a transition to a higher energy state, S_1 or S_2 (1), from which energy can be lost in nonradiative ways, by vibrational relaxation in S_1 (2), by internal conversion (3), by external quenching (4). Molecules in the S_1 lower energetic state can undergo a downward transition by emitting fluorescence (5). Emission of fluorescence usually does not proceed until the ground state, this occurs usually by vibrational relaxation, where there is again an energy loss (6). Intersystem crossing from the singlet excited state (S_1) to the triplet state (T_1) is an alternative to fluorescence as no photon is emitted. However decay from T_1 to S_0 results in phosphorescence. The various vibrational relaxations (10^{-12}s) occur faster than the downward transitions. That is why they happen prime and after fluorescence (Adapted from Macey, 2007).

Before the term quenching was mentioned. In fluorescence spectroscopy quenching refers to any process that leads to the decrease in fluorescence intensity Thus, this term basically encompasses all the mechanisms involving excited electronic species that have been enumerated before, excluding fluorescence itself and the vibrational relaxations, part of the pathway of fluorescence.

It is named collisional quenching when the excited-state fluorophore is deactivated on the contact with another molecule in solution, which is named as quencher. A wide number of molecules may act as collisional quenchers, for instance oxygen, halogen, amines, and electron-deficient molecules like acrylamide, and within different mechanisms such electron transfer and intersystem crossing to the triplet state (*e.g.* quenching by halogen and heavy atoms realized by spin-orbit coupling). Another type of quenching is known as static quenching. It occurs in the ground state, and does not rely on diffusion and molecular collisions. It can for instance consist on the formation of non-fluorescent complexes between the quencher and the fluorophore. Quenching can also occur in several via several other non-molecular mechanisms, for instance attenuation of light by the fluorophore itself or other absorbing (Lakowicz, 2006).

Another important process specific to fluorescence that may occur in the excited state is resonance energy transfer (RET). It takes place whenever the emission spectrum of a fluorophore, named the donor overlaps with the absorption spectra of another molecule. The acceptor does not have to be a fluorophore. RET does not involve the emission of light by the donor, and absorption by the acceptor. The donor and acceptor are coupled by a dipole-dipole interaction. The degree of energy transfer is dependent on the spatial distance between donor and acceptor, and the extent of spatial overlap, characterized in terms of the Förster distance.
Besides these characteristic distances, the energy transfer is dependent on a broad number of parameters, as the lifetime of the donor, diffusion and if the pair is covalently bounded (Lakowicz, 2006).

3.2.2. Protein Fluorescence

Fluorescence spectroscopy is a widely used tool in protein studies, are they directed to structural features, folding, denaturation, association reactions, substrate binding, etc. It stands as a fast method of analysis, implicates low-cost operations, and provides a relatively high sensitivity.

Proteins contain three amino-acid residues that contribute to their UV fluorescence: Tyrosine (Tyr, Y), tryptophan (Trp, W), and Phenylalanine (Phe, F). These intrinsic fluorophores are particularly rare in proteins. Trp, the major contributor for protein fluorescence is usually present in 1 mole % of proteins. When proteins contain one or few fluorophores, the spectral data is easy to interpret.

For convenience of analysis the absorption and emission spectra of these amino acids in neutral solution are shown in Figure 3.5.

The emission of proteins is dominated by Trp, which absorbs at longer wavelength and presents the highest extinction coefficient. Moreover, energy absorbed by Phe and Tyr can be further transferred to Trp residues in the same protein. Phe shows the shortest absorption and

emission wavelengths, presenting a structured emission in water environment with a maximum near 282 nm. As for Tyr, the emission takes place at approximately 303 nm and is quite insensitive to solvent polarity. Oppositely, Trp emission is highly dependent on polar parameters and local environment as further can be observed. The emission of Trp in water takes place usually around 350 nm.

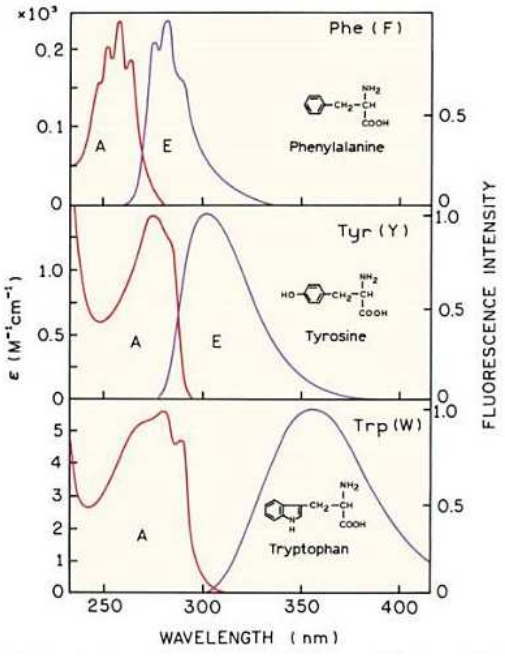

Figure 3.5: Absorption and emission spectra of the protein intrinsic fluorophores in pH 7 aqueous solution (Adapted from Lakowicz, 2006).

The excitation of protein fluorescence is generally realized at the absorption maximum 280 nm or at higher wavelengths, meaning that Phe is not excited most of times. At wavelengths longer that 295nm, as can be neatly seen in Figure 3.2, the absorption is mainly responsibility of Trp. Thus, one can excite selectively Trp fluorescence at 295-305 nm, permitting a better resolution and understanding of the spectral data (Lakowicz, 2006).

Solvent effects on Tryptophan Emission Spectra

One of the major characteristics that allow the use of protein fluorescence to extract conclusions regarding the structure features and behavior of a protein is the way Trp emission is affected by local environment.

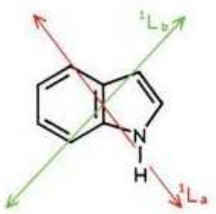

Figure 3.6: The two excited-state dipole moments of tryptophan (Adapted from Lakowicz, 2006)

Whereas the emission of Tyr is not so sensitive to local environment, Trp is highly sensitive to change in its microenvironment, especially to polar solvents. This strange duality is explained by the unique character of Trp as a fluorophore. In Tyr the emission appears two occur from only one of its two electronic states. On the contrary Trp presents two nearly isoenergetic transitions correspondent to two nearly perpendicular excited state-dipole moments, ^1L_a and ^1L_b (Figure 3.6). This electronic transitions display distinct absorption and emission, and are differently sensitive to solvent polarity. The relative population of these excited states depends first on the excitation wavelength, wavelengths higher than 290nm favor the ^1L_a transition, whereas at 270 nm is favored the other transition. By other hand the emission of ^1L_b is mostly structured, compared to the ^1L_a emission.

Depending on the solvent, emission can take place from ^1L_a or ^1L_b states, though emission from the ^1L_b is infrequent. This is due to the fact that Trp emission is highly sensitive to hydrogen bonding to the imino group. The ^1L_a transition is more sensitive to polar solvents (like ethanol), shifting to lower energy on their presence, which makes sense since this transition involves more directly the polar nitrogen atom of indole. In a complete nonpolar environment the ^1L_b state has the lower energy and may dominate the emission, whereas in the reverse situation ^1L_a dominates.

In a protein the spectral implications can be interesting for analysis. Once the ^1L_A transition shifts to lower energies with the increase of polarity and hydrogen bounding, the relative position of the Trp residues in the protein structure can be checked by the position of the emission maximum. If the Trp residue is buried inside the protein, the emission occurs at lower wavelengths. When the Trp residue is exposed in solution, typically aqueous and polar for proteins, the ^1L_a transition transits to lower energies, resulting in a red-shift[a] of fluorescence emission. This effect can be depicted in Figure 3.7, and can be used for instance to follow protein unfolding. Moreover few proteins display the characteristic structured emission of the ^1L_b transition since few Trp residues are in completely nonpolar environments. Furthermore one can specifically excite the ^1L_a at wavelengths superior to 290 nm and have a clear notion of the events (Lakowicz, 2006).

[a] A red-shift means that the maximum of emission is shifted to higher wavelengths, on opposition to a blue-shift.

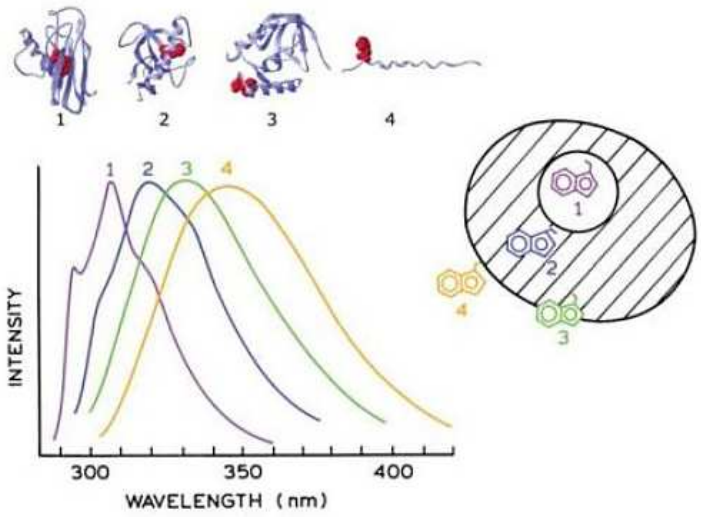

Figure 3.7: Effect of tryptophan environment on the emission spectra. The higher is the exposure of the Trp in the protein structure, more will be its maxima of absorption red-shifted (1 to 4). This effect can be noticed upon the degree of unfolding of a protein. The emission spectra are those of apoazuerin Pfl, ribonuclease T_1, staphylococcal nuclease, and glugagon, for 1 to 4 respectively (Adapted from Lakowicz, 2006).

Excited-State Ionization of Tyrosine

Tyr is regularly regarded as a simple fluorophore, and is not so sensitive to external conditions as Trp. Nonetheless Tyrosine can display complex spectral properties in certain situations. Tyr can suffer excited-state ionization, inducing the loss of the proton in the aromatic hydroxyl group. In the ground-state the pK_a of the hydroxyl group is approximately 10, while on the excited state it decreases to 4. Consequently, in neutral solution the excited state can dissociate during the lifetime of the excited state, leading to quenching of the Tyrosine fluorescence. Tyrosinate, the ionized form of Tyr, is weakly fluorescent at 350nm, an emission that can be confused with Trp fluorescence.

Nevertheless experience tells that excited state ionization is not the major decay pathway for Tyr, and for that reason it is only observed in some proteins (Lakowicz, 2006).

Resonance Energy Transfer

Due to the spectral properties of the intrinsic fluorophores, resonance energy transfer can take place between them. The spectral overlap of the absorption and emission spectra of Phe, Tyr and Trp can induce usually an energy transfer from Phe to Tyr and subsequently to Trp. This type of energy transfer has been frequently noticed in various proteins, specially the Tyr-Trp transfer, and is also accounted as a reason to the reduced contribution of Phe and Tyr in the emission of most proteins. Blue-shifted Trp residues can also transfer excitation energy to longer wavelength Trp. (Lakowicz, 2006)

Quenching of the Protein Fluorescence

Protein intrinsic chromophores are, in similarity to the other fluorophore particularly sensitive to external solvent quenching. In addition once again Trp is the most affected residue.

Besides being extremely affected with solvent polarity, Trp fluorescence is also uniquely sensitive to collisional quenching, owed seemingly to the tendency of the excited-state indole to donate electrons. Tryptophan can be quenched by externally added groups (present in the solvent) or by nearby groups in the protein. This results in highly variable quantum yields of tryptophan fluorescence. A broad number of quenching factors has been reported for Trp fluorescence:

- quenching by proton transfer to neighbor amino groups - histidine and lysine residues can be agents of such quenching;
- quenching by electron acceptors, for instance protonated carboxyl groups;
- electron transfer quenching by SSs and amides such as the ones present in the peptide backbone;
- electron transfer quenching by peptide bonds in the peptide backbone.

Similarly to RET these interactions are strongly dependent on distance, especially the rate of electron transfer, decreasing exponentially with distance. The extent of electron transfer may depend as well on the location of close charged groups, which act in stabilizing or destabilizing the charge transfer state. The quenching effect of electron transfer conjugated with RET can sometimes result that Trp residues display almost no fluorescence (Lakowicz, 2006).

Remarks

From the statements previously realized it can concluded that protein fluorescence is indeed a powerful tool, since one can extract pretty important conclusions regarding local features of the protein, where the intrinsic fluorophores are localized. For instance, while the fluorescence spectra obtained by excitation at 280 nm provide a general perspective on the protein conformation, where the generality of the residues stand, if they are quenched or not; at 295 nm we excite uniquely the Trp, and the information retrieved is far more specific of the protein areas where these are localized.

Spectral interpretation can reversely be far trickier to process. In the presence of multiple aromatic residues in the protein, particularly Trp, spectra overlap is undesirable side-effect, which occurs at most usable wavelengths. These residues are not located in the same environments in the protein, and to evaluate which residue contributes more on the fluorescence is hard to trace.

3.3. ULTRAVIOLET LIGHT INDUCED REACTION MECHANISMS IN PROTEINS

It is known that the exposure of proteins to light can induce dramatic changes in protein structure, leading eventually to its degradation, physical or chemical. Photoxidation of the protein UV sensitive species is regarded as one of the major contributors for the protein partial destruction (Kerwin and Remmele, 2006).

In proteins, the major targets of UV radiation are evidently the intrinsic fluorophores Trp, Tyr, Phe, and two important structural elements: the peptide backbone and cystines (cysteines linked by SS bridge). In aqueous solution the absorption wavelengths are 260–290 nm for Tyr, 240–270 nm for Phe, 180–230 nm for the peptide backbone, and 250–300 nm for cystines (Kerwin and Remmele, 2006). As previously described, Trp can absorb in solution through its the two dipole moments. Trp absorption maxima are centered at 220nm (ε~36000 $M^{-1}cm^{-1}$), 280nm (ε~5500 $M^{-1}cm^{-1}$) and 288nm (ε~4500 $M^{-1}cm^{-1}$) with a shoulder at 265nm (ε~4500 $M^{-1}cm^{-1}$) (Neves-Petersen *et al*., Paper Submitted).

The specific mechanisms triggered in these targets encompass the broad picture described schematically in Figure 2.2. Aside the processes in which the excited entity is relaxed to the ground state, like fluorescence, thermal relaxation or transfer of energy, the other pathways usually involve the degradation of this specie, thus termed generally photolysis or photodegradative mechanisms (Kerwin and Remmele, 2006).

In this section it is pretended to review these events in the protein intricate context, a complex net of interactions, where diverse deciding factors are in play, like the pH of the solution, temperature, polarity, nearby side-chains, etc. Since the experimental work was primarily focused in the photo-induced mechanisms in Trp, this will be the major issue in analysis. However, some notions regarding the pathways of excited states of Tyr and cystine will be introduced, pertinent to further speculations and understanding. In attention will also be the influence of the external conditions on these pathways. Evidently the particular mechanisms of SS bond disruption by UV light will be taken in strong consideration.

3.3.1. Main Photochemical and Photophysical Reaction Mechanisms

Among the natural occurring amino acids Trp displays the highest absorption in the near-UV, and is for that reason a major player in the photochemical and photophysical processes in proteins. The fate of Trp excited species (lifetime of about 3 ns) has been widely studied and reviewed in literature. Flash photolysis studies have allowed the identification of two major

pathways of non-radiative relaxation for the excited specie of tryptophan (Trp* lifetime of about 3 ns, Sherin *et al.*, 2004):

(a) ejection of an electron to the solvent, generating a solvated electron e_{aq}^- (wide absorption peak centered at ~720 nm), and a tryptophan radical cation $Trp^{\bullet+}$ (absorbs at ~560 nm) (3.2). $Trp^{\bullet+}$ rapidly deprotonates forming a indolyl neutral radical $Trp^{\bullet}$ (absorbs at ~510 nm) (3.3) (Neves-Petersen *et al.*, Paper Submitted).

$$Trp + h\nu \rightarrow Trp^{\bullet+} + e_{aq}^- \quad (3.2)$$

$$Trp^{\bullet+} \rightarrow Trp^{\bullet} + H^+ \quad (3.3)$$

The formed $Trp^{\bullet}$ can then further react with neighbor amino acids. It may, for instance, extract a hydrogen atom from a neighbor Tyr or cysteine (RSH), and self-repair, yielding reactive radical species such as cysteine neutral radical $RS^{\bullet}$ and tyrosine radical cation $Tyr^{\bullet+}$. Alternatively $Trp^{\bullet}$ might attack the peptide bond leading ultimately to its cleavage. In the presence of oxygen, it can form a peroxy radical, which can suffer further reaction producing two analogs of Trp: N-formylkyneurine and kyneurine (absorption at 300-400 nm - Snytnikova *et al.*, 2007). These two species absorb light at longer wavelengths than Trp, and upon absorption in aerobic conditions induce further damage to the protein (Kerwin and Remmele, 2006).

(b) intersystem crossing from the excited singlet state Trp to the triplet state ^3Trp (3.4 and 3.5), which absorbs at ~450 nm (lifetime of approximately 10μs). ^3Trp may afterwards transfer an electron to a nearby SS bridge yielding $Trp^{\bullet+}$ and $RSSR^{\bullet-}$ (absorbs at ~420 nm) (3.6). Under aerobic conditions the ^3Trp might also react with molecular oxygen to give once more $Trp^{\bullet+}$ and a strong reactive oxygen radical $O_2^{\bullet-}$ (3.7), which advents further damage to the protein (Neves-Petersen *et al.*, Paper Submitted; Kerwin and Remmele, 2006).

$$^1Trp + h\nu \rightarrow {}^1Trp^* \quad (3.4)$$

$$^1Trp^* \rightarrow {}^3Trp \quad (3.5)$$

$$^3Trp + RSSR \rightarrow Trp^{\bullet+} + RSSR^{\bullet-} \quad (3.6)$$

$$^3Trp + O_2 \rightarrow Trp^{\bullet+} + O_2^{\bullet-} \quad (3.7)$$

The solvated electrons e_{aq}^- yielded from the excited state ionization of Trp can latter trigger further reactive mechanisms in the protein. They may recombine with Trp, generating radical anions (3.8), or be captured by electrophylic species such as cystines (3.9), molecular oxygen (3.10), or by H_3O^+ at acidic pH (3.11).

$$e_{aq}^- + Trp \rightarrow Trp^{\bullet-} \quad (3.8)$$

$$e_{aq}^{-} + RSSR \rightarrow RSSR^{\bullet -} \quad (3.9)$$

$$e_{aq}^{-} + O_2 \rightarrow O_2^{\bullet -} \quad (3.10)$$

$$e_{aq}^{-} + H_3 0^{+} \rightarrow H^{\bullet} + H_2O \quad (3.11)$$

Cystine radicals $RSSR^{\bullet -}$ formed upon electron transfer (3.6 and 3.9) might further cleave, inducing the breakage of the SS, forming thyil radicals and thyols (3.12 and 3.13).

$$RSSR^{\bullet -} \rightarrow RS^{\bullet} + RS^{-} \quad (3.12)$$

$$RSSR^{\bullet -} + H^{+} \rightarrow RS^{\bullet} + RSH \quad (3.13)$$

The hydrogen radical resulting of electron capture at acidic pH can react with a SS bridge in the vicinity and also lead to its disruption (3.14).

$$H^{\bullet} + RSSR \rightarrow RS^{\bullet} + RSH \quad (3.14)$$

Additionally, the solvated electron e_{aq}^{-} may react with the peptide chain, to generate a hydroxide ion and a ketyl radical (3.15).

$$e_{aq}^{-} + \text{-CONH-} \rightarrow OH^{-} + \text{-}\dot{C}(OH)NH\text{-} \quad (3.15)$$

The latter can propagate along the side chain, and upon the encounter with a SS bridge react, generate once more a $RSSR^{\bullet -}$ radical, whose repercussions were already explicated, with the subsequent reductive splitting of the SS bridge (Neves-Petersen *et al*., Paper Submitted).

Evidently, cystines are also prompt to photodegradation by direct absorption of UV-light, and in the same range of wavelengths than Trp residues, primarily below 300 nm. At this event rupture can occur either in the R-S bond or in the S-S bond (3.16).

$$RSSR + h\nu \rightarrow 2RS^{\bullet} \; or \; R^{\bullet} + RSS^{\bullet} \quad (3.16)$$

The photolytical radical products $R^{\bullet}$ and $RSS^{\bullet}$ can experience further reactions with other amino acids, with molecular oxygen and possibly with water, which may respectively result in crosslinking, a variety of acids, and disproportionation to cysteine sulfonic and sulfinic acids. However, the share of this direct photodegradation is reduced, principally in proteins containing Trp and Tyr, since the molar extinction coefficient (ε) of cystine is reasonably lower than the ones of these two fluorophores (in water: ε_{280}cystine = 125 $M.cm^{-1}$; ε_{280}Trp = 5500 $M.cm^{-1}$;ε_{280}Tyr = 1490 $M.cm^{-1}$ (Walker, 2005). Moreover, the absorption wavelength is dependent on the R-S-dihedral bond angle and can red-shift to longer wavelengths that 300nm, which do were not used for excitation in this work (Kerwin and Remmele, 2006).

The photolytical yielded free thiyl radicals $RS^{\bullet}$ and thiol groups RSH can further react with other free thiol groups, is it within the protein reforming or forming a intra-disulphide bond, or externally forming SS bridges with other molecules (*e.g.* with another irradiated protein molecule resulting in aggregation). Alternatively the free thiyl radical can react with other amino acids or oxygen. Finally the thiyl radicals may even cross-link with a SS bond in a protein resulting in an unpaired electron shared between the two SS bridges followed by rupture resulting in a mixture of species: ones keeping the original bond and other with a mixed SS formed with the thiyl radical (Neves-Petersen *et al*., Paper Submitted; Kerwin and Remmele, 2006).

3.3.2. Influence of external factors on the reaction mechanisms

In the previous section were introduced a multitude of pathways that can be triggered upon UV irradiation of proteins, and the photo-induced mechanisms in Tyr and Phe were not even discussed. The succession of the mechanisms enabled by the excitation of Trp is not a determined fact. However it is strongly influenced by external conditions and by the reaction microenvironment.

First of all, external factors like pH, temperature or solvent particularities can affect the initial fate of the excited specie, is it the return to the ground state by relaxation coupled with fluorescence, ejection of an electron and ionization, or intersystem crossing.

At acidic pH values, the excited S1 state of Trp can be highly quenched due to the protonation of the NH group of the indole ring (pKa ≥ 2.2). The protonation may be followed by fast intersystem crossing into protonated triplet state $^{T}TrpH^{+}$ (pKa = 3.2, lifetime of 26 ns), suppressing significantly the return to ground state by fluorescence, and the two major non-radiative pathwaysof Trp here referred (Sherin *et al*., 2006). For pH values between 3 and 10, there is no direct influence of pH on the fate of excited Trp in solution. High pH values are generally favorable for e^{-}_{aq} formation (Kerwin and Remmele, 2006).

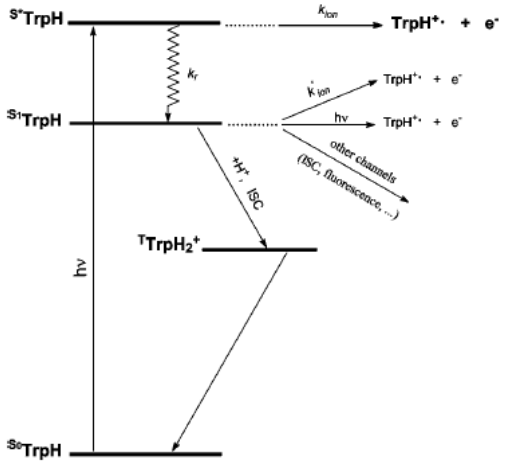

Figure 3.8: Channels of Trp photoionization.

Temperature has also a major effect on the pathway taken by the excited Trp specie. An increase of temperature from 4 to 37ºC or greater can raise e^-_{aq} formation from singlet excited Trp in solution in a fivefold fashion or more, with the parallel decrease in triplet state formation (Kerwin and Remmele, 2006).

In neutral solutions two decay pathways of Trp are dependent on temperature: the ionization of Trp excited species and intramolecular proton transfer from the protonated NH_3^+ group to the C-4 position of the indole ring, both processes being favored with the temperature increase. The second is not generally possible in proteins, since the NH_3^+ group is involved in the peptide bond and Trp residues are not generally found in N-terminals. Therefore this increase in e^-_{aq} formation with temperature can only be due from an increase in the ratio of ionized species and not the decrease in the yield of the other relaxation pathways. Fluorescence, intersystem crossing, or even internal conversions are not directly dependent on temperature (Sherin *et al.*, 2004). Photoionization of Trp can occur from diverse channels (Figure 3.8). Photoexcited Trp can absorb the second quantum of light and suffer biphotonic ionization. As already mentioned, it can undergo protonation of the indole ring, followed by intersystem crossing to the triplet state. Another precursor for the TrpH ionization is an extremely shorted-lived non-relaxed prefluorescent excited state, which apparently competes with the relaxation thermal equilibrium. Finally, singlet excited state of tryptophan may undergo thermal ionization from the S_1 relaxed state, the only process known to be temperature-dependent (Sherin et al., 2006).

The solvent used may affect also the fate of the excited specie: a raise in ionic strength or solvent polarity can stabilize the solvation of the electron, resulting in higher solution lifetimes and the probabilities of its formation (Kerwin and Remmele, 2006).

In the protein intricate environment the influence of external conditions can be felt differently since the Trp residues can be buried within the macromolecule. Thus, solvent polarity and ionic force will not affect in the same magnitude the excited state of Trp.

In a protein, another major factor that will influence the fate of the excited specie is the presence of other groups in the vicinity of the Trp residues. As previously discussed in the Protein Fluorescence section (3.2.2), Trp fluorescence is highly quenched by close groups that can accept electrons from the Trp (protonated carboxyl groups, disulphides, amides, peptide bonds) or receive protons (histidine and lysine residues). Hence, the close presence of these groups may drive the Trp excited specie in a particular pathway and favor determined mechanisms such as ionization. The mechanism of SS bond breakage can be particularly dependent on the distance between the bond and the tryptophan residue, as will be described in the next section.

On other hand external solvent conditions can also affect indirectly the photophysics and photochemistry of Trp within a protein since factors like pH, temperature, ligands or salts can

affect the conformation of the polypeptide. In experiments with the same protein, differences can be noticed from case to case if the conditions are shifted, since upon these structural changes, the relative position of the Trp residues and other groups is changed. Indeed, in tests realized in bovine serum albumin it was noticed that changes in structure induced by pH altered the final sites at which the reactive radicals resided. Analogous differences were detected between the folded and unfolded states of mellitin and beta-lactalbumin (Kerwin and Remmele, 2006).

3.3.3. Consequences of Protein Photo-degradation, SS Bond Breakage and Light Induced Immobilization

Since a wide number of mechanisms can be activated in proteins upon UV radiation, originating extremely reactive species like peroxy radicals or singlet oxygens it is natural that the structural modifications within the protein will quite serious, including the modification of amino acids, breakage of the peptide chain, and other effects reported in section 3.3.2. These modifications may lead to the structural disarrangements of binding sites and enzyme inactivation (Neves-Petersen *et al.*, 2007).

Protein photo-degradation and inactivation of enzymes or functional proteins is classically attributed to the photo-oxidation of cystines (Neves-Petersen *et al.*, 2002). SS bonds sustain the tertiary structure of the protein, and their disruption may affect terribly certain conformational features. Cystine photo-degradation is shown to be highly dependent on its microenvironment (Neves-Petersen *et al*., 2002). Additionally, in proteins cystine residues have a natural preference for aromatic residues as spatial neighbors (Petersen *et al*., 1999). The two precedent observations correlate well with the photo-induced reactions here presented. Upon excitation of Trp residues, several of the activated mechanisms may lead to breakage of intra-molecular SS bonds.

Moreover, the distance between Trp residues and the SS bonds can be an extremely important factor for the event. Studies in lysozyme and a model system allowed to verify that previously described interaction between ^{3}Trp and cystine (expression 3.5) is based on direct electron transfer between the two species. It consists on a very short range interaction that decays exponentially with the increase of distance beyond Van der Vaals overlap between the donor and acceptor (Neves-Petersen *et al.*, Paper Submitted).

Cutinase, from *Fusarium solani pisi*, has been one of the most extensive studied models since it displays only one Trp that is in direct contact with a SS bridge (closest distance ~3.8 Å). In this enzyme, the disruption of SS bond mediated by Trp excitation has been proven to be a statistical phenomenon (Neves-Petersen *et al.*, 2002). In this simple model, formation of the solvated electron from excited Trp has been noticed in the flash photolysis studies, and this yielded product follows several fates here described, including recombination with H_30^+ and SS

bonds, or with other electron scavengers. Formation of $RSSR^{\bullet -}$, which advents the splitting of SS bridge, is resultant of both solvated electron recombination and reaction with the ^{3}Trp (Neves-Petersen *et al.*, Paper Submitted). Therefore, even in this simple model, diverse pathways may be involved. For cutinase, it was also noticed that the longer the UV excitation of the aromatic residues, the larger is the proportion of broken SS bonds and free thiols, originated from splitting of $RSSR^{\bullet}$. The concentration of solvated electrons increases also over the time in the flash photolysis studies (Neves-Petersen *et al.*, 2002; Neves-Petersen *et al.*, Paper Submitted).

Though the breakage of SS bonds can induce conformational changes on the protein, the full inactivation of its properties or loss of catalytical activity in enzymes is not an acquired fact.

Besides reacting with other protein free thiols, the photo-yielded solvent accessible free thiol groups can react with gold (Au) or thiol-rich surface to form covalent bonds (Neves-Petersen *et al.*, 2006; Duroux *et al.*, 2007; Snabe *et al.*, 2006). This is the principle behind the light induced immobilization technique that was described in section 2.2. The technique makes use of the natural existence of closely spaced triads of residues aromatic/cystines that was referred previously. This constellation is ubiquitous in many protein families such as hydrolases, oxidoreductases, transferases, lyases, Major Histocompability Complex (MHC) class proteins, and membrane receptor proteins, and is present in all members of the immunoglobulin superfamily (Neves Petersen *et al.*, 2006), which make them potential and interesting targets for light-mediated immobilization.

This immobilization approach overcomes several inconvenients of classic protein immobilization techniques. The most common techniques for protein immobilization usually require one or more termochemical/chemical steps, which may have deleterious effects on the structure and function of the protein bound. The available methods rely on noncovalent adsorption or on covalent attachment to chemically modified surfaces with aldehydes, activated esters or epoxide cross-linkers. These attachment procedures lead to the random orientation of immobilized protein molecules, and poor control in the density of immobilized molecules. The methods can be also invasive, when foreign groups are introduced into the protein, which can provoke denaturation, or lower the biological activity and substrate specificity (Duroux *et al.*, 2007).

Light-induced immobilization avoids the non-specific exposure of the protein, prior or during the binding procedure, to structurally modifying chemical agents. Furthermore, the size of the area of immobilization is limited to the area of illumination. Finally, the immobilized molecules are oriented through precise and known covalent bonding onto the surface.

In the Nanobiotechnology Group of the University of Aalborg, an immobilization experimental setup is installed in a clean room for light-induced molecular immobilization (LIMI). The setup includes a laser source, whose beam can be focused onto the surface of flat quartz

slides. The slides may be thiol-derivatized, allowing the bond to the thiol groups of the protein upon illumination. The immobilization procedure implies the deposition of one microdroplet of protein solution onto the slide, and posterior exposure to the laser-beam of UV-light (Duroux *et al.*, 2007).

Using this technique several proteins belonging to the above mentioned groups were immobilized, including cutinase, lysozyme, alkaline phosphatase, immunoglobins of antigen binding, the MHC class protein I (Neves-Petersen *et al.*, 2006; Duroux *et al.*, 2007; Snabe *et al.*, 2006), bovine serum albumin and prosthetic serum albumin (Parracino, A., Personal Communication). All these proteins have a great biomedical interest since they can act as sensors for a wide number of applications. For instance, immunoglobulins have a great relevance in disease diagnostics, in microarray probing of specific diseases, or in the identification of particular biomarkers by biomolecular interaction.

With the laser setup previously, the beam can be focused to precise locations with sub-micrometer dimensions, enabling the creation of dense microarrays, immobilization of biomolecules according to specific patterns (recurring to specific masks) (Neves-Petersen *et al.*, 2006; Duroux *et al.*, 2007; Skovsen *et al*., 2008; Neves-Petersen *et al*., 2008).

An important aspect regarding the immobilization procedures that were realized is that the native and functional properties of the proteins were maintained (Duroux *et al.*, 2007; Neves-Petersen *et al.*, 2006).

The spot size of the created arrays or patterns is reduced and covers only the illuminated surface of the microdroplet, with a high density of immobilized biomolecules. Protein activity is preserved as a dense monolayer (Duroux *et al.*, 2007).

The immobilization technology is ideal to couple, proteins and peptides. It is not limited to slide immobilization. The coupling can also be realized to nanoparticles, such as gold nanospheres, that may subsequently be used as molecular carriers into cells (drug-delivering) for therapeutic applications (Parracino *et al.*, 2008).

4. THE PROTEIN MODEL: α-LACTALBUMIN

4.1. CONTEXT AND FUNCTIONS OF THE PROTEIN

Milk has been regarded for ages as an important nutritional product, derived from the experience-based acquired knowledge. However, only in the last decades has been characterized the paper of its constituents as functional foods. Whey, a by-product of cheese manufacturing, the fluid remaining after straining and curdling of milk, was once regarded as a chemical waste difficult to treat. The high costs associated to its disposal and the evolution of the analysis techniques allowed the identification of whey as a valuable co-product (Brown and Ernstrom, 1982). Indeed, whey contains a considerable fraction (20%) of the proteins from the milk; the remaining fraction, constituted mostly by caseins, is separated upon curdling. Whey proteins are globular proteins unique for its nutritional value and functional properties. Properties like emulsification or gelation raise the interest in whey proteins isolates and concentrates, making them desirable assets for a broad range of foods, (Gao *et al.*, 2008; Pedersen *et al.*, 2006).

The second major component of the whey protein agglomerate is α-lactalbumin (LA), representing about 20-25% of its composition, (Pedersen *et al*., 2006; Hong *et al*., 2002)

LA is a small (MW~14.2 kDa), acidic (isoelectric point: *IP*~4-5) calcium (Ca^{2+}) binding protein, present in the milk whey of diverse mammalians. Expressed exclusively during lactation, LA plays an important role in the biosynthesis of lactose. It resides as one of the two components of the lactose synthase complex, responsible for the catalysis of the lactose biosynthesis final step in the lactating mammary gland, as shown in expression (4.1). The other component of this enzymatic complex is β1,4-galactosyltransferase (GT), which is involved in the processing of proteins in various secretory cells by transferring galactosyl groups from Uridine 5'-(trihydrogen diphosphate)-Galactose (UDP-GAL) to glycoproteins containing N-acetylglucosamine. LA modulates the activity of GT through a reversible protein-protein interaction, increasing its affinity and specificity for glucose, and thereby changing its sugar acceptor specificity from N-acetylglucosamine (GlcNAc) to glucose, enabling the synthesis of lactose, the major carbohydrate component of the milk. The reaction occurs in the Golgi lumen of the cell, in the required presence Mn^{2+} ions. (Chysina *et al.*, 2000; Permyakov and Berliner 2000; Ramakrishnan and Qasba, 2001).

$$\text{UDP-GAL} + \text{glucose} \xrightarrow{\text{GT}/\alpha\text{-LA}} \text{lactose} + \text{UDP} \qquad (4.1)$$

Besides the natural role of LA, this protein has important characteristics that reinforce its interest as a model of study. LA contains a strong binding site for Ca^{2+} ions, which activity affects

considerably the conformation and activity in solution. Therefore, it is often chosen as a simple model for the calcium binding phenomenon in proteins, for instance in the calcium binding effects in the interaction of protein with other proteins, peptides, membranes, and low molecular weight. Moreover, this binding site responds also to other ions like Mg^{2+}, Mn^{2+} and Na^{+}, besides the existence of other Zn^{2+} binding sites, each case resulting in different conformations of the protein. The modulation of the protein structure by ions is an interesting enigma for molecular biology, particularly the functions that these conformations may have. This protein has been also studied extensively in recent years as a model for protein folding studies, particularly due to native-like conformational states that it adopts under certain conditions, called molten-globules (MGs), which are similar to protein folding intermediates.

This protein displays a close evolutionary relationship with c-type lysozyme. They share only 40% homology in amino acid sequence, but show comparable gene organization and similar three-dimensional fold (*vide supra*, section 3.2). Although structurally similar, in terms of functionality they reveal large differences. C-type lysozyme is an enzyme which binds and cleaves the glycosidic bond linkage in sugars, for instance it degrades the peptidoglycan of bacterial cell walls. Such lytic capacity is much reduced in LA, displaying in its native form only 10^{-6} of the specific activity of egg-white lysozyme. It is believed that specific amino acid substitutions in LA are responsible for the loss of the enzyme activity of lysozyme and acquisition of features required for its role in the lactose synthesis. (Chysina *et al.*, 2000; Mizuguchi *et al.*, 2000; Qasba and Kumar, 1997; Permyakov and Berliner 2000).

On other hand, some variants of LA have shown antimicrobial activity, others induction of apoptosis in tumor cells (Permyakov and Berliner 2000).

This work, aims at studying UV-light induced structural effects on LA and the temperature and pH stability of the protein. The protein used was the calcium depleted form. Hence, this chapter will focus on two major issues:

- description of the three-dimensional structure of the protein, and subsequent features important for the assessment of light-induced reactions in the protein (*e.g.* position of the fluorescent residues and the disulphide bridges);
- stability of the protein under the depletion of calcium, thermal and pH shifts.

4.2. PRIMARY, SECONDARY & TERTIARY STRUCTURE

4.2.1. Main Features

The majority of α-lactalbumins (LAs) found in mammalian's milk, including human, guinea pig, bovine, baboon, goat, and buffalo versions, are 123 amino acid residues long and share

homologous three-dimensional structures (*vide* Table 3.1). Only Rat LA distinguishes itself by containing 17 additional C-terminal residues (Permyakov and Berliner, 2000).

Table 4.1: Comparison of different LA structures. The values displayed are the root mean square deviations (in Å) obtained after superposition using the least square fitting function applied to C_α atoms of residues 1-120 (values in bold font) and to the core of the molecule (values in normal font). LA core comprises the residues 5-11, 23-40, 50-61, and 71-104. Apo-bLAc: Ca^{2+} depleted form of bovine LA at 2.2 Å (PDB code: 1F6R). Holo-bLAc: Ca^{2+} bound form of Bovine LA at 2.2 Å (PDB code: 1F6S). mLA: recombinant bovine LA at 2.3 Å (PDB code: 1HFZ). Baboon LA at 1.7 Å (PDB code; 1ALC). Guinea pig LA at 1.9 Å (PDB code, 1HFX). Goat LA at 2.3 Å (PDB code, 1HFY). Buffalo LA at 2.3 Å (Calderone *et al*., 1996). Human LA at 1.7 Å (Acharya *et al*., 1991). The values were calculated using the program O (Extracted from Chrysina *et al*.., 2000).

The deviations displayed, presenting generally values bellow 1 Å, demonstrate a high rate of structural alignment between the different versions of the protein.

	Apo-bLAc	Holo-bLAc	mLA (Bovine)	Baboon	Guinea pig	Goat	Buffalo	Human
Apo-bLAc		**0.68**	**0.8**	**0.93**	**1.01**	**0.75**	**0.8**	**0.99**
Holo-bLAc	0.39		**0.51**	**0.89**	**0.82**	**0.61**	**0.6**	**0.87**
mLA (Bovine)	0.41	0.28		**0.94**	**0.84**	**0.77**	**0.7**	**0.92**
Baboon	0.65	0.65	0.65		**1.06**	**1.06**	**1.04**	**0.41**
Guinea pig	0.57	0.44	0.44	0.66		**1.11**	**1.08**	**1.01**
Goat	0.6	0.45	0.54	0.8	0.7		**0.52**	**1.05**
Buffalo	0.53	0.95	0.48	0.76	0.63	0.27		**1.01**
Human	0.66	1	0.65	0.27	0.63	0.81	0.78	

The high homology between the first mentioned sources results in a comprehensive interchange of experimental results and subsequent interpretations realized with the different variants of the protein. For that reason, in this introductory text, when a result or interpretation will be mentioned, the specie in question will only be invocated when pertinent.

Number of amino acids: 123

Molecular weight: 14186.0

Theoretical pI: 4.80

Amino acid composition:

Ala (A)	3	2.4%
Arg (R)	1	0.8%
Asn (N)	8	6.5%
Asp (D)	13	10.6%
Cys (C)	8	6.5%
Gln (Q)	6	4.9%
Glu (E)	7	5.7%
Gly (G)	6	4.9%
His (H)	3	2.4%
Ile (I)	8	6.5%
Leu (L)	13	10.6%
Lys (K)	12	9.8%
Met (M)	1	0.8%
Phe (F)	4	3.3%
Pro (P)	2	1.6%
Ser (S)	7	5.7%
Thr (T)	7	5.7%
Trp (W)	4	3.3%
Tyr (Y)	4	3.3%
Val (V)	6	4.9%
Pyl (O)	0	0.0%
Sec (U)	0	0.0%
(B)	0	0.0%
(Z)	0	0.0%
(X)	0	0.0%

Figure 4.1: Amino-acid composition of bLA. Data obtained using the tool ProtParam on the Expasy Server (**www.espasy.org**) by submitting the fasta sequence of the PDB Entry 1F6S.

In Figure 4.1 is listed the amino-acid composition of Bovine LA (bLA), the selected model protein in this studies. The protein is rich in aromatic and cysteine (Cys, C) residues, displaying 4 tryptophans, 4 tyrosines, 4 phenylanalynes, and 8 cysteines. These residues are quite rare, existing generally in low numbers in the constitution of proteins. According to Creighton (1992), the random frequency of these residues in the amino acid composition of proteins is 1.3% for Trp, 3.2 % for Tyr, 3.9% for Phe, and 1.7% for Cys. In bLA the molar percentage of Trp and Cys is 3.3 % and 6.5%, values reasonably higher than the average, making it an unusual target of UV-triggered mechanisms.

It is important to notice that LA contains a variable number of Trp from species to species, presenting for instance 3 Trp in the human LA and 4 in the bovine and goat variant. Since the model studied is bLA, any further considerations regarding the position of Trp in LA will attend to the structure with 4 Trp at positions 26, 60, 103, and 118. Throughout this work the three-dimensional structures of bLA used for analysis correspond to the crystallized forms at 2.2Å resolution and high ionic strength by Chrysina *et al.* (2000). The two crystallized folds are: LA with Ca^{2+} bounded (holo-bLAc, PDB entry: 1F6S) and LA depleted of Ca^{2+} (apo-bLAc, PDB entry: 1F6R). The first corresponds to the native bLA, which exists in the presence of Ca^{2+} ions. The second is a Ca^{2+} depleted form, which is used for mere qualitative analysis in this section and in section 4.2.2, given that LA in the absence of Ca^{2+} displays variable configurations dependent on the solvent conditions (discussed in detail in section 4.3.4).

Tertiary Structure of Native LAs

Typically, the native tertiary structure of LAs (Ca^{2+} bound form) fold shows two sub-domains separated by a cleft: a large α-helical subdomain and a small β-sheet subdomain (further mentioned as α-subdomain and β- subdomain respectively), connected by a calcium binding loop (Figure 4.2). The α- subdomain is formed by three main α-helices (H1, H2 and H3; residues 5-11, 23-24 and 86-98 respectively) and two short 3_{10} helices[b] (h1b and h3c; residues 18-20 and 115-118 correspondingly). The β-subdomain is constituted by a serie of nonstructured loops, a small three-stranded antiparallel β-pleated sheet (S1, S2 and S3; residues 41-44, 47-50, and 55-56 respectively) and a short 3_{10} helix (h2, residues 77-80).

The high affinity Ca^{2+} binding site is located at the junction of the subdomains and is composed of a contiguous chain (residues 79-88) linking the 3_{10} helix of the β-subdomain and the helix H3 of the α-subdomain (residues 86-98). This region is considered the most rigid part of LA structure. The site includes Ca^{2+} linking highly conserved aspartates and one lysine. The ligands responsible for Ca^{2+} binding are the two carbonyl groups corresponding to Lys79 and Asp84, and three carboxyl groups corresponding to Asp82, Asp87, and Asp88. A secondary calcium binding

[b] 3_{10} helix: structure characterized by 3 residues per turn and 10-member hydrogen-bounded loops.

site was also identified 7.9 Á away from the main one (Pike *et al.*, 1996; Chrysina *et al.*, 2000; Permyakov and Berliner, 2000; Kim and Baum, 1999).

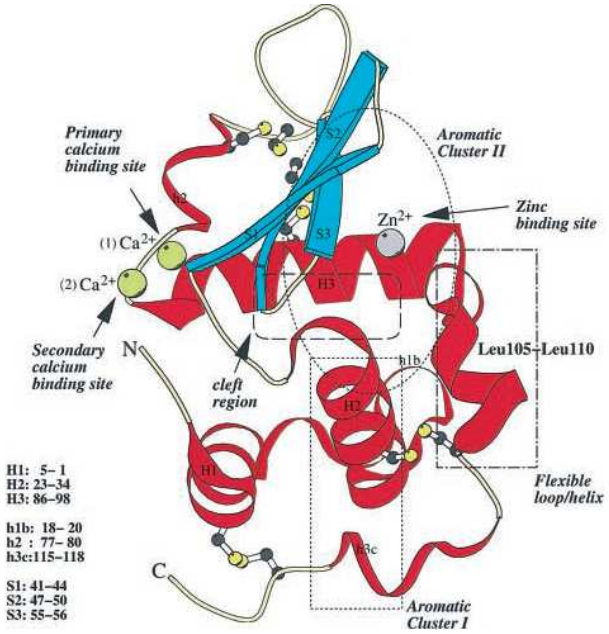

Figure 4.2: Three-dimensional structure of LA and the functional regions of the molecule showing the location of metal ions identified in LA crystal structures. Secondary structural elements are marked (*S,* b-strand in blue; *H* , α-helix and *h,* 3_{10} helix in red). The 8 cysteine residues are also represented, between the close pairs of cysteine are formed the 4 disulphide bridges of the protein (Adapted from Chrysina *et al.*, 2000).

Overall, the tertiary structure of LA is stabilized by four disulphide (SS) bridges. The SS bridge Cys73-Cys91 holds together the two subdomains, forming the Ca^{2+} binding loop. Located in the small β-sheet subdomain, another important SS bridge, Cys61-Cys77, links nonstructured loops, connecting both subdomains as well. The other two bridges, Cys6-Cys120 and Cys28-Cys111, are situated in the α-helical subdomain (Vanhooren *et al*., 2006**a**; Permyakov and Berliner, 2000), the first one being reduced with extreme rapidity (Ikegushi *et al*. 1998), and the second one plays an important stabilizing role (Wu and Kim, 1998; Horng *et al.*, 2003; Ikegushi *et al.*, 1998).

Besides the Ca^{2+} binding site, LA contains three other important structural regions: two aromatic clusters and one flexible helix/loop region.

The two aromatic clusters are integrated on two separate hydrophobic cores of the protein. They are both localized in the α-subdomain and comprise the majority of the protein fluorophores as can be observed in the structure of holo-bLAc enhanced in yellow in Figure 4.3. Together with the Ca^{2+} binding site they form the most rigid part of the structure.

.Aromatic cluster I is constituted by residues involved in interactions between one helix 3_{10} and one α helix of the α-subdomain, in a zone further from the binding site, comprising one

Phe (F31) and one Trp (W118). The aromatic cluster II, part of the second hydrophobic core (also named hydrophobic box), is formed by packed interactions between residues of the α-helices H2 and H3 and is situated in the vicinity of the cleft region located at the opposite side of the Ca^{2+} binding site (enhanced in Figure 4.2). It comprises the remaining Trp residues (W26, W60, and W104), one Tyr (Y103) and one Phe (F53) (Chrysina *et al.*, 2000; Wu *et al.*, 1998, Pike *et al*., 1996).

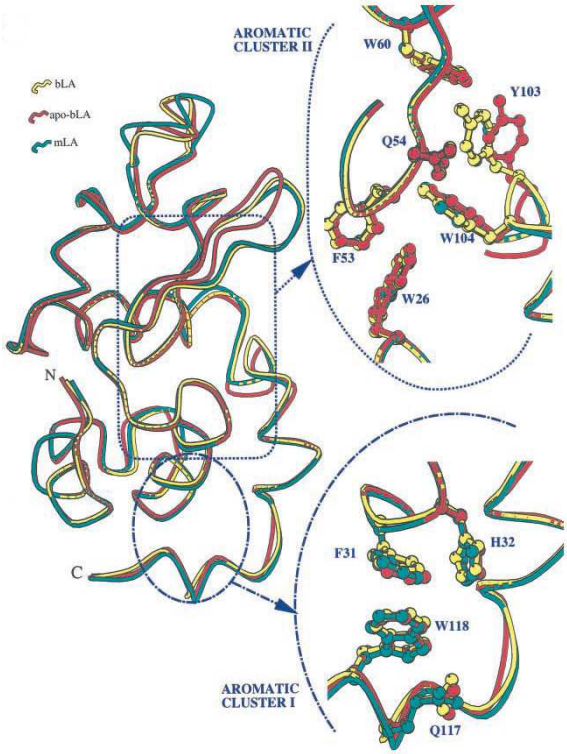

Figure 4.3: Localization of the Aromatic Clusters I and II in the structure of bLA. apo-bLAc structure (PDB entry: 1F6R) is shown in *red*, holo-bLAc structure (PDB entry: 1F6S) is shown in *yellow,* and recombinant bLA (mLA) structure in *green*. The superposition of the structures was performed with program O (35) (Adapted from Chrysina *et al.*, 2000).

The crystallized structures are very similar, only showing some small deviations. The insets show the details of packing interactions in aromatic clusters I and II (the hydrophobic box). Aromatic cluster I comprises one phenylalanine (F31) and one histidine (H32) localized in the end of helix H2, and one glutamine (Q117) and one tryptophan (W118) located in the terminal tail of LA. Aromatic cluster II contains residues from the H1, H2 and one of the 3_{10} helices, including three tryptophans (W26, W60 and W104), one tyrosine (Y103), one phenylalanine (F53), and one glutamine (Q54).

The flexible helix/loop region is constituted by the residues 105-110 (Leucine 105, Alanine 106, Histidine 107, Lysine 108, Alanine 109 and Leucine 110 - Enhanced in Figure 4.2), and is adjacent to the lower end of the cleft interacting with the C-terminal end of helix H2. It is a particularly interesting region since it flanks the aromatic cluster I and adopts different conformations, loop or distorted helix, depending of the molecular environment, particularly upon the pH of the crystallization medium. It seems that at higher pH values(6.5– 8.0) this loop adopts the helical conformation and at low pH (4.6), the “loop” conformation (Pike *et al*., 1996;

Ramakrishnan and Qasba, 2001) For both crystallized structures of bLA (apo-bLAc and holo-bLAc) this flexible region adopts a distorted helical conformation.

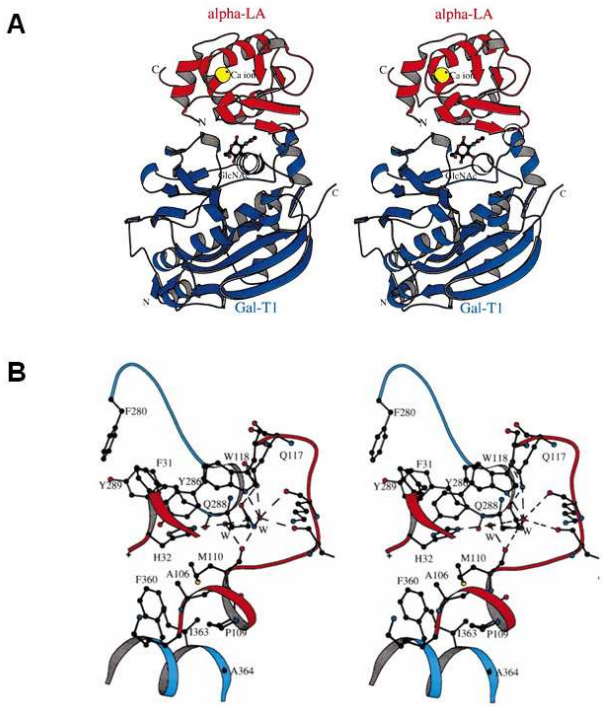

Figure 4.4: A – Molecular structure of lactose synthase, a complex between the catalytic domain of bovine GT (Gal-T1) and mouse LA (alpha-LA). The complex is shown with the acceptor GlcNAc. **B –** Stereo view of the molecular interactions between the same GT and LA. The secondary elements of LA are colored in red, while those of GT are in blue. The interactions between the proteins are principally hydrophobic. Two water molecules are trapped between the two proteins, and one of them has extensive hydrogen bonding interactions with both protein molecules. Adapted from Ramakrishnan and Qasba (2001).
.

Both aromatic cluster I and the flexible helix/loop region are particularly important for the lactose synthase regulation function, as they are the major active sites for interaction with GT. Ramakrishnan and Qasba (2001) described the structural role of both components in the catalysis reaction through a crystallographic study of the lactose synthase complex formed by recombinant mouse LA and bovine GT. The interactions between the LA and GT molecules are primarily hydrophobic and near of the acceptor site of GT (Figure 4.4 A). The aromatic cluster I of LA interacts with a corresponding hydrophobic patch in GT (Figure 4.4 B). The flexible loop/helix region of LA (in the mouse structure in a helix conformation) interacts with phenylalanine 360 and one of the α-helix of GT. Proline 109 sidechain of LA also interacts with the same α-helix of GT. Two residues of the aromatic cluster I of LA, histidine 32 and phenylanine 31 are said to be important in the binding of glucose to the complex.

In terms of structure details, it is finally important to outline the main differences between LA and c-type lysozyme. Lysozyme has the same fold organization than LA, with the two distinct

subdomains. The main differences reside on the non-existence of a Ca^{2+} binding site in lysozyme and in the cleft region, in which is located the binding site for monosaccharides in lysozyme. In LA the cleft region is blocked by Tyr 103. The truncations of the site, along with amino acid substitutions in the lower reaches of the cleft perturb the capability of LA to bind monosaccharides (Pike *et al.*, 1996).

4.2.2. Structural Elements Involved in the UV-sensitivity of LA

The location of the major part of the protein fluorophores in bLA has already been mentioned as they integrate primarily the two aromatic clusters of the protein. In this project, the most important positions are those of the Trp residues, since the intrinsic Trp fluorescence was used to probe their position within the protein (and the local structure), and the Trp residues were selectively excited to study the UV-induced reactions.

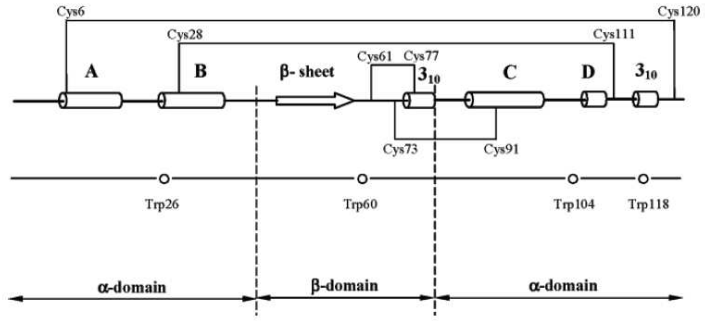

Figure 4.5: Schematic representation of LA. Secondary structure elements and the disulfide bonds in native GLA are indicated at the top. The domain boundaries are shown as dashed lines. Each of the tryptophan residues (O) is indicated (Adapted from Vanhooren *et al.*, 2006**a**).

The four Trp, major contributors for the protein fluorescence, are all located in the two clusters of bLA. Trp 26, Trp 60 and Trp 104, constituents of the aromatic cluster II are buried within the protein, displaying low values of accessible surface area[c] (ASA) in holo-bLAc: 0, 2.06, and 5.86 $Å^2$ respectively. Trp 118, present in the aromatic cluster I, is more exposed to the solvent with a calculated ASA of 30.3 $Å^2$. In apo-bLAc, the Ca^{2+} depleted form at high ionic strength, the tendency is the same, though Trp 60 is quite more exposed and Trp 104 the inverse. The ASA determined values for apo-bLAc are respectively 0, 0.12, 9.45, and 26.73 $Å^2$ for Trp 26, Trp 60, Trp 104 and Trp 118.

Trp 60, the only one of these residues that belongs to the β-subdomain (Figure 4.5), is located near two disulphide bonds (Cys61-Cys77 and Cys73-Cys91) in native bLA as can be depicted in the three-dimensional representation of holo-bLAc (Figure 4.6 A).

[c] The ASA values were calculated using the program *Surface Racer*© 5.4, upon submission of the PDB files for holo-bLA (1F6S) and apo-bLA (1F6R), considering a probe radius of 1.4 Å that approximates the radius of a water molecule, and the Van der Vaals radii sets of Richards – 1977 (Tsodikov *et al.*, 2000).

Considering a 5.2 Á cut-off distance for Van der Vaals contact between two atoms in proteins (as defined in Li and Nussinov, 1998), Trp60 is in direct contact with Cys73-Cys91 (calculated value of 4.67 Á) and very close to Cys 61-Cys77 (6.43 Á), which make them potential targets of UV-induced reduction, and consequently probable quenchers of Trp60 fluorescence. Trp 118, located in the opposite end of bLA, in direct contact with Cys28-Cys-118 (5.15 Á), is another likely trigger of UV induced SS bond disruption.

As observed by Vanhooren *et al*.(2006**b**) for goat LA, the indole side-chains of Trp60 and Trp118 in bLA are located on opposite sides of those of Trp26 and Trp104, that form a couple. The indoles side-chains of these two coupled Trp residues are in direct contact with each-other (calculated distance of 3.78 Á in *RasMol* – data not displayed in Figure 4.6), adequate situation for exchange and resonance of their excitation energy. Trp26 and Trp104 are not in direct contact with any SS bond. However, the indole ring of Trp104 and a potential quenching group, the peptide bond of Val92-Lys93, are within the delimited contact (calculated distance of 5.06 Á) as can be pictured in Figure 4.6 A.

In the same zone of the peptide backbone, the peptide bond Lys94-Ile95 is in direct contact with Trp 60 (3.76 Á) and may act also as quencher for this fluorophore. Similarly, Trp118 is also in presence of other quenching groups, other than the SS bond Cys28-Cys111. Its indole ring is in direct contact with the imizidole ring of one histidine (His32, 3.86 Á) and close to the peptide bond between Val27 and Cys26 (6.62 Á).

The characteristics of the Trp residues in the structure of apo-bLAc are similar to those of the correspondent residues in holo-bLAc described, which is natural given high homology degree of the two folds (see deviation values in Table 4.1, superposed structures in Figure 4.3 and section 4.3.5). In fields A and B of Figure 4.7 is represented the three-dimensional structure of apo-bLAc with the relative positions of Trp regarding correspondingly the SS bonds and the other potential quenchers. It can be noticed in both fields that the direct contacts mentioned for holo-bLAc are maintained, meaning that for this form of the Ca2+ depleted LA, the same UV-reactions noticed in native bLA may also occur.

The relative distances calculated for both structures are summarized in Table 4.2, where are also present other proximity distance values between SS bonds and Trp residues.

Experimental observations sustain partly the observations here realized. Through fluorescence studies using mutants of human LA containing only one Trp residue, Chakraborty *et al.* (2001) proved that the fluorescence signal of Trp 60 and Trp 118 is significantly quenched by disulphide bonds in their vicinity. Native human LA contains only three Trp residues, lacking Trp 26. However the structures of bLA and human LA are very similar, so the same quenching should occur in bLA, as suggest the distances here determined.

Table 4.2: Distances between the Trp residues of holo-bLAc and Apo-bLAc and its potential quenchers. The values were determined in *Rasmol* 2.6 using the "monitor" tool. In green are highlighted the Trp-quencher pairs for which there is direct contact (≤ 5.2 Å).

Pair		Distance (Å)	
Tryptophan	**Potential Quencher**	**Holo-bLAc**	**Apo-bLAc**
Trp26	Trp104	3.78	3.61
Trp26	Cys28-Cys111	8.37	8.38
Trp26	Cys6-Cys120	14.81	13.36
Trp60	Cys61-Cys77	6.43	6.24
Trp60	Cys73-Cys91	4.67	4.20
Trp60	Lys94-Ile95	3.76	4.09
Trp104	Val92-Lys93	5.06	5.08
Trp104	Cys28-Cys111	9.06	8.95
Trp104	Cys73-Cys91	7.80	7.93
Trp118	Cys6-Cys120	9.60	8.07
Trp118	Cys28-Cys111	5.15	4.74
Trp118	His32	3.86	4.12
Trp118	Val27-Cys28	6.62	5.70

More recently, Vanhooren et al. (2006**b**) studied the fluorescence of four mutants of goat LA, each one lacking one of the Trp residues. Compared to the wild-type the fluorescence of mutants lacking Trp60, Trp104 and Trp118 was higher, while for the mutant lacking Trp 26 it was lower. First of all, these results indicate that Trp26 dominates fluorescence, which can be explained by the lack of quenching groups around it (which is also verified in bLA). The increase in Trp fluorescence of the other mutants is explained differently. Trp60 and Trp118 are highly quenched by vicinal groups, including the disulphide bonds (observed as well in bLA). There are strong evidences that in LA these groups indirectly quench the group Trp26-Trp104, by transfer of energy to Trp60 and Trp118 (Sommers and Kronman, 1980; Vanhooren *et al.*, 2005). Despite the exchange of excitation between Trp 26 and Trp 104, there is an increase of fluorescence intensity in the mutant lacking Trp 104. This could be again due to the presence of quenchers of Trp 104 (again here verified for bLA), and indirect quenching of Trp26 by transfer of energy from Trp26 to Trp104. Resuming, in the mutants lacking Trp60, Trp104 and Trp118, the indirect quenching of Trp26 by the quenchers and the transfer of energy from Trp26 to each of these residues would not occur, resulting in the increase of fluorescence yield.

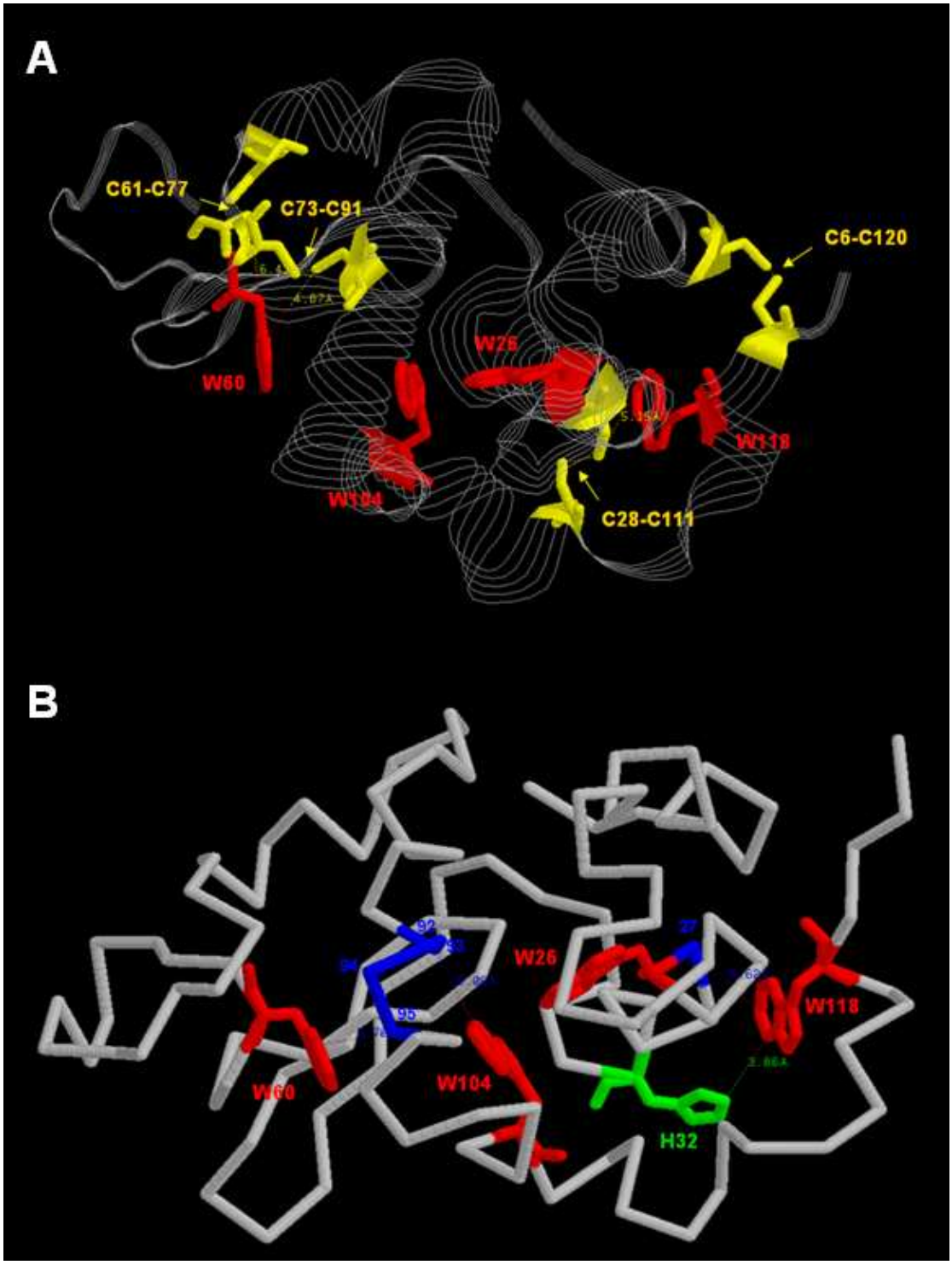

Figure 4.6: Crystal structure of holo-bLAc at 2.2 Å resolution (PDB entry: 1F6S) generated in *RasMol* 2.6. **A-** Peptide backbone is represented in grey strands. The 4 Trp and the 8 Cys residues of bLA are displayed in a stick configuration respectively in red and yellow. Dashed yellow lines represent the SS bonds of the protein highlighted by yellow arrows. Potential contact between the indole nucleus of a Trp residue and a disulphide bond is indicated mixed red-yellow dash line and the distance in Å. **B-** The peptide backbone is represented in grey strands and the backbone of five residues (Val27, Val92, Lys93, Lys94, and Ile95) is in blue. Val 32 is in stick configuration and in green. Contact between the indole nucleus of a Trp residue its potential quenchers is indicated in mixed red-green/blue dash line and the distance in Å.

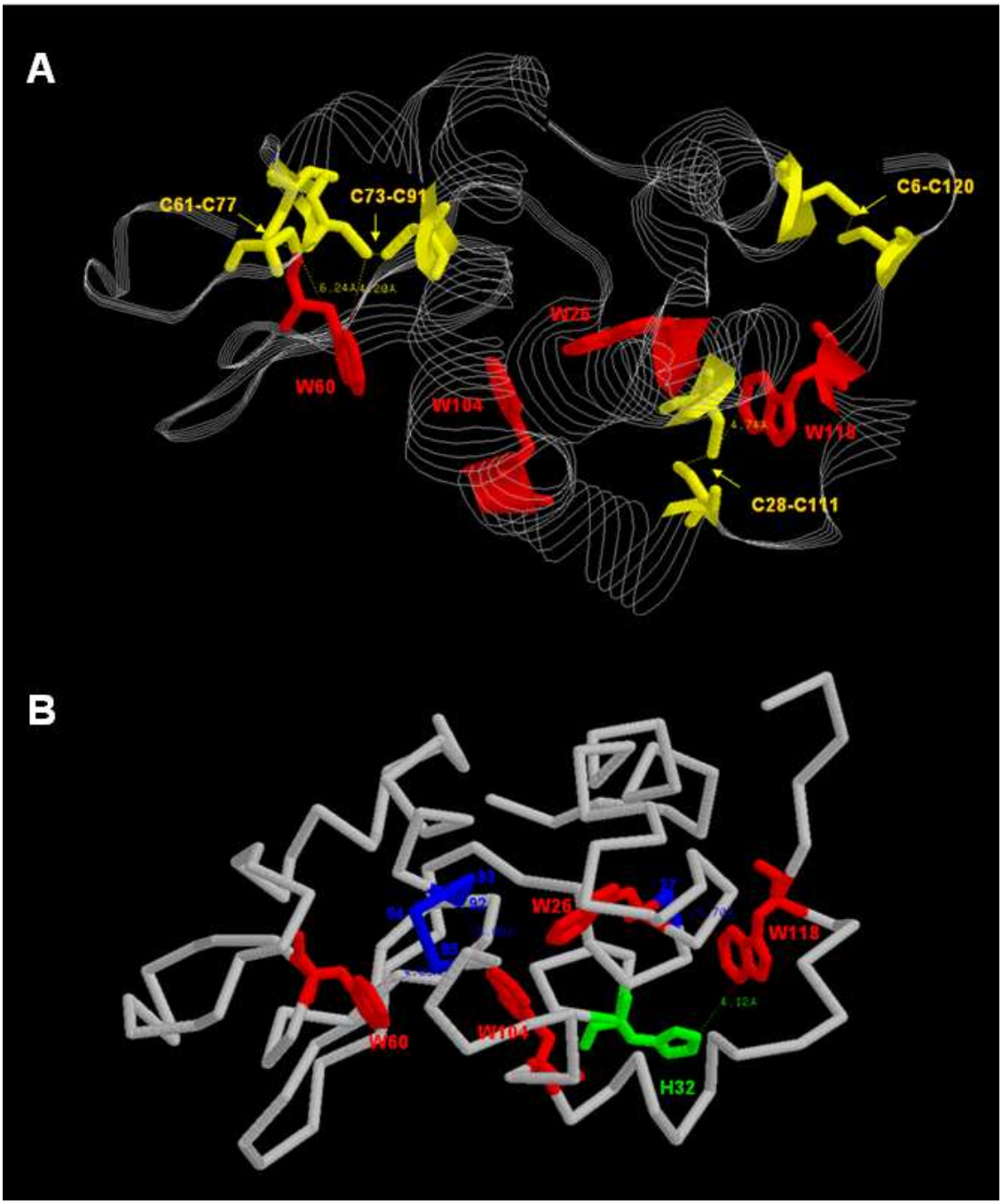

Figure 4.7: Crystal structure of apo-bLAc at 2.2 Å resolution (PDB entry: 1F6S) generated in *RasMol* 2.6. A- Peptide backbone is represented in grey strands. The 4 Trp and the 8 Cys residues of apo-bLAc are displayed in a stick configuration respectively in red and yellow. Dashed yellow lines represent the SS bonds of the protein highlighted by yellow arrows. Potential contact between the indole nucleus of a Trp residue and a disulphide bond is indicated mixed red-yellow dash line and the distance in Å. B- The peptide backbone is represented in grey strands and the backbone of five residues (Val27, Val92, Lys93, Lys94, and Ile95) is in blue. Val 32 is in stick configuration and in green. Contact between the indole nucleus of a Trp residue its potential quenchers is indicated in mixed red-green/blue dash line and the distance in Å.

4.3. CONFORMATIONAL STABILITY OF LA

The denaturation of proteins is evidently closely related to the stability of their structures. For LA a great deal of studies has been carried out using denaturation and unfolding procedures, is it in the ambit of protein folding studies, or in the context of aggregation studies of the protein for food engineering. For insight into protein stability and denaturation phenomena please see Appendix A (Denaturation of Proteins). It was not integrated in this part to avoid the natural succession in the text.

In the next section the denaturation of LA (the molten globule states) will be discussed, followed by a literature overview on the conformational stability under the conditions stated previously (temperature, pH, absence of calcium).

4.3.1. Molten Globule States

Globular proteins, and specially LA, have been extensively studied protein models for the understanding of protein stability, folding, and unfolding. Proteins can exist in particular low-entropy but energically equivalent states, “quasi-native” states, usually called molten-globules (MGs), that do not involve major changes in protein structure (Damodaran and Paraf, 1997; Chang *et al.*, 2001). These states are created under a wide variety of conditions, generated at equilibrium after unfolding upon the exposition to acid solutions, mild denaturants, by remotion of protein-bound prosthetic groups or metal ions, as well as protein chain truncation (Laureto *et al.*, 2002).

A molten globule (MG) state has been classically described as a relatively compact folding state of the protein, a collapsed state of the whole polypeptide chain, that retains some native-like secondary structure and overall backbone-folding topology, but lacks some of the specific side-chain interactions of the native structure that permit the existence of a clear tertiary arrangement. “Globule” refers to the structure compactness and “molten” to the increased enthalpy and entropy on the transition from the native to the new state. The MG state may therefore be interpreted as a stable partially folded conformation that can be distinguished from either the native or the fully denaturated form. (Laureto *et al.*, 2002; Van Dael *et al.*, 2005; Tarek *et al.*, 2003; Damodaran and Paraf, 1997).

MG-like states are particularly attractive since they have been shown to resemble kinetic intermediates in the folding process of the proteins, LA being one of these cases (Wijesinha-Bettoni *et al.*, 2007; Tarek *et al.*, 2003). The full understanding of the mechanism of protein folding, an active quest in molecular biology and biophysics nowadays, requires the knowledge of the structure, relative energetics and dynamics of the species populating the folding pathways of the protein. The acquired knowledge could help to understand the nature and role of these

diverse kinetic intermediates, intriguing for itself along the folding pathway. In some cases they display progressive structural shifts along the folding process, while in other situations one can find intermediates that display large structural deviations in comparison with the precedents, yielding conformers that even delay the process. (Van Dael *et al.*, 2005). MG-like states can be used as a model to fulfill these needs of analysis, besides presenting the advantage fact of being formed at equilibrium, permitting an easier identification and characterization with the help of spectroscopy techniques, on opposition to the case of regular protein folding intermediates, seemingly intricate due to their transient nature (Laureto *et al*., 2002).

Although the MG is currently accepted as a concept, there have been raised several polemics around its meaning, particularly if it should be considered as thermodynamically distinct state in comparison to the unfolded one (Laureto *et al.*, 2002; Pfeil *et al.*, 1998). The structure of the MG is highly heterogeneous and disordered and, like the large majority of denaturated or partial denaturated state of proteins, it comprises also a large number of conformational isomers (Chang *et al.*, 2001), complicating the achievement of a structural picture of this its conformational states.

In the specific case of LA, unfolding of the protein to MG-like states has been reported upon exposition of the protein to acid solutions (acid denaturation), to mild denaturants (*e.g.* with guanidine hydrochloride at neutral pH LA suffers a three-state denaturation from the native state N, with an intermediate MG-like state and the further fully denaturated form), thermal variations, in cases of calcium depletion at low ionic strength, among others (Kuwajima *et al.*, 1996; Laureto *et al.*, 2002). In this thesis, relevant notions about the thermal stability of the protein, its conformational state at different pHs, and structural changes induced by calcium depletion will be mentioned. The focus will not be the MG and the study of folding intermediates. Nevertheless, discussing the MG state is inevitable, given that the thematic in issue and the MG are intrinsically related, and along the chapter some questions will be raised

4.3.2. Thermal stability of LA

The thermal stability of a protein is an intricate and complex issue: Thermal induced changes involve primarily the destabilization of major non-covalent interactions. Hydrogen bonds, electrostatic, and Van der Vaals interactions, which stabilize the native structure mainly at the different secondary level of its structure, are exothermic (enthalpy driven) in nature. Hence, they are destabilized at high temperatures and stabilized at low temperatures. However, the peptide hydrogen bonds are mainly buried in the interior of the protein, so they remain stable at a wide range of temperatures. In contrast, hydrophobic interactions are endothermic (entropy driven), and favored with the temperature increase, and the hydrophobic residues are more susceptible of interacting with water at lower temperatures. Another important factor is the conformational

entropy of the polypeptide chain: with a temperature increase, the thermal kinetic energy of the polypeptide chain increases, which greatly facilitates the unfolding of the polypeptide chain (Fennema, 1996).

The thermal stability of proteins is consequently strongly dependent on the amino-acid content and on the network of bonds in the protein structure. In fact, the first observed change in a protein's structure upon temperature increase will be the unfolding on its tertiary structure, due to the weakening and breakage of long-range interactions. The progressive flexibility obtained by the protein chain leads to solvent exposure of groups once buried. Cooperative hydrogen bonds will now maintain the secondary structure of the protein. Then the disruption of non-covalent interactions leads the unfolding, and the hydrophobic groups, on the unfolding and hydration of the structure, take a role in the rearrangement of the structure, since they interact less with water. On the other hand, the stability of the proteins can also be compromised by lowering of temperature, such as myoglobin that displays maximum stability around 30ºC, and that upon storage below 0ºC suffers cold-induced denaturation. Protein stability depends on the relative magnitude of contributions from polar and non-polar interactions. When polar interactions are favored in a protein, it will be more stable at low temperatures than at higher temperatures, while when non-polar interactions are favored, the protein will be more stable at ambient temperature than at low temperatures (Fennema, 1996).

LA has a high content in hydrophobic amino-acids (like Leu, Cys, Ile ; *vide* Figure 3.1), factor that can contribute positively for its thermal stability (Fennema, 1996). This is reinforced by the compact tertiary structure of globular proteins and the absence of free thiols groups (Wang *et al.*, 2006). Indeed, in its native conformation, at physiologic conditions (whey milk), neutral pH and calcium-rich environment, LA shows a high thermal stability. In these conditions, the T_d (denaturation temperature) (~62%) is the lowest among the whey proteins but this process is 90% reversible, as measured by calorimetry (Chaplin and Lyster, 1986; Wit and Klarenbeek, 1984). Irreversible changes happen in the native protein only at 70-80ºC, which results in minimum protein aggregation. At a temperature superior to 90ºC aggregation is fully noticed (McGuffey *et al*., 2007). The thermal unfolding is also appointed to form partly denaturated species with characteristics similar to MG-like conformations, these species being noticed at temperatures superior to 60 ºC. These partially unfolded state exhibit an increased linear dimension and hydrophobicity as well as better accessibility of the disulfide bonds to a thiol exchange reaction (Wijesinha-Bettoni *et al.*, 2007; Vanderheeren and Hanssens, 1994; Wang *et al.*, 2006).

Though native LA can be classified as thermal resistant protein (maintaining its structure intact at high temperatures), it is not always the case since its conformation is largely affected by external solvent conditions, thus so is its stability. Indeed, any denaturation transition in LA is highly dependent on metal ion concentration and pH values (Permyakov and Berliner, 2000).

Thermal stability data is very useful in terms of providing clues on the structural effects induced to the protein by different external parameters, like pH or other solvent specificities (Pedersen *et al.*, 2006). Structural changes are detectable since the protein will have a different susceptibility to thermal unfolding upon changes in physic chemical parameters of the solution. For that reason it is a tool frequently used on studies with LA, involving pH or calcium concentration changes.

4.3.3. pH Influence in the Conformational Stability of LA

At neutral pH LA and at temperature way below its T_d is in its native state in the milk whey (Gao *et al.* 2008). From preliminary studies it was concluded that LA undergoes intermolecular interactions leading to varying degrees of polymerization depending on the pH. At acidic pH values, the protein is characterized a rapid reversible association and slow aggregation. Between pH 6 and 8.5 there is very little association, being the protein in a native-like structure and above pH 9.5 there is expansion without aggregation (Boye *et al.*, 1997). It is interesting in the ambit of this study to look at the molecular changes that occur at these different pH values.

As mentioned before, the isoelectric point of native LA is determined by previous analysis to be around 4-5 (acidic protein).

Therefore, upon pH shifts towards acidic values, LA turns progressively more positively charged. The titrable groups of the protein (with different pK_as) will be gradually protonated at low pH values, leading ultimately to the denaturation of the protein due to electrostatic repulsion forces. The transition to a denaturated state happens progressively, as a cooperative event, triggered by the protonation of residues in the calcium binding pocket, rich in Glu and Asp (model pK_as around 4-5, Creighton, 1992), leading to Ca^{2+} release from the protein (Pedersen *et al.*, 2006; Kim and Baum, 1998). This event takes place in the vicinity of the isoelectric point, as described by nuclear magnetic resonance (NMR) and near-UV (250-400 nm) CD spectroscopy (Kim and Baum, 1998), in agreement with previous studies (Griko et al., 1994). Above pH 5.0 the protonation of residues does not contribute to the formation of a compact denaturated state. The transition is noticed below 4.2, where larger population of denaturated states is detected, displaying a reduced signal at 280 nm (in the near-UV) in the CD spectrum (Kim and Baum, 1998). Probably, the structure is destabilized for two reasons: the release of calcium and the possible to breakage of salt bridges mediated by the protonation of Asp and Glu. The result is a structure with fewer constraints, and risking concomitant rupture of H-bonds.

The acidic pH-induced unfolding results in a calcium depleted acid denaturated form (A-state), a MG-like conformal state, which is analogous to an early protein folding intermediate, and frequently regarded as the MG *prototype*, usually defined at pH 2 (De Laureto et al. Kim and Baum, 1998). In this form, the thermal stability of the protein is largely affected, the T_d lowers from 62ºC at pH 8 to 32ºC at pH 2.5 (Pedersen *et al.* 2006).

This partly folded state retains some of its tertiary features, in a bipartite structure conformation. When pH drops, the helical content of the native structure, constituted by the α-subdomain plus helix 3_{10} h2 (residues 1-37 and 85-123) is preserved, albeit dynamical, with the typical helical secondary structure retained by helices H2 and H3, formed by loose hydrophobic interactions. On the other hand, the majority of the β-subdomain, encompassing the three β-strands of the protein (residues 38-84) is disordered and unstructured (Laureto *et al.*, 2002, Kuwajima *et al.*, 1996).

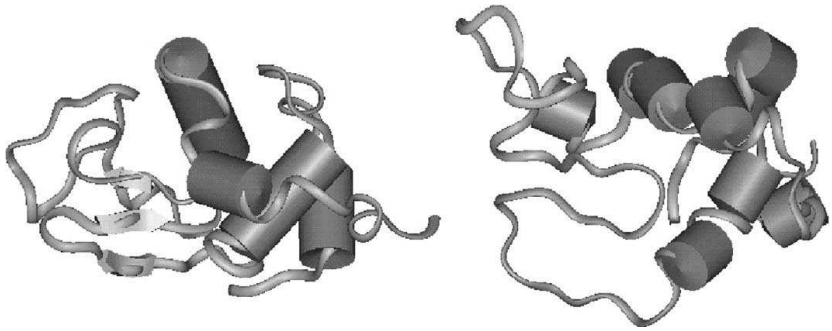

Figure 4.8: Snapshots of LA configurations in the native state (left) and molten globule state at pH 2 (right) from the molecular dynamics simulations. Helices are displayed as barrels and β-sheets as large arrows (Adapted from Tarek *et al.*, 2003).

This bipartite picture of LA can be confirmed by snapshots of LA generated from molecular dynamics simulations displayed in Figure 4.8 (Tarek *et al.*, 2003). Two snapshots are represented: to the left is displayed protein in its native conformation (pH 8) and to the right in its A-state (pH 2). It can be clearly noticed the loss of the structure in the β-subdomain (triple-stranded antiparallel β-sheet) when pH is lowered to pH 2, while most of the α-subdomain (helices) is conserved.

The reduced signal obtained with near-UV CD spectroscopy (De Laureto *et al.*, 2002; Kim and Baum, 1999), in consonance with quenching experiments with acrylamide (Pedersen *et al.*, 2006), indicate that, at low pH, some specific and rigid side-chain packing of aromatic chromophores of the protein is possibly lost, and that an opening of the hydrophobic part of the protein may occur.

Although at low pH Trp 26 and Trp 104 (part of the aromatic cluster II) remain buried in the acid state and the hydrophobic cluster that they integrate is maintained, there is a clear possibility of structural re-arrangement in this area, as documented by nuclear magnetic resonance (NMR) and hydrogen exchange of tryptophan indole ions (Kuwajima et al., 1996). The observed conformational change is likely to be in this area since the main stabilizing hydrophobic core is considered to be oppositely the aromatic box I. An analysis of a set of point mutations in the α-subdomain of the protein led to consider this subset of hydrophobic residues (aromatic box I) most important for the formation of the native-like topology (Wu and Kim, 1998; Permyakov and Berlinder, 2001), as it could be for the maintenance of the α-subdomain structure.

This expected opening of the structure and the exposure of certain hydrophobic parts of the protein are confirmed by the following observations.

- the radius of gyration of native calcium-loaded LA is 15.7 Á in contrast with the value of 17.2 Á for the acid molten globule Permyakov and Berliner, 2000);
- it is a highly hydrated conformation comprising 270 bound water molecules (Permyakov and Berliner, 2000);
- the mass density of the interior of the protein is 5% less and the intrinsic compressibility coefficient two times higher than in the native protein (Permyakov and Berliner, 2000);
- a 15-fold increase in hydrophobicity is noticed when it converts to the acid state (Gao *et al.*, 2008).

LA retains therefore a globular shape in acidic conditions however swollen when compared to the native state. At very low pH values the opening of the structure leads eventually to protein aggregation (Pedersen *et al.*, 2006).

The effect of alkaline pHs in the structure of the protein is less described in literature. Upon shift to basic pH values, the protein will become negatively charged. At pH 9 the protein is probably quite stable, since no aggregation is still observed and no thermal transition is noticed in differential scanning calorimetry experiments (Boye *et al.*, 1997). At higher pH values, the destabilized negative charged protein may loose a large part of its favorable electrostatic interactions leading to its partial denaturation, mentioned to have a MG-like conformation (Harata and Muraki, 1992).

4.3.4. Calcium Induced Conformation Changes in LA

Chelating agents, metal cations, and buffer components are known to induce dramatical structural changes in the LA molecule and thereby alter its binding properties in solution (Griko *et al.*, 1999). In particular, the influence of the Ca^{2+} ion will be discussed.

The native form of the LA is the calcium-bound, which is the major form under physiological conditions (milk whey) (Hong *et al.*, 2002). However, during the refolding process LA is mainly in its calcium depleted form (named apo-LA on opposition of holo-LA, which is the metal-ion bounded form), and the role of binding of Ca^{2+} in lactose synthesis is still unclear (Permyakov and Berliner, 2000). LA assumes probably other forms than the calcium-bound *in vivo* in the variable environments where it intervenes, and the apo-form is probably one of them.

The binding of Ca^{2+} to LA induces prominent changes in its 3D structure and function but not the secondary structure (Permyakov and Berliner, 2000). The calcium ion in LA has a structural role, being required for folding and native SS bond formation in the reduced denaturated protein (Chrysina *et al.*, 2000). In the denatured form, with the disulphide bridges

intact, LA refolds slowly to its native structure, a process at least 2 orders faster upon Ca^{2+} binding by folding intermediates (Kuwajima *et al*., 1989)

Though several reports exist on the role of calcium in the stabilization of LA structure, there is no agreement about the conformation of the calcium depleted form of LA, probably due to its structural instability. Divergent opinions are reported, shifting from a classical MG devoid of the cooperative thermal transition, to a partly native folded state with some maintained native proprieties and oppositely showing cooperativity (Laureto *et al.*, 2001).

The apo-LA thermal stability has been probed by differential calorimetry, fluorescence emission, Raman spectroscopy, and near UV-CD at different solvent conditions (pH, ionic strength). All observed T_m (temperature of mid-transition) values were lower than the T_m of the native Ca^{2+} bound state (Hendrix *et al.*, 1996; Wilson *et al.*, 1995; Laureto *et al.*, 2001; Veprintsev *et al*., 1997; Pfeil, 1998; Wijesinha-Bettoni *et al*., 2001). T_m is reported to be highly dependent of the physic chemical parameters of the solution.

One important solvent parameter that can affect the results and the conformation of apo-LA is ionic strength. NaCl and KCl were both shown to stabilize substantially the folded state: in the presence of 0.5 M NaCl the thermal stability is reported to increase by 30ºC (Wijesinha-Bettoni *et al.*, 2001). The stability of calcium-bound LA is not influenced by variations in ionic strength at neutral pH indicating that no charged groups affect protein stability in this pH range. However removal of calcium ion exposes negatively charged residues originally coordinated to Ca^{2+} in the holo-LA, destabilizing the conformation of the protein (Griko *et al*., 1999). The salt stabilizing effect is probably due to ionic interactions and not a specific binding effect of the cations like Ca^{2+} replacement, achieved by partial neutralization of the unfavorable charge. This is supported by previously referred X-ray crystallography studies (Chrysina *et al.*, 2000) and NMR studies (Wijesinha-Bettoni *et al.*, 2001) carried on apo-LA in the presence of high contents of salts. In both studies only subtle changes are observed between the apo and the calcium loaded form, at the calcium binding sites. Parallel to the minor instability in the structure, no ion was found in binding site in the crystallized apo-LA and no chemical shifts were observed in the aspartates of the calcium binding site, excluding this way any Ca^{2+} substitution.

Without the stabilizing presence of calcium in the binding site, LA is also more vulnerable to pH shifts. Between pH 5.5 and 8.5, apo-LA is stable, in similarity to the native form. However, its stability decreases remarkably below pH 5 (Griko *et al.*, 1999)

Crystallographic studies show the presence of a more open cleft structure in the Ca depleted form, induced by a perturbation of interactions between the α and β-subdomain of LA at an inter-subdomain region located it at the edge of the hydrophobic box. The authors argue that this perturbation propagated from the main calcium binding pocket, where a small expansion is observed (at high ionic strength), causing a slight tilt of the helix 3_{10} h2 relatively to the H3-helix, leading to the disruption of some of the native interactions in the Aromatic Cluster II. The NMR

studies concurs partially with the crystallization study showing that the major shifts occur in the residues on the main Ca^{2+} binding loop and on the nearby α-helix(H3-helix). Nonetheless, the NMR chemical shifts in the Aromatic Cluster II are not so elevated (mostly for the Tyr103, which is the residue that shows a wider change in the crystallographic study). These small divergences in both studies may be attributed to differences between the crystallized form and the solution (NMR) form of apo-LA, or simply by differences in the experimental conditions used in both studies.

The areas with changed structure in the calcium depleted form are the same areas where the MG of the A-state (LA at pH 2) is apparently altered, which could signify that this form at high ionic strength is representative of an initial step for the transition to a MG-form. The MG-conformation could be favored at low ionic strength, with a further dispersion of these zones.

Studies using limited proteolysis on apo LA (Laureto *et al.*, 2002), where the conformation was well characterized as native-like by means of near-UV CD show that the destabilization of apo LA under different denaturating conditions (moderate heating, presence of Trifluoroethanol and Oleic acid), occurs only in residues 34-57, giving origin to a MG like conformation. These residues are part of the β-subdomain, the major zone disordered in the A-form. One can imagine therefore apo-LA in terms of a compact protein with a short disordered segment, easily destabilized by ionic strength, temperature, among others, that in under strong destabilization resembles the A-state pictured in Figure 4.8.

4.4 REMARKS

From this literary overview of the protein, some broad notions can be traced about its reaction to destabilizing conditions. The unfolding of LA comes generally in a bipartite fashion, with the β-lobe more disorganized and the α-lobe retaining some compactness, which makes sense since the two sub-domains are well separated as can be depicted from the three-dimensional structure of the native protein (Figure 4.2). The apo-form is less stable and reacts in an amazing diversity upon diverse solvent conditions, implying that, for each experimental approach, a judicious characterization of the specific effects of different solvent factors on protein structure must precede premature speculation and discussion of controversial results.

However, it is interesting to observe that the molecular flexibility of LA is probably influenced and controlled by solvent conditions and modulated by binding ions, which might serve as a regulatory mechanism for this protein.

Indeed, in the several biochemical roles advanced for the protein other than the intervention in the lactose biosynthesis, LA is not in its native conformation. Calcium-depleted forms, as the one analyzed in this study, are known to interact with lipid membranes and oleic acid. The association of LA with the latter is known to generate a multimeric MG variant, HAMLET

(human LA made lethal to tumor cells) that induces apoptosis specifically in tumor cells. (Permyakov and Berliner, 2000; Laureto *et al.*, 2002; Fisher *et al.*, 2004). Furthermore, a MG state of the human protein has been shown to have antimicrobial activity (Wijesinha-Bettoni *et al.*, 2007).

It makes sense also, that in the different environments of the human and mammals' body, LA assumes different conformations. The reactivity to different metal ions is a possible regulating mechanism.

For the reasons presented above the apo-forms of LA are by itself clearly attractive models of study, though care must be taken on analysis.

On the other hand it is important to analyze the protein and the apo-form as models for the study of UV reactions. As a model, LA is not a simple case of study like *Fusarium solani pisi* cutinase that displays only one Trp and one SS bond, which allows the link between the excitation of Trp and disruption of SS-bridge to be easily made. Moreover, the four Trp residues of LA are located in different environments of the protein, exposed to different quenchers and may be enrolled in a wide number of interactions. Such variety makes not only the process of fluorescence data analysis quite harder, since it is not easy to understand how the Trp residues contribute for the protein intrinsic fluorescence, as it opens doors for a wide number of possible UV triggered mechanisms. However, the richness of SS bonds and Trp residues in this small protein suggests that the SS induced breakage in study is probable in several ways.

In fact, the disruption of SS bonds in LA upon Trp excitation has been verified for Ca^{2+} loaded and apo-versions of bovine, human (Permyakov *et al*., 2003), and goat (Vanhooren et al., 2002; Vanhooren *et al.*, 2006**a**) LA. In these studies was proven the light-induced breakage of two SS bonds in human and goat LA: Cys61-Cys77 and Cys 73-91. Additionally, in the studies regarding the goat version (for apo and Ca^{2+} loaded LA) was proven the disruption of Cys6-Cys120. Strangely, no breakage of the bond Cys28-Cys111 was found in either study. This bridge is in close Van der Vaals contact with Trp 118, and its photo-reduction would be more expected than the others SS bonds. This SS bond is located in a zone with very high preference for native-like topology. Thus, this activated SS bond may not be susceptible to cleaving, or even upon cleaving, the resulting thiyl radicals may not tend to migrate away for each-other, and the SS bond may reform before any other reaction (Vanhooren *et al.*, 2006**a**).

Studying an apo-form is presumably more difficult since the structure is more instable and unpredictable. Nevertheless, the SS bridges in this state are probably still intact and the aromatic residues compact even in a MG-like state. It is appealing to probe the effects of UV light on apo-bLAs since they are not so well characterized in this particularity. The characteristics of apo-forms may be also favorable for an immobilization procedure since the disulphide bonds of LA are in principle less stable, and possibly it will adhere easily onto surfaces due to the stronger inherent hydrophobic character of these forms (compared to the native LA).

5. CHARACTERIZATION OF THE MODEL

5.1. PREMISSES

The main goals of the characterization procedure were, as previously stated, to evaluate the protein model as a candidate for light induced immobilization and check the ideal conditions to proceed with this technique with the model. Taking in consideration the main features of the model chosen, a calcium depleted form of LA, the characterization procedure regarded two distinct issues, reflected in the organization of the results here presented.

First it was needed to verify the SS bond light induced disruption for the apo-form of LA obtained in solution. As stated before, from literature it is known that this mechanism can occur in calcium depleted forms of the protein but it was desirable to verify it, and confirm its specific features for the apo-form and the conditions used. Moreover, it was important to check the impact of distinct factors such as temperature or pH in the UV-sensitivity of the protein in order to plan a desired immobilization.

On a second hand, it was required to qualify and define the specific apo-form obtained in the experimental conditions used above. Calcium depleted forms LA are particularly unstable, and for that reason it was important to figure out the conformation that it adopts initially in solution, and assure if the model is stable during the experiments, focusing already in the immobilization procedure. Furthermore, for comparisons with other works, this step is clearly essential.

The primary tool used for both sets of analyses was fluorescence spectroscopy. The basic principles and concepts behind the analysis procedure will be described throughout the results presentation.

To avoid confusions with either the native form or other apo-forms of the protein, the protein form used in the experiments and described in the Materials and Methods (section 5.2.1) will be further named as eLA, standing for “bovine α-lactalbumin used in the experimental procedure”.

5.2. MATERIALS AND METHODS

5.2.1. Materials

Protein Solutions

Bovine α-Lactalbumin from bovine milk type III was purchased from Sigma-Aldricht (product labeled as L6010a) as lyophilized powder and the same was used without any further preparation in all the experiments here mentioned. The product in question had been previously prepared directly from raw, unpasteurized milk, purified by ion-exchange chromatography using DEAE-agarose, and depleted of calcium via remotion by precipitation with sodium sulphate. The degree of purity is ≥85% (Sigma Product Information, www.sigmaaldrich.com).

eLA concentrations in solution were determined by absorbance at 280nm using an extinction molar coefficient of 28500 $M^{-1}.cm^{-1}$ (Masaki *et al.*, 2000; Permyakov *et al.*, 2003)

Buffer Preparation

In all spectroscopy studies protein and other solutions were dissolved in buffers prepared with Milli-Q water (conductivity below 0.2 µS.cm-1). The salts used for buffer preparation, as the respective purity and their provenience are displayed in Table 5.1.

Table 5.1: Salts used for Buffer preparation, Molecular Formula, Purity, and Provenience.

Buffer	Salt	Formula	Purity	Provenience
Tris HCl	TRIZMA® BASE	$NH_2C(CH_2OH)_3$	≥99.9%	Sigma
Phosphate Buffer	Potassium Phosphate Monobasic	KH_2PO_4	≥99.0%	Sigma
	Potassium Phosphate Dibasic ACS Reagent	K_2HPO_4	≥98.0%	Sigma-Aldricht
Sodium Citrate	Sodium Citrate Tribasic Dihydrate	HOC(COONa)(CH2COONa)2 · 2H2O	≥99.0%	Sigma-Aldricht
Sodium Carbonate	Sodium Carbonate Anydrous	Na_2CO_3	≥98.0%	Fluka

pH of the prepared buffer stock solutions was adjusted by addition of hydrochloric acid 2.5 M and sodium hydroxide 2 M and pH values were checked using a standard pHmeter (PHM 210).

Ellman's reagent

DTNB (5,5´-dithiobis-(2-nitrobenzoic acid)) or Ellman's reagent was purchased from Molecular Probes (Invitrogen) as a powder. 1 mM of this powder was dissolved in TRIS HCl 100 mM. The pH was adjusted to 6.56 in order to favor the dissolution. 0.7 mM DTNB stock used in the experiments consisted on the supernatant extracted. The stock concentration was determined by absorbance at 324nm using an extinction molar coefficient for DTNB in TRIS HCl of 16600 $M^{-1}.cm^{-1}$ (Riddles *et al.*, 1983). The stock solution was stored in the fridge at 4 ºC.

Cysteine solutions

L-Cysteine was obtained from Fluka as a lyophilized powder (degree of purity ≥ 98.5%). A 200 mM stock solution was prepared in Tris HCl 10 mM pH 7.56 after weighting in an analytical balance. All solutions used experimentally were diluted from this stock.

5.2.2. Methods

5.2.2.1. Experimental Methods

Time-dependent Fluorescence Emission of eLA

UV-light triggered reaction mechanisms in eLA were probed by monitoring the time-dependent fluorescence intensity of eLA upon constant irradiation with UV-light. A 1.86 µM eLA solution was prepared after dilution in TRIS HCl 25 mM pH 8.55 from a stock solution of the protein. Three milliliters of the prepared solution was illuminated in a quartz macro cuvette (1 cm pathlenght) in diverse irradiation sessions each of them corresponding to different illumination duration (1h, 2h, 3h, 4h, 5h), this way characterizing the extent of the reaction. Continuous illumination at 295 nm was realized using a 75-W Xenon arc lamp coupled to a monochromator from a RTC 2000 PTI spectrometer. Temperature was maintained constant at 25 ºC in the thermostated cuvette by means of a peltier element installed in the spectrofluorimeter, and controlled externally by a thermometer plunged in the solution. The sample was continuously magnetically stirred at 900 rpm to preserve the homogeneity of the solution. The fluorescence intensity of eLA at 340 nm was monitored during the plenitude of the sessions through the detector 1 of the equipment, and the emission at 295 nm, the scattering of the light, was scanned synchronously in the detector 2, turning on the time-based mode of the equipment. Emission was detected through two photomultiplier tubes each coupled to a monochromator. Excitation and emission slits were set at 5 nm.

In the PTI software used to control the experiment, real-time correction was enabled, set at 1.8 V for excitation at 295 nm, in order to correct the oscillations of the lamp in excitation. Two

data sets of emission *versus* time are obtained in this procedure for both channels (detectors), one with the detected values and one with the correction applied. In the results analysis and presentation the corrected values are only used when mentioned.

After each illumination emission and excitation spectra were recorded. The slits were all maintained at 5nm. Excitation in the emission spectra was realized first at 295 nm and secondly at 280 nm. Emission was fixed at 340 nm in the channel 1 and 320 nm in the channel 2 for the excitation spectra.

The same emission and excitation spectra were realized for in the same conditions with the fresh solution (non-illuminated), and with just the buffer (TRIS HCl 25 mM pH 8.55), in order to correct for *Raman Contribution* (see definition in Appendix C).

Detection of free Thiol Groups with DTNB on UV illumination of eLA

Detection and quantification of the free protein thiol groups was carried on with the spectrophotometric assay based on the reaction of thiol groups with DTNB As can be observed in Figure 5.1, when the thiolate ion ($R\text{-}S^-$) or a thiol (R-SH) reacts with the Ellman's reagent ($DTNB^{2-}$ in solution), a mixed disulphide and one equivalent of nitrothiobenzoate ion (TNB^{2-}) are formed. The latter absorbs intensively at 412 nm (ε_{412} = 14150 $M^{-1}.cm^{-1}$), while the mixed disulphide and $DTNB^{2-}$ show the same weak absorption signal at this wavelength. Hence, the net change in molar absorptivity at 412nm felt upon the reaction is equal to the molar absorptivity of the intensely colored by-product TNB^{2-}, which is by its turn proportional to the concentration of the $R\text{-}S^-$ or/and R-SH that reacted (Riener *et al.*, 2002, Neves-Petersen *et al.*, 2002).

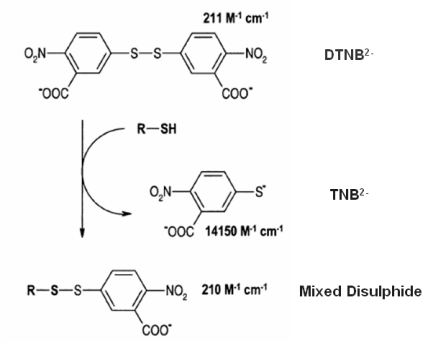

Figure 5.1: Reaction of a thiol with Ellman's reagent, originating a mixed disulphide and one equivalent of TNB^{2-}. The extinction molar coefficients at 412 nm are displayed for the different chemical species and all refer to pH > 7.29 (Adapted from Riener *et al.*, 2002).

In order to realize the quantification procedure on α-LA, after each of the illumination sessions described in the previous section, the irradiated solutions present in the cuvette were extracted. An excess of DTNB (100 µL of a 0.7 mM stock solution of DTNB in Tris HCl) was added to 900 µL of each of the illuminated solutions (immediately after the extraction) and to 900 µL of a non-illuminated eLA. The absorbance at 412 nm was measured with a UV/visible

spectrophotometer (UV1 VWR International – Thermo Electron Corporation), and using always 1 –cm path quartz cuvettes. The absorbance of the solution was checked immediately after mixing of the two components, and on several turns in the following minutes. The sample was kept in the dark between measurements, and agitated manually before each reading. The absorbance value at 412 nm stabilized after approximately 20 minutes of reaction. For quantification was considered the absorbance value read at 22 minutes of reaction. Furthermore, absorbance at 412 nm was checked immediately after manual agitation for two blanks, a protein blank and a reagent blank, in order to correct the assay determined absorbances. The compositions of the assay solution and of the two blanks are described in table 5.2:

Table 5.2: Composition of the solutions used for the Ellman's assays and of the two blanks.

	Absorbance Value	**Volume (µL)**	**Components and Concentration**	**pH**
DETECTION ASSAY:	$A_{412S\ 22min}$	900	eLA 1.86 µM Illuminated and non-illuminated	8.55
		100	DTNB 0.7 mM	6.75
REAGENT BLANK:	A_{412r}	900	Tris HCl 25 mM	8.55
		100	DTNB 0.7mM	6.75
PROTEIN BLANK:	A_{412p}	900	eLA 1.86 µM non-illuminated	8.55
		100	Tris HCl 100 mM	6.75

Since the detection assay on the non-illuminated protein was not realized in the same time scale than the illumination of the eLA 1.86 µM samples, the blanks were repeated for this one. The final values of absorbance (A_{412}) are proportional to the number of free thiol groups present in the protein that react with DTNB and were determined using the following expression:

$$A_{412} = A_{412S\ 22\,min} - A_{412R} - A_{412S} \quad (5.1)$$

To evaluate the sensibility of the assay, the same procedure was realized for diluted L-cysteine solutions of known concentration. L-Cysteine presents a single thiol group that reacts easily with the Ellman's reagent and for that reason is often used as a thiol standard (Riener *et al.*, 2002). 900 µL of each solution and of buffer used for dilution (Tris HCl 10 mM pH 7.56) were mixed each turn with 100 mM. Once more the absorbance at 412nm was checked immediately after mixing. For the cysteine solutions the protocol was the same than before, with the stabilized value after 22 minutes of reaction registered. The absorbance values obtained in this fashion are plotted in function of cysteine concentration in the calibration curve obtained (Figure 5.2) A reasonable linear correlation is noticed between the two variables, which reinforces the reliability of the assay used.

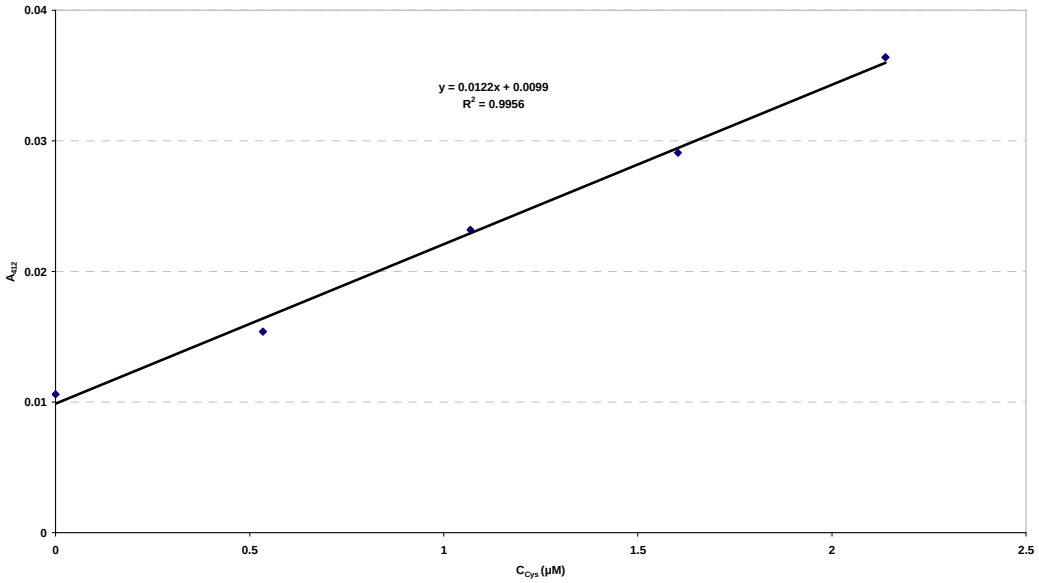

Figure 5.2: Absorbance values at 412 nm *versus* cysteine concentration in the assay. The absorbance values correspond all to a reaction time of 22minutes except for the 0µM solution.

Time-dependent Fluorescence Emission of eLA at different temperatures

The effect of temperature in eLA UV-sensitivity was investigated using the same approach as the previously described study of extent of reaction mechanisms over the irradiation time. The time-dependent fluorescence intensity of eLA was once more monitored using the same steady-state setup in the RTC 2000 PTI spectrometer with constant irradiation with UV-light. However, in this case the solution in the cuvette was maintained at different temperatures in the diverse sessions, and illumination was always carried out over the same duration. The experimental set-up used for the constant UV-light irradiation was identical and the procedures realized prior and after the sessions were exactly the same. Thus, here will only be described the conditions used on all illumination sessions, summarized in Table 5.3.

Table 5.3: Conditions and settings used in the temperature-dependent illumination sessions of eLA samples.

Protein sample	eLA 1.85µM in Tris HCl 25mM pH 8.55
Volume (mL)	3
Stirring (rpm)	900
Irradiation duration (h)	3.5
Excitation wavelength (nm)	295
Wavelength set in Detector 1 (nm)	340
Wavelength set in Detector 2 (nm)	295
Real-time Correction - Excitation at 295 nm	1V

Temperature was maintained constant throughout the each session at the value of interest, and the sessions were realized respectively at 9.3, 12.9, 15.6, 20.4, 24.9, 29.9 and 34.6ºC. Emission spectra were also recorded in the end of each session, upon excitation at 295 nm and 280 nm, as well as excitation spectra fixing the emission in detector 1 at 340 nm and in detector 2 at 320 nm. Temperature was still maintained constant in these recordings. Moreover, these measurements were performed in fresh samples of the protein, at each of the temperatures above mentioned, considering the same delay time to reach each temperature, and with just the buffer (TRIS HCl 25 mM pH 8.55), in order to correct for *Raman Contribution*.

In all experiments and procedures excitation and emission slits were set at 5 nm.

The detection of free thiol groups was also realized in the end of each irradiation session, except for the irradiation session realized at 9.3 ºC. The protocol used was exactly the same than for quantification procedure of different irradiation times, with the Ellman's assay. The difference here resided on the samples used for detection, all collected from the irradiation procedures of 3.5 h described in this session. The absorbance value considered was the one at 20 minutes of reaction, since the value at 412 nm stabilized earlier. Protein and Reagent blanks were also realized for each trial.

Time-dependent Fluorescence Emission of eLA at different pH values

The study of pH influence in the UV-sensitivity of eLA was in all similar to the one realized in the previous section. All conditions and experimental set-ups of illumination were equal except the temperature, which was maintained constant at 25 ºC in all sessions, the illuminated sample, which presented different pH values from session to session, and the voltage selected for Real-time correction, which was 1.81 V for the selected excitation at 295 nm.

Table 5.4: Buffers used for the protein solutions used in the illumination sessions and correspondent pH values.

pH	Buffer
4.56	Sodium Citrate 0.01 M
5.7	Phosphate Buffer 0.1 M
6.48	Phosphate Buffer 0.1 M
7.56	Tris HCl 10 mM
8.55	Tris HCl 25 mM
9.48	Sodium Carbonate 0.05 M
10.49	Sodium Carbonate 0.05 M

eLA concentration in the cuvette was always 1.85 μM, but the buffer used for the previous dilution was different, each of them specific for the pH value pretended (Table 5.4).

eLA UV-light irradiation coupled to CD measurements

The far UV-region of a circular dichroism (CD) spectrum assures a qualitative evaluation on the average secondary structure content of proteins (Neves-Petersen *et al.*, 2002). In particular, proteins containing a high content in α-helix, such as LAs, present a strong double minimum in far-UV CD spectra, at 222 nm and 210-208 nm. The intensity of these peaks reflects the amount of helicity in these proteins (Fasman *et al.*, 1996). Hence, CD spectroscopy was used to scan the relative changes induced by UV illumination in the conformation of eLA.

Table 5.5: Selected settings in the RTC 2000 PTI spectrometer for eLA steady-state illumination.

Temperature (ºC)	25.2
Stirring (rpm)	900
Excitation wavelength (nm)	295
Wavelength set in Detector 1 (nm)	340
Wavelength set in Detector 2 (nm)	295
Excitation slit (nm)	5
Emission slits (nm)	3
Real-time Correction - Excitation at 295nm	1 V

For that purpose a eLA sample was irradiated with 295 nm light using the same spectrofluorimeter and a similar experimental set-up than the referred in the previous sections. In order to obtain a clear far-UV CD spectra, a higher concentration of eLA was illuminated, 11.5 μM, and a 10 mM concentration was selected for the buffer (Tris HCl pH 8.55). The settings used for the illumination procedure are resumed in Table 5.5.

Before illumination, 3.5 mL of the eLA sample were introduced in the cuvette. The sample was illuminated during 10000 s but each 2000 s the experiment was stopped to remove a 300 μL sample for the further analysis. The stability of each removed sample (2000 s, 4000 s, 6000 s, 8000 s, and 10000 s) was immediately evaluated after extraction by far-UV CD spectroscopy. Non-illuminated eLA and the buffer were also probed by far-UV CD with the respective purposes of comparison and correction of the spectra.

The experimental parameters selected for acquiring the standard CD spectra are listed in Table 5.6. The 300 μL samples were placed in a quartz macrocuvette, with a pathlenght of 0.1 cm to check the amount of secondary structural feature of eLA in function of the illumination time. The CD wavelength scans were realized at room temperature in a JASCO J-715 spectropolarimeter and the measurements were controlled by the JASCO hardware manager.

Table 5.6: Experimental parameters for the standard CD spectra of a wavelength scan at 25ºC.

Parameters	
Mode	CD/HT
Range	240-200 nm
Band width (nm)	0.5
Resolution	1.0
Accumulation	3
Speed (nm/min)	5
Sensitivity (mdeg)	100
Response (s)	1
Buffer	10mM Tris HCl (pH 8.55)
Sample	eLA 11.5 µM
Test	0-, 2000-, 4000-, 6000-, 8000-, 10000-s illumination

Experimental set-up used for acquiring the fluorescence emission spectra at different temperatures

For obtaining a thermal unfolding profile of the protein form used approach consisted on recording the intrinsic fluorescence emission of the protein in a wide range of temperatures. For that aim, emission spectra of fresh samples of protein at different temperatures were recorded using the previously described RTC 2000 PTI spectrometer.

Two sets of spectra were measured, in one the excitation was fixed at 280 nm and in the other at 295nm. In the first set of experiments eLA concentration in the samples was 16.63 µM, while in the second 17.54 µM. In both protein in the samples was solubilized in 25 mM Tris HCl at pH 8.55.

The sample volume in the 1-cm path cuvette was 3mL and the stirring was maintained in the scans constantly at 650 nm. The excitation slits were selected at 5 nm, while the emission slits at 1 nm. Spectra were recorded with an integration time of 0.1 seconds. The pretended solution temperature was reached through the peltier element and the same hold time (at the temperature pretended) was selected in the PTI software. Since the scans were realized progressively (from the lowest to the highest temperature), after the introduction of a new fresh sample, the temperature pretended was reached rapidly and in a similar time gap in all cases. Temperature was maintained during the scans. Spectra with excitation fixed at 280 nm were recorded at 10.2, 18.2, 26.1, 33.6, 40.9, 49.4, 56.3, 63.9, 71.1, and 77.4 ºC. Spectra with excitation fixed at 295 nm were measured at 10.0, 18.2, 26.0, 33.6, 41.0, 49.0, 56.5, 64.0, 71.6, and 78.7 ºC.

The spectra with the excitation fixed at 295 nm were also realized with the buffer, in order to correct for *Raman Contribution*. No temperature effect was noticed in the *Raman Contribution* and for that reason only the spectra registered at 26.0 ºC was used for correction. The equivalent spectra were not recorded for the excitation fixed at 280 nm since the Raman signal does not affect in this case the maximum of emission.

5.2.2.2. Data Treatment and Analysis

Raman Correction

In certain emission and excitation spectra it was necessary to correct the values for *Raman Contribution* (*vide* Definition in Appendix C). The corrected emission values consisted simply on the subtraction between the original ones and the values obtained for the buffer, which at the wavelengths in play only absorbed and emitted light derived from the vibration of water molecules.

Smoothing Procedures

Some spectra obtained throughout the results displayed a considerable noise that was not convenient for visualization and for calculation procedures. Thus, in certain cases, which are outlined along the results presentation, a smoothing treatment of the data points was required. All smoothing procedures were performed by adjacent averaging in the program *Origin 7.5*. The emission and the far-UV CD spectra were smoothed using a 5 points average, while for the excitation spectra a 2 points average was chosen. Smoothing operations were realized prior to normalization procedures, if both were carried out.

Data Normalization

The normalized emission values of emission spectra, excitation spectra, and time-based fluorescence measurements consisted on the ratio between each data point (emission value) and the maximum value of emission registered in the whole spectra or over the entire illumination session.

Fittings and Plots

Non-linear fitting operations were realized using the program *Origin 7.5*. Linear fittings and plotting of the data were performed in *Excel*.

5.3. RESULTS ANALYSIS AND PRESENTATION

5.3.1. Time-dependent Disruption of Disulphide Bridges

5.3.1.1. Verification and Quantification

The first step of the characterization procedure consisted on verifying and quantifying the disruption of SS bonds upon UV irradiation on eLA. The stability issues of the protein will not be presented in this section; they will be addressed later on. It is just important to state that the experiments were realized at 25 ºC, and in 25mM of Tris HCl at pH 8.55, conditions for which eLA should be still stable. To probe the breakage of disulphide bonds over time, the intrinsic Trp fluorescence was scanned in solution, under constant illumination of UV light. Changes in the fluorescence intensity can provide clues regarding the UV induced mechanisms, since upon irradiation, the excited Trp species can be driven in a multitude of pathways, and consequently the fluorescence emission is indirectly affected. Particularly, it is known that in LA SS bonds quench substantially the excited state of Trp residues in LA. Upon breakage, the resultant thiols no longer act as quenching agents. Therefore, an increase in Trp fluorescence intensity may occur, if the broken SS bond was previously quenching a Trp residue.

Time-dependent fluorescence profile upon UV light exposure

The time-dependent fluorescence intensity of eLA at 340 nm upon illumination using 295 nm light is presented in Figure 5.3. During the first 6000 seconds (~1.7 hours) an accentuated increase in fluorescence (~17%) is observed, followed by stabilization in a short plateau region (from 2h to 3h of illumination) where the fluorescence intensity remains stable, and a posterior decrease in the counts.

This increase in fluorescence intensity is in agreement with a light-induced transformation of eLA. It could be due do light-induced separation between quenching groups and Trp residues or photoinduced chemical changes in the same groups (*e.g.* cleavage of SS bonds). The Trp residues, selectively excited, would no longer be as initially quenched, and could fluoresce more. As the sample is irradiated, the larger would be the number of protein molecules photo-transformed (with the quenching groups damaged), since they are spread in the agitated medium. At a certain point few would be the non-transformed protein molecules in solution, as the fluorescence intensity remains constant in the plateau, until other mechanisms overrule, which lead probably to the photobleaching (photodegradation) of Trp residues and decay in Trp fluorescence.

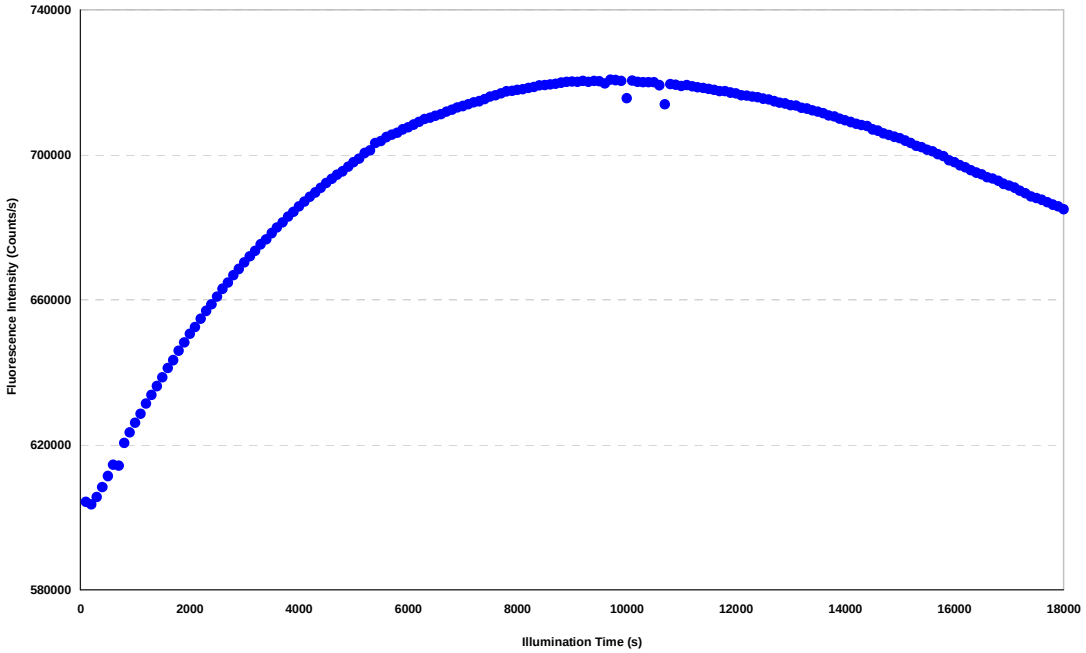

Figure 5.3: Fluorescence intensity of eLA *versus* illumination time. Excitation was fixed at 295 nm and emission was monitored at 340 nm. Temperature was maintained at 25ºC using a peltier element. Measurements were performed using a RTC 2000 PTI spectrofluorimeter as described in Materials and Methods (section 5.2).

The fluorescence profile displayed in Figure 5.3 corresponds to an illumination session of 5 h. In order to characterize the fluorescence behavior of the protein intrinsic fluorophores (Trp, Tyr and Phe) along the illumination procedure, the same experiment was also performed during other illumination periods (1h, 2h, 3h, 4h) (*vide* Materials and Methods, section 5.2). The fluorescence emission profiles obtained at 340nm were very similar to the one shown on Figure 5.3 (*vide* Figure B1, Supplementary Results in Appendix B), confirming the reproducibility of the 5h results.

Excitation (emission set at 340 and 320 nm) and emission spectra (excitation at 295 and 280 nm) were recorded at the end of each illumination session and for a fresh sample of eLA. The spectra were corrected for *Raman contribution* (description in Materials and Methods, section 5.4).

An assembly of the results respecting the first three hours of illumination (where the increase in fluorescence intensity is still observed), is displayed in Figure 5.4, including the emission spectra read after excitation at 295 and the excitation spectra taken with emission fixed at 340 nm. The increase in intensity is confirmed in the in the excitation spectra over the first 2 h of illumination and is correlated with the increase in the fluorescence readings in the emission spectra. In fact, in Figure 5.4, the emission is only probed at 340 nm and it is important to assure that the fluorescence increase is not just dependent on a possible wavelength shift of Trp

emission. Indeed, as can be noticed in Figure 5.4 the emission spectrum becomes strongly red-shifted with the illumination of the protein, presenting a maximum around 322 nm at the start of illumination and migrating until approximately 338 nm in the plateau region (~3h). Oppositely the excitation spectrum turns slightly blue shifted with the illumination of the protein.

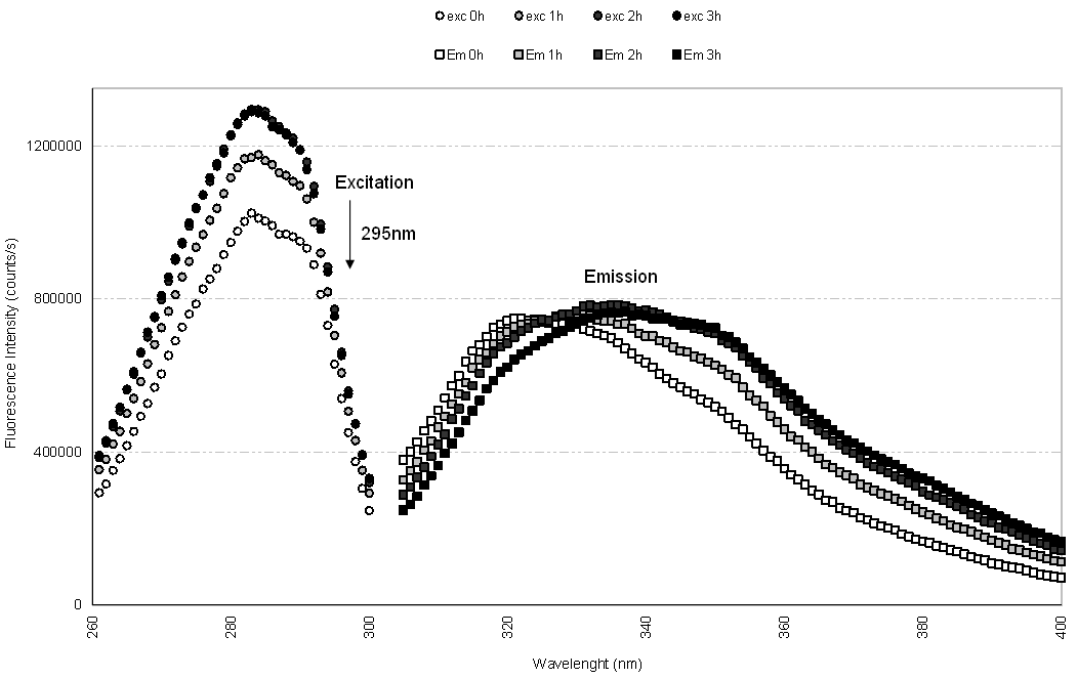

Figure 5.4: Effect of illumination time on the spectrum of excitation and emission. The spectra were recorded fixing the emission at 340 in the excitation spectra and the excitation at 295 in the emission one as described in Materials and Methods (Section 5.2).

The gradual red-shift of Trp fluorescence is clearly observed in Figure 5.5, where are gathered the normalized emission spectra recorded upon 295 nm light excitation for all irradiation sessions broadening the different time periods of illumination. It continues besides the plateau region (irradiation time > 2h), though the wavelength distance between emission maxima of two consecutive spectra turns lower with the extent of illumination. Ultimately the maximum of emission is swept to 340 nm at 5h of illumination. The first important detail that should be outlined is the existence of a red shoulder between 345 nm and 355 nm in the spectrum taken for the fresh sample. The emission of the four eLA Trp residues is overlapped in the emission spectra. This zone may be resultant of the fluorescence contribute of a Trp residue which sensitive to polarity due to solvent exposure, and thus emitting at higher wavelengths. From the structural analysis performed previously the most likely candidate would be Trp 118, which presents the higher ASA values for the crystallized proteins (*vide* section 4.2.2), and is located in a separate zone of the protein (aromatic cluster I). The remaining Trp residues dominate the emission, and should be more buried in the non-illuminated eLA, since the emission maximum of the spectrum

is located around 322 nm. Indeed, the other Trp residues of bLA (Trp 26, Trp 108 and Trp 60) are quite shielded from solvent and integrate aromatic cluster II, comprised within the main hydrophobic core of the protein.

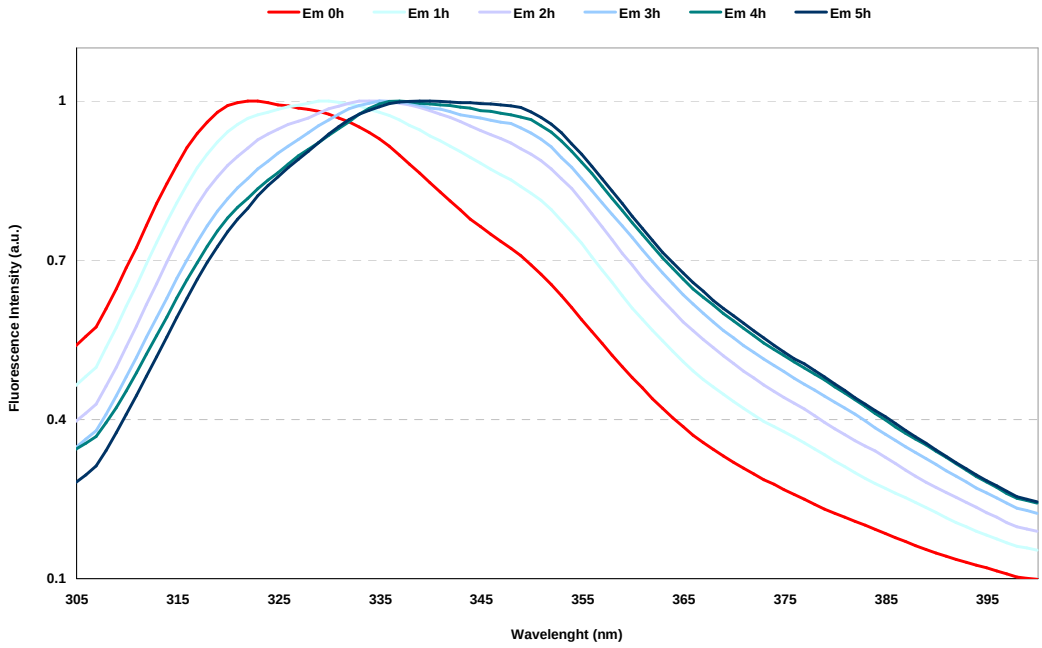

Figure 5.5: Normalized emission spectra of illuminated samples of eLA over different time periods and non-illuminated eLA. Excitation was realized at 295nm. The spectra were first smoothed and normalized as described in Materials and Methods (section 5.2).

The constant irradiation results in an increase of the fluorescence contribution in the shoulder region, while at lower wavelengths a blue shoulder is gradually formed (~315-325 nm). The shifts here described can be derived from the migration of one or more specific Trp residue(s) to more solvent accessible zones of the protein. It could be due to opening of the SS bonds e reconfiguration of the aromatic clusters of the protein, which results at least in the local unfolding of eLA in these zones.

Upon normalization, another interesting feature is also unveiled: the emission spectra took after 2, 3, 4 and 5h of illumination apparently cross each-other at approximately 337 nm. This crosspoint can be eventually an *isosbestic point* (see definition - Appendix C). Though different interpretations can be provided for the existence of *isosbestic points* in sets of electronic spectra, the situation in this case is probably simpler to read. Only one chemical specie should be involved, since the Trp residues are selectively excited. Thus, the *isosbestic* point could indicate the presence of an equilibrium in a photo induced reaction. On the reagent side would be present the Trp species which are characterized by an emission at lower wavelengths, which are slowly inter-converting into red-shifted products species, object of the illumination and possibly SS-bond breakage.

For the correspondent normalized spectra read after excitation at 280 nm (*vide* Figure B2, Supplementary Results – Appendix B), the red-shift is also visible, and takes place over the same distances. Such results indicate that Trp dominates fluorescence emission in the protein. This is expected since near 280 nm the Tyr groups are responsible for only one-fifth of goat LA absorption (Vanhooren *et al.*, 2002), which is similar to bLA in structure. The red shoulder is still visible for the non-illuminated sample, while the *isosbestic* point is not clear anymore.

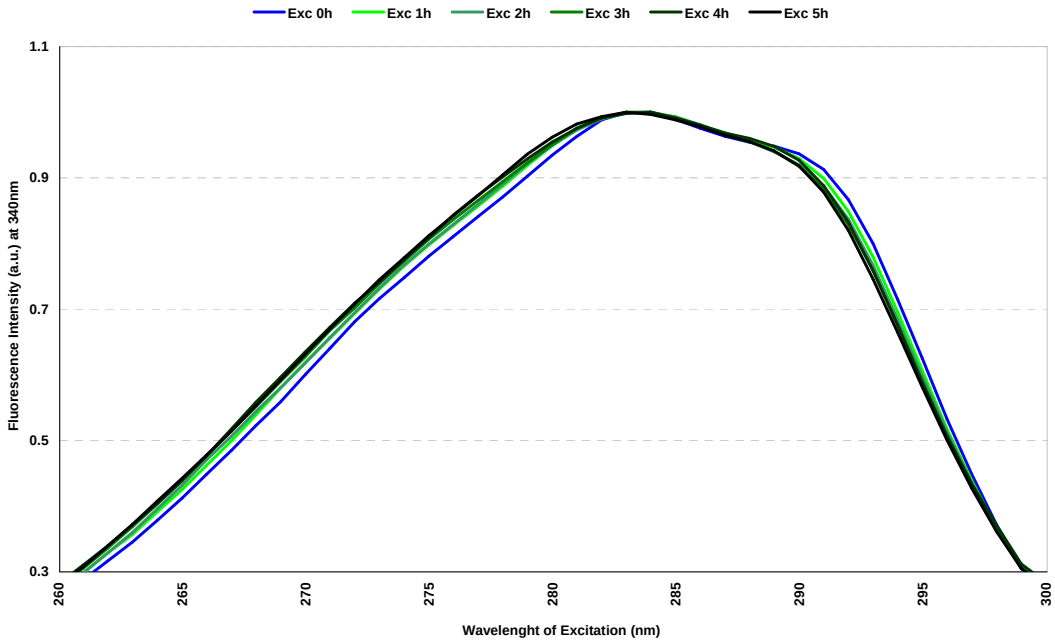

Figure 5.6: Normalized excitation spectra of illuminated samples of eLA over different time periods and non-illuminated eLA. Emission was selected at 340nm. The spectra were first smoothed and normalized as described in Materials and Methods (section 5.2).

The normalization of the excitation spectra provides further insight into the events in play. Both the spectra recorded with emission fixed at 340 nm and 320 nm (Figure 5.6 and Figure 5.7 respectively) show, in similarity to the observed for the emission spectra, that the fluorescence behavior of the intrinsic fluorophores is affected all along the illumination, even in the decay region. This shift signifies that with the illumination of the protein occurs an increase of the proportion of species that are excited at lower wavelengths in detriment of species excited at higher wavelengths.

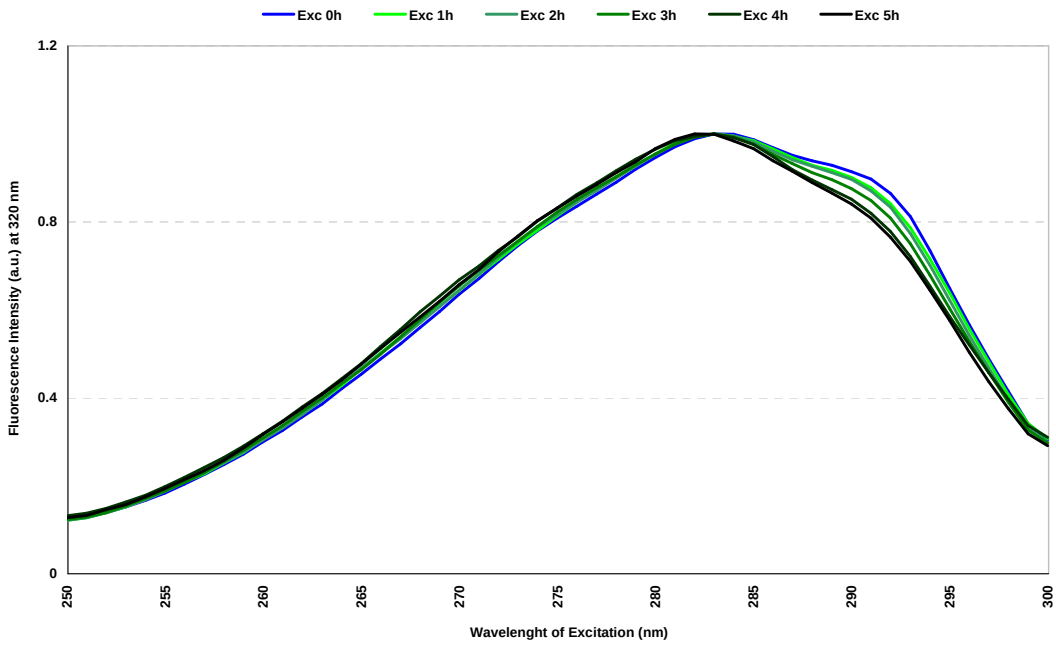

Figure 5.7: Normalized excitation spectra of illuminated samples of eLA over different time periods and non-illuminated eLA. Emission was selected at 320 nm. The spectra were first smoothed and normalized as described in Materials and Methods (section 5.2).

For an emission around 320 nm, this result is expected, since Trp species, as observed previously, tend to emit at higher wavelengths with the long-term irradiation, resulting in a reduced number of Trp emitting in that area and in an increase in proportion of the other protein fluorophores (Phe and Tyr) that are excited at lower wavelengths. This predictable shift is most likely reflected in the normalized excitation spectra on a large shoulder-decrease clearly visible in Figure 5.5 (285-296 nm interval).

The ratios between the normalized excitation spectra of the illuminated samples and the spectrum of the fresh sample provide an enhanced resolution on the spectral changes (Figures 5.8 and 5.9). In both plots (with emission fixed at 340 nm and 320 nm) can be observed a gradual ratio decrease in the zone where Trp selectively absorbs (290-306 nm), coupled to an increase in ratio below 283 nm that turns more intense at lower wavelengths. In the plot correspondent to the excitation spectra with emission fixed at 320 nm, there is a larger decrease of the ratio in magnitude and the specific spectral change spreads in a wider area (282-300 nm). This is mainly due to the overlapping effect of the shoulder-decrease before mentioned.

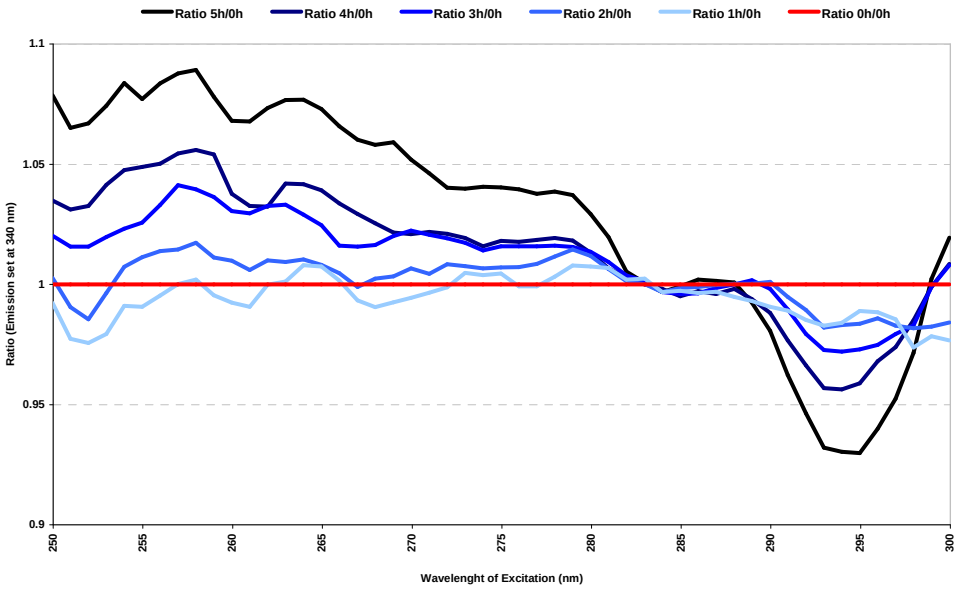

Figure 5.8: Ratio between the normalized spectra with the emission fixed at 340 nm displayed in Figure 5.6. The ratio is realized between the spectra took after different periods of illumination and the spectrum of the fresh eLA.

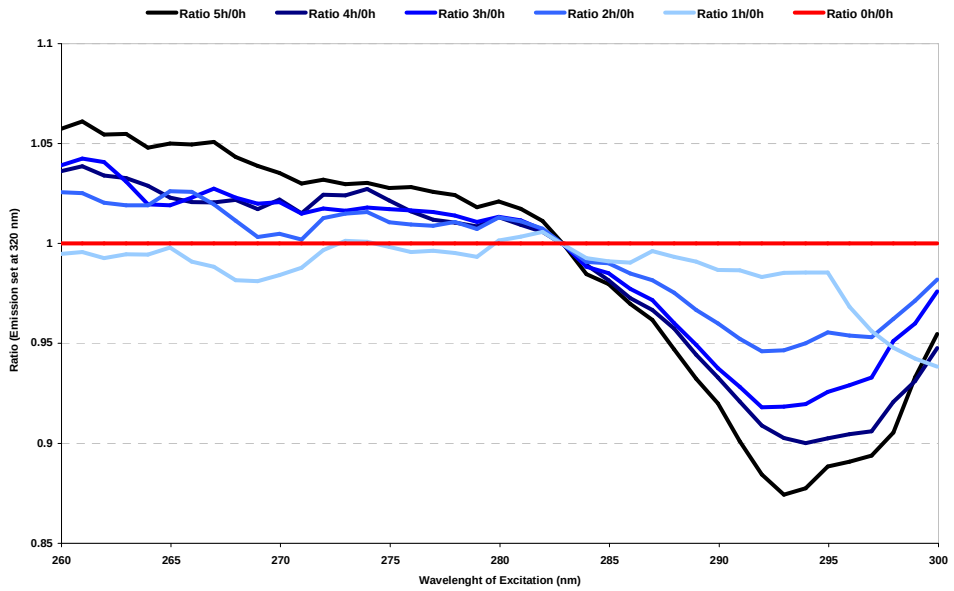

Figure 5.9: Ratio between the normalized spectra with the emission fixed at 320nm displayed in Figure 5.7. The ratio is realized between the spectra took after different periods of illumination and the spectrum of the fresh eLA.

This effect, whose causes were already advanced, may not be the only influence felt when fixing the emission 320 nm. The same event that affects the other excitation spectra

(emission fixed at 340 nm) could also be influencing the ratios at this wavelength. This general event that is characterized by a gradual decrease of ratio at 283-305 nm and increase at 290-305 nm could be due to the photobleaching of Trp residues. Upon illumination the proportion of Trp in the excited population would diminish, provoking the increase in proportion of other protein fluorophores (Tyr, Phe) in the population.

Quantification of the SS bond light-induced breakage with DTNB

In order to verify and quantify the possible disruption of the disulfide bridges under the UV illumination, a reaction assay was performed with DTNB after each illumination session previously mentioned (1h, 2h, 3h, 4h and 5h) and for a sample of non-illuminated eLA (*vide* Materials and Methods, section 5.2). In Figure 5.10 are displayed the absorbance values at 412 nm (A_{412}) obtained for each irradiation time and the time-dependent fluorescence emission increase at 340 nm obtained for the session of 5-h illumination.

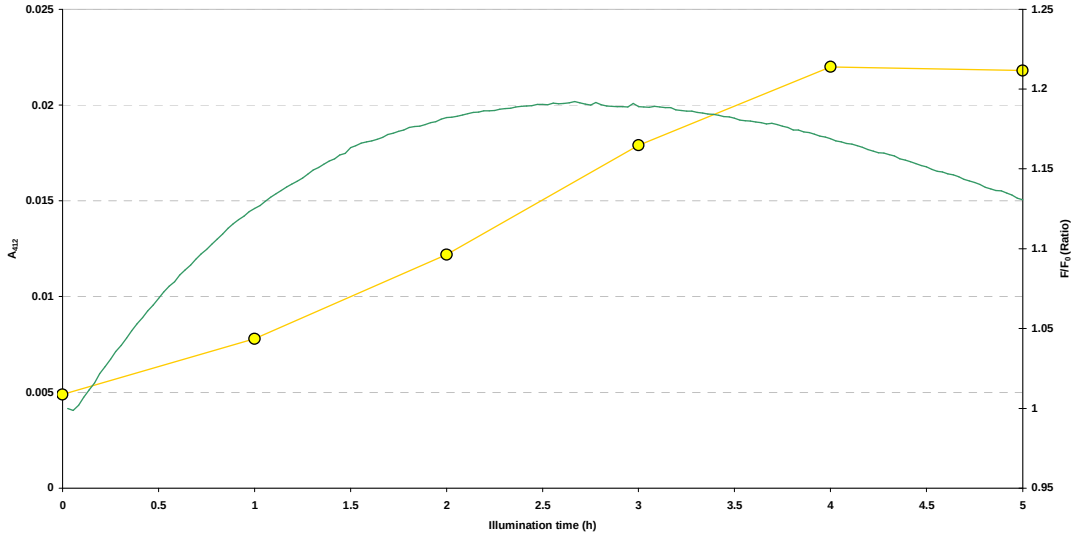

Figure 5.10: Values of Absorbance read at 412 nm (closed yellow circles A_{412}) *versus* illumination time. In green is displayed time-dependent fluorescence intensity increase at 340nm (F/F_0). The presence of free thiols was evaluated after reaction with 5,5´-dithiobis-(2-nitrobenzoic acid), after 0-, 1-, 2-, 3-, 4- and 5-h of illumination with 295 nm light, considering that the free thiol concentration is proportional to the absorbance value at 412 nm, as described in Materials and Methods (Section 5.2). F/F0 values displayed consist on the ratio between the monitored values fluorescence emission at 340 nm and the initial fluorescence emission value at 340 nm obtained for the 5-h illumination session. The values were corrected for lamp intensity oscillations as described in Materials and Methods (Section 5.2).

It can be noticed that A_{412} increases rapidly with Trp excitation in the first three hours of illumination, corresponding to the same zone where is noticed an exponential increase in fluorescence intensity. In the decay zone a raise of A_{412} is still noticed (between the assays realized for 3 and 4h of illumination) culminating in a lower value obtained at 5 h of illumination. Since the free thiol concentration is proportional to the value read at 412 nm (*vide* Materials and

Methods section 5.4), these results indicate that the continuous illumination with 295 nm induces an increase in thiol concentration. Therefore, it is confirmed in eLA the excitation of Trp residues provokes the cleavage of SS bonds. However, from these results no direct correlation can be realized between the increase of fluorescence intensity and breakage of SS bonds. Probably the absence of the SS bonds and other sterical configurations provoked by the breakage provoke a direct of indirect increase in fluorescence.

One of the absorbance values obtained was not expected. The value for 0 h of illumination presented a residual value, even after deduction of the blanks (*vide* Materials and Methods section 5.2). This result is doubtful since the protein even in the apo-form should not display any free thiol groups, since the four SS bridges should not easily be broken or reduced without the presence of an external agent. One plausible reason resides on the fact that the experiments with illuminated samples and the non-illuminated one were not realized in the same time frame. The blank assays were realized separately also, which could raise differences in the detection capacity of the instrument, and in the solution of DTNB stored in the cold. Indeed when compared the corrected spectra (reagent blank subtracted) of the irradiated samples and the fresh one (*vide* Figure B3 Supplementary Results – Appendix B), the characteristic peak of the absorbing 412 nm TNB^{2-} is only noticeable for the first ones. Nonetheless, ideally, the whole experiment should be repeated, which at the time was not possible.

Static light scattering

Since the irradiation of eLA leads to the presence of free thiol groups it was important to verify during the illumination procedure that there was no association or aggregation of protein molecules by means of inter SS bond formation. This was realized by simple measurement of the intensity of the light scattered in the illuminated samples. Upon illumination with light the dipoles set in oscillation emit also a secondary radiation with the same wavelength of incoming radiation, called Rayleigh scattering, or elastic scattering. For particles much smaller that the wavelength of light (radius $R < \lambda / 20$), which is the case of small globular proteins such as eLA , the intensity of the scattered light is only dependent on the size of the particles and not on the structure or their concentration. Therefore, if protein monomers associate, there should be a large increase in the emission signal at the wavelength of excitation.

In this line of thought the 295 nm emission of the samples irradiated with 295 nm light was constantly monitored in each of the previously mentioned illumination sessions (1h, 2h, 3h, 4h and 5h). The time-course of the normalized scattered light during each illumination is displayed in Figure 5.11. In the illumination sessions of 2h, 3h, 4h and 5h a decrease in intensity is noticed in the majority of the illumination session, despite that in the profiles of the 3h and 4h session there is a small initial increase in fluorescence. In the session of 1h illumination there is an increase in emission, though the slope turns less steep in the last minutes. Curiously, these

sessions in which an increase in 295 nm emission is found, present all a small initial decrease in the 340 nm fluorescence, for unknown reasons. Possibly, if the session of 1h illumination was proceeded, the decrease in light scattering intensity would be verified further in time. Despite these small incongruences, these results indicate that, in principle, very little or even no association takes place between proteins upon illumination with 295 nm UV light and for the concentration value here used.

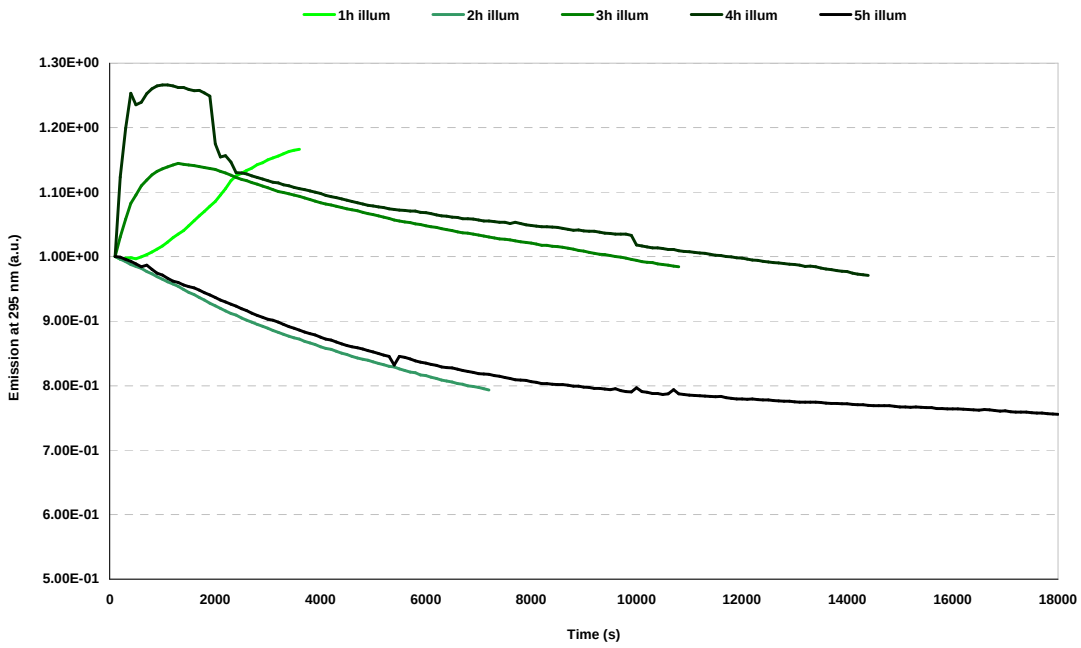

Figure 5.11: Ratio of the emission values at 295 nm during the illumination sessions. The emission of 295 nm light was checked constantly during the sessions of irradiation (1h, 2h, 3h, 4h, 5h) with 295 nm light using the second channel of the spectrofluorimeter. The values are corrected for the light source oscillation and were normalized as described in Materials and Methods (Section 5.2).

Choice of the Concentration

The majority of the illumination sessions realized in the characterization procedure were run using protein solutions with concentrations of about 2 μM. This reference value was chosen in virtue of earlier experiments with the protein. From these trials it was deduced that higher concentrations could imply longer illumination sessions for obtaining the whole fluorescence emission profile (zone of fluorescence increase, plateau, decay) (Data not shown). Since the all the profile is needed for analysis, this time gap could complicate the scaling and planning of the experimental procedures and even jeopardize the integrity of the protein. Using high concentrations of protein can also have natural implications in a good fluorescence reading of the sample, *e.g.* inner filter effect. Higher concentrations could also drive to a closer proximity

between protein molecules. Upon disruption of the SS bonds this proximity can favor the possibility of cross-linking.

5.3.1.2. Influence of external parameters

In sequence to the verification of SS bond disruption upon UV illumination it was interesting to check the effect of external parameters like temperature or pH in the mechanisms involved. Such evaluation could, for instance, help to understand the conditions in which the immobilization process would be more favored.

Temperature Dependence

To study the effect of temperature on the photo-triggered mechanisms in eLA a similar approach than the one realized for the verification procedure was realized. In this case, instead of illumination time, the changed variable from session to session was temperature.

The normalized time-based fluorescence measurements realized with emission fixed at 340 nm upon constant irradiation with 295 nm light are displayed in Figure 5.12. The fluorescence time-dependent profile recorded for the majority of the temperatures follows the same tendency than the presented in Figure 5.3, *i.e.* a strong initial increase in fluorescence intensity, followed by stabilization in a plateau region, and eventually a decay phase (only visible for some temperatures in the 3.5 hours of illumination). The exception to this common fluorescence behavior is the experiment at the most elevated temperature, 34.6 ºC, for which can be noticed a constant decay in fluorescence emission all along the illumination session.

As can be observed in Figure 5.12, in the trial realized at 9.3 ºC data points are lacking in the last 2000 seconds of illumination, resulting in an incomplete profile. This was due to experimental problems. Unfortunately, it revealed difficult to maintain the solution temperature at such low values with the peltier element used, during the whole period of illumination. The profile here displayed corresponds to the experiment for which the peltier element remained longer efficient. Thus, the data points in display correspond to the phase where the temperature was still maintained at 9.3 ºC.

The effect of temperature is at first sight evident. The lower the temperature is, the steeper the slope of initial fluorescence increase, originating fluorescence increases superior to 25 % for the three lowest temperatures. Coupled to this, is the fact that for lower temperatures, the plateau is only reached further in time. Only for the illumination procedures realized at 12.9 and 15.9 ºC, it is hard to trace this general pattern, since they present very similar profiles, which is natural since the temperature margin between these two experiments is the lowest among all.

Assuming that the increase in fluorescence is originated from SS bond breakage as described in the previous section, this influence of temperature in the fluorescence increase

indicates that at least one of the processes or reactions that originate this rupture in this protein is temperature dependent.

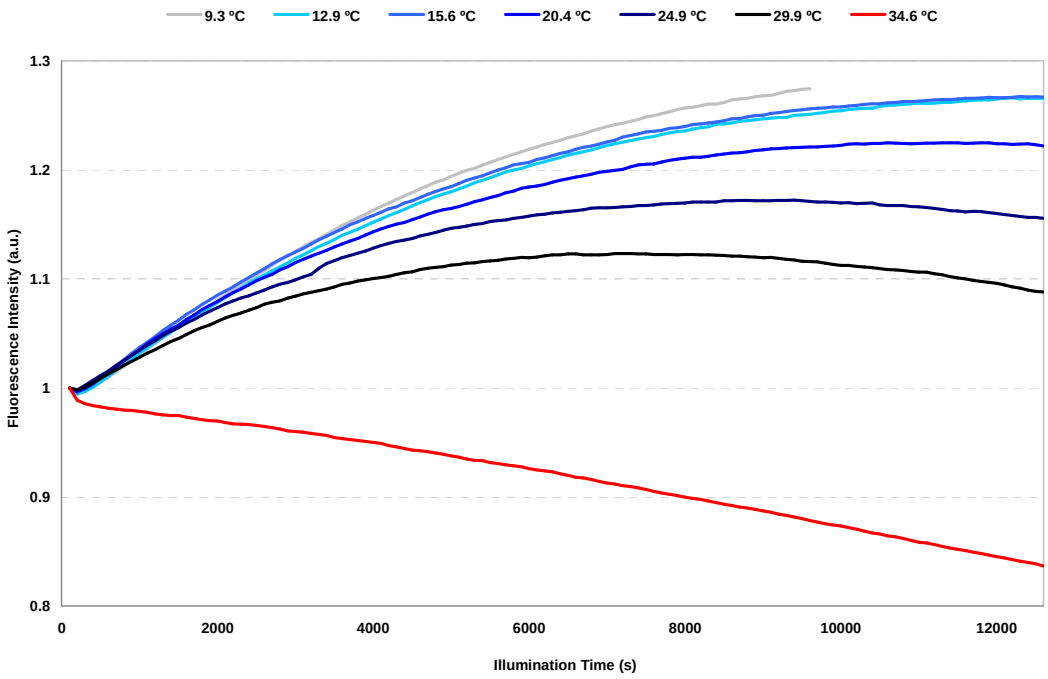

Figure 5.12: Fluorescence intensity of Bα-L in function of the illumination time at different temperatures (9.3, 12.9, 15.6, 20.4, 24.9, 29.9 and 34.6 ºC). Excitation was realized at 295 nm and emission measured at 340 nm. Measurements were effectuated using a PTI spectrofluorimeter during 3.5 hours. The temperature of the solution was maintained constant using a Peltier element. The curves were normalized and corrected for the oscillations of lamp intensity as described in Materials and Methods (Section 5.2).

In order to understand the effect of temperature in the kinetics of a possible reaction, the fluorescence emission time-based curves obtained for the different temperatures (Figure 5.12) were fitted using an exponential function. Since for the curve obtained at 24.9 ºC within this experimental set-up presented a deviation around 3000s, for the fitting was used a different run realized also at 24.9 ºC within the same time period, with a very similar profile.

$$F(t) = C_1 + C_2 e^{-kt} \tag{5.2}$$

The curves were fitted according to Equation 5.2, where $F(t)$ is the fluorescence intensity measured at time t, C_1 and C_2 are constants, and k the rate constant of exponential fluorescence increase. The physical interpretation of this equation is that the irradiation of Trp species (one or more Trp of the protein) induces a first order reaction involving only one protein molecule.

A fitting criterion was adopted, to overcome the divergence in the temperature profiles, and to exclude the initial small decrease in fluorescence (first minutes). The fitting was realized in all assays for the data sets between the first point in time which that majored 80% of the

maximum fluorescence emission and the first that overcome 95% of the maximum fluorescence emission, so only in the emission increase zone. This way the fittings are comparable since they were realized considering data points located in same zone of the profiles for all temperatures. The fittings were also realized for the normalized data points. The fitted parameters, as the correspondent errors, mean square errors (R^2), and reduced Chi square errors, for each of the fitted temperature curves, are displayed in Table 5.8.

Table 5.7: Parameters values and correspondent errors, root mean square errors, and reduced chi square errors obtained after fitting of time-based fluorescence curves using equation 5.2.

T (ºC)	C_1	C_2	k (s^{-1})	R^2	Red. Chi^2
9.3	1.37 ± 0.004	-0.402 ± 0.003	1.64E-04 ± 2.73E-06	0.99986	4.90E-07
12.9	1.33 ± 0.002	-0.356 ± 0.001	1.71E-04 ± 1.44E-06	0.99995	1.41E-07
15.6	1.32 ± 0.002	-0.340 ± 0.001	1.87E-04 ± 1.67E-06	0.99994	1.60E-07
20.4	1.25 ± 0.002	-0.274 ± 0.001	2.26E-04 ± 2.57E-06	0.99992	1.42E-07
24.9	1.20 ± 0.003	-0.221 ± 0.002	2.49E-04 ± 5.64E-06	0.99989	9.28E-08
29.9	1.16 ± 0.008	-0.174 ± 0.007	2.88E-04 ± 2.07E-05	0.99977	6.39E-08

The fitting curves, and the correspondent residual plots, are present in the supplementary results (Appendix B) for further insight.

The fitted values obtained for the constants show that temperature affects the time-dependent fluorescence intensity of the sample in a bivalent fashion. Both constants C_1 and C_2 decrease (in module) with rise of temperature, whereas the rate constant k increases. The values of C_1 and C_2 cannot be used to quantify any phenomenon, since the values used for fitting were normalized, to overcome possible divergences between the diverse experiments. Despite this fact, the important notion that should be extracted is that these two constants counteract the effect of the rate constant upon temperature change, and dominate the shape of the curve. This explains why in the curves of Figure 5.12 the slope of fluorescence intensity is steeper with the decrease of temperature, while the rate constant of exponential increase k decreases.

On the contrary to the other constants, k has a physical meaning, characterizing the one-step reaction. The constant should thus be dependent on temperature in accordance to the Arrhenius law:

$$k = Ae^{-Ea/RT} \tag{5.3}$$

where Ea is the energy of activation ($J.mol^{-1}$), R the universal gas constant for perfect gases (8.135 $J.K^{-1}.mol^{-1}$), and T the temperature in Kelvin. The linear relationship between the logarithm

of the rate constant values displayed in Table 5.8 and the inverse of temperature is confirmed in Figure 5.13, with the correspondent linear fitting and mean square error (R^2).

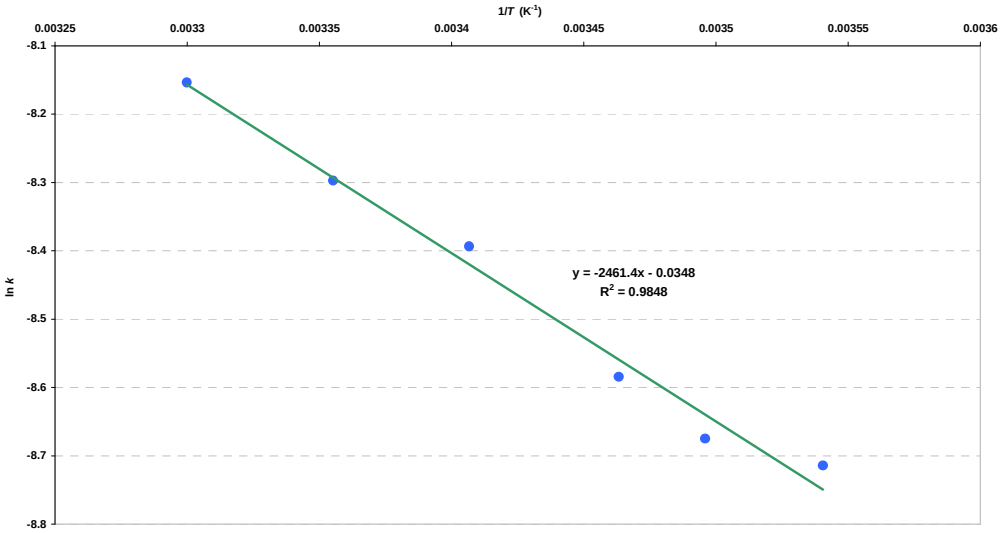

Figure 5.13: Linear relation between the logarithm of the rate constant ln *k* and the inverse of temperature 1/*T*. The linear regression trendline is also displayed in the plot as the equation and the root mean square error R^2.

The energy of activation can be then calculated from the slope of the linear regression (-*Ea*/*R*). The energy of activation obtained characterizes the process affected by temperature, presenting a value of about 20.5 kJ.mol^{-1}.

Following the same approach than the used in the study of illumination time influence, excitation (emission set at 340 and 320nm for each channel) and emission spectrum (excitation at 295 and 280nm) were also recorded after each fluorescence illumination session (run at different temperatures) and for fresh samples of α-L (with the temperature set previously in the spectrofluorimeter). To be noticed that the spectra were corrected for *Raman contribution*. The emission spectra recorded upon excitation at 295nm before and after illumination (3.5 h) are displayed respectively in Figures 5.14 and 5.15.

When comparing both figures it is possible to confirm the raise of Trp emission noticed in fluorescence time-based profiles (Figure 5.12) for the temperatures concerned (15.6 to 29.9 ºC), coupled here again to a red-shift, presenting the same transition spectral traces (upon illumination) than the ones focused at 25 ºC in section 5.2.1.1. For evident reasons it was not possible to record the emission spectrum after illumination at 9.3 ºC. The fluorescence increase screened in emission is again coupled to the increase in the excitation of the protein fluorophores as depicted in the excitation spectra taken (Data not shown).

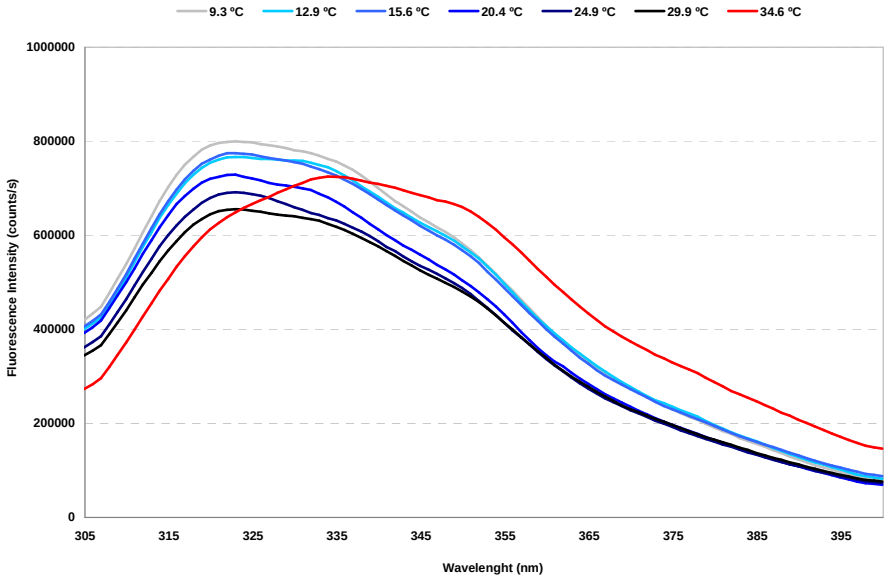

Figure 5.14: Emission spectra of non-illuminated eLA at different temperatures (9.3, 12.9, 15.6, 20.4, 24.9, 29.9 and 34.6ºC). Solution temperature was previously set using the peltier element. Excitation was realized at 295nm. The spectra were first smoothed as described in Materials and Methods (section 5.2).

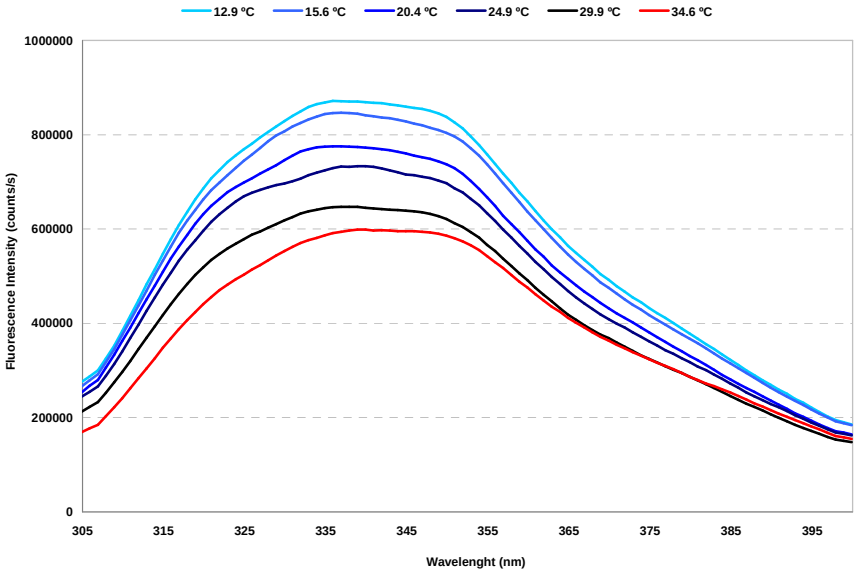

Figure 5.15: Emission spectra of eLA recorded after 3.5h of 295nm light irradiation at different temperatures (12.9, 15.6, 20.4, 24.9, 29.9 and 34.6ºC). Excitation was realized at 295nm and the temperature of the solution was still maintained after the precedent irradiation and during recording of the spectra. The spectra were first smoothed as described in Materials and Methods (section 5.2).

In the fresh solutions, at 34.6 ºC Trp fluorescence is already red-shifted to 334 nm when compared to the lower temperatures, which present all the same emission maximum at approximately 323 nm. This could explain the absence of a fluorescence increase profile, in virtue

of a structural modification of the protein. Nonetheless, illumination at this temperature provokes a red-shift of 4nm in the emission maximum coupled to the decrease in the counts.

The emission spectra recorded at 280 nm (*vide* Figures B16 and B17 Supplementary Results – Appendix B) display the same pattern, indicating roughly that between 29.9 ºC and 34.6 ºC there should be a thermal transition in this form of eLA.

This matter will be further discussed when addressed the thermal stability of the protein.

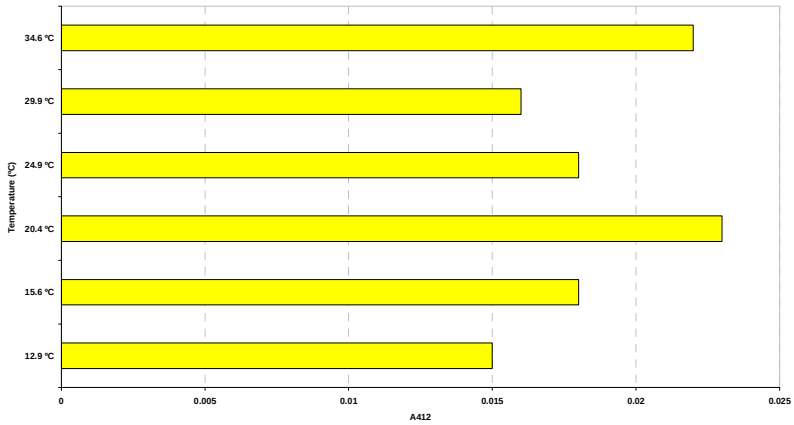

Figure 5.16: Values of absorbance at 412 nm after 20 minutes of reaction between the irradiated samples at different temperatures, and DTNB (*vide* Materials and Methods, section 5.2).

The Ellman's assay with DTNB was also performed immediately after each illumination session to verify the presence of free thiols and the breakage of the SS bonds, in the irradiated solutions. As can be noticed in Figure 5.16 there a relatively strong absorbance signal was noticed after mixing with DTNB for all the samples, with the same magnitude as the values for the plateau region in the verification procedure presented before (section 5.2.1.1), attesting the presence of free thiols, even after irradiation at 34.6 ºC. No explicit correlation with temperature can be outlined, just in the three lowest temperatures there seems to exist an increase in thiol concentration with the temperature increase.

pH Dependence

The influence of pH on UV light-triggered reaction mechanisms was studied considering the same approach than the used in the case of temperature. The time-dependent fluorescence intensity at 340nm upon irradiation with 295 nm UV-light was checked for diverse solutions of eLA, which were prepared from different buffers and presenting different pH values (4.56, 5.7, 6.48, 7.56, 8.55, 9.48, and 10.49). The corresponding time-based fluorescence profiles are displayed in Figure B18 in the Supplementary Results section (*vide* Appendix B).

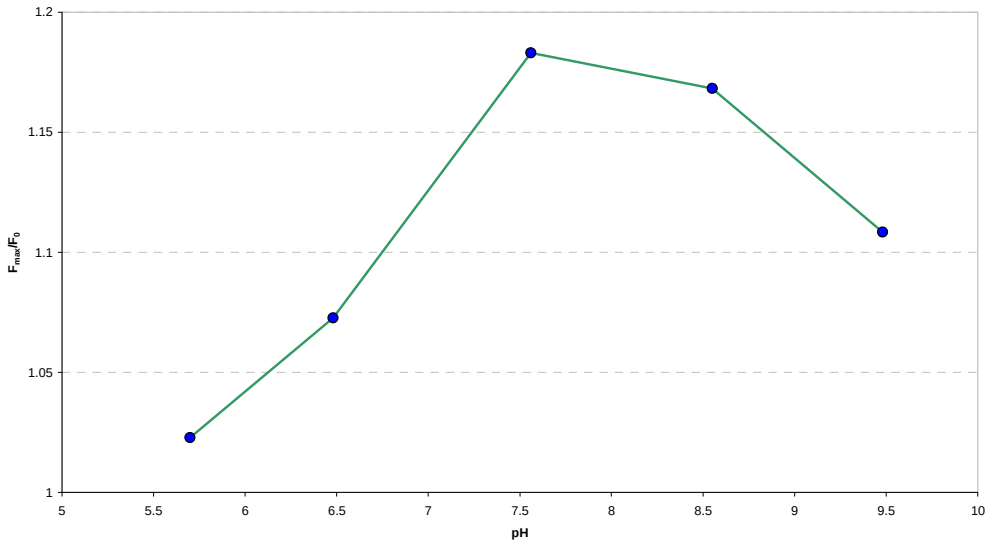

Figure 5.17: Fluorescence emission maximum increase at 340 nm of eLA upon prolonged 295 nm UV-light irradiation for different pH values. The points F_{max}/F_0 consist on the ratio between the maximum emission value of the time-based fluorescence emission profile (at the plateau) and the fluorescence emission at time zero. The fluorescence time-dependent curves from where these values were obtained are present in the Supplementary Results (Appendix B).

No increase in fluorescence emission was noticed for the solutions characterized by extreme pH values (4.56 and 10.49), just a constant decay. For the intermediate pH values, an increase in fluorescence was noticed with the same time-dependent profile than the presented in Figure 5.3. The maximum fluorescence emission increase (emission at the plateau) obtained for each of these pH values at 340 nm is displayed in Figure 5.17. The higher values of increase are noticed for pH values near neutrality: 7.56 and 8.55. This probably indicates that at neutral pH values the quenching of the Trp residues is less prominent. However, it is not possible to affirm, based only on these results, that the photo-degrading mechanism of quenchers or cleavage or SS bonds is favored at these pH values. Since the protein is in the apo-form the conformational structure is strongly affected by the pH of the solution. Moreover the buffers used presented diverse ionic strengths and the implications to protein conformation could be variant and unpredictable from experiment to experiment. Thus, one cannot predict if the relative positions of the quenchers relative to the Trp are affected.

5.3.1.3. Effects of illumination on the secondary structure

Acknowledged that irradiation of eLA with 295 nm UV light induced specific structural changes in this form of eLA, including the breakage of SS bonds, and exposure of Trp residues, it was important to evaluate the implications of such modifications in the general conformation of the protein. For that aim, far-UV circular dichroism (CD) spectroscopy was used to check possible conformational changes in the secondary structure of the protein over different periods of UV-light illumination, complementing the fluorescence studies presented in 5.2.1.1.

As previously described in Materials and Methods, a 11.5 µM eLA sample was irradiated with 295 nm, and the fluorescence intensity was monitored at 340 nm. The experiment was stopped each 2000s to remove a sample for further analysis. The stability of each removed sample (2000s, 4000s, 6000s, 8000s, and 10000s) and of a non-illuminated one was evaluated by far-UV CD spectroscopy. The steady-state fluorescence profile of the entire illumination session is displayed in Figure 5.18.

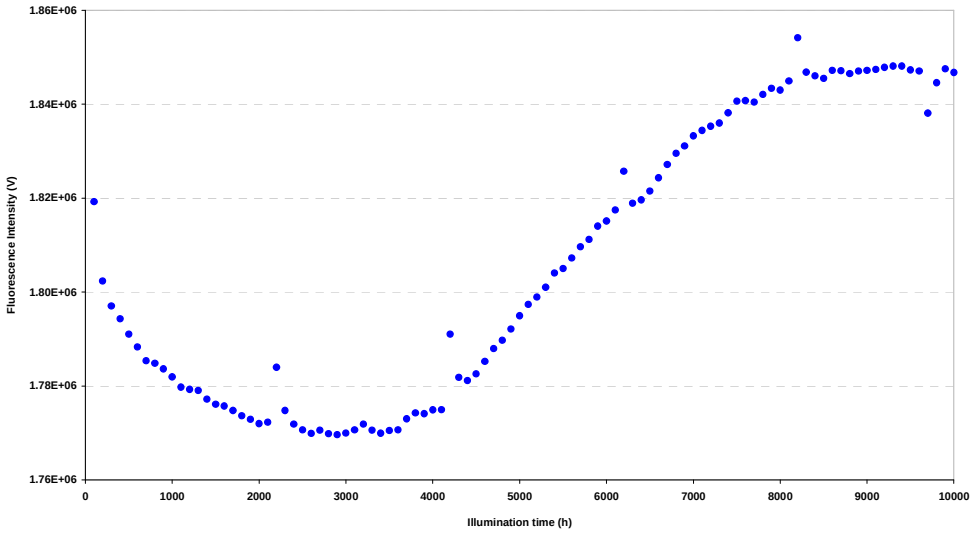

Figure 5.18: Fluorescence intensity of eLA *versus* illumination time. Excitation was fixed at 295 nm and emission was monitored at 340 nm. Temperature was maintained at 25ºC using a peltier element. The experiment was stopped each 2000s to remove a protein sample. The emission values are corrected for the oscillations of lamp intensity. Measurements were performed using a RTC 2000 PTI spectrometer as described in Materials and Methods (section 5.2).

The time-dependent fluorescence emission upon irradiation with 295 nm of the 11.5 µM protein sample is similar to the previously observed in the verification procedure (Figure 5.3) and in the temperature experiments (Figure 5.12), just with the difference in a small decrease in intensity in the early phase of the experiment.

The effects of illumination on the secondary structure can be observed in Figure 5.19, where is displayed an overlay of the recorded far-UV CD spectra. Although some fluctuations are noticed, the overall trend is the partial loss of the secondary structure the longer the sample was illuminated, with progressive slight loss of ellipticity. Although these changes are noticed, irradiated eLA should still present a considerable amount of secondary features, since the spectra of the irradiated spectra still present the minimum at ~210-208 nm.

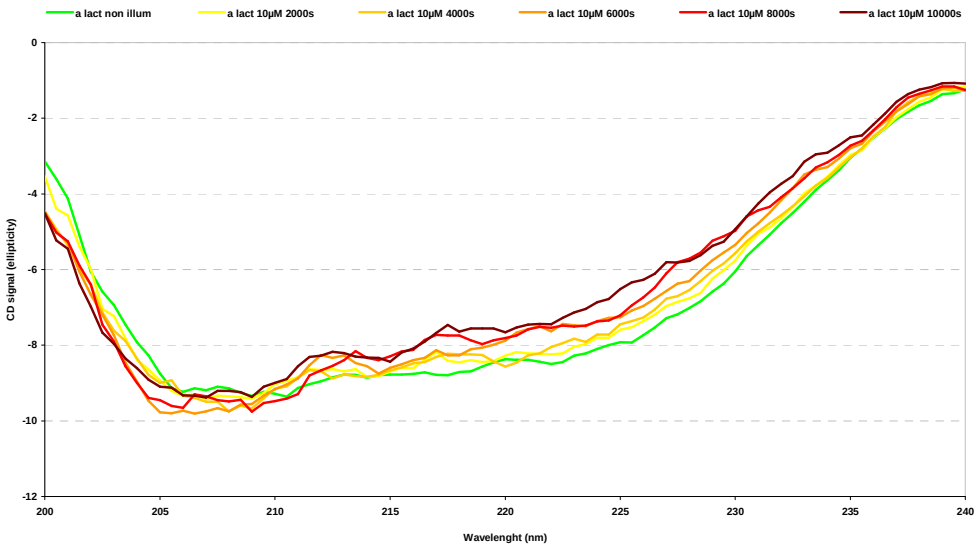

Figure 5.19: Far-UV CD scan of 295 nm light irradiated eLA samples (0-, 2000-, 4000-, 6000-, 8000-, and 10000-s of illumination) recorded at pH 8.55 and room temperature. The measurements were realized in a JASCO J-715 spectropolarimeter. The spectra were corrected for the buffer contribution in ellipticity and smoothed as previously described in Materials and Methods (Section 5.2). Although some fluctuations are noticed, the overall trend is the partial loss of secondary structure the longer the collected sample was illuminated.

It is not possible to correlate the increase of fluorescence with the changes in the secondary structure. The experimental set-up should affect the fluorescence emission, since the volume removed at each stop (clearly visible in the time profile by a raise in fluorescence emission) is considerable (8% of the initial volume), resulting in a final volume of 2 mL compared to an initial of 3.5 mL. The usage of this setup was forced by the experimental conditions needed in a clear far-UV CD scan. Protein concentration of approximately 10 µM is needed for a clear spectra in far-UV CD, along with a buffer concentration of 10 mM (*vide* Material and Methods). In the required conditions the fluorescence profiles were extremely different at each illumination session, probably due to the joint effect of using higher concentrations and lower ionic strength. This last variable specially is probably the destabilizing factor, rendering the protein more sensitive to external changes.

Nonetheless, with the approach used, the effect on the secondary structure is clear, even if the effect over illumination time could not be reasonably quantified.

5.3.2. Thermal Stability of the Protein

As was advanced in the literary review realized over α-LA (Chapter 4), this protein, especially in its apo-form, is very sensitive to external factors, like ionic strength or temperature. Thus, it is required to evaluate the conformation adopted by the protein in the experimental conditions used for characterization. Once again, fluorescence spectroscopy was used to the

thermal stability of the protein form, since temperature was the main destabilizing agent in the experiments, and to explore the conformational features of the protein, in the apo-form obtained.

The thermal stability of the protein was checked by probing the intrinsic fluorescence of fresh solutions of protein stabilized at a wide range of temperatures (10-80ºC). The emission of the protein at a certain temperature was checked by excitation of fresh 17.54 µM eLA solutions at 295 nm and at 280 nm.

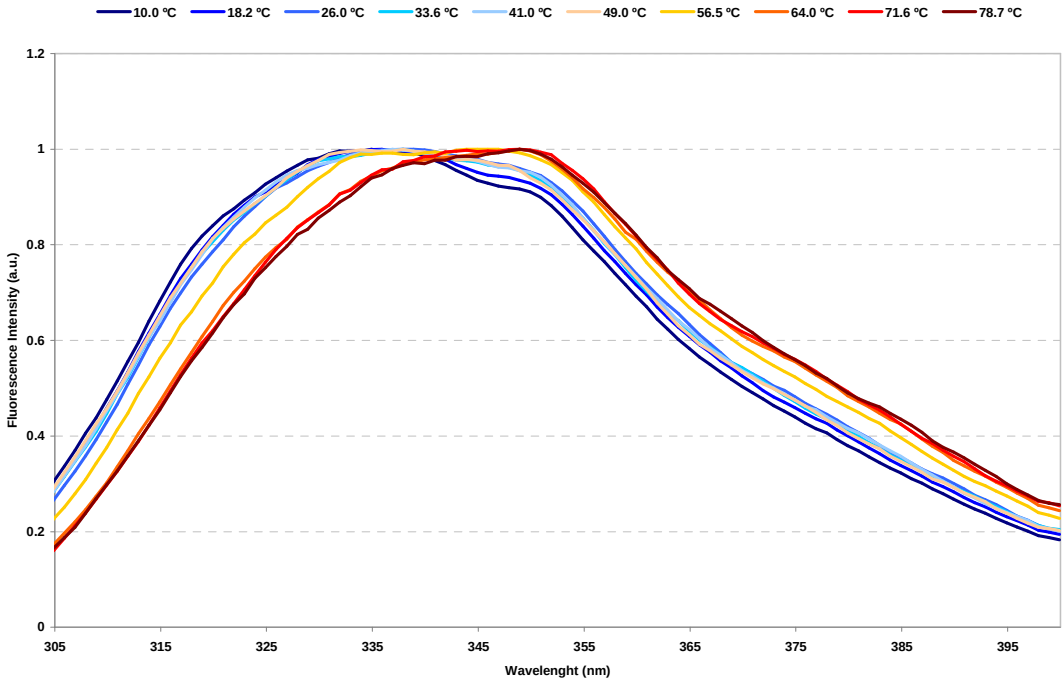

Figure 5.20: Normalized emission spectra of fresh eLA solutions recorded at different temperatures (10.0, 18.2, 26.0, 33.6, 41.0, 49.0, 56.5, 64.0, 71.6, and 78.7 ºC). Excitation was realized at 295nm and the temperature of the solution was set before the recording of the spectra and during the short irradiation. The spectra were smoothed and normalized as described in Materials and Methods (section 5.2).

The solution temperature was set previously, considering the same hold stabilization time for each temperature, and the resulting emission spectra after excitation at 295nm were corrected for *Raman contribution* as described in Materials and Methods (Section 5.2). In Figure 5.20 are displayed the normalized emission spectra correspondent to excitation with 295 nm light for the different temperatures tested. A red-shift is noticeable in Trp fluorescence when the spectrum is taken at higher temperatures. This red-shift is quite similar to the observed when the protein is irradiated with UV-light (section 5.2.1.1), with an increase in the population of exposed Trp in the red-shoulder area, which is severed at temperatures higher than 48.0 ºC. Besides the red-shift is there is a decrease in fluorescence emission with the temperature increase, which can be noticed in the original spectra (non-normalized – *vide* supplementary results, Appendix B). This was already verified in the temperature characterization (section 5.3.1.2). In the spectra recorded

upon excitation at 280 nm, the same red-shift is noticed, as also the increase in fluorescence counts (*vide* supplementary results, Appendix B).

In order to clearly visualize the occurring red-shift, the wavelengths values of emission maxima (λ_{max}) after excitation at 295 and 280 nm are plotted in function of temperature in Figures 5.21 and 5.22.

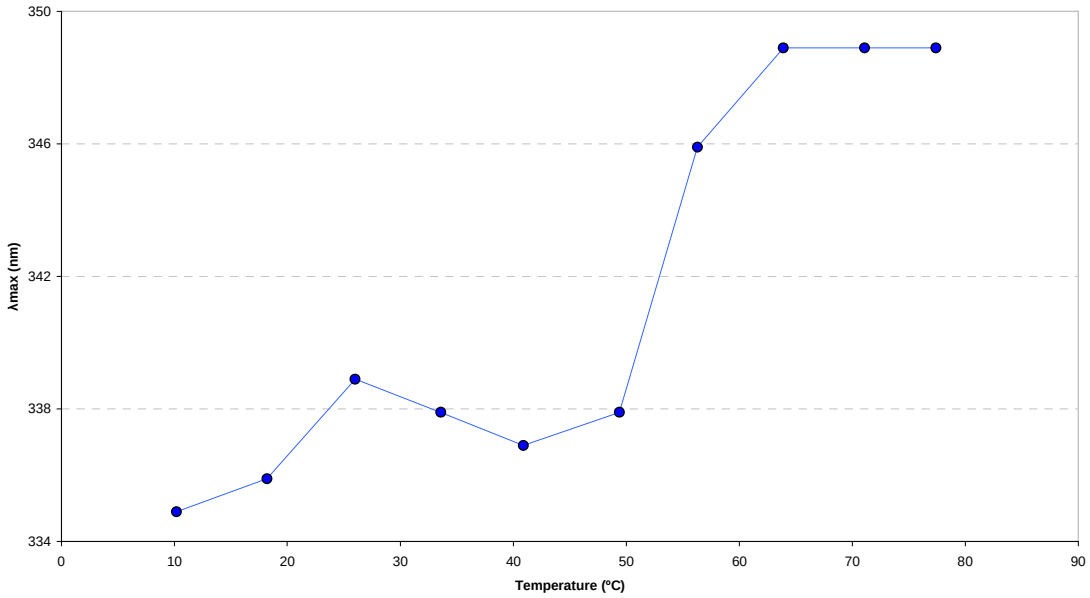

Figure 5.21: Maximum of emission of eLA upon excitation at 295 nm (λ_{max}) *versus* the solution temperature.

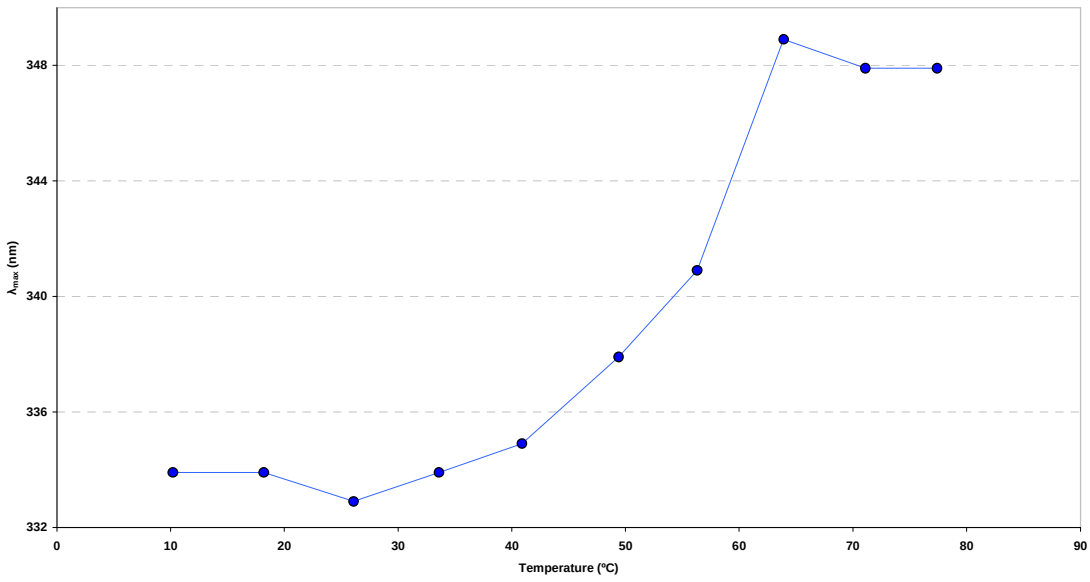

Figure 5.22: Maximum of emission of eLA upon excitation at 295 nm (λ_{max}) *versus* the solution temperature.

The first important fact that should be retained from both figures is that the λ_{max} noticed in these results for low temperatures (<25ºC) are quite higher than the observed in the temperature characterization procedure (Figures 5.14 and B.16 in Appendix - λ_{max} ~322-324 nm for excitation at 295 nm and 280 nm). The main experimental difference between the two sets of experiments is eLA concentration, which here is ten times higher. The Trp residues, sensitive to solvent polarity, are here more exposed, for higher concentrations of eLA.

Both the figures describe in a general form the thermal unfolding of the protein. Upon excitation at 295 nm there are two experimental points that could be outliers and erroneous, the ones corresponding to temperatures of 28.0 and 33.6 ºC. The unfolding at 295 nm (Figure 5.22) characterizes only the Trp residues, and probably only part of them, given the already debated increase of fluorescence intensity in the red shoulder area of the spectrum for high temperatures. If the two experimental points before mentioned are not considered, the profile of the unfolding denotes a transition characterized with by T_m between 50 and 70 ºC. The thermal unfolding is more patent in the points obtained from the excitation procedures realized at 280 nm (Figure 5.21), characterizing the exposure of part of both Trp and Tyr residues of the protein, and shows more clearly the existence of a cooperative thermal transition of the apo-form in these conditions, with a T_m between 40 and 70 ºC.

In the temperature characterization procedure, a strong wavelength red-shift was felt between spectra of lower temperatures, 29.9 and 34.6 ºC, from ~323 nm of λ_{max} to 334 nm (Figures 5.14 and B16) . The strong shift in that case probably induces a conformational transition in eLA since after 3.5 h of illumination, only at 34.6 ºC is not noticed an increase in fluorescence intensity.

This particular thermal transition is not noticeable in these results. The aromatic clusters should be already partly destabilized at this range of temperatures as described before. Since the concentration is higher in these experiments, it could be that the impact of ionic strength in eLA (the concentration of the buffer is the same in both experimental procedures) is more felt in the experiments realized for the temperature characterization procedure. Thus, these eLA samples, which are more concentrated, could be more instable.

5.4. DISCUSSION

Before analyzing specifically the UV sensitivity of the protein model it is important to clarify the conformational features of the apo-forms of LA obtained here in solution. In most part of the characterization procedure eLA concentration was ~2 µM in 25 mM Tris HCl pH 8.55. In non-irradiated samples corresponding to these conditions and at low temperatures Trp emission is typically centered at ~322 nm (*vide* Figures 5.5 and 5.14). In solution and at neutral pH Ca^{2+} loaded bLA shows a fluorescence emission maximum of 325 nm (Engel *et al.*, 2002). The

proximity of both values indicates that most of the Trp residues in the eLA apo-form are buried as in native bLA. Moreover in diverse procedures the behavior of this eLA apo-form upon exposure to UV-light is similar, showing similar spectral traces, and reproducible results.

To study the stability of the eLA in solution, its thermal unfolding was probed by fluorescence spectroscopy (section 5.3.2). However, these experiments were conducted using higher concentrations of eLA (17.44 μM) and spectral changes in Trp emission were noticed for low temperatures (<30ºC). Probably the ionic strength is not high enough to stabilize completely eLA in the absence of calcium for these concentrations. Nonetheless, eLa at 17.54 μM (and in 25mM Tris HCl pH 8.55) presents apparently a cooperative thermal unfolding in the regions where Trp is located. MG forms of eLA, which are typical products of LA unfolding under denaturating conditions, do not present usually a cooperative unfolding (Pfeil *et al.*, 1998), and generally are an equilibrium mixture of substates (Chang *et al.*, 2001), so probably this form of eLA in solution presents still a native-like structure, as the model described for apo-LA in Chapter 4. In the temperature characterization realized for the form of eLA at 2 μM, the Trp emission spectra of non-irradiated samples show a possible conformational transition between 29.9 and 34.6 ºC (Figure 5.14), which was not observed in this thermal denaturation. The fluorescence behavior at 34.6 ºC upon continuous UV-irradiation is markedly different than at lower temperatures, not presenting an increase in fluorescence intensity at 340 nm. It is possible that this transition, not observed in the thermal unfolding, is a first step of eLA unfolding, in which the aromatic clusters are disarranged, particularly relatively to quenching groups, not yielding the same fluorescence spectral changes than at low temperatures.

At low temperatures (<29.9 ºC) for the samples of ~2μM, eLA should be stable in solution, presenting a native-like conformation, and retain the majority of the packing interactions in the aromatic clusters, as it is indicated by he degree of Trp burial. The Trp emission spectra of all non-irradiated of eLA shows an interesting red-shoulder, which is not noticed in previous fluorescence experiments is it with bLA (Engel *et al.*, 2002), or apo and native goat LA (Vanhooren et al., 2002). This shoulder could derived from the fluorescence contribute of the more exposed Trp118, attending that this Trp may be less quenched in this form of LA displaying an increased fluorescence than usual, and that the aromatic cluster I may be more disarranged. Trp118 could be extremely more exposed than expected.

It is patent, though, that the concentration of eLA and buffer influenced tremendously the experiments, which is natural considering the analysis of the protein model realized before (Chapter 4). For instance in CD experiments, which were conducted at the lowest ionic strength (10 mM Tris HCl pH 8.55), no reproducible results for the time-dependence of the fluorescence emission of eLA were obtained. eLA in solution adopts probably in these conditions a more unstable conformation.

Prolonged excitation of Trp residues in eLA induces an increase in fluorescence yield coupled with a red-shift in Trp emission. This fluorescence behavior of this apo-version of bLA (2 µM sample) was observed for temperatures below 29.9 ºC. It correlates well with previous observations realized in Ca^{2+} loaded and depleted human, bovine (Permyakov *et al*., 2003) and goat (Vanhooren et al., 2002; Vanhooren *et al.*, 2006**a**) forms of LA, for which light induced SS bond breakage was noticed.

The increase in fluorescence yield with the illumination time is presumably related to the progressive cleavage of SS bonds mediated by Trp excitation, and with the absence of these groups as potential quenchers. In eLA the time-dependent profile of fluorescence emission at 340 nm shows a relatively strong increase in intensity in the first hours of illumination of (Figure 5.3 and 5.12). The rate at the fluorescence intensity increases seems to diminish in an exponential way. This was confirmed by the fitting procedures realized in the temperature characterization (Section 5.3.2 – Table 5.7). Fluorescence quantum yields stabilize latter in a plateau region, with a final decrease in last minutes of irradiation. Such time-dependent emission profile has been observed previously in other UV sensitive proteins like cutinase (Neves-Petersen et al., 2002) and horseradish peroxidase H2 (Neves-Petersen *et al.*, 2007). In both cases the increase in fluorescence yield was attributed to putative light-induced dissociation and/or photoinduced damage of strong fluorescence quenchers proximal to aromatic residues of the proteins. While in horseradish peroxidase H2, this increase was attributed to damage of the close prosthetic group, in cutinase was proven the direct relationship with disulphide bond cleavage. Cutinase displays only one Trp residue in direct contact with a disulphide bond and for that reason it is easy to relate the two events (*vide* Sections 3.3.3 and 4.4). The increase in thiol groups was found to be correlated to the time-dependency of fluorescence increase. In bLA, the richness in SS bonds, Trp residues and other quenchers requires a more extensive analysis to prove that cleaving of SS bonds is really the cause of this phenomenon, and determine the Trp residue(s) involved. To be noticed that the fluorescence increase noticed on eLA is quite reduced when compared to the observed in cutinase (*vide* Figure 5.3 - a maximum of 19% increase is registered in the plateau *vs* an increase superior to 8 fold in cutinase), and the plateau phase is only reached way further in illumination time.

For eLA, disruption of SS bonds was observed upon prolonged excitation of Trp residues recurring to the Elmann's assay (Figure 5.10), but the experimental data is insufficient to relate directly the cleavage and fluorescence increase. For an apo-form of goat LA (which presents the same four Trp residues and a similar structure to native bLA – *vide* Table 4.1), Vanhooren et al. (2003) noticed that upon constant UV light irradiation the rate at which the free thiol groups were formed apparently decreased in an exponential way. Such rate dependence, noticed at different temperatures and also for Ca^{2+} loaded forms of goat LA, is concordant with the remarks above. This correlation indicates that the relation exist probably, and could be verified upon repetition

and optimization of the Elmann's assays here executed. A larger number of samples irradiated during different periods of 295 nm-light should be tested.

The fluorescence increase felt at 340 nm is also partly provoked by the pronounced red-shift in eLA Trp fluorescence. After 5 h of constant irradiation Trp emission maximum is swept from 322 nm to 340 nm (Figure 5.5), which indicates a progressive local unfolding of eLA under irradiation, as Trp residues are dislocated to solvent accessible areas of eLA. Trp in water has an emission maximum of 348 nm, and the fully denaturated form of native goat LA on 6 M guanidinium hydrochloride has a maximum of emission of 345 nm (Vanhooren et al., 2006**a**). Thus, the hydrophobic clusters of eLA should not be completely unfolded upon irradiation. Curiously, emission around 340 nm is a typical property of molten globule forms of LA, particularly the acidic form at pH 2 (Vanhooren et al., 2002).

It is hard to predict the global conformational changes that the tertiary structure of eLA suffers upon irradiation. As stated previously, breakage of Cys61-Cys77 and Cys73-91 was found in goat and human LA upon Trp prolonged excitation (Vanhooren *et al.*, 2006**a**; Permyakov *et al.*, 2000). As mentioned before Cys73-91 holds together the two subdomains of LA and Cys61-Cys77 is located within the β-subdomain. Upon their breakage the α-subdomain remains structured while the β-subdomain is disarranged, as shows a construct of LA where the cysteines that form this SS bonds are substituted by alanines (Wu *et al.* 1995). In goat LA is also found the light-induced cleavage of Cys6-Cys120 (Vanhooren *et al.*, 2006**a**). The three-disulphide form of LA with a reduced Cys6-Cys120 is similar to intact native LA in secondary and tertiary structure (Moriarty *et al.*, 2000). The far-UV CD spectra of eLA irradiated samples here recorded (Figure 5.19) show a progressive but low loss of secondary features on irradiation with 295 nm light. The helical structures of eLA should be retained even after illumination. Vanhooren *et al.* (2003) noticed similar changes far-UV CD spectra for an apo-version of goat LA. Reversely the far UV spectrum recorded by the same authors revealed profound losses of ellipticity. These remarks indicate that the UV-triggered cleavage of disulphide bridges in LA induces the loosening of the tertiary structure of the protein, mostly in the aromatic clusters (where are located the intrinsic fluorophores), but not in the secondary features, maintaining most of the α-helical content.

Upon continuous Trp excitation in human α-LA, Permyakov *et al.*(2003), found three types of protein components after gel chromatography of the irradiated sample. One was representative of the native protein (emission upon excitation centered at ~328-329 nm), the other with a red-shifted Trp fluorescence (emission maxima at ~339-340 nm), and the last with non-tryptophan fluorescence. In the eLA Trp emission spectra recorded here after distinct durations of irradiation at 25ºC (Figure 5.5), the formation of such red-shifted species is also noticed. Upon illumination, there is a progressive increase of intensity in the red-shoulder region

of the spectrum, dislocating the emission maximum to 340 nm. The blue-shoulder formed gradually with irradiation could advent of the overlapped emission of the remaining native protein portion that did not suffer any conformational changes (*e.g.* splitting of SS bonds). The presence of an *isosbestic point* indicates that a reaction may occur yielding these red-shifted Trp species from lower wavelength emitting Trp species. The red-shifted species display also higher fluorescence quantum yields, this indicating that they should be related to the SS-bond breakage. The validity of this *isosbestic point* could be discussible, since it is originated from the normalization of spectra. However, in several other procedures was proven that hidden *isosbestic points* such as this one may appear after normalization of electronic spectra and have a significative meaning (Panda and Datta, 2008; Pouet *et al.*, 2004). Here, since the two species present divergences in fluorescence quantum yield, it is not possible to notice the *isosbestic point* without normalizing.

The last component described by Permyakov et al. (2000) displaying nontryptophan fluorescence corresponds evidently to the protein fraction that has its Trp residues photochemically degraded by exposure to UV-light. The photochemical destruction of Trp residues is probably the main responsible for the decay of fluorescence intensity felt after 2.5 h of illumination (Figure 5.3). It also explains the increasing the blue shift displayed in the excitation spectra with the extent of illumination (Figures 5.6 and 5.7). The ratio of Trp available to be excited is diminished, which results in a raise in ratio of Tyr and Phe excited, which absorb at lower wavelengths (Figures 5.8 and 5.9). Upon excitation at 313 nm this component in human LA emits with a maximum centered at ~417 nm, resembling the emission of N-formylkynurenine. The absorption spectra of irradiated goat LA present a shoulder at 310-325 nm, which increases with time of irradiation. Oppositely to the observations in human LA, the irradiated protein does not fluoresce upon excitation at these wavelengths. Therefore, it is possible that several fates for Trp photochemical destruction exist, depending on the specie and conditions. It is important to empathize that human LA possesses only three Trp residues, lacking the most fluorescent Trp 26, which could greatly influence these reaction pathways.

It is interesting to look more profoundly into the equilibrium translated by the presence of an *isosbestic point*. For the light-induced cleavage of the SS bond in cutinase, Neves-Petersen et al. (2002), proposed a theoretical model which assumed a chemical exchange between two species that slowly interconvert. The original species are the protein molecules with their SS bonds intact, yielding the photo-cleaved species that are characterized by a higher quantum fluorescence yield. Due to internal processes after Trp excitation the excited low quantum yield species would convert to high the high quantum yield species. The conversion is regarded in the model as a probabilistic event, and the time-dependent fraction of low quantum yield species depends on factors such as power of the irradiation or the absorption (volume, concentration).

The model successfully described the time-dependency of the fluorescence intensity in cutinase (increase).

The presence of an *isosbestic point* in the eLA successive spectra suggests that a similar event occurs in this protein, with the UV triggered conversion between the original low quantum yield species to transformed species characterized by a red-shifted emission and higher quantum yields. The presence of these two elements in the separated products of human LA irradiation supports such reaction mechanism.

It was not possible to fit the time-dependent fluorescence curves of eLA with the expressions resultant of the model proposed by Neves-Petersen et al. (2002), since the application of model can not be applied satisfactorily in the experimental conditions used the irradiation procedure of eLA. Certain criteria are not fulfilled, such as the full illumination of sample volume.

Alternatively, the temperature time-dependent fluorescence eLA curves (Figure 5.13) were fitted with an exponential function. It is assumed that excited Trp are involved in a first order reaction, and that the extent of the reaction (rate constant) is proportional to the rate constant of fluorescence exponential increase (*k*). The products of the reaction would be the 340 nm fluorescent Trp species. In this model possible reactions that lead to fluorescence intensity decrease are despised, such as the reverse reaction or photo-destruction of Trp residues. In that case a bi or tri-exponential function should be used for fitting, and the decay phase of the profile should be included. Irradiation was realized always for 3.5 h and the decay phase was not present in most of the profiles. With the determination of *k* for different temperatures it was expected to learn more about the possible reaction kinetics.

The errors obtained for the fittings (Table 5.8) and the fitting curves and residues (Supplementary Results in Appendix B), indicated that the model above can successfully be applied to describe the time-dependent fluorescence of eLA.

The values of the fitted parameters show, as evidenced in the presentation of the results, two distinct tendencies. *k* increases with the temperature raise, while C_1 and C_2 diminish. The increase of *k* with temperature signifies that the reaction mechanism in which the Trp excited species of eLA are driven is favored by temperature increase. On the other hand, the Trp excited species, upon involvement in reaction pathways do not radiate emitting fluorescence, which explains the diminishment of fluorescence for higher temperatures, mathematically translated in the values of C_1 and C_2.

As advanced before, for Trp alone in solution an increase of temperature from 4 to 37 ºC can raise aqueous electron formation (e_{aq}^-) from excited singlet Trp states in a fivefold way or more (*vide* section 3.3.2). The increase of *k* with temperature quite considerable, the fitted value at 29.9 ºC is almost the double of the one at 9.3 ºC. The only decay pathway of Trp excited

species that is known to be temperature dependent is the thermal ionization from the S_1 relaxed state (5.4) (*vide* section 3.3.2).

$$^1\mathrm{Trp} \xrightarrow{k_{ion}} \mathrm{Trp}^{\bullet+} + e_{aq}^{-} \quad (5.4)$$

Sherin *et al.* (2003) studied the temperature dependence of Trp excited states ionization. This group determined that the rate constant of Trp thermal ionization (k_{ion}) at pH 7.1 varied with temperature according to the Arrhenius Law yielding pre-exponential factor $A_{ion} = 2.3\times10^{15}$ s and energy of activation Ea_{ion} = 50 kJ/mol. As described in the Analysis of the results *k* shows similar temperature dependence with an Ahrrenius activation energy Ea = 20.5 kJ/mol. The values of the activation energies are quite proximal indicating the thermal photoionization is one of the major mechanisms activated upon excitation of the Trp species, and precedes the increase in fluorescence intensity. The energy of activation required for photoionization in eLA is smaller than for Trp in solution. In eLA the presence of other groups in the vicinity of Trp residues could both favor the ionization of the excited Trp, diminishing the energy barrier required for this mechanism. For instance, it is known that lysine and histidine may quench the Trp excited species by proton transfer to neighbor amino groups. The proximity of electron acceptor groups such as protonated carboxyl groups, SS bonds, amides, and the peptide bond could be another factor (section 3.2.2). Indeed, while studying the 3D structures of the two bLAs (Figures 4.6 and 4.7), the close proximity of lysine residues, SS bonds and peptide chain was referred.

This mechanism yields the formation of a solvated e_{aq}^-, which as described previously (*vide* section 3.3.1). The e_{aq}^- may trigger a wide number of photoinduced mechanisms in proteins, including the breakage of SS bonds. The latter probably occurs in eLA, if the correlation between SS bond breakage and exponential fluorescence increase is considered. In that case it would be probably the sole pathway described by exponential fluorescence increase upon e_{aq}^- electron release. Temperature dependence is observed for all the temperature curves, so this mechanism is expected to occur in the range of temperatures 9.3 – 29.9 ºC. For higher temperatures it is not excludable that the same mechanism occurs. In fact cleavage of SS bond is noticed at 34.6 ºC. eLA is probably folded differently at this temperature, implying changes in the positions of the Trp residues and probably the quenching groups, which modify its fluorescence behavior.

The cleavage of SS bonds upon e_{aq}^- release can occur by several mechanisms (*vide* section 3.3.1), is it by direct capture of the e_{aq}^- by the cystine residues (5.5), or indirectly implying the reaction with the peptide chain (5.6), yielding of ketyl radical $-\dot{C}(OH)NH-$ that can propagate along the chain and react with the SS bond.

$$e_{aq}^{-} + RSSR \rightarrow RSSR^{\bullet -} \quad (5.5)$$

$$e_{aq}^{-} + \text{-CONH-} \rightarrow OH^{-} + \text{-}\dot{C}(OH)NH\text{-} \quad (5.6)$$

The second mechanism does not depend on the distance between the excited Trp residues and SS bond, as the first one or as the electron transfer from the triplet state ^{3}Trp (*vide* sections 3.3.1 and 3.3.3)., Vanhooren *et al.* (2006**a**) observed that the light-cleavage SS bonds in goat LA is associated with the cross-linking of cysteine with lysine residues. Such event is noticed for breakage of Cys6-Cys120 and Cys73-Cys91 with formation of Cys6-Lys122 and Cys91-Lys79 or Cys73-Cys93 (only one free thiol radical is formed in each case). Through the construction of four goat LA mutants, each one with a Trp residue substituted by a Phe, this group discovered also that the breakage of Cys6-Cys120 is exclusively mediated by Trp26. The two entities are too distant for a direct contact (in goat LA the distance is 14.5 Á), so a plausible mechanism would be a propagation reaction like the described here (5.6). The formation of Cys6-Lys122 sustains such possibility. Moreover, lysine radicals are known to form intramolecular –S–NH– with cysteine residues when radicals (Fu et al., 2002). The similarity between bLA and goat LA, and the observed distance between the two referred entities in holo-bLAc and apo-bLAc (14.81 and 13.36 Á respectively) indicate that the cross-linking could also occur in eLA.

By the same approach Vanhooren *et al.* (2006**a**) determined the mutual presence of Trp26 and Trp104 may be essential for the photo-cleavage of Cys73-Cys91 in goat-LA. Again the distances between these Trp residues and this bonds are far elevated (10.9 and 7.7 Á), and the lysine cross-linking is found, indicating a possible important contribute of e_{aq}^{-} in the cleavage.

Evidently, it is not excluded that other mechanisms are involved in the fluorescence increase and SS bond breakage, such as the electron transfer from the triplet state to neighbor SS bonds. Indeed for goat LA, Trp60 is the major contributor for SS bond cleavage and is in proximity of the broken Cys 61-77 and Cys73-Cys91. Furthermore, for the first of the bonds no cross-linking with lysine was observed.

Observation of the successive Trp emission spectra of eLA (Figure 5.5), for which the *isosbestic point* is visualized, can help to trace some conclusions regarding the Trp species involved in the reaction mechanisms. If the red-shoulder present in the emission spectrum at 0h irradiation represents truly the fluorescence contribute of Trp118, this residue should not be involved in reaction equilibrium translated by the *isosbestic point* and possibly in the fluorescence increase. In fact for goat LA Trp 118 is considered the Trp residue that contributes the less to the thiol formation. This is likely due to the fact that Cys28-Cys111 is not found broken after illumination (Vanhooren *et al.*, 2006**a**).

One of the other Trp residues should be involved in this equilibrium upon excitation, the most likely being Trp26, that dominates emission in LA (*vide* section 4.2.2).

As mentioned before the contribute constants C_1 and C_2 counteract the increase of fluorescence dictated for higher values of *k* with temperature raise. The increase of temperature favors the yielding of e_{aq}^-. This should result in an increase of SS bond formation and consequently of fluorescence quantum yield. However e_{aq}^- can be driven to other reaction pathways (*e.g.* reaction with molecular oxygen or H_30^+ ion from the buffer – section 3.3.2) and induce further damage to the Trp residues or to the protein itself. Therefore, at higher temperature these mechanisms are also favored, which would explain also the decrease in fluorescence yield for higher temperatures.

Finally it is important to discuss other important experimental indications regarding eLA as a candidate for eLA immobilization. Assuming that the increase in fluorescence is correlated to the cleavage of SS bonds the pH characterization procedure indicates that neutral pH values favor the breakage mechanisms (Figure 5.17). At alkaline pH values the production of e_{aq}^- should be favored, but eLA is also more unstable, which could invalidate the increase in fluorescence, and does not interest for immobilization since the molecule is not kept intact.

Static light scattering measurements in eLA (Figure 5.11) indicate that little or almost no association takes place between eLA molecules with broken SS bonds. In the studies realized by Permyakov *et al.* (2003), the SDS-page electrophoresis data of the illuminated human LA showed no oligomeric forms. Oppositely, SDS-page and gel filtration results of Vanhooren *et al.* (2003), demonstrate that after 6 h UV-irradiation of an apo-form of goat LA monomers, dimmers, trimers and polymers are formed. However the fraction of intact monomers (0.66) is still considerably high. Therefore it should be expected that the indications of the static light measurements are accurate and polymerization by intra-SS bounding is not a problem for the proposed light-induced immobilization. However, it is hard to predict which thiol reactive group would be immobilized.

The implications of SS bond breakage in the structure of the protein are difficult to predict, as advanced *supra*. UV-modified human LA shows no cooperative thermal spectral changes, showing that the protein should be mostly in a denaturated form (Permyakov *et al.*, 2002). The implications to the protein functionality are not well defined. The UV-changed component of human LA above mentioned still shows Ca2+ binding capability, though with lower affinity than the native-like human LA (Permyakov *et al.*, 2002). Since several conformational changes are expected near or in the active site (aromatic cluster I, and hydrophobic cores)for lactose synthase regulation, it is expected that eLA looses most of this functionality in the products of irradiation (340 nm Trp emitting proteins – with SS bonds broken). In native-like goat LA ~35 % of the original lactose synthase regulatory activity is conserved after 3 h irradiation (Vanhooren et al., 2006**a**). However it is not known if this activity is originated from the still intact

goat LA or photo-transformed protein. This test should be realized in eLA in the photo-transformed protein after separation of the irradiation products.

Since the cleavage of three disulphide bonds can be expected in LAs (Cys61-Cys77, Cys73-91 and Cys6-Cys120), a potential immobilization of eLA onto a surface could occur by all these three possibilities, which would have different impacts on the protein structure. Of the three disulphide bonds, Cys6-Cys120 should be the most accessible for surface binding upon cleavage, since it is locate in exposed areas of both holo-bLAc and apobLAc. On the other hand, Cys61-Cys77 and Cys73-Cys91 are almost completely shielded from the solvent, which would difficult an immobilization. Additionally, only for Cys6-Cys120 is not noticed cross-linking with lysine residues in goat LA, so two thyil radicals could be available for reaction, and the radicals should be free of sterical interference in the bounding. Nonetheless, the effects of illumination on the position of these Cys radicals are not known.

Resuming, characterizing eLA as a potential candidate light-induced immobilization candidate is a delicate issue. Light-immobilization onto thiol derivatized surface or gold surfaces should be expected since the formation of thiol groups is confirmed and is favored by prolonged illumination with UV-light. However, the reaction mechanisms in which are driven the excited species of Trp are extremely complex and no strong conclusions can be taken for the best conditions for immobilization. Neutral pH and low temperatures should be preferable since the protein should be relatively stable and the cleavage of SS bonds still takes place. Moreover the calcium depleted forms of eLA revealed in solution a high instability upon slight changes in solvent conditions.

6. IMOBILIZATION PROCEDURE

6.1. PREMISSES

During the extent of the project, considering the progressive uptake of information resultant of eLA characterization, several light immobilization procedures were tried. The disruption of SS bonds in the protein upon Trp excitation was early confirmed using the Elmann's reaction, as displayed in the characterization results. Therefore it was assumed that free thiol groups should be present to react with thiol derivatized surfaces or gold upon prolonged UV-illumination, at least in the experimental conditions used in that assay.

Before and during this project, immobilization of eLA in quartz derivatized slides was tried using the LIMI technology developed by the group, and previously described. For a wide number of solvent conditions and eLA concentrations, (covering the used in the characterization procedure), and output power, the immobilization was not successful (Parracino, A., Kold, A., Personal Communication).

As an alternative, light induced immobilization was attempted in solution, using gold nanoparticles (AuNP). Bain *et al.* (1989) demonstrated that molecules carrying thiol groups can absorb with extreme efficiency onto gold surfaces, upon the covalent binding of the thiol moiety to the gold atoms in the surface. As previously reviewed (section 3.3), the thiol groups provenient from photo-reduction in proteins are very reactive, which should facilitate the covalent bonding,

In solution eLA is perfectly hydrated and the molecules can be homogeneously illuminated upon stirring. Furthermore, with the agitation of the medium, the reaction between the free solvent thiol groups of the protein and the gold atoms of the nanoparticles surface is promoted. Moreover, if well dispersed in solution, AuNP provide a high surface area for immobilization.

The light-immobilization into AuNP was realized with a similar experimental set-up than the used in characterization for probing the fluorescence time-based emission of eLA. An eLA sample is constantly illuminated with UV-light in the spectrofluorimeter, in order to break the disulphide bonds. The kinetics of cleavage are already known, since similar experiments were realized during the characterization procedure of eLA, and the fluorescence emission of the protein can be probed during the experiment. At the desired moment, AuNP can be introduced in the cuvette to react the produced thiol groups of the protein in solution. This can be either during the process, by pausing the illumination session, or in the beginning, before this procedure. Replacement of one molecule with another is favored by using an excess of a new molecule while providing enough heat and/or sonication (Templeton *et al.*, 1999). Consequently, the concentration of eLA used in solution was always approximately 2.5 times higher than the

concentration of AuNP after addition. Heat and/or sonication were not possible to use in risk of damaging the protein, so during reaction, magnetic agitation was always promoted. After reaction the particles (with or without eLA immobilized) and eLA were separated by centrifugation, due to the difference in molecular weight.

The size estimation of separated, fresh particles and eLA was carried out using Dynamic Light Scattering (DLS). The purification technique (removal of excess protein) and characterization of immobilization procedure (verification of protein immobilization into AuNp were studied using UV-visible spectroscopy. Additional characterization was realized by probing the fluorescence of the nanoparticles, and by further measurements using Scanning Electron Microscopy coupled to Energy Dispersive X-ray spectroscopy (SEM-EDS).

6.2. MATERIALS AND METHODS

6.2.1. Materials

Preparation of AuNP

Sodium Citrate ($C_6H_5Na_3O_7.2H_2O$), Gold (III) chloride tryhydrate ($HAuCl_4,3H_2O$) were procured from E-Merck. 0.01 M Au^{3+} and 0.1 M sodium citrate mother solutions were used for synthesis.

Protein and Buffer Solutions

Protein and buffer solutions were prepared using the same sources and procedures than the presented in the Materials section of the eLA characterization procedure (Section 5.2.1).

6.2.2. Methods

6.2.2.1. Preparation of AuNP

Gold cation in the form of $AuCl_4^-$ can be reduced by using biocompatible weaker reducing agents (Cushing *et al.*, 2004). Moreover, the reducing agent can also serve as an organic capping agent that is normally used to prevent agglomeration of nucleated particles. Turkevich process is the well-known example for the same, where the synthesis of citrate capped AuNP was carried out by boiling a mixture of dilute $HAuCl_4$ and sodium citrate (Enüstun *et al.*, 1963).

2 ml of the 0.01 M gold salt solution transferred into 48 ml of de-ionized water. The solution was heated to boil on constant stirring. On boiling, 0.4 ml of 0.1 M sodium citrate solution was added rapidly and left at the same temperature and stirring for 30 min. The solution turned to deep red color of characteristic gold colloids indicating the reduction of Au^{3+} to metallic gold (Au^0).

The suspension was cooled to room temperature and washed twice with water using the centrifugation technique. The suspension was centrifuged at 10000 RPM for 10 min. and supernatant liquid that contains very small particles, excess surfactant and reaction byproduct salts was decanted. Bottom agglomerated particles were re-dispersed in water and the same process was repeated for another time. After second wash, bottom settled citrate coated gold particles re-dispersed in buffer solution. The suspension was used for characterization and further immobilization experiments. From the molarities of the above reaction, the concentration of gold nanoparticles (AuNP) and citrate surfactant is determined. Respective concentrations of 0.4 mM and 0.8 mM were obtained.

6.2.2.2. Light Induced Immobilization of eLA on AuNP Surface

Two immobilization procedures of eLA were realized. The experimental set-up for immobilization was the same than the used for probing the time-dependent fluorescence emission of eLA (described in Section 5.2.2.1). In both procedures two milliliters of eLA solution was illuminated in a quartz macro cuvette (1 cm pathlenght). Illumination was stopped at a certain point to introduce AuNP solution, and continued afterwards with AuNP in solution. Continuous illumination at 295 nm was once more realized in the previously described RTC 2000 PTI spectrometer. Emission was monitored using the two detection channels of the spectrometer. Real-time correction was not enabled. Magnetic stirring of the illuminated sample was kept during the extent of both procedures. Temperature inside the cuvette was maintained constant using a peltier element.

The experimental settings used in both immobilization procedures (A and B) are described in Table 6.1.

Table 6.1: Experimental settings used in the immobilization procedures.

Immobilization Procedure	**A**	**B**
Protein sample	eLA 10 μM in Tris HCl 10 mM pH 8.55	
Volume (mL)	2	
AuNP sample	AuNP 400 μM in Tris HCl 10 mM pH 8.55	
Volume of AuNP solution introduced (μL)	20	15
NP concentration in the cuvette (μM)	3.96	3
Time of introduction of AuNP (h)	1	1.7
Total time of illumination (h)	2.3	4
Temperature (ºC)	25.2	25
Stirring (rpm)	900	
Excitation wavelength (nm)	295	295
Wavelength set in Detector 1 (nm)	340	330
Wavelength set in Detector 2 (nm)	295	330
Excitation slits (nm)	5	
Emission slits (nm)	3	5

In the case of the immobilization procedure B the illuminated sample was removed and stored at 4 ºC and under constant agitation overnight to promote reaction b between the thiol groups and the gold surface.

After illumination in procedure A, and reaction in procedure B, the samples were washed twice to remove the excess of protein which did not bind to the AuNP. Each time (wash), the samples were centrifuged at 13400 rpm in a Minispin® (Eppendorf) during 10-15 minutes. After centrifugation the AuNP were clearly visible in the bottom of the liquid as a black color agglomerate. The supernatant was removed and AuNP were resuspended in 10 mM Tris HCl pH 8.55. AuNP dispersed immediately in solution, showing that they were still stable. After the two washes the final resuspension should contain almost no free eLA in solution.

6.2.2.2. Characterization Procedure

UV-visible Absorption Spectroscopy

Thermo scientific UV-Visible spectrophotometer (model: VWK International UV1 v4.60) was used to characterize the diverse washing steps of the separation procedure after immobilization procedure A (the two supernatants), the final resuspension of AuNP resulting of immobilization procedure A, and a AuNP blank (fresh sample of 3.96 µM concentration in 10 mM Tris HCl pH 8.55). The absorption spectra were recorded between 200 and 600 nm. The measurements were performed in black 1 cm path length cuvettes.

Fluorescence Spectroscopy

Measurements were once more carried out in RTC 2000 PTI spectrometer in a black 1 cm path length cuvette. The analyzed samples were the diverse washing steps of the separation procedure after immobilization procedure A (the two supernatants), the final resuspension of AuNP resulting of immobilization procedure A, and a AuNP blank (fresh sample of 3.96 µM concentration in 10 mM Tris HCl pH 8.55). Emission Spectra were recorded upon excitation at 280 nm. Emission and excitation slits were fixed at 5 nm. The final spectra are resultant of average of 3 spectra. The same measurements were realized with 10 mM Tris HCl pH 8.55 in order to correct for *Raman Contribution*. All the precedent spectra were corrected by subtraction of the emission spectrum of this buffer.

Dynamic Light Scattering (DLS)

DLS experiments were performed in a NanoZS, a zeta sizer from Malvern. The instrument automatically fits the autocorrelation function with various fitting algorithms to extract

the diffusion coefficient and Stokes-Einstein equation uses to convert the diffusion coefficient to the hydrodynamic radius. The average size and size distribution of fresh AuNP, eLA and AuNP after immobilization were estimated. For that purpose were used respectively a freshly prepared solution of 10 μM AuNP (in 10 mM Tris HCl pH 8.55), the supernatant of the first wash from immobilization procedure A, and the final resuspension of AuNP from immobilization procedure A. The measurements were realized in 1 cm path length disposable polystyrene cuvettes.

Scanning Electron Microscopy – Energy Dispersive X-ray spectroscopy (SEM-EDS)

Carl Zeiss 1540XB SEM-EDS was used for estimation of AuNP composition. Scanning electron microscopy (SEM) images were collected optimizing the voltage between 5 - 12 kV on silicon substrate where the dried AuNP particles are placed. X-rays, which are also produced by the interaction of electrons with the sample was detected by Energy Dispersive X-ray Spectroscopy (EDS). In order to improve the EDS analysis in SEM, the sample was excited with X-rays. During the X-ray acquisition for particle's composition analysis, the electron beam focused over the particle projection area. The X-ray spectrum was acquired for 60s, at an acceleration voltage of 12 kV. NORAN system six version 2.0 software from Thermo Fischer scientific was used to analyze the EDS data.

Two samples were analyzed using SEM-EDS:

- final resuspension provenient from immobilization procedure B;
- AuNP blank - diluted fresh sample prepared from the mother solution containing 3μM of AuNP in 10 mM Tris HCl pH 8.55.

6.3. RESULTS ANALYSIS AND PRESENTATION

In the first immobilization procedure (Immobilization A) a sample of eLA was illuminated with 295 nm light in the spectrofluorimeter as described in Materials and Methods (Section 6.2). The time-profile of fluorescence emission at 340 nm is displayed in Figure 6.1.

An increase in fluorescence is observed during the first hour of illumination. The experiment was stopped after approximately 1 hour of illumination to introduce the AuNP, which can be noticed in the profile by a temporary intensity decrease. Considering the previous trials with the Elmann's reagent, it was assumed that the increase fluorescence intensity is proportional to the number of free thiol groups formed. By introducing the AuNP in an advanced part of the illumination session it was pretended that free thiol groups were already formed upon mixing with the protein solution. After one hour of illumination there should be already a considerable number of broken SS, translated by an 13% increase in fluorescence intensity. Furthermore, in the

characterization procedure of eLA it was noticed that for breakage of a considerable amount of SS bridges, was required a considerable exposition time to UV. The late introduction of AuNP permits to avoid that they interfere with the process of illumination (e.g. scattering of the light). After the introduction of the AuNP, an increase in fluorescence intensity is still noticed, though the slope is less steep. After ~1.8 h of illumination a plateau is reached, followed by a decay phase until the end of the session (~2.3 h).

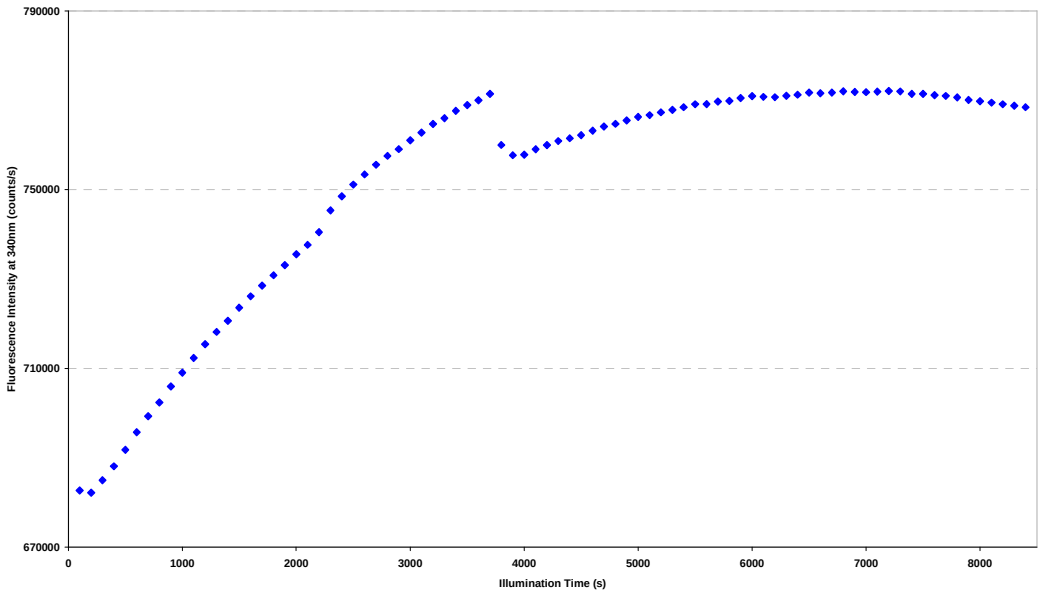

Figure 6.1: Fluorescence intensity of eLA *versus* illumination time. Excitation was fixed at 295 nm and emission was monitored at 340 nm. Temperature was maintained at 25ºC using a peltier element. Measurements were performed using a RTC 2000 PTI spectrofluorimeter as described in Materials and Methods (section 6.2).

The elastic scattering of the light was monitored during the whole extent of the session, by probing the emission at 295 nm in the second channel of the spectrofluorimeter. The emission did not increase, just decayed, even after the introduction of AuNP (Data not Shown), suggesting that no aggregation took place through inter-disulphide bonding between protein molecules.

Subsequently, the irradiated solution (containing the AuNP) was centrifuged and washed twice, as described in Materials and Methods, in order to remove the excess of protein. Three solutions were stored, one correspondent to supernatant of the first wash, the equivalent of the second wash, and the resuspended AuNP (with eLA immobilized or not). These samples were characterized through UV-absorption, Fluorescence Spectroscopy and DLS as described previously in Materials and Methods (Section 6.2).

In Figure 6.2 are displayed the absorption spectra of the liquid supernatants obtained after each wash procedure. In the spectrum recorded with the supernatant extracted from the first wash (in green), two typical protein peaks are clearly observed, at 220 nm and 280 nm, wavelengths for which the peptide bonds and aromatic residues respectively absorb. After the

first wash the majority of the protein in excess is removed, since in the spectra corresponding to the supernatant resultant of the second wash and resuspended AuNP (blue and red respectively, visible in the zoomed area), these two peaks are not sharp anymore. The peak corresponding to gold (~520 nm) is only visible for the spectrum of resuspended AuNP which confirms that the separation was successful.

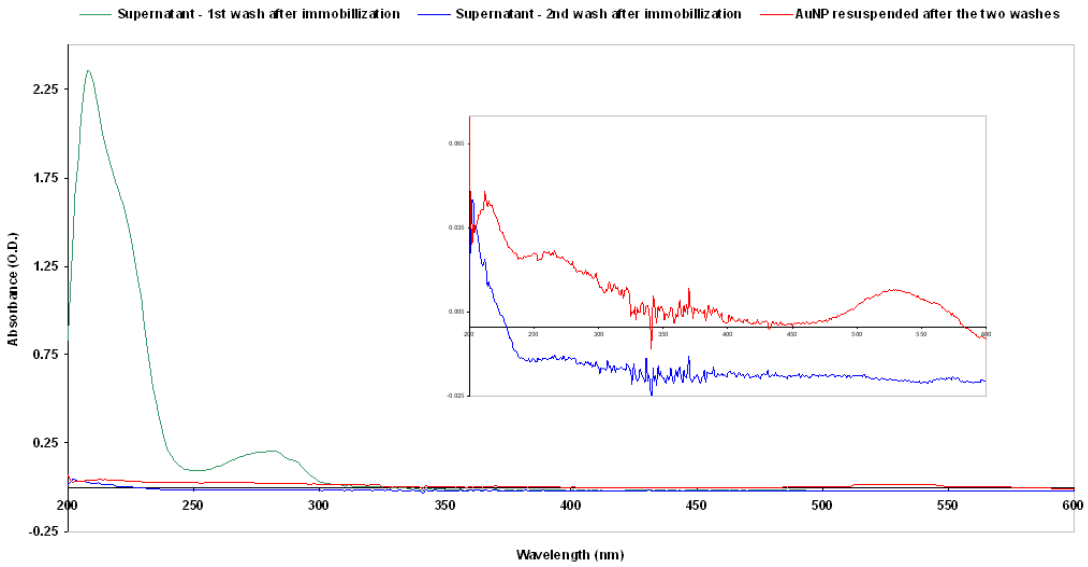

Figure 6.2: Absorption spectra of the supernatants of the two washes and the final resuspended AuNP solution. The box displayed within the area of the plot is a zoom of the absorption spectra of the second wash supernatant and the final resuspension of AuNP. The spectra were recorded in a UV-visible absorbance spectrophotometer as previously described in Materials and Methods (Section 6.2)

In Figure 6.3 are displayed the absorption spectra of the resuspended AuNP (red), and a fresh solution of AuNP prepared with the same concentration (wine red). The gold peak is present in either one of the spectra. The difference between these two spectra (orange), shows a peak at 220 nm, which could represent the absorption of peptide bonds of immobilized eLA. The absorption peak of the aromatic residues is not so clear. There could be a peak indeed, but centered at ~260 nm.

The fluorescence characterization data reflects similar results. The fluorescence emission spectrum of the supernatant resultant of the first wash (upon excitation with 280 nm light) presents a broad peak centered at ~335 nm (*vide* Figure B22 – Supplementary Results, Appendix B). The supernatant resultant of the first wash still displays some protein intrinsic fluorescence, but with far lower emission counts. Compared to the latter, the resuspended AuNP seemingly display no emission peak upon excitation with 280 nm (*vide* Figure B23 – Supplementary Results, Appendix B). The emission spectra difference between the resuspended AuNP and the fresh AuNP displays however a peak at ~335 nm (*vide* Figure B24 –

Supplementary Results, Appendix B), though at these low fluorescence counts the accuracy of the results is not to be trusted.

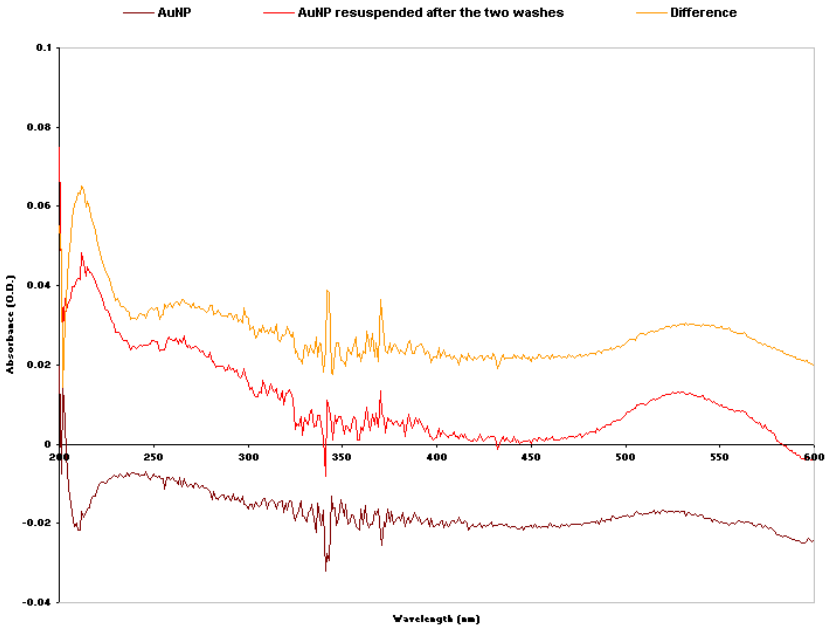

Figure 6.3: Absorption spectra of the final resuspension of AuNP (red), fresh AuNP (wine red) and the difference between these two (orange). Spectra were recorded using a UV-visible spectrophotometer as described in Materials and Methods (section 6.2).

To confirm if eLA was successfully immobilized onto the AuNP, the size of eLA, fresh AuNP, and the final resuspended AuNP was estimated using DLS. For a solution of 10 μM of fresh AuNP the measurements show an intense peak at 50.37 nm (*vide* Figure B25 – Supplementary Results, Appendix B). The measurement realized for the final resuspension of AuNP shows a modest difference in AuNP size after the immobilization procedure, presenting an intense peak at 50.81 nm (*vide* Figure B26 – Supplementary Results, Appendix B). eLA size was estimated by DLS measurement of the second wash supernatant. The peak which probably corresponds to the protein, at ~5.5 nm (*vide* Figure B27 – Supplementary Results, Appendix B), is not the most intense (15% intensity), showing that the sample may have been contaminated with some larger impurity. Nonetheless, given the probable hydrodynamic diameter (5.5 nm) of eLA, these results do not support a scenario of a successful immobilization, since no significative difference is noticed between the diameter values of the two tested particles.

In order to check the previous results the immobilization procedure was repeated (Immobilization B). This rehearsal presented some differences. After the illumination procedure the removed irradiated mixture of protein and AuNPs was left overnight at 4ºC under constant

agitation. This way it was expected to promote the binding reaction, and allow all the free thiol groups of the protein to react with the AuNP. The AuNP were also introduced latter in the illumination process, after about 1.7h of illumination, which proceeded until a final time of 4h.

Fluorescence emission was probed at 330 nm upon excitation with 295 nm light and no increase in fluorescence was noticed (Data not shown).

After overnight reaction the sample was submitted to the same washing protocol. The characterization procedure was this turn realized using SEM-EDS. The images obtained for the final resuspension of AuNP (after immobilization) and for the AuNP blank (fresh sample) are displayed in the Figures 6.4 and 6.5 respectively. In both images are visible the groups of AuNP. The enhanced areas in the images (1 and 2), corresponding to two distinct zones where AuNP were or not present, were analyzed though EDS.

The X-ray spectra of the two exposed areas (Figures 6.4 and 6.5) can provide quantitative information of the particles constitution. However this information may not correlate exactly the particles content due to the presence of the buffer salts and surfactant. Moreover, the sample placed on the sample holder may not be homogeneous and the amount of sample may be variable between detections. Furthermore, individual AuNP are in nanometer size, and the area exposed (> 2.5 μm in length and height) comprise a large portion of area non-occupied by AuNP, in which other molecules could be present.

However, this experimental analysis qualitatively confirms the presence of the elements C, O, N, Si, Au and Cl (Fig. 5). C and O peaks can be expected from sodium citrate surfactant and the buffer salts; the N peak can also be expected from the buffer salts and Au from AuNP. Proteins display also high contents in N, C and O, so these peaks could also be representative of eLA attached to AuNP.

In Figure 6.4, exposed area 2 does not contain any AuNP, since no Au peak is noticed in the X-ray spectrum, and presents all the atomic entities of the buffer salts (Tris HCl). Therefore this area should be representative of atomic composition of the buffer salts and surfactant. In the spectrum corresponding to exposed area 1, the presence of AuNP is confirmed by a gold peak at ~2.1 kV. A peak of smaller intensity is also noticed for nitrogen. In Figure 6.5, the X-ray spectrum, corresponding to the zone where fresh AuNP lay (exposed area 1) shows again the Au peak and quite reduced N peak this time.

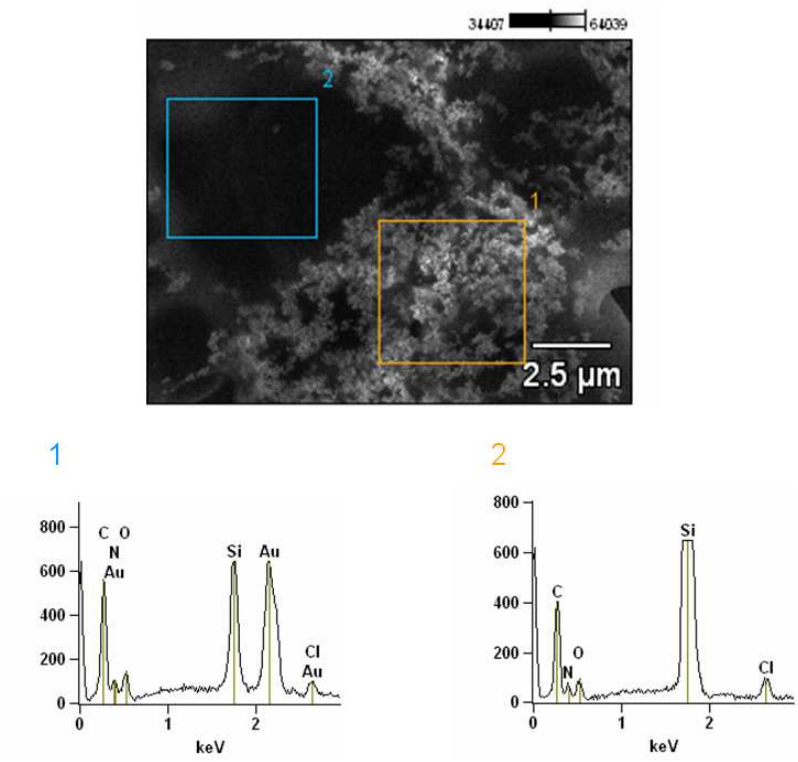

Figure 6.4: SEM image of the final AuNP resuspension (after immobilization). Accelerating Voltage: 7.0 keV; Magnification: 18272. The squares represent the area exposed to EMS. X-ray spectra of the exposed areas are displayed in the bottom. The peaks corresponding to each atom are labeled.

Table 6.2: Experimental atomic values obtained after EMS analysis of each exposed zone - AuNP resuspension (after immobilization).

Parameter	ZAF Value		Weight %		Atomic %	
Atom/Exposed area	**1**	**2**	**1**	**2**	**1**	**2**
C	1.84	3.95	16.41	24.84	46.34	41.78
N	2.06	3.01	6.63	4.5	16.07	6.49
O	1.7	1.96	4.77	2.99	10.1	3.77
Si	0.88	1.06	12.09	62.87	14.6	45.22
Cl	0.97	1.21	3.23	4.79	3.09	2.73
Au	1.34		56.87		9.79	

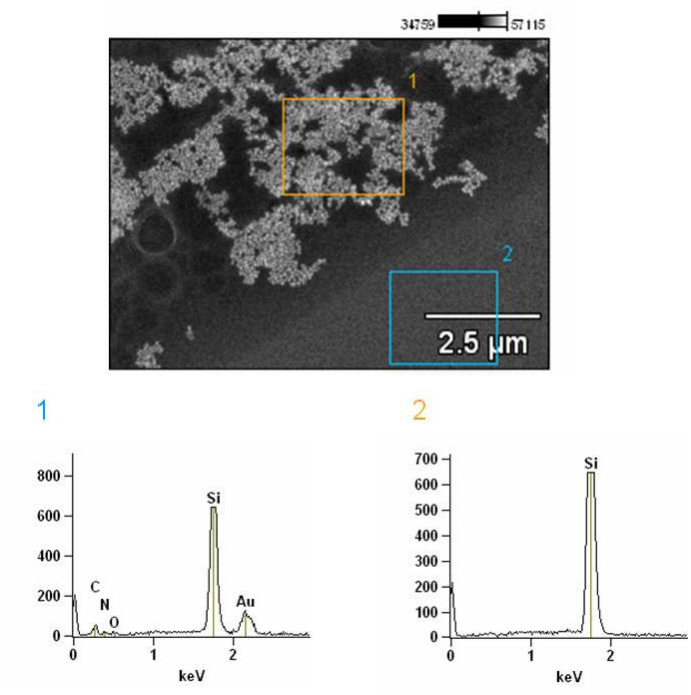

Figure 6.5: SEM image of the final AuNP blank (fresh, non-exposed particles). Accelerating Voltage: 7.0 keV; Magnification: 29881. The squares represent the area exposed to EMS. X-ray spectra of the exposed areas are displayed in the bottom. The peaks corresponding to each atom are labeled.

Table 6.3: Experimental atomic values obtained after EMS analysis of each exposed zone - AuNP blank (fresh, non-exposed particles).

Parameter	ZAF Value		Weight %		Atomic %	
Atom/Exposed area	**1**	**2**	**1**	**2**	**1**	**2**
C	3.07		6.14		17.77	
N	2.18		2.32		5.76	
O	1.63		1.22		2.65	
Si	0.91	1	54.59	100	67.52	100
Au	1.53		35.73		6.3	

The experimental EMS values (Tables 6.2 and 6.3), provide further insight into the possible AuNP composition. In the zone where resuspended AuNP lay (exposed area 1 – Figure 6.4) the atomic content in N (16.07 %) is considerably higher compared to the zone characterizing the exposed buffer and the surfactant (6.49 %) (exposed area 2 – Table 6.2). As said before, the homogeneity of the sample can not be assured and the quantity of sample tested

may not be the same in both areas. However, such a difference of values could indicate that eLA is in fact immobilized on the surface of AuNP, though in low quantities. The ratio between N and atomic content of gold could be a reasonable indicative of the presence of eLA in the AuNP. The values of these ratios for the zone where resuspended (exposed area 1 – Figure 6.4) and fresh (exposed area 1 – Figure 6.5) are present are respectively 0.117 and 0.065. Though the particles can behave differently in solution and the two analyses can present divergences, the value for the resuspended AuNP is almost the double, providing another indication of successful immobilization.

6.4. DISCUSSION

The results obtained from the two immobilization procedures of eLA onto AuNP are contradictory. The DLS analysis of immobilization A shows no apparent difference in hydrodynamic diameter between the product of immobilization (final resuspended AuNP) and the fresh AuNP. Though the surfactant surrounds AuNP in the fresh sample, the width of the surface film it may form should not be even detectable, while with eLA immobilized, a macromolecule, a difference in hydrodynamic diameter should be noticed. The UV-absorption characterization procedure shows on the other hand some indications of possible immobilization. In the difference spectra between final resuspended and fresh AuNP a peak is observed at 220 nm, where peptide bond absorbs, and a residual peak is found at ~260 nm, where aromatic residues absorb. Furthermore, these peaks are not found or very reduced in supernatant of the second wash, excluding the possibility of being representative of free eLA in solution. However the fluorescence spectroscopy characterization shows once more negative results, with no emission upon 280 nm excitation in the resuspended AuNP.

Oppositely, immobilization procedure B provides a scenario of successful immobilization, since the resuspended AuNP provenient from this procedure present, seemingly present nitrogen contents, after characterization analysis with SEM-EDS.

The two immobilization procedures present differences, not only in protocol (diverse times of introduction of AuNP, longer time of irradiation reaction in immobilization B) but also in the fluorescence behavior of eLA upon irradiation. The increase in fluorescence intensity was not noticed in immobilization B, while for immobilization A the typical increase described in eLA characterization procedure is noticed. These divergences in fluorescence behavior spell once more the instability noticed eLA once the low ionic strength is too low. The immobilizations were realized with eLA concentration of 10 μM in 10 mM TrisHCl. It corresponds to the lowest case in ionic strength. At the time of the experiments the knowledge regarding apo-forms of bLA was limited. In future immobilizations this effect should be considered. Nonetheless the breakage of

SS bonds could be expected, even in these destabilized forms. The denaturated forms of LA are generally folded in MG-like conformations, and part of the native interactions should be kept.

Light-induced immobilization of other proteins onto nanoparticles was already attempted in the Nanobiotechnology group of the University of Aalborg. Bovine Serum Albumin and Prosthetic Serum Albumin were already successfully immobilized onto gold coated magnetite nanoparticles and AuNP respectively (Personal Communication, Parracino A.). After immobilization it was found not that not also Bovine Serum Albumin molecules are covalently bounded on the surface of the nanoparticles, but also that they form aggregates around the immobilized protein, increasing the measured hydrodynamic diameter in DLS from 27.4 to 200 nm (Parracino *et al.*, 2008). Another protein, esterase, an enzyme that does not present SS bonds, but contains four free cysteines, was immobilized through affinity reaction with gold coated magnetite nanoparticles, without the use of light. The average hydrodynamic diameter of the particles (DLS), protein and complex of protein and nanoparticles was respectively 37 nm, 49.4 nm and 74.6 nm, signifying that the enzyme forms a single layer on the gold surface.

Evidently, each protein can display a particular mechanism of immobilization and attachment to the gold derivatized nanoparticles, depending on its structural and chemical features. Though LA immobilization to metallic surfaces is not well described in literature, there are several reports concerning the adsorption properties of LA. Upon interaction with colloidal polystyrene nanospheres native bLA the protein adsorbs particularly well on the polystyrene surface through stable hydrophobic interactions (neutral pH - both LA and polystyrene are negatively charged) and hardily desorbs. Upon adsorption bLA suffers denaturation to a partly folded state and remains in a MG-like conformation (Engel *et al.*, 2002). LA also adsorbs particularly well onto negatively charged planar poly(acrylic) acid brushes (Holmann *et al.*, 2007). Neutron Reflectometry data showed that despite its net negative charge (neutral pH), LA was penetrating deeply into the polymeric brush. Moreover, no protein accumulation was found at the inner poly(styrene) or the outer solution interface of the polymeric brush. Total Internal Reflection Fluorescence data indicated also a high degree of reorientational mobility of LA within polymeric brush. It was concluded that this high mobility of LA within the polymeric brush could partially be understood by the presence of repulsive electrostatic interactions.

Upon thiol immobilization to the gold surface, eLA might also rearrange in a partly denaturated form as the described above. Since eLA is negatively charged and upon adsorption does not tend to accumulate, aggregation of the protein is not expected, due to electronic repulsion. Hence, the eLA molecules may occupy completely the surface of the AuNP, forming a thin film, not allowing other molecules to adsorb.

Given that eLA is a particularly small protein (average hydrodynamic radius obtained from DLS is 5.5 nm), the difference in hydrodynamic radius of the complex AuNP-eLA may not be distinguishable within the resolution of the DLS measurements, unlike esterase. Moreover the

hydrodynamic radius of the AuNP may not be constant, which could yield some divergences between samples.

Nevertheless, such event does not overrule the unsatisfactory results obtained on the Fluorescence Spectroscopy characterization, where no fluorescence emission is found for the resuspended AuNP.

Gold is known for having a polemic and discussible paper in fluorescence emission. Classically, gold is known to be a stronger fluorescence quencher. However it has been advanced recently that gold may also have a reverse role, enhancing the fluorescence of fluorophores. Fluorophores on the excited may undergo near-field interactions with metal particles to create plasmons, a phenomenon called Metal-Enhanced Fluorescence (MEF). MEF by was already verified for AlexaFluor derivatized Rat Immunoglobin G immobilized in gold films (Zhang and Lakowicz, 2006). According to radiating plasmons model for MEF the absorption component of metal particle extinction contributes to quenching, while the scattering component contributes to MEF. Therefore the size of gold particles may have a particular influence on the paper of gold in fluorescence.

Here, the estimated hydrodynamic radius of AuNP is 50.37 nm, which could signify a high light scattering yield from the particles. However if total adsorption of eLA on the surface is considered, this implies that the aromatic residues are in direct or almost in direct contact with the gold molecules, which could favor the quenching of their fluorescence by the gold (Zhang and Lakowicz, 2006), explaining the emission spectrum obtained. Furthermore, quenching of fluorescence was observed recently by Delphino and Cannistaro (2009) for the well described hybrid complex of Azurin-AuNP. In this case azurin molecules form a monolayer in the surface of the 20 nm AuNP. Binding of azurin molecules to the AuNP surface results in the red shift of the nanoparticle resonance plasmon band and in the quenching of the azurin single tryptophan fluorescence signal.

Even if the model advanced (thin film of eLA around the AuNP) explains partly the results obtained for both immobilizations, and the SEM-EMS results point out the binding of eLA to AuNP, the data presented here is not sufficient to prove a successful light-induced immobilization of eLA.

7. CONCLUSIONS

The first step of this experimental work consisted on evaluating bLA as a potential candidate for light-assisted immobilization. Calcium depleted form of bLA was chosen as model for this characterization procedure. This choice reflected both the biomedical interest of apo-LA forms (regarding its potential functionality), and the need of further investigating the light induced cleavage of SS bonds in these LA forms, which was not so well characterized.

The characterization procedure of apo-bLA forms brought evidence of some interesting results. Prolonged irradiation of a native-like apo-bLA resulted in an increase in fluorescence yield, coupled to a pronounced red-shift in Trp fluorescence. These spectral changes are probably caused by involvement of Trp excited species into first order reactions that will yield conformational changes on the protein, as indicate the hidden *isosbestic* point and the exponential fluorescence increase at 340 nm. The original Trp excited species are converted upon reaction to high fluorescence quantum yield and red-shifted products. Breakage of SS bonds is probably another product of this reaction. Upon cleavage of these bridges in eLA, the quenching of the Trp residues is considerably reduced, explaining the raise in Trp emission. This cut-back is probably due to the absence of these bonds as strong fluorescence quenchers, but can also advent of photodegradation and displacement of other quenching groups upon cleavage. For instance it is known that the SS bonds breakage in goat-LA can be resultant of crosslinking of a cysteine to a lysine. The latter can be a strong fluorescence quencher, as integrated in the peptide bond. Furthermore, the red-shifted emission of the product Trp species indicates a displacement of these residues to solvent accessible areas upon cleavage. It could also alter the appetence of the red-shifted Trp species for quenching.

One of mechanisms activated upon Trp irradiation and responsible of SS bond cleavage is the thermal photoionization of excited singlet Trp species and production of e_{aq}^-, as pointed out by the temperature dependency of the exponential rate of fluorescence increase.

Acquirement of fluorescence lifetime components and use of flash photolysis studies in bLA is a next step for understanding deeply the mechanisms and Trp residues involved in the UV-triggered reactions here described.

Though these observations provide supplemental knowledge on the UV-triggered mechanisms in apo-forms of bLA, and LA in general, the informations regarding apo-bLA as candidate for light-assisted immobilization are scarce.

The verified presence of free thiol groups is evidently a fulfilled criterion for the technique. Nevertheless it is not known which thiol groups will be available to react with a derivatized surface upon immobilization. They are detected by the Elmann's reagent and Cys6-Cys120, that suffers photlysis in goat LA, is in an accessible region, so they should be solvent accessible, but it is not

excludable that sterical interferences exist. SS bond breakage seemingly is favored at low temperatures and neutral pH, another indication that should be considered for immobilization.

The integrity of the protein and its functionality is not guaranteed upon UV-light irradiation. The polypeptide probably reorganizes as a MG-form maintaining most of its native-like structural features (mostly secondary content), but drastical changes are expected in the aromatic clusters, which could jeopardize the active site for lactase synthase activity and other potential functionalities.

The instability and unpredictability of bLa in an apo-form is an additional problem for using this model. Slight modifications in the experimental conditions, typically required for using diverse analytical techniques, resulted in large discrepancies in results obtained. In the future, it would be preferable to use the most stable Ca^{2+} loaded form, in order to have reproducible results. The UV-sensitivity of both forms could also be compared this way.

The final evaluation of apo-bLA as candidate was performed by executing the light-immobilization procedure on gold nanoparticles. The results suggest the possibility of thin-film formation on the AuNP surface. Even so, these experiments consisted only on a test phase, since at the time the knowledge of the apo-form of bLA was reduced, as also the UV-sensitivity of the candidate. The conditions used in both immobilizations destabilized particularly apo-bLA. In the future higher ionic strengths should be used.

The model for thin-film formation in apo-bLA should be confirmed by rehearsal of the immobilization and all the characterization procedures. Labeling of the protein with a powerful fluorophore may also help in characterization procedure. Moreover it would allow the use of other identification techniques (for the tagging of eLA onto the fold surface), such as fluorescence and confocal microscopy.

Light-induced immobilization of LA onto gold AuNP has a considerable biomedical interest. Given the broad range of LA functional properties, upon binding to AuNP, this complex could be used futurelly as biosensor for a wide number of metal ions, or as molecular carrier. The latter application is particularly appealing given two possible distinct LA functions: lactose synthase regulation and anti-tumorogenic agent. Moreover, the protein can be successfully delivered in the interior of cells. This is due to the nature of covalent bond that links the thiol to the gold surface, resulting in the detachment of the protein when the carrier (AuNP) enters the reducing cell environment. The specific delivery of the protein to certain cells can also be controlled by magnetic field, if the AuNP are substituted by gold coated magnetite nanoparticles, which above certain dimensions, display paramagnetic properties.

Concluding, this work brought further insight into UV-light activated mechanisms in Ca^{2+} depleted forms of LA, especially in what respects the breakage of SS bonds. In this form LA is not the best candidate for light-induced immobilization, since it is very unstable and susceptible to conformational changes.

BIBLIOGRAPHY

Acharya KR, Ren JS, Stuart DI, Phillips DC, Fenna RE. (1991) *Crystal structure of human alpha-lactalbumin at 1.7 A resolution*. J Mol Biol., **221**(2), 571-81.

Bain C.D., Troughton E.B., Tao Y.T., Evall J., Whitesides G.M. and Nuzzo R.G. (1989), *Formation of Monolayer Films by the Spontaneous Assembly of Organic Thiols from Solution onto Gold*. J. Am. Chem. Soc*.,* **111**, 321-335.

Boye J. I., I. Alli and A. A. Ismail. (1997). *Use of Differential Scanning Calorimetry and Infrared Spectroscopy in the Study of Thermal and Structural Stability of α-Lactalbumin*. J. Agric. Food Chem., **45**, 1116-1125

Brown R. J. and Ernstron C. A. (1982). *Incorporation of Ultrafiltration Concentrated Whey Solids into Cheddar Cheese for Increased Yield*. J. Dairy Sci., **65**, 2391-2395

Calderone V., M. G. Giuffrida, D. Viterbo, L. Napolitano, D. Fortunato, A. Conti, K. R. Acharya. (1996). *Amino acid sequence and crystal structure of buffalo α-lactalbumin.* FEBS Letters, **394**, 91-95

Canet D, K. Doering, C. M. Dobson, and Y. Dupont. (2001). *High-Sensitivity Fluorescence Anisotropy Detection of Protein-Folding Events: Application to α-Lactalbumin.* Biophysical Journal, **80**, 1996–2003

Chakraborty S., Ittah V., Bai P., Luo L., Haas E., Peng Z.Y. (2001) *Structure and dynamics of the alpha lactalbumin molten globule: fluorescence studies using proteins containing a single tryptophan residue*. Biochemistry, **40**, 7228–7238

Chang J-Y and Li L. (2001). *The Structure of Denatured a-Lactalbumin Elucidated by the Technique of Disulfide Scrambling.* The Journal of Biological Chemistry, **276**, 13, Issue of March 30, pp. 9705–9712

Chaplin L. C. and Lyster, R. L. J. (1986). *Irreversible heat denaturation of bovine α-lactalbumin*. Journal of Dairy Research, **53**, 249–258.

Chrysina E.D., K. Brew and K. R. Acharya. (2000). *Crystal structures of apo- and holo-bovine alpha-lactalbumin at 2.2-Å resolution reveal an effect of calcium on inter-lobe interactions.* J Biol Chem, **275**, 37021– 37029.

Creighton T. E. (1992) *Proteins: Structures and Molecular Properties*. W. H. Freeman; Second Edition

Cushing B. L., Kolesnichenko V. L., O'Connor C. J. (2004) *Recent advances in the liquid-phase syntheses of inorganic nanoparticles.* Chem. Rev., **104**, 3893-3946

Damodaran and Paraf (1997) *Food proteins and their applications*. Marcel Dekker Inc, New York

Delfino I., Cannistraro S. (2009) *Optical investigation of the electron transfer protein azurin–gold nanoparticle system*. Biophysical Chemistry, **139**, 1–7

Duroux M, E. Skovsen, M. T. Neves-Petersen, L. Duroux, L. Gurevich and S. B. Petersen. (2007). *Light-induced immobilisation of biomolecules as an attractive alternative to microdroplet dispensing-based arraying Technologies*. Proteomics, **7**, 3491–3499

Engel M. F. M., C. P. M. van Mierlo and A. J. W. G. Visser. (2002). *Kinetic and Structural Characterization of Adsorption-induced Unfolding of Bovine α-Lactalbumin.* The Journal of Biological Chemistry, **277**, 3, Issue of March 29, 10922–10930

Enüstün B. V., Turkevich J. (1963) *Coagulation of Colloidal Gold.* J. Am. Chem. Soc., **85** (21), 3317–3328

Fasman G. D. (1996) *Circular Dichroism and the Conformational Analysis of Biomolecules*. Springer

Fenemma O. (1996) *Food Chemistry.* Marcel Dekker Inc, New York

Fischer W., L. Gustafsson, A-K Mossberg, J. Gronli, S. Mork, R. Bjerkvig and C. Svanborg. (2004). *Human α-Lactalbumin Made Lethal to Tumor Cells (HAMLET) Kills Human Glioblastoma Cells in Brain Xenografts by an Apoptosis-Like Mechanism and Prolongs Survival*. Cancer Research, **64**, 2105–2112

Fu X. Y., Mueller D. M., and Heinecke J. W. (2002) *Generation of intramolecular and intermolecular sulfenamides, sulfinamides, and sulfonamides by hypochlorous acid: A potential pathway for oxidative cross-linking of low-density lipoprotein by myeloperoxidase*. Biochemistry, **41**, 1293-1301.

Gao C., R. Wijesinha-Bettoni, P. J. Wilde, E. N. C. Mills, L. J. Smith and A. R. Mackie. (2008). *Surface Properties Are Highly Sensitive to Small pH Induced Changes in the 3-D Structure of α-Lactalbumin.* Biochemistry, **47**, 1659-1666

Griko Y. V. and Remeta D. P. (1999). *Energetics of solvent and ligand-induced conformational changes in α-lactalbumin.* Prot Sci, **8**, 554–561.

Griko YV, Freire E, Privalov PL. (1994) *Energetics of the α-lactalbumin states: A calorimetric and statistical thermodynamic study*. Biochemistry, **33**, 1889-1899.

Harata K. and Muraki S. M. (1992). *X-ray Structural Evidence for a Local Helix-Loop Transition in α-Lactalbumin.* The Journal of Biological Chemistry, **267**, 3, 1419-1421

Hendrix T. M., Y. V. Griko and P.L. Privalov. (1996). *Energetics of structural domains in α-lactalbumin*. Prot Sci, **5**, 923–931.

Hollmann O., Steitz R., Czeslik C. (2008) *Structure and dynamics of α-lactalbumin adsorbed at a charged brush interface*. Phys. Chem. Chem. Phys.,**10**, 1448–1456

Hong Y-H and Creamer L. K. (2002). *Changed protein structures of bovine β-lactoglobulin B and α-lactalbumin as a consequence of heat treatment*. International Dairy Journal, **12** (2002) 345–359

Horng C-H, S. J. Demarest, and D. P. Raleigh. (2003) *pH-Dependent Stability of the Human α-Lactalbumin Molten Globule State: Contrasting Roles of the 6-120 Disulfide and the β-Subdomain at Low and Neutral pH.* PROTEINS: Structure, Function, and Genetics, **52**,193–202

Ikeguhi M., M. Fujino, M. Kato, K. Kuwajima and S. Sugai. (1998). *Transition state in the folding of α-lactalbumin probed by the 6-120 disulfide bond.* Protein Science, **7**, 1564-1574.

Kerwin B. A, and Remmele R. L. Jr. (2006). *Protect from Light: Photodegradation and Protein Biologics*. Journal of Pharmaceutical Sciences, **96**, 6, 1468-1479

Kim S. and Baum J. (1998). *Electrostatic interactions in the acid denaturation of α-lactalbumin determined by NMR.* Protein Science, **7**, 1930-1938.

Kuwajima K. (1996). *The molten globule state of α-lactalbumin*. FASEB J,**10**,102–109

Kuwajima K., Y. Ogawa, and S. Sugai. (1979). *Application of the pH-Jump Method to the Titration of Tyrosine Residues in Bovine α-Lactalbumin.* Biochemistry, 878

Kuwajima, K., Mitani M., Sugai, S. (1989) *Characterization of the critical state in protein folding. Effects of guanidine hydrochloride and specific Ca_2^+ binding on the folding kinetics of alpha-lactalbumin*. J Mol Biol., **206**(3), 547–561.

Lakowicz J. R. (2006). *Principles of Fluorescence Spectroscopy*. Springer, 3rd edition

Laureto P. P., E. Frare, R. Gottardo and A. Fontana. (2002). *Molten Globule of Bovine α-Lactalbumin at Neutral pH Induced by Heat, Trifluoroethanol, and Oleic Acid: A Comparative Analysis by Circular Dichroism Spectroscopy and Limited Proteolysis*. PROTEINS: Structure, Function, and Genetics, **49**, 385–397

Li A-J and Nussinov R. (1998). *A Set of van der Waals and Coulombic Radii of Protein Atoms for Molecular and Solvent-Accessible Surface Calculation, Packing Evaluation, and Docking.* PROTEINS: Structure, Function, and Genetics, **32**, 111–127

Macey M. (2007) *Flow Cytometry: Principles and Applications*. Humana Press; 1st edition

Masaki K., Masuda R., Takase K., Kawano K. and Nitta K. (2000) *Stability of the molten globule state of a domain-exchanged chimeric protein between human and bovine α-lactalbumins*. Protein Engineering, **1**, 1-4

Matsumura Y and Ananthaswamy H. N. (2004). *Toxic effects of ultraviolet radiation on the skin.* Toxicology and Applied Pharmacology, **195**, 298–308

McGuffey M. K., D. E. Otter, J. H. van Zanten and E. A. Foegeding. (2007) *Solubility and aggregation of commercial α-lactalbumin at neutral pH.* International Dairy Journal, **17**, 1168–1178

Mizuguchi M., D. Hashimoto, M. Sakurai and K. Nitta. (2000). *Cold Denaturation of α-Lactalbumin*. PROTEINS: Structure, Function, and Genetics, **38**, 407–413

Moriarty D.F., Demarest S.J., Robblee J., Fairman R., Raleigh D.P. (2000) *Local interactions and the role of the 6–120 disulfide bond in_α-lactalbumin: implications for formation of the molten globule state*. Biochim Biophys Acta,**1476**, 9–19.

Neves-Petersen M. T., M. Duroux, E. Skovsen, L. Duroux and S. B. Petersen. (2008) Journal of Nanoscience and Nanotechnology, in print.

Neves-Petersen M. T., S. Klitgaard, A. S. L. Carvalho, S. B. Petersen, M. R. A. de Barros and E. Pinho e Melo. (2007) *Photophysics and Photochemistry of Horseradish Peroxidase A2 upon Ultraviolet Illumination.* Biophysical Journal, **92**, 2016–2027

Neves-Petersen M. T., S. Klitgaard, E. Skovsen, T. Pascher, T. Polivka, A. Yartsev, V. Sundström and S. B. Petersen. (Paper submitted). *Flash photolysis of cutinase: identification and decay kinetics of transient intermediates formed upon UV excitation of aromatic residues*.

Neves-Petersen M. T., Z. Gryczynski, J. Lakowicz, P. Fojan, S. Pedersen, E. Petersen and S. B. Petersen. (2002). *High probability of disrupting a disulphide bridge mediated by an endogenous excited tryptophan residue.* Protein Sci., **11**, 588-600

Neves-Petersen M.T., Snabe T., Klitgaard S., Duroux M., Petersen S.B. (2006) *Photonic activation of disulfide bridges achieves oriented protein immobilization on biosensor surfaces.* Protein Sci., **15**, 343-51

Panda D. and Datta A. (2008) *Implications of Area Normalization of Multi-Component Spectra*. Appl. Spectrosc., **62**, 341-344

Parracino A., Prakash G., Kold A., Correia M., Neves-Petersen M.T., and Petersen S. B. (2008) *Novel photonic immobilisation technique provides a new approach to couple biomolecules onto superparamagnetic nanoparticles for nano-medical applications*.

Conference Talk, **NanoSMat 2008** - 3rd International Conference on Surfaces, Coatings and Nanostructured Materials

Pedersen J. B., P. Fojan, J. Sorensen and S. B. Petersen. (2006) *Towards Control of Aggregational Behaviour of α-Lactalbumin at Acidic pH.* J. Fluoresc., **16**, 611–621

Permyakov E. A. and Berliner L. J. (2000). *α-Lactalbumin: Structure and function*. FEBS Lett, **473**, 269–274.

Permyakov E. A., S. E. Permyakov, G. Y. Deikus, L. A. Morozova-Roche, V. M. Grishchenko, L. P. Kalinichenko and V. N. Uversky. (2003). *Ultraviolet Illumination-induced Reduction of α-Lactalbumin Disulfide Bridges.* PROTEINS: Structure, Function, and Genetics, **51**, 498–503

Petersen, M.T.N., Jonson, P.H., and Petersen, S.B. (1999) *Amino acid neighbours and detailed conformational analysis of cysteines in proteins.* Protein Eng. **12**, 535–548.

Pfeil W. (1998). *Is the molten globule a third thermodynamic state of proteins? The example of alpha-lactalbumin*. Prot Struct Funct Genet, **30**, 43–48

Pike A. C. W., K. Brew and K. R. Acharya1. (1996). *Crystal structures of guinea-pig, goat and bovine α-lactalbumin highlight the enhanced conformational flexibility of regions that are significant for its action in lactose synthase.* Structure, **4**, 691–703

Pöpp J. and Strelle M. (2008) *Biophotonics - Visions for Better Health Care*. Wiley-VCH, 1st edition

Pouët M., Baures E., Vaillant S., and Thomas O. (2004) *Hidden Isosbestic Point(s) in Ultraviolet Spectra*. Appl. Spectrosc., **58**, 486-490

Prasad N. (2003) Introduction to biophotonics. Wiley

Qasba P. K. and Kumar S. (1997). *Molecular Divergence of Lysozymes and α-Lactalbumin*. Critical Reviews in Biochemistry and Molecular Biology, **32**, 4, 255-306

Ramakrishnan B. and Qasba P. K. (2001). *Crystal Structure of Lactose Synthase Reveals a Large Conformational Change in its Catalytic Component, the b1,4-Galactosyltransferase-I.* J. Mol. Biol., **310**, 205-218

Riddles P. W., Blakeley R. L., Zerner B. (1983). *Reassessment of Ellman's reagent*. Meth. Enzymol., **91**: 49–60

Riener C. K., Kada G., Gruber H. J. (2002) *Quick measurement of protein sulfhydryls with Ellman's reagent and with 4,4'-dithiodipyridine*. Anal. Bioanal. Chem., **373**, 266–276

Sherin P. S., O. A. Snytnikova and Y. P. Tsentalovich. (2004). *Tryptophan photoionization from prefluorescent and fluorescent states*. Chemical Physics Letters, **391**, 44–49

Sherin P. S., Snytnikova O. A., Tsentalovich Y. P. (2006) *Competition between ultrafast relaxation and photoionization in excited prefluorescent states of tryptophan and indole*. The Journal OF Chemical Physics, **125**, 144511

Sinha R. P. and Häder D. P. (2002). *UV-induced DNA damage and repair: a review*. Photochem. Photobiol. Sci., **1**, 225–236

Skovsen E., M. T., Neves-Petersen, A. Kold, L. Duroux and S. B. Petersen. (2008) Journal of Nanoscience and Nanotechnology, in print.

Snabe T., Røder G. A., Neves-Petersen M. T., Buus S., Petersen S. B., (2006) *Oriented coupling of major histocompatibility complex (MHC) to sensor surfaces using light*

assisted immobilisation technology. Biosens. Bioelectron. 2006, **21**, 1553–1559

Snytnikova O. A., P. S. Sherin, L. V. Kopylova, and Y. P. Tsentalovich. (2007). *Kinetics and mechanism of reactions of photoexcited kynurenine with molecules of some natural compounds*. Russian Chemical Bulletin, International Edition, **56**, 4, 732—738

Sommers, P. B., and Kronman, M. J. (1980) *Comparative fluorescence properties of bovine, goat, human and guinea pig α-lactalbumin. Characterization of the environments of individual tryptophan residues in partial folding conformers*. Biophys. Chem.,**11**, 217-232.

Tarek M., D. A. Neumannb and D. J. Tobias. (2003) *Characterization of sub-nanosecond dynamics of the molten globule state of α-lactalbumin using quasielastic neutron scattering and molecular dynamics simulations.* Chemical Physics, **292**, 435–443

Templeton A.C., Cliffel D.E., and Murray R.W. (1999) *Redox and Fluorophore Functionalization of Water-Soluble, Tiopronin-Protected Gold Clusters.* J. Am. Chem. Soc., **121**, 7081-7089

Tsodikov O. V., M. T. Jr. Record, and Y. V. Sergeev. (2002*). A novel computer program for fast exact calculation of accessible and molecular surface areas and average surface curvature.* J. Comput. Chem., **23**, 600-609.

Van Dael H., A. Chedad, A. Vanhooren and I. Hanssens (2005). *Influence of experimental conditions and Trp mutations on the stability and the folding characteristics of goat α-lactalbumin.* Journal of Molecular Structure, **744–747**,155–160

Vanderheeren G. and Hanssens I. (1994) *Thermal Unfolding of Bovine α-Lactalbumin. Comparison of circular dichroism with hydropphobicity measurements*. The journal of Biological Chemistry, **269**, 10, 7090-7094

Vanhooren A., B. Devreese, K. Vanhee, J. Van Beeumen and I. Hanssens. (2002). *Photoexcitation of Tryptophan Groups Induces Reduction of Two Disulfide Bonds in Goat α-Lactalbumin*. Biochemistry, ***41,*** 11035-11043

Vanhooren A., Chedad A., Farkas V., Majer Z., Van Dael H., Joniau M., Hanssens I., (2005) *Tryptophan to phenylalanine substitution allows to differentiate between short and long range conformational changes during denaturation of goat α-lactalbumin*. Proteins, **60**, 118–130

Vanhooren A., E. Illyes, Z. Majer and I. Hanssens. (2006**b**). *Fluorescence contributions of the individual Trp residues in goat α-lactalbumin*. Biochimica et Biophysica Acta, **1764**, 1586–1591

Vanhooren A., K. De Vriendt, B. Devreese, A. Chedad, A. Sterling, H. Van Dael, J. Van Beeumen and I. Hanssens. (2006**a**). *Selectivity of Tryptophan Residues in Mediating Photolysis of Disulfide Bridges in Goat α-Lactalbumin*. Biochemistry, **45**, 2085-2093

Veprintsev D.B., S. E. Permyakov, E. A. Permyakov, V. V. Rogov, K. M. Cawtherm and L. J. Berliner. (1997). *Cooperative thermal transitions of bovine and human apo-lactalbumins: evidence for a new intermediate state*. FEBS Lett, **412**, 625–628.

Walker J. M. (2005) *The Proteomics Protocols Handbook*, Humana Press, 571-607

Wang Q., A. Tolkach and U. Kulozik. (2006). *Quantitative Assessment of Thermal Denaturation of Bovine α-Lactalbumin via Low-Intensity Ultrasound, HPLC, and DSC.* J. Agric. Food Chem., **54**, 6501-6506

Wijesinha-Bettoni R, C. M. Dobson and C. Redfield. (2001). *Comparison of the structural and dynamical properties of holo and apo bovine alpha-lactalbumin by NMR spectroscopy.*

JMol Biol, **307**, 885–898.

Wijesinha-Bettoni R., C. Gao, J. A. Jenkins, A. R. Mackie, P. J. Wilde, E. N. C. Mills and L. J. Smith. (2007). *Heat Treatment of Bovine α-Lactalbumin Results in Partially Folded, Disulfide Bond Shuffled States with Enhanced Surface Activity*. Biochemistry, **46**, 9774-9784

Wilson G., S. J. Ford, A. Cooper, L. Hecht, Z. Q. Wen and L. D. Barron. (1995). *Vibrational Raman Optical Activity of a-Lactalbumin: Comparison with Lysozyme, and Evidence for Native Tertiary Folds in Molten Globule States*. J. Mol. Biol., **254**, 747–760

Wit J. N. and Klarenbeek, G. (1984). *Effects of various heat treatments on structure and solubility of whey proteins*. Journal of Dairy Science, **67**, 2701–2710.

Wu L. C. and Kim P.S. (1998). *A Specific Hydrophobic Core in the α-Lactalbumin Molten Globule*. J. Mol. Biol., **280**, 175-182

Wu, L. C., Peng, Z., and Kim, P. S. (1995) *Bipartite structure of the α-lactalbumin molten globule*. *Nature Struct. Biol.* 2, 28 1-286

Zhang J. and Lakowicz J. R. (2007) *Metal-enhanced fluorescence of an organic fluorophore using gold particles*. Opt. Express, **15**, 2598-2606

APPENDIX

A. DENATURATION OF PROTEINS

The denaturation processes of proteins are frequently used as simplified situations for the analysis of phenomena such as protein stability, folding, and unfolding. Indeed, denaturation appears like an unfolding process, reversal occurring when refolding takes place, and can be use to mimic such mechanisms.

The denaturation generally is considered like a two-state sharp transition from native (N) to denaturated (D) protein, where the structure of the protein is disordered under a certain stress (*e.g.* heat, mild denaturant like urea), and its functionality can be remarkably lost.

This is simplistic description of the process that does not consider the eventual intermediate transitions occurring during protein denaturation. At any instant of time a protein molecule in population of an unfolding protein has a unique conformation which is not static, but constantly being altered by rotation around single bounds. The kinetic pathways of unfolding and refolding process in denaturation phenomenon can be determined by which intermediate conformational state (I_i) the molecule passes through, where the reaction can be described as a succession of transitions, as it can be depicted in Figure A1.

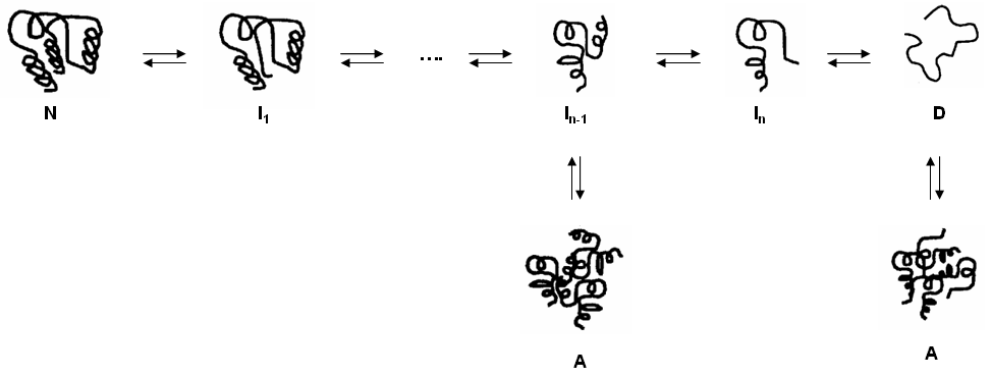

Figure A1: Schematic representation of the kinetic pathways of unfolding and folding in a denaturation process. The states are pictured as a hypothetic protein during its unfolding. Letters: N – native protein; I_i – intermediate species; D – denaturated form; A – state of aggregation.

The general picture given by Figure A1 can be further explored, and simplified for specific cases. Along the process, denaturation can be reversible or irreversible, depending on the transient state where the defolding is, *i.e.* if the reverse path is still energetically viable. Some of intermediates are also stable enough and can exist in equilibrium states. The extent of denaturation can be also variable, affecting largely or not the structure of the protein (on the

quaternary, tertiary, secondary structure), is it confined to a region specific region and resulting only on the partial unfolding of the protein, or involving the complete molecule.

The denaturation can also consist in a “all-or-none” reaction that shows cooperativity nature, or in a more confusing process where the transition is not defined from molecule to molecule in the pool of denaturating species generating even diverse intermediate forms. In a cooperative unfolding there will be no partially unfolded molecules in the set, since structures that exist partly intact or partly are not thermodynamically stable and only exist transiently. In this case the denaturation process can be really approximated to a two-state unfolding (taking place from the native or a transient thermodynamically stable specie to the denatured final form or stable denaturated specie).

Though each protein possesses a unique native three-dimensional structure, the same protein can also adopt several different structures according to the type and extent of denaturating treatment.

Aggregated species (A) may also be formed at different steps of the process, either in the case stable intermediate (due mainly to hydrophobic interactions between exposed hydrophobic groups during denaturation), or in the advent of the denaturated form (disulphide and hydrogen bonding, as ionic forces are responsible for bonding (Damodaran and Paraf, 1997).

Thus, each case must be separately considered, and specific models of defolding must be for the protein in study.

The analysis of denaturation processes is clearly an important issue. Usually, a physical or chemical property of the protein that is related with its structure is measured along an increase in the denaturating conditions (for instance a denaturant concentration or temperature). The property can indicate the local unfolding of a protein, like the fluorescence emission of the protein chromophores (using fluorescence spectroscopy), or the global unfolding of the protein, accessed for instance with the ellipticity measured at far-UV (using circular dichroism spectroscopy), helpful in characterizing of the peptide bond in proteins. In that way a profile can be obtained that describes the denaturating process, and the eventual changes in protein structure, along the diverse intermediates formed. The typical profiles for a two-state denaturation showing cooperativity are illustrated in Figure A2. They show the shift in signal (y) when one pass from a native specie (y'_N and y_N) to a denaturated form (y'_D and y_D), signal this that characterizes a part of the structure and its shift in position.

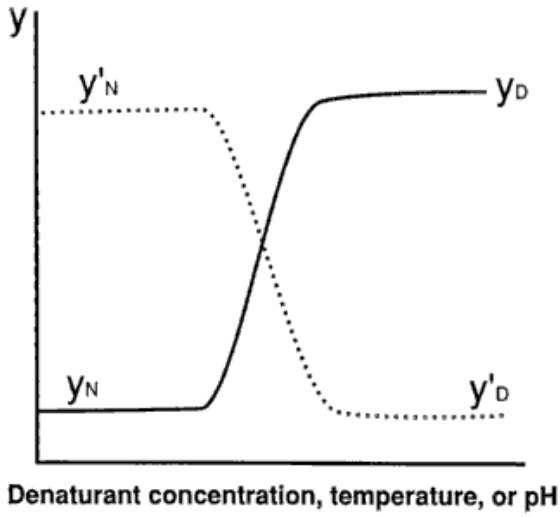

Figure A2: Typical protein denaturation curves; *y* represents any measurable physical or chemical property of the protein that varies with protein conformation; y_N and y_D are the values for the native and denaturated state respectively (Adapted from Fenemma, 1996).

It is also important to notice that monomeric proteins that contain two or more domains with different properties may exhibit multiple transition steps in a unfolding profile.

The denaturation curves further allow the quantification of the denaturation process. When cooperativity is present in a transition between two species, the "two-state transition" model can be applied. For this model the equilibrium between the native and the denaturated state in the cooperative transition region can be expressed as:

$$N \underset{}{\overset{K_D}{\rightleftharpoons}} D \qquad \text{(A.1)}$$

$$K_D = [D]/[N] \qquad \text{(A.2)}$$

where K_D is the equilibrium constant. Since the concentration of denaturated protein molecules in the absence of a denaturant is extremely low, estimation of this constant is not possible. However, in the transition region, where the concentration of denaturant is sufficiently high, an increase in the population of denaturated protein specie allows the determination of the apparent equilibrium constant, K_{app}. In the transition region, where both native and denaturated protein species are present, the value of *y* is given by:

$$y = f_N y_N + f_D y_D \qquad \text{(A.3)}$$

where *fn* and *fd* are the fractions of the protein in the native and denaturated state, and y_N and y_D are y values for the native and denaturated states respectively. From Figure A2 one can deduce the values of each fraction (here is considered that the denaturated specie has a higher signal, the inverse would imply the correspondent calculations):

$$f_N = (y_D - y)/(y_D - y_N) \quad \text{(A.4)}$$

$$f_D = (y - y_N)/(y_D - y_N) \quad \text{(A.5)}$$

Since the fractions of denaturant and native protein are correspondent to their concentrations, the apparent equilibrium constant is then obtained by:

$$K_{app} = f_D / f_N = (y - y_N)/(y - y_D) \quad \text{(A.6)}$$

The free energy of denaturation is finally given by:

$$\Delta G_{app} = -RT \ln K_D \quad \text{(A.7)}$$

R is the perfect gas constant in J.mol^{-1}.K^{-1}, T temperature in K. A plot of $-RT \ln K_D$ versus denaturant signal (concentration, temperature, pH) results in a straight line. The value of mid-transition is the value for which the free energy of denaturation ΔG_{app} is zero, *i.e.* at equilibrium.

In the case of chemical denaturants, the enthalpy of change ΔH_D can be obtained from the variation of the free energy change with temperature using the Van't Hoff equation.

$$\Delta H_D = -R \frac{d \ln K_D}{d(1/T)} \quad \text{(A.7)}$$

One can compare the process under different conditions (which would rely on a variable distinct from the responsible for denaturation) by means of the value at mid-transition, is it the temperature of mid-transition (T_m), concentration of denaturant at mid-transition (C_m), or pH of mid-transition (pH_m). The value of mid-transition will then one for which in the set of proteins in analysis, half of them are still in the original state and half of them in the denaturated one. One classical example is the melting temperature, or denaturation temperature (T_d), which is simply the T_m for proteins and other biomolecules that present a two-state sharp thermal transition (from the N-state to the D-state). It is often used characterize the thermal denaturation of several enzymes and proteins, and other biomolecules, like for instance the DNA on its denaturation from double to single chain (Damodaran and Paraf, 1997; Fenemma, 1996).

B. SUPPLEMENTARY RESULTS

Time-dependent Disruption of Disulphide Bridges

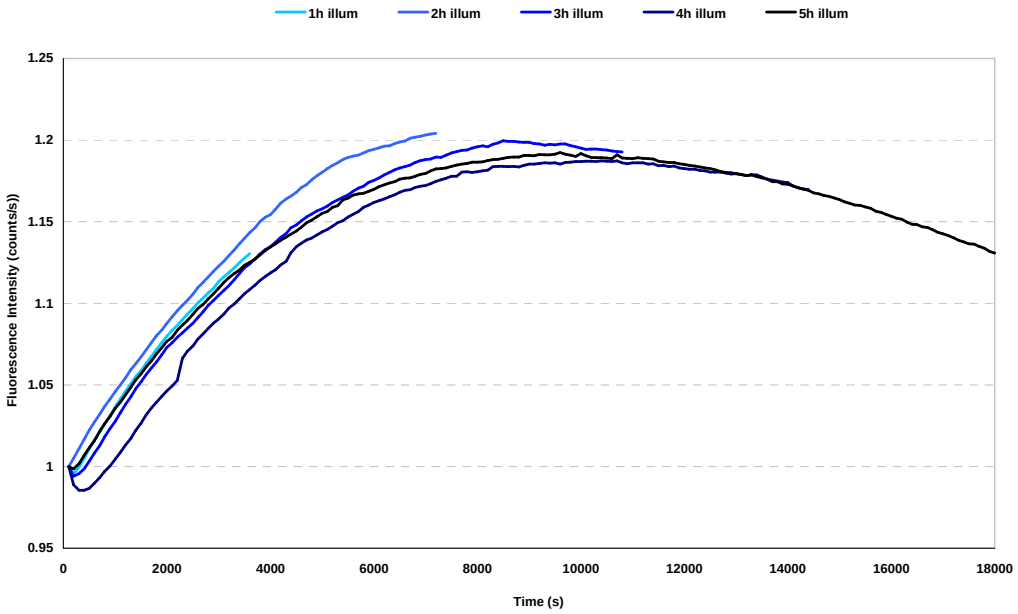

Figure B.1: Fluorescence intensity of eLA *versus* illumination time in the diverse irradiation sessions (1-, 2-, 3-, 4-, and 5-h). Excitation was fixed at 295 nm and emission was monitored at 340 nm. Temperature was maintained at 25ºC using a peltier element. Measurements were performed using a RTC 2000 PTI spectrofluorimeter. The curves were normalized and corrected for the oscillations of lamp intensity as described in Materials and Methods (Section 5.2).

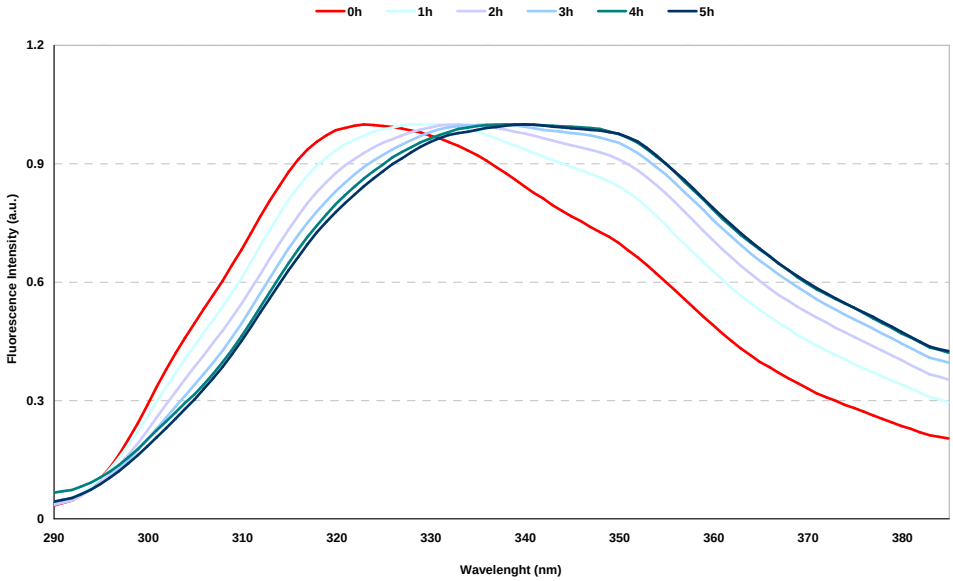

Figure B.2: Normalized emission spectra of illuminated samples of eLA over different time periods and non-illuminated eLA. Excitation was realized at 280 nm. The spectra were first smoothed and normalized as described in Materials and Methods (section 5.2).

Figure B.3: Corrected absorbance spectra recorded after 22 minutes of reaction between irradiated (1-, 2-, 3-, 4-, and 5-h) and non-irradiated (0h) eLA and DTNB. The correction was realized by subtracting the experimentally obtained spectra and the spectra for the reagent blanks, enlighten by colored dashes in the Plot. The characteristic peak at 412 nm can be noticed for the irradiated samples, while for the non-irradiated sample, no peak is visible, the value at 412 nm being merely residual.

Influence of temperature in the time-dependent fluorescence emission of eLA - Fitting Results

9.3 ºC

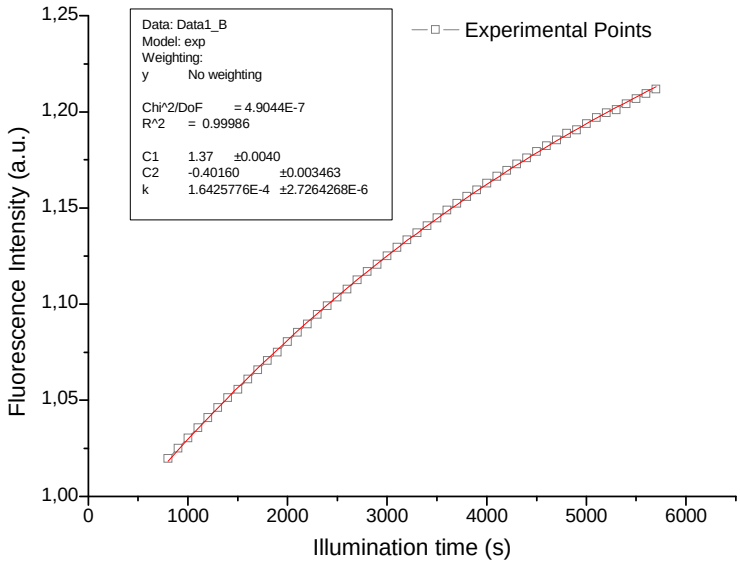

Figure B.4: Fitting curve obtained for fluorescence time-dependent intensity at 340 nm upon irradiation with 295 nm UV-light for 9.3 ºC (red). The experimental points are also displayed (squares). In the box are presented the fitting parameters, correspondent errors, mean square error, and chi square error.

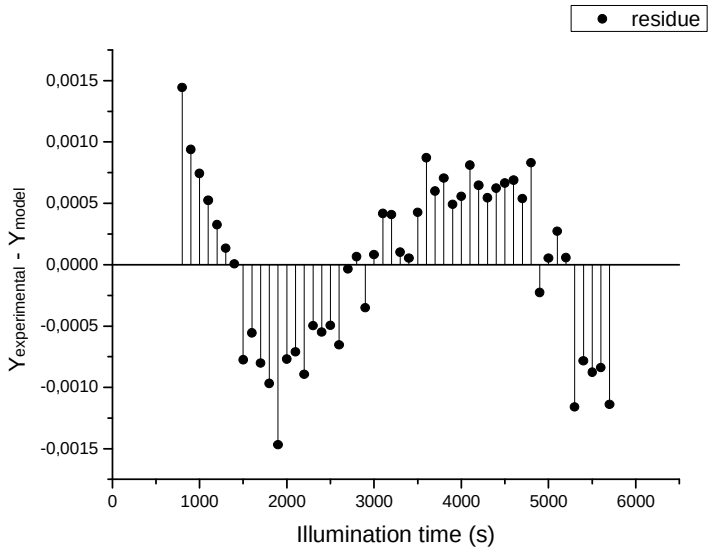

Figure B.5: Residual Plot obtained for the fitting of the fluorescence time-dependent intensity curve obtained at 9.3 ºC. Each residue corresponds on the difference between the experimental point and the value predicted by the model.

12.9 ºC

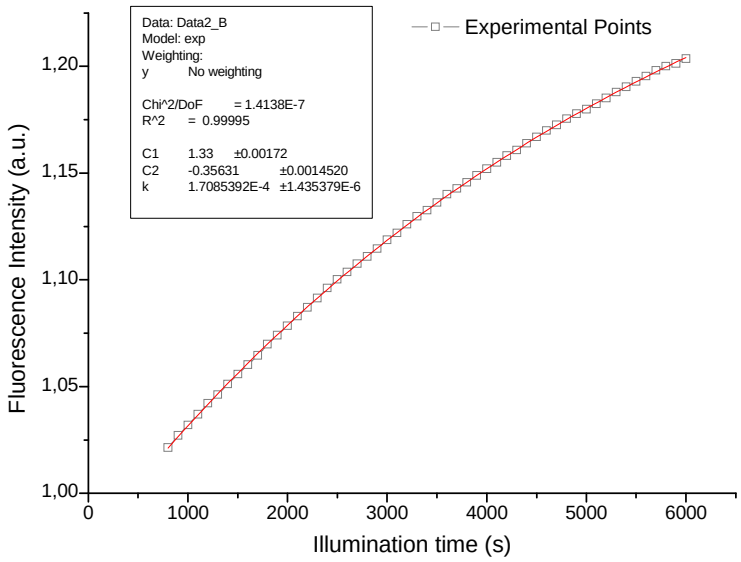

Figure B.6: Fitting curve obtained for fluorescence time-dependent intensity at 340 nm upon irradiation with 295 nm UV-light for 12.9 ºC (red). The experimental points are also displayed (squares). In the box are presented the fitting parameters, correspondent errors, mean square error, and chi square error.

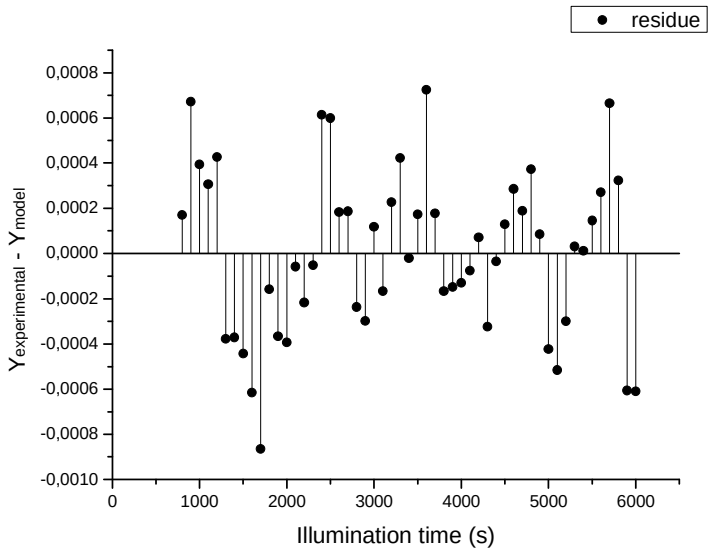

Figure B.7: Residual Plot obtained for the fitting of the fluorescence time-dependent intensity curve obtained at 12.9 ºC. Each residue corresponds on the difference between the experimental point and the value predicted by the model.

15.6 ºC

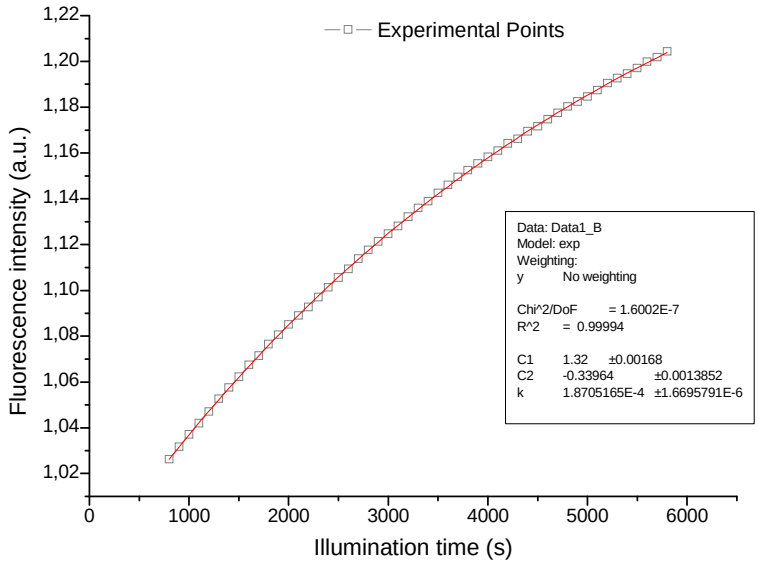

Figure B.8: Fitting curve obtained for fluorescence time-dependent intensity at 340 nm upon irradiation with 295 nm UV-light for 15.6 ºC (red). The experimental points are also displayed (squares). In the box are presented the fitting parameters, correspondent errors, mean square error, and chi square error.

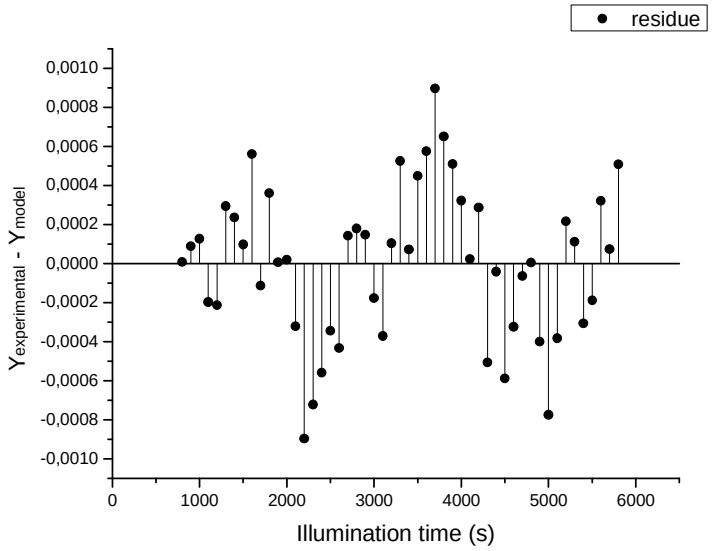

Figure B.9: Residual Plot obtained for the fitting of the fluorescence time-dependent intensity curve obtained at 15.6 ºC. Each residue corresponds on the difference between the experimental point and the value predicted by the model.

20.4 ºC

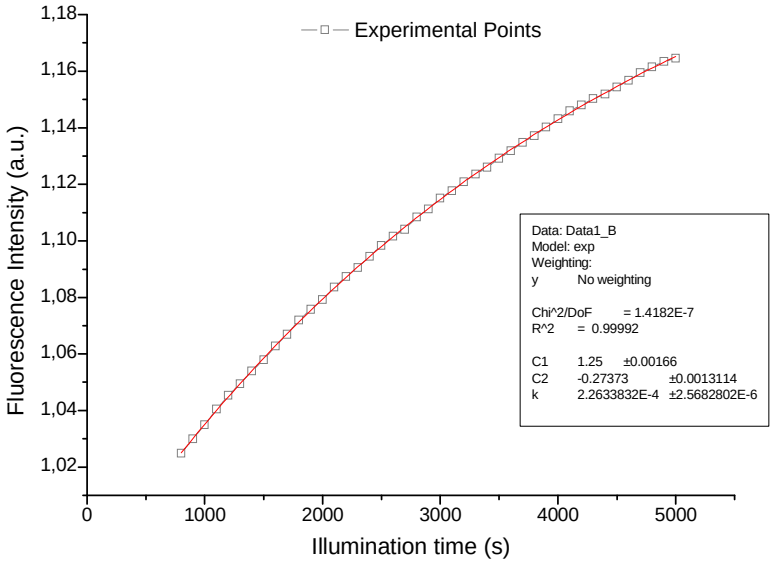

Figure B.10: Fitting curve obtained for fluorescence time-dependent intensity at 340 nm upon irradiation with 295 nm UV-light for 20.4 ºC (red). The experimental points are also displayed (squares). In the box are presented the fitting parameters, correspondent errors, mean square error, and chi square error.

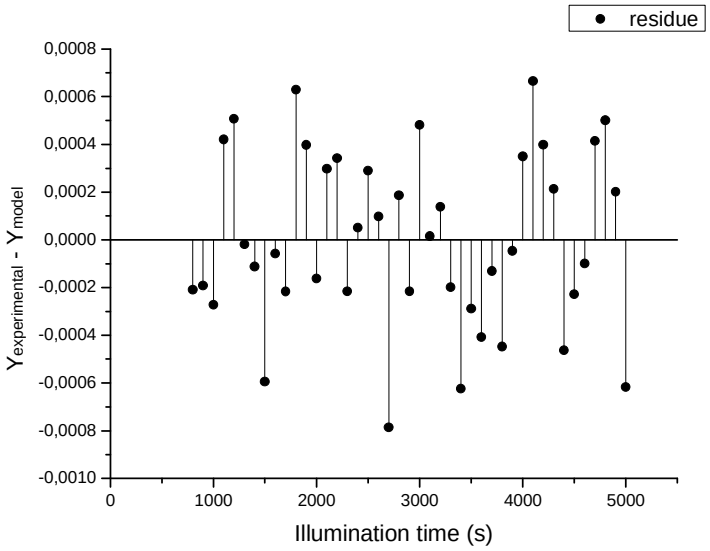

Figure B.11: Residual Plot obtained for the fitting of the fluorescence time-dependent intensity curve obtained at 20.4 ºC. Each residue corresponds on the difference between the experimental point and the value predicted by the model.

24.9 ºC

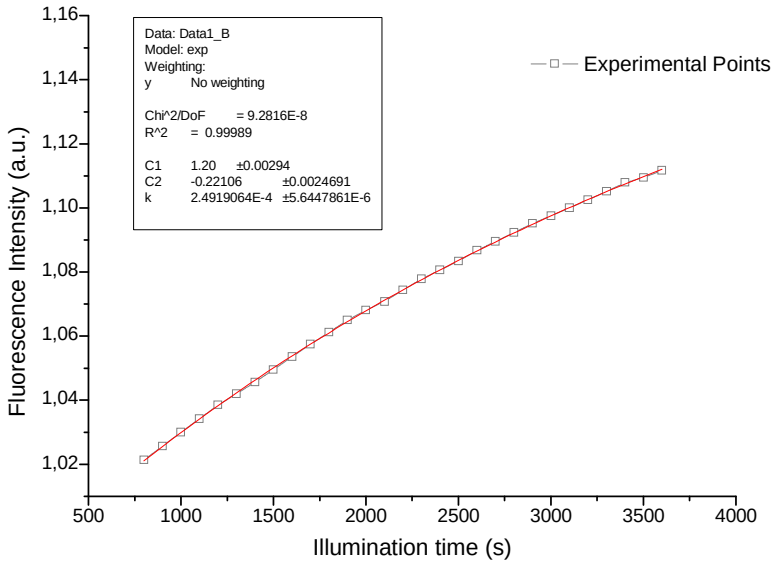

Figure B.12: Fitting curve obtained for fluorescence time-dependent intensity at 340 nm upon irradiation with 295 nm UV-light for 24.9 ºC (red). The experimental points are also displayed (squares). In the box are presented the fitting parameters, correspondent errors, mean square error, and chi square error.

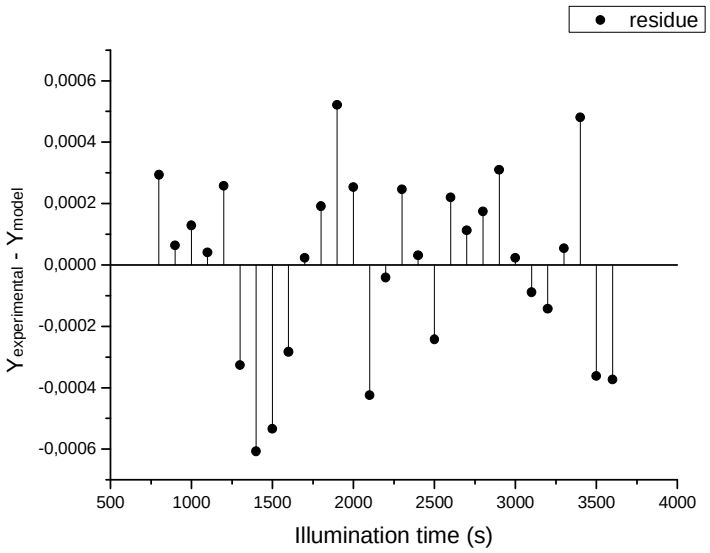

Figure B.13: Residual Plot obtained for the fitting of the fluorescence time-dependent intensity curve obtained at 24.9 ºC. Each residue corresponds on the difference between the experimental point and the value predicted by the model.

29.9 ºC

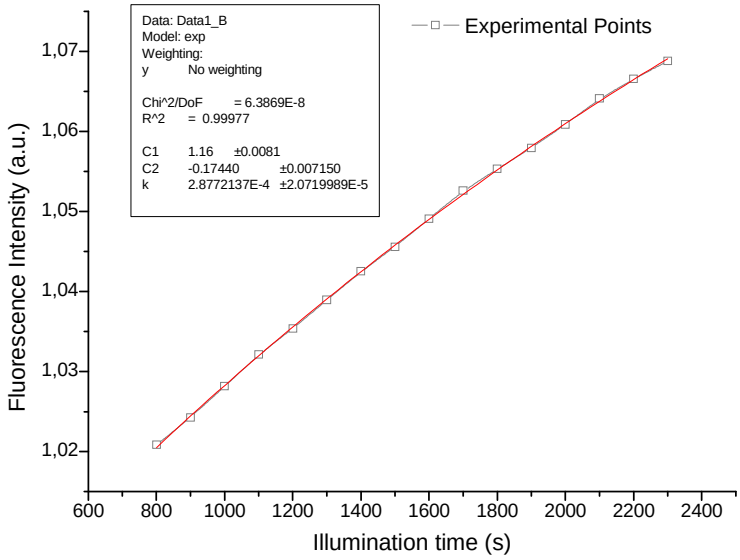

Figure B.14: Fitting curve obtained for fluorescence time-dependent intensity at 340 nm upon irradiation with 295 nm UV-light for 29.9 ºC (red). The experimental points are also displayed (squares). In the box are presented the fitting parameters, correspondent errors, mean square error, and chi square error.

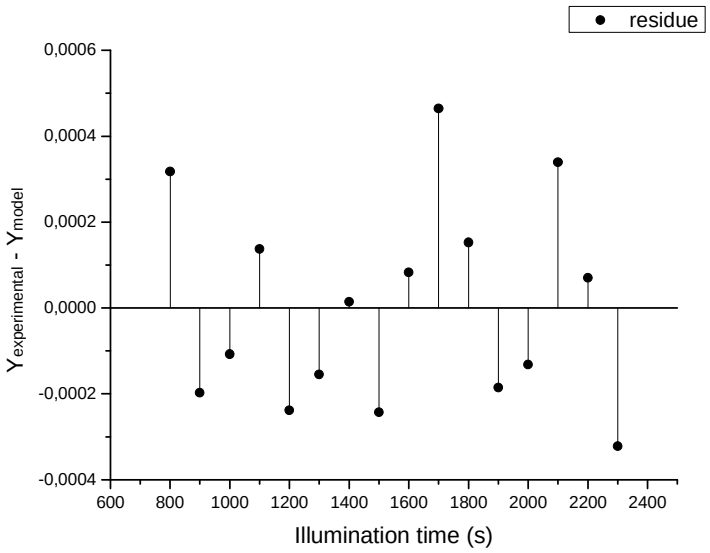

Figure B.15: Residual Plot obtained for the fitting of the fluorescence time-dependent intensity curve obtained at 29.9 ºC. Each residue corresponds on the difference between the experimental point and the value predicted by the model.

Influence of temperature in the time-dependent fluorescence emission of eLA – Emission Spectra

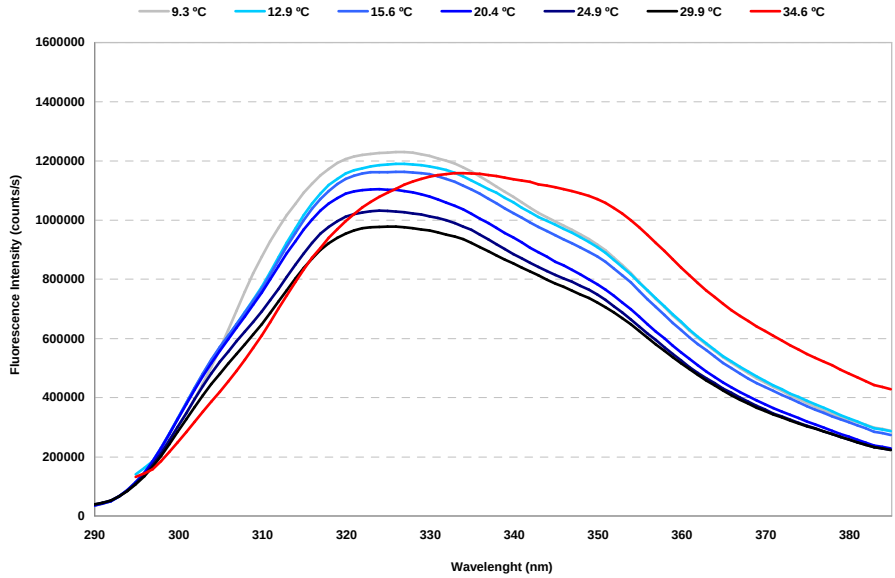

Figure B.16: Emission spectra of non-illuminated eLA at different temperatures (9.3, 12.9, 15.6, 20.4, 24.9, 29.9 and 34.6ºC). Solution temperature was previously set using the peltier element. Excitation was realized at 280 nm. The spectra were first smoothed as described in Materials and Methods (section 5.2).

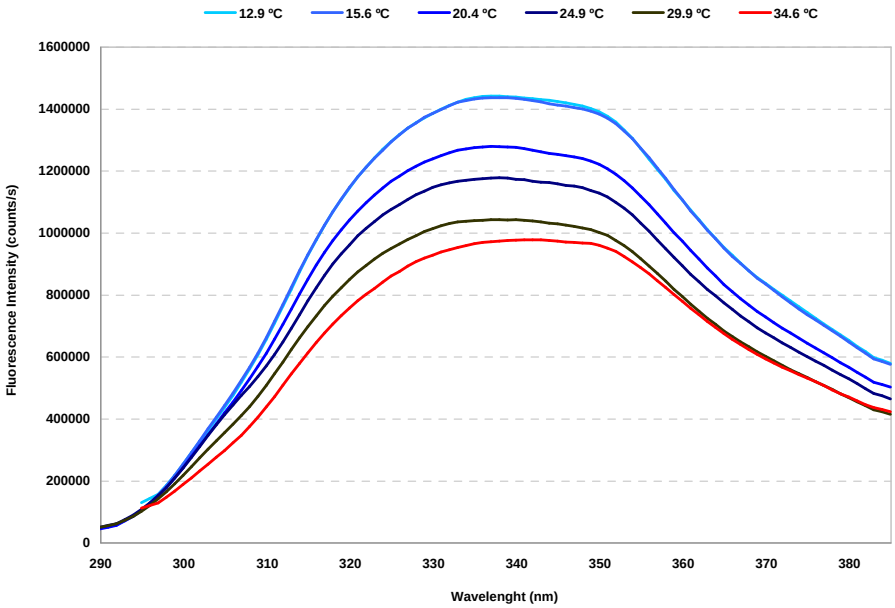

Figure B.17: Emission spectra of eLA recorded after 3.5h of 295 nm light irradiation at different temperatures (12.9, 15.6, 20.4, 24.9, 29.9 and 34.6ºC). Excitation was realized at 280 nm and the temperature of the solution was still maintained after the precedent irradiation and during recording of the spectra. The spectra were first smoothed as described in Materials and Methods (section 5.2).

Influence of pH in the time-dependent fluorescence emission of eLA

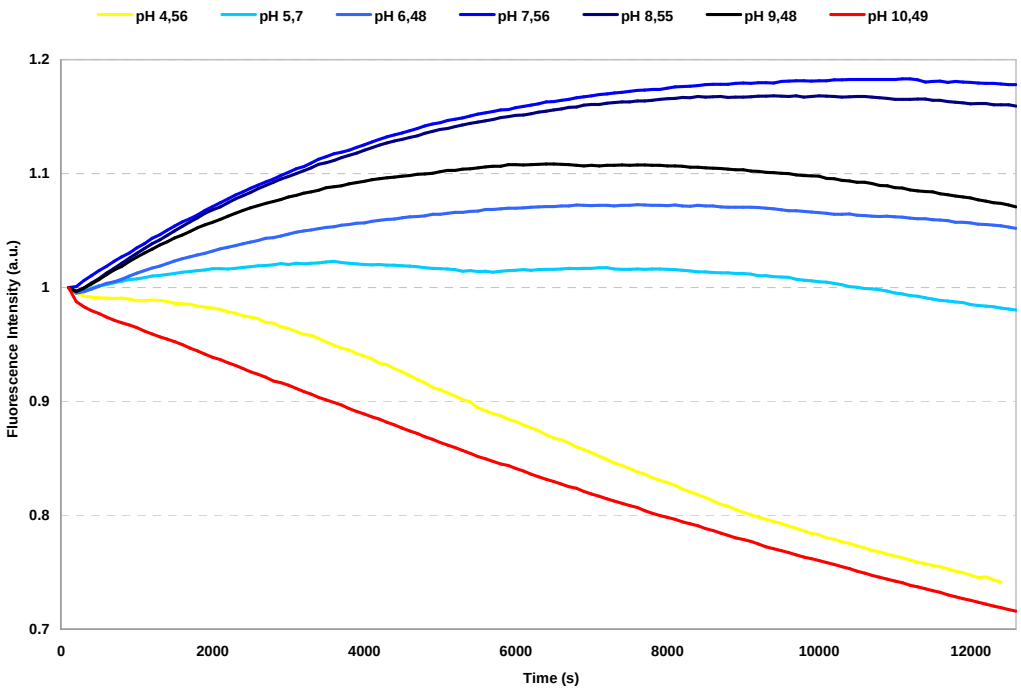

Figure B.18: Fluorescence intensity of Bα-L in function of the illumination time at pH values (4.56, 5.7, 6.48, 7.56, 8.55, 9.48, and 10.49). Excitation was realized at 295 nm and emission measured at 340 nm. Measurements were effectuated using a PTI spectrofluorimeter during 3.5 hours. The temperature of the solution was maintained constant using a Peltier element. The curves were normalized and corrected for the oscillations of lamp intensity as described in Materials and Methods (Section 5.2).

Temperature Influence on Fluorescence Emission

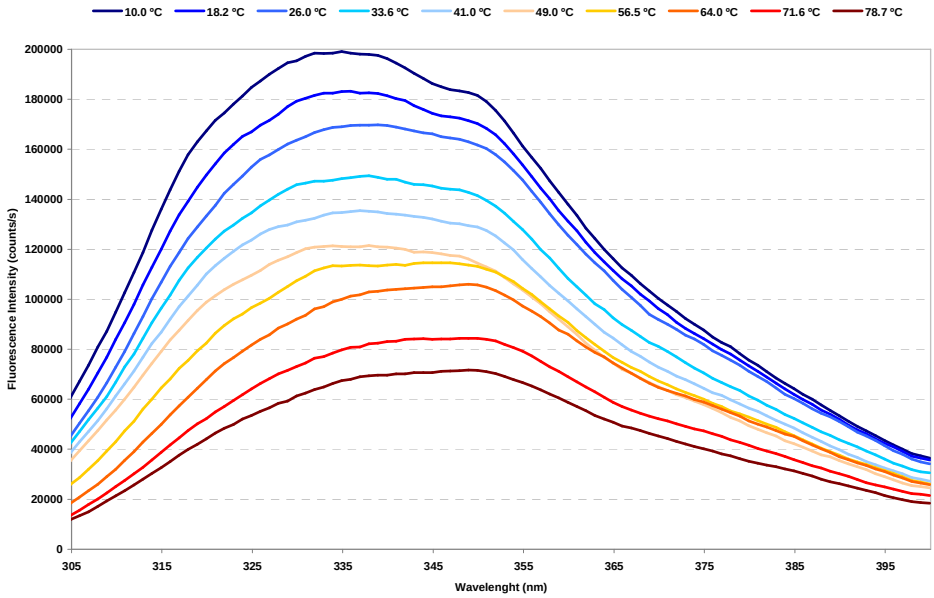

Figure B.19: Emission spectra of fresh eLA solutions recorded at different temperatures (10.0, 18.2, 26.0, 33.6, 41.0, 49.0, 56.5, 64.0, 71.6, and 78.7 ºC). Excitation was realized at 295 nm and the temperature of the solution was set before the recording of the spectra and during the short irradiation. The spectra were smoothed as described in Materials and Methods (section 5.2).

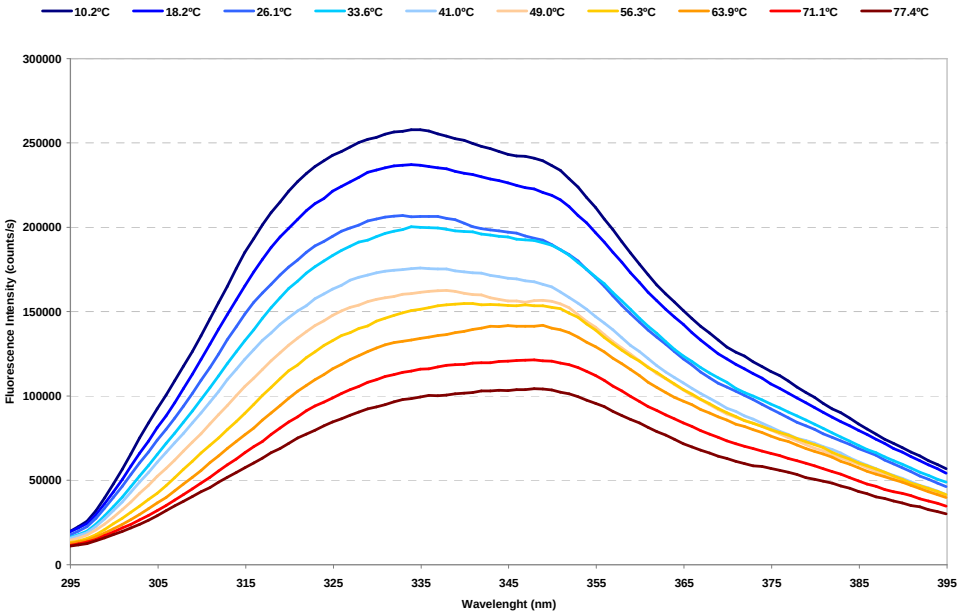

Figure B.20: Emission spectra of fresh eLA solutions recorded at different temperatures (10.2, 18.2, 26.1, 33.6, 40.9, 49.4, 56.3, 63.9, 71.1, and 77.4 ºC). Excitation was realized at 280 nm and the temperature of the solution was set before the recording of the spectra and during the short irradiation. The spectra were smoothed as described in Materials and Methods (section 5.2).

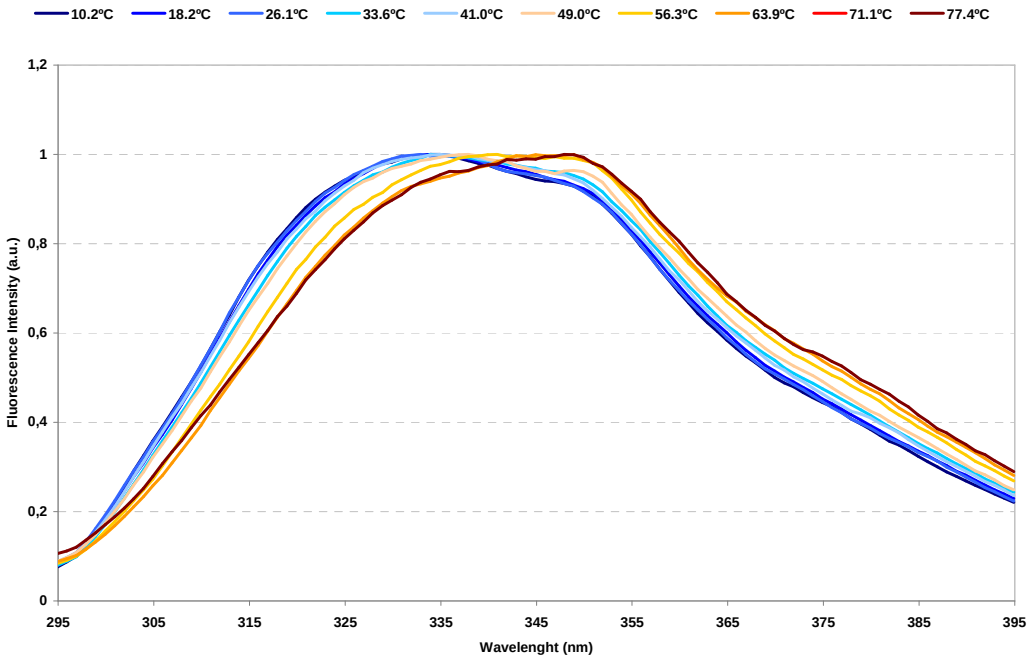

Figure B.21: Normalized emission spectra of fresh eLA solutions recorded at different temperatures (10.2, 18.2, 26.1, 33.6, 40.9, 49.4, 56.3, 63.9, 71.1, and 77.4 ºC). Excitation was realized at 280 nm and the temperature of the solution was set before the recording of the spectra and during the short irradiation. The spectra were smoothed and normalized as described in Materials and Methods (section 5.2).

Immobilization Procedure

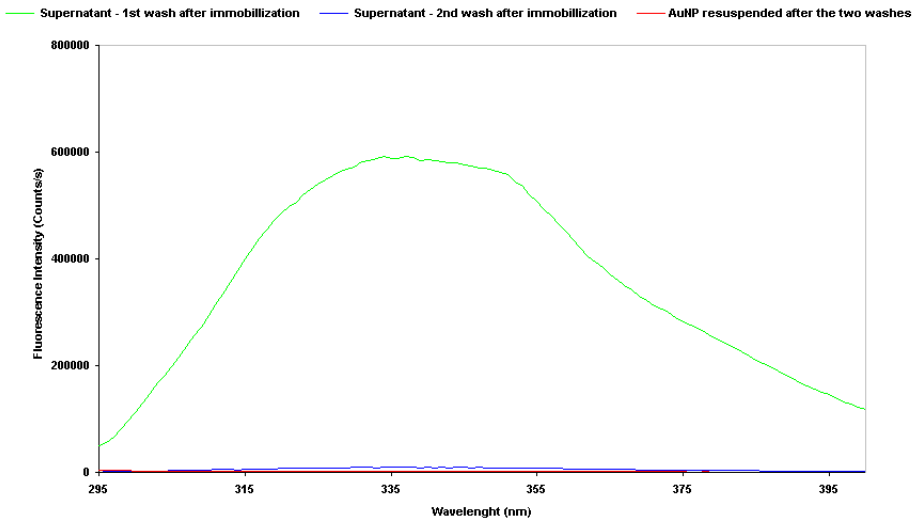

Figure B.22: Emission spectra of the supernatants of the two washes and the final resuspended AuNP solution. The spectra are corrected for *Raman contribution*. The spectra were recorded in a PTI spectrofluorimeter as previously described in Materials and Methods (Section 6.2)

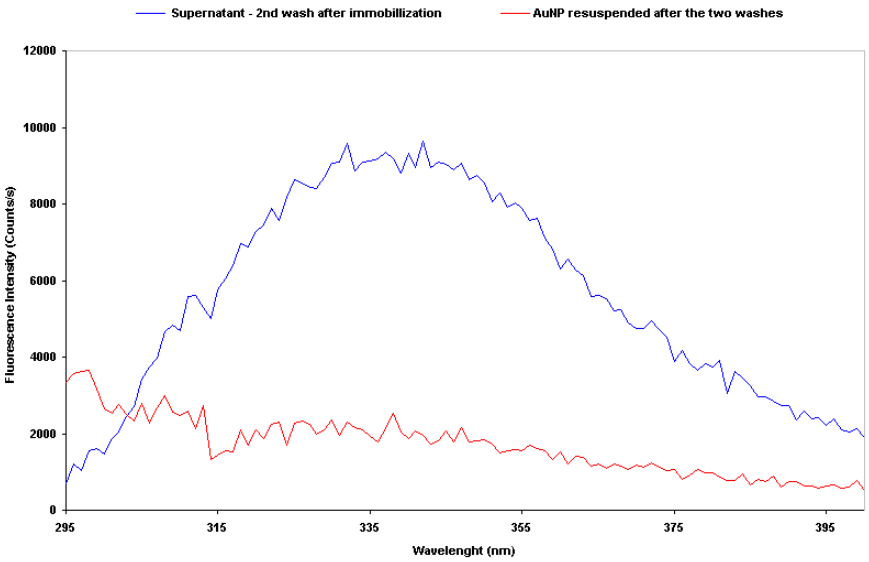

Figure B.23: Emission spectra of the supernatants of the second wash and the final resuspended AuNP solution. The spectra are corrected for *Raman contribution*. The spectra were recorded in a PTI spectrofluorimeter as previously described in Materials and Methods (Section 6.2)

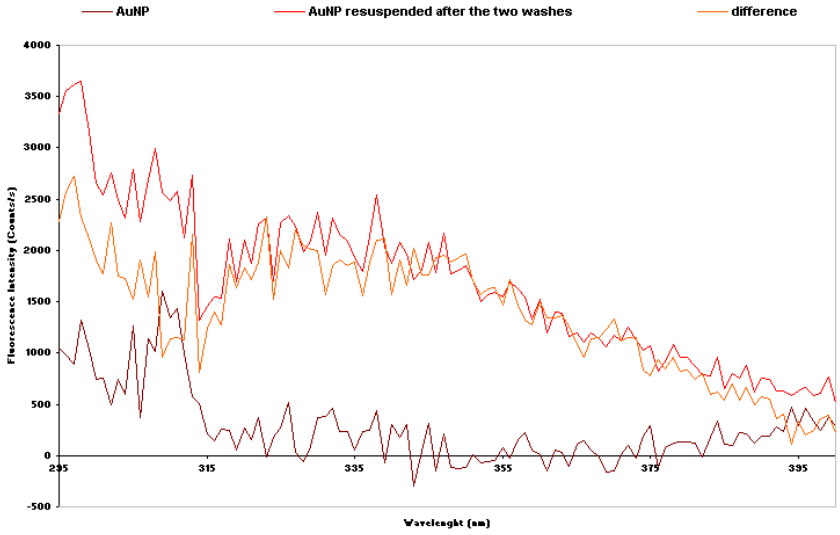

Figure B.24: Emission spectra of the final resuspended AuNP solution, a fresh solution of AuNP and the difference between them. The spectra are corrected for *Raman contribution*. The spectra were recorded in a PTI spectrofluorimeter as previously described in Materials and Methods (Section 6.2)

		Diam. (nm)	% Intensity	Width (nm)
Z-Average (d.nm): 22,86	Peak 1:	50,37	82,4	19,64
PdI: 0,596	Peak 2:	3,398	17,6	1,059
Intercept: 0,820	Peak 3:	0,000	0,0	0,000

Result quality : Refer to quality report

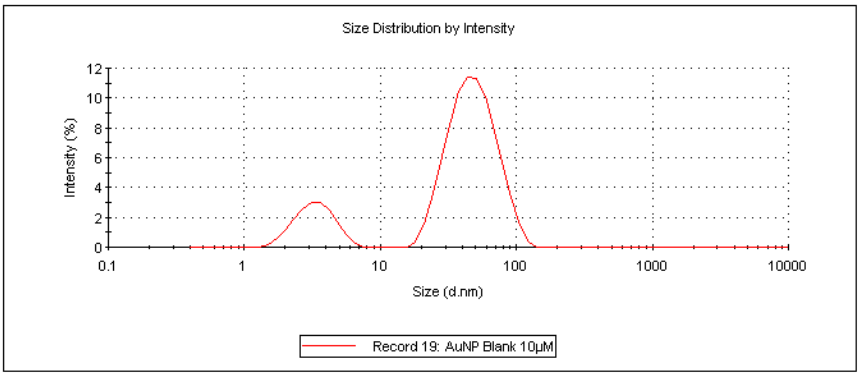

Figure B.25: Size distribution by Intensity. The intensity is related to the number of measurements that originated a peak with for a certain particle size. A strong intensity means that in solution is present a considerable amount of molecules with the particular size where the peak is centered. Results obtained for a AuNP fresh solution of 10 µM. The dynamic light scattering measurements were realized in a Zeta Sizer NANO ZS as described in Materials and Methods (section 6.2).

		Diam. (nm)	% Intensity	Width (nm)
Z-Average (d.nm): 34,01	Peak 1:	72,10	85,0	29,98
PdI: 0,622	Peak 2:	5,477	15,0	1,976
Intercept: 0,667	Peak 3:	0,000	0,0	0,000

Result quality : Refer to quality report

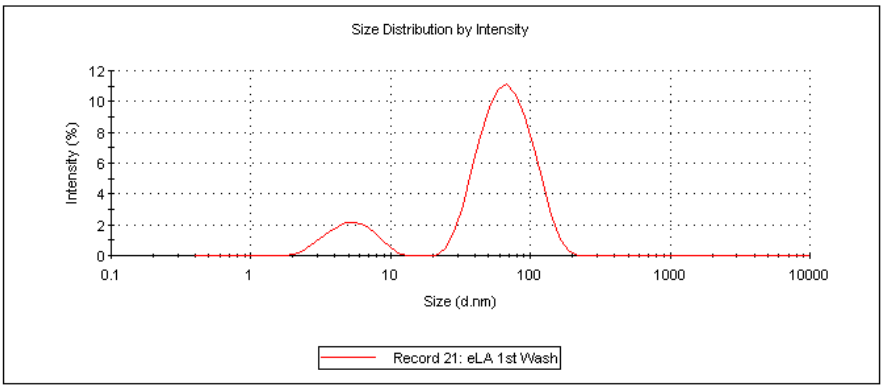

Figure B.26: Size distribution by Intensity. The intensity is related to the number of measurements that originated a peak with for a certain particle size. A strong intensity means that in solution is present a considerable amount of molecules with the particular size where the peak is centered. Results obtained for the supernatant of the first wash. The dynamic light scattering measurements were realized in a Zeta Sizer NANO ZS as described in Materials and Methods (section 6.2).

			Diam. (nm)	% Intensity	Width (nm)
Z-Average (d.nm):	25,90	Peak 1:	50,81	86,3	20,84
PdI:	0,579	Peak 2:	3,767	13,7	1,170
Intercept:	0,829	Peak 3:	0,000	0,0	0,000
Result quality :	Refer to quality report				

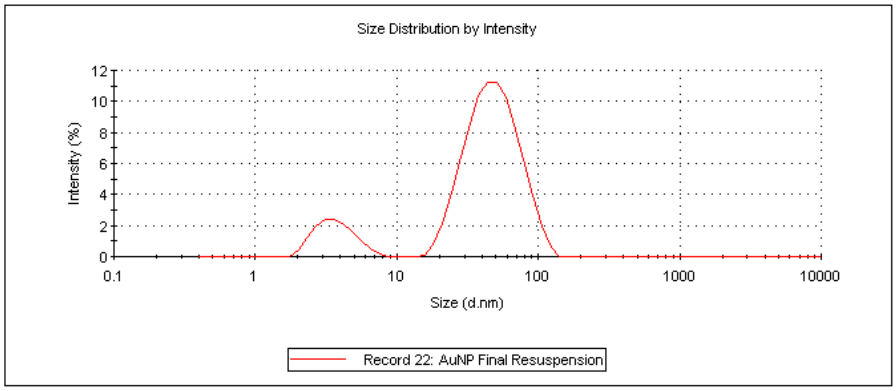

Figure B. 27: Size distribution by Intensity. The intensity is related to the number of measurements that originated a peak with for a certain particle size. A strong intensity means that in solution is present a considerable amount of molecules with the particular size where the peak is centered. Results obtained for the final resuspension of AuNP. The dynamic light scattering measurements were realized in a Zeta Sizer NANO ZS as described in Materials and Methods (section 6.2).

C. DEFINITIONS

Raman Contribution

Spectral data obtained experimentally upon excitation of a certain fluorophore in solution do not translate explicitly the real emission of this molecule. A wide number of factors can affect the signal and distort the observation. Raman scattering can be one of these artifacts, and it will occur from all solvents. For water the Raman peak appears at a wavenumber 3600 cm^{-1} lower than the wavenumber of the incident EM radiation. For excitation at 280 nm the Raman peak from water surges at ~311 nm, which can interfere with protein intrinsic fluorophores emission. Highly fluorescence samples generally dominate the emission and overwhelm the Raman peak. However, if the gain of the instrument is increased to compensate a diluted solution or a low fluorescing sample, the Raman peak may become significant and distort the emission spectrum (Lakowicz et al., 2006).

Isosbestic Point

Isosbestic points are commonly found when spectra plotted on the same chart are taken for a set of solutions where two or more absorbing components are present varying their proportions from solution to solution, provided that their total concentration is constant. The

meaning of isosbestic points is though polemic, and the knowledge about them is still scarce. An isosbestic point can arise in diverse situations, for instance:

- when the electronic spectra are taken on a solution where a chemical reaction is taking place, in which case the two absorbing components are a reactant and a product A and B;
- a solution where the two absorbing species A and B are in equilibrium and their relative proportions are controlled by the concentration of some other component (*e.g.* the protonated and deprotonated forms of a acid-base indicator; in this case the other component would be hydrogen ions);
- in the spectra of two unrelated components non-interacting components that present the same total concentration.

In all these examples, A (and/or B) may be either a single *chemical species* or a mixture of chemical species present in invariant proportion. If A and B are single chemical species, isosbestic points will appear at all wavelengths at which their molar absorption coefficients (formerly called extinction coefficients) are the same. (A more involved identity applies when A and B are mixtures of constant proportion.) (IUPAC, Pouet *et al.*, 2004)